An Analysis of the Relationship Between Respired Gases, Mixed Venous Oxygen, and Cardiac Output

Don Tishan Wellalagodage

Oriel College

A thesis submitted for the degree of

Doctor of Philosophy

University of Oxford

Trinity 2025

Abstract

An Analysis of the Relationship Between Respired Gases, Mixed Venous Oxygen, and Cardiac Output

Tishan Wellalagodage, Oriel College *Trinity 2025*

The focus of this thesis is the estimation of cardiac output and mixed venous O_2 saturation ($S_{\bar{v}}O_2$) through the analysis of respired gases. Current methods for measuring these parameters are limited by invasiveness, inaccuracy, or impracticality. Computed cardiopulmonography (CCP) is a novel technique for the assessment of respiratory and cardiac function, where each of these limitations may be addressed. CCP combines a molecular flow sensor (MFS) with a comprehensive cardiopulmonary model to provide non-invasive estimates of these, along with other cardiopulmonary parameters, through highly accurate and contemporaneous measurements of respired gases. Here, its application is tested in three different cohorts.

Chapter 1 provides an overview of the physiology and conditions relevant to the cohorts studied. In addition, the development of the various methods of measuring and estimating cardiac output are discussed, along with the historical context for the experimental methods discussed in this thesis.

In Chapter 2, CCP is introduced. The physical principles which allow for the MFS to record precise and contemporaneous breath-by-breath data, and the computational model, which is comprised of separate sub-models, is discussed in detail. Previous work undertaken with CCP is also presented.

Chapters 3 and 5 describe the results of the two clinical cohorts studied, the pulmonary hypertension and cardiac surgery patient cohorts, respectively. Both studies were conceived with the aim of comparing non-invasive CCP estimates of cardiac output and $S_{\bar{v}}O_2$ against

the invasive clinical reference standards of measurement. The pulmonary hypertension cohort study involved awake and spontaneously breathing participants, while the cardiac surgery cohort study included participants who were mechanically ventilated, following their postoperative admission to the intensive care unit. For the pulmonary hypertension cohort, CCP estimates for cardiac output were slightly biased towards underestimating the direct Fick cardiac output (mean difference: -0.25 L/minute, limits of agreement -1.9 to 1.4 L/min). For the cardiac surgery cohort, significant technical limitations made comparison between CCP cardiac output and $S_{\bar{v}}O_2$ estimates against the reference measurements difficult. The adjustments necessary to the respective CCP-based protocols due to these differences were explored.

Chapter 4 involves the study of healthy volunteers, with the primary objective of bridging the protocols used for awake participants in chapter 3 and mechanically ventilated ones in chapter 5. Due to the invasive nature of reference measurements for cardiac output and $S_{\bar{v}}O_2$, participants in this study instead underwent multiple protocols with different experimental configurations for comparison. Intraclass correlation coefficients (ICC) were calculated for each protocol. The open-circuit exogenous tracer gas protocol had the highest (best) cardiac output ICC at 0.87. Conversely, the closed-circuit exogenous tracer gas protocol was the worst of the four protocols at 0.64. The two identical CO_2 based protocols differed in their ICC values at 0.71 and 0.86.

Chapter 6 provides the overall conclusions gained from the results of the studies in this thesis. The potential for future work, which has been directed by these results, is also discussed.

Acknowledgements

I would firstly like to thank my supervisors, Peter Robbins and Andy Johnson. Peter, whose seemingly unlimited patience and enthusiasm for science guided me through all aspects of the doctorate. Andy, without whom the surgical study and my clinical efforts would never have gotten off the ground. I am eternally grateful for their contributions to my growth as an academic and clinician.

Thank you to my viva examiners, Professors Mike Grocott and Neil Herring (who also examined my Confirmation of Status), for making the process a thoroughly enjoyable and stimulating one—even with a midnight start.

It has been a pleasure to work with the other members of the Robbins and Ritchie groups. The work carried out in this thesis would simply not have been possible without their contributions. This list includes, but is not limited to, Dominic Sandhu, Graham Richmond, Nicholas Smith, Grant Ritchie, Jessica Luiz, Haopeng Xu, Asma Alamoudi, Nick Talbot, and John Couper.

My thanks also to Luke Howard and Francesco Lo Guidice at the Hammersmith Hospital for being so accommodating and helpful during my research there. At the John Radcliffe, I am equally grateful to the staff in the Cardiothoracic Intensive Care Unit who made every effort to help wherever possible. Special thanks must go to Liv Johnson for allowing our research device to overstay its welcome in the unit and to Mohammed Salem for helping me recruit a significant number of the patients in that cohort, including the very first one.

To my friends and colleagues at Oriel College, where I found a home away from home. Thanks to Juliane, Rob, Marta, Dan, Izzy, Cara (Oriel in spirit), Azmi, John, Cécile, Valerio, Tristan, Caitlin, Zelim, and Angelica. Words cannot express how much their friendship and support have meant to me over these years. To Marta, Dan, Izzy, and Cara especially, thank you for sticking with me through everything.

Back home, I must acknowledge St Paul's; there would be no Oxford and no DPhil if I had not been there. To Antone, for encouraging and advising me on how to make it possible and to Ash for maintaining an impossibly high energy in supporting me in everything from athletics to space to, of course, anaesthesia—we did it.

Finally, my love and thanks to my family. This thesis is as much the product of your work as it is of mine. Thank you to my parents for giving me everything, and to Kevin for believing in me and standing with me throughout this journey.

Abbreviations

ABG Arterial Blood Gas

AD Alveolar Dead Space

BTPS Body Temperature, Pressure, Saturated

CBGS Circulatory and Body Gas Stores

CCP Computed Cardiopulmonography

CV Coefficient of Variation

DF Direct Fick

ETT Endotracheal Tube

F_iO_2 Fraction of Inspired Oxygen

FRC Functional Residual Capacity

FT FloTrac

HME Heat and Moisture Exchanger

ICC Intraclass Correlation Coefficient

ICU Intensive Care Unit

LNL Lognormal Lung

MAC Minimum Alveolar Concentration

MFC Mass Flow Controller

MFS Molecular Flow Sensor

MIGET Multiple inert gas elimination technique

MRI Magnetic Resonance Imaging

MVBG Mixed Venous Blood Gas

PAC Pulmonary Artery Catheter

PEEP Positive End-Expiratory Pressure

REC Research Ethics Committee

RER Respiratory Exchange Ratio

RQ Respiratory Quotient

$\mathbf{S_pO_2}$ Peripheral Oxygen Saturation

STPD Standard Temperature, Pressure, Dry

$\mathbf{S_{\bar{v}}O_2}$ Mixed Venous Oxygen Saturation

TD Thermodilution

TG Tracer Gas

$\dot{\boldsymbol{V}}$ Ventilation

$\dot{\boldsymbol{Q}}$ Perfusion/cardiac output

$\dot{\boldsymbol{V}}/\dot{\boldsymbol{Q}}$ Ventilation-Perfusion Ratio

$\dot{\boldsymbol{V}}\boldsymbol{CO_2}$ Carbon Dioxide Production

$\dot{\boldsymbol{V}}\boldsymbol{O_2}$ Oxygen Consumption

Contents

1 Introduction

1.1 The Cardiopulmonary System

The cardiopulmonary system is a collective term for the cardiovascular system, comprised of the heart and vasculature, and the respiratory system, made up of the lungs and airways. These interlinked systems are primarily responsible for the transport of O_2 and CO_2 in blood and facilitating the exchange of metabolic nutrients, waste products, and water.(1; 2)

Air from the atmosphere flows through the conducting zone of the respiratory system where it is warmed, humidified, and filtered before reaching the respiratory zone. The conducting zone of the respiratory system begins with the trachea and ends with the terminal bronchioles. The respiratory zone includes the respiratory bronchioles, alveolar ducts, and alveolar sacs. The lung parenchyma is made up of the alveolar walls and interstitium. Gas exchange, specifically the diffusion of O_2 into the blood and the uptake of CO_2 out of the blood, occurs at the interface between the pulmonary capillaries and alveolar walls.(2)

Ventilation is not a perfectly efficient process. Dead space, the regions in the lung which are not involved in gas exchange, result in a fraction of each breath being exhaled unchanged. Dead space can be further categorised into anatomical, alveolar, and physiological dead space.(2) Anatomical dead space is the volume of air in the conducting airways. True alveolar dead space is air within the alveolar spaces that receive no perfusion; this volume is considered to be negligible in the healthy population.(3) Apparent alveolar dead space may also arise from ventilation/perfusion mismatch in the lung. Physiological dead space is the sum of anatomical and alveolar dead space. In the mechanically ventilated patient, apparatus dead space is an additional form of dead space. Apparatus dead space is the volume of air within the endotracheal tube and other components such as connectors and humidifiers.

The heart is the pump of the cardiovascular system which transports blood through

the systemic and pulmonary circulation. Venous, deoxygenated blood flows through the right atrium and into the right ventricle where it is pumped through the pulmonary vasculature. At the same time, oxygenated blood from the pulmonary vasculature is collected in the left atrium and is circulated through the aorta and into the systemic arterial tree.(2)

1.2 Medical and Surgical Disorders of the Cardiopulmonary System

This thesis is concerned primarily with the measurement of cardiac output and mixed venous oxygenation in two groups of patients who have particular measurement requirements in these areas. The two cohorts who took part in the experimental work presented in this thesis were either pulmonary hypertension or postoperative cardiac surgery patients. The disorders of the cardiopulmonary system relevant to these patients are described below.

1.2.1 Pulmonary hypertension

Pulmonary hypertension (PH) is diagnosed when the resting mean pulmonary artery pressure is greater than 20 mmHg.(4) The diagnosis can be further classified based on the diagnosis. Five different classifications for PH exist, with groups 2 and 3 being the most common(5; 6):

- **Group 1- Pulmonary arterial hypertension (PAH):** PAH is characterised by the obstruction of small pulmonary arteries due to endothelial dysfunction and vascular remodelling. PAH can be caused by inherited conditions, a wide array of acquired systemic disorders, drugs, and can also be classified as idiopathic.(7)

- **Group 2- PH due to left-sided heart disease:** Group 2 PH occurs as a result of increased hydrostatic pressure in the pulmonary vasculature due to left heart disorders such as aortic and mitral stenosis, heart failure (with either preserved or reduced ejection fraction), and rheumatic heart disease.(5)

- **Group 3- PH due to lung disease or hypoxia:** Lung disease which contributes to the reduction of pulmonary capillary area, due to hypoxic pulmonary vasoconstriction, destruction of the lung parenchyma, and/or vascular remodelling may cause this class of PH.(8) Chronic obstructive pulmonary disease and interstitial lung disease are significant contributors to this group.(6)

- **Group 4- Chronic thromboembolic PH (CTEPH) and other pulmonary artery obstructions:** CTEPH occurs due to thromboembolic obstruction of the pulmonary arteries. Additionally, the shear stress caused by obstruction leads to vascular remodelling, contributing to a worsening of the pressure within the pulmonary circulation.

- **Group 5- PH with multifactorial mechanisms:** This group includes PH caused by disorders which do not fall under any of the other four classes. Examples include chronic renal failure, sarcoidosis, and haemoglobinopathies including sickle cell disease, thalassaemia, and spherocytosis.(6)

The diagnosis of PH requires right heart catheterisation using a pulmonary artery catheter (PAC) in order to obtain right heart pressures, including the mean pulmonary artery pressure. Prior to this, however, patients are extensively worked up for the purposes of investigating possible differential diagnoses, identifying the class of PH, and for overall assessment of functional status. These investigations include electrocardiography (ECG), blood tests (including but not limited to haematology, biochemistry, thyroid function tests, and immunology), chest computed tomography, transthoracic echocardiography, pulmonary function tests, and cardiopulmonary exercise testing.(9) In addition to the mean pulmonary artery pressure, other right heart and pulmonary artery pressures, cardiac output, mixed venous O_2 saturation, and arterial O_2 saturation are also recorded. These values are then used to calculate other parameters, including pulmonary vascular resistance, cardiac index, stroke volume, and pulmonary arterial compliance.

1.2.2 Disorders requiring cardiac surgical intervention

Cardiac surgery encompasses the surgical treatment of heart and thoracic aortic pathologies. Coronary bypass grafting (CABG) for ischaemic heart disease, aortic and mitral replacement or repair for either valvular regurgitation or stenosis, and a combination of the aforementioned are the most commonly performed surgeries.(10) Most major cardiac surgery is performed using cardiopulmonary bypass (CPB). CPB involves diverting venous blood into a heat and gas exchanger and back into the arterial circulation. During this time, the heart is stopped using a cardioplegia solution and the aorta is cross-clamped to separate the systemic and coronary circulation.(11)

Ischaemic heart disease

CABG is a surgical option for ischaemic heart disease manifesting in various ways, including acute ST-segment myocardial infarction, complex multivessel disease, and left ventricular dysfunction. Arteries or veins harvested from the patient are used to bypass obstructed coronary arteries.(12)

Aortic stenosis and regurgitation

The aortic valve is a tri-leaflet valve that opens to allow blood to flow from the left ventricle to the aorta. Aortic stenosis, whereby the valve is pathologically narrowed and restricts blood flowing out of the left ventricle, is the most common valvular disease in Europe and America. It is usually due to age-related calcific degeneration in these regions. Aortic regurgitation causes backflow of blood from the aorta into the left ventricle during diastole. The causes of aortic regurgitation range from congenital defects such as a bicuspid aortic valve (can also cause aortic stenosis) and acquired pathologies such as rheumatic fever and infective endocarditis. Both aortic stenosis and regurgitation can be treated with an aortic valve replacement (AVR) using either a mechanical or bioprosthetic valve.(13)

Mitral stenosis and regurgitation

The mitral valve is a bicuspid valve separating the left atrium and ventricle, allowing the

flow of blood from the former into the latter during diastole. A regurgitant mitral valve can be caused by various pathologies affecting the valve specifically or due to dilation of the left atrium, annulus, or ventricle causing a functional failure of the cusps to converge. Mitral valve stenosis has fewer causes than regurgitation, these include rheumatic heart disease and infective endocarditis.(14) Where possible, mitral valve repair (MVr) is preferred over mitral valve replacement (MVR) due to reduced mechanical stress on the valve postoperatively.(14; 15; 16)

Tricuspid regurgitation

Clinically significant tricuspid regurgitation is most often due to secondary causes such as left heart disease and pulmonary hypertension rather than valve-specific pathologies. Tricuspid valve surgery is far less common than aortic and mitral valve surgery. Similar to the approach for mitral valve regurgitation, tricuspid valve repair (TVr) is preferred over replacement of the valve and is associated with a lower perioperative mortality.(17)

1.3 Respiratory-based Cardiac Output Measurement

Cardiac output measurement may be dichotomised into respiratory and non-respiratory techniques. An overview of the former is presented below.

1.3.1 The Fick principle

The Fick principle describes the relationship between the arteriovenous difference of a respiratory gas (usually either CO_2 or O_2, but not necessarily) and the production or consumption of the same gas.(18; 19) Named for Adolf Fick, who first demonstrated the principle in 1870 in a canine subject, it provides the theoretical basis for what is considered the gold standard of cardiac output measurement, the direct Fick method.

Taking O_2 as the subject gas, the Fick principle can be expressed mathematically with the Fick equation:

$$\dot{Q} = \frac{\dot{V}O_2}{c_{aO_2} - c_{\bar{v}O_2}}$$

Where $\dot{Q}$ is cardiac output, $\dot{V}O_2$ is consumption of O_2, c_{aO_2} is the arterial content of O_2, and $c_{\bar{v}O_2}$ is the mixed venous content of O_2.

Calculating the consumption or production of the subject gas requires sampling of respired gases. Paired arterial and mixed venous blood gas samples are required for the calculation of the arteriovenous difference of the subject gas. The direct Fick cardiac output can be calculated if all of the components of the Fick equation are measured. In cases where this is not possible, various methods of estimation of one or more components of the equation can be used in order to calculate an indirect Fick cardiac output.

The assumptions necessary to calculate a Fick cardiac output are that there is no intracardiac shunt and that both pulmonary and systemic circulations are at a steady state at the time of measuring the consumption/production and arteriovenous difference of the subject gas.(20)

1.3.2 Development and application of the Fick method

Right heart catheterisation for the purposes of cardiac output measurement was first performed by Otto Klein in 1930.(21; 22) It was not until the 1940s, however, that Cournand and Richards extended the evidence base for direct Fick and indicator-based cardiac output measurement and developed the technique to obtain a wider breadth of haemodynamic measurements.(23; 24; 25) They, along with Werner Forssmann who performed the first human right heart catheterisation (on himself), were recognised for their contribution to the field with the Nobel Prize in 1956.(26)

Cournand and Ranges demonstrated the application of right heart catheterisation and the subsequent calculation of direct Fick cardiac output in one subject.(23) Of note is that sampling right "auricular" (atrial) blood was considered to be a true mixed venous sample.

This work was built upon a few years later in 1945 with a larger cohort of 34 to show that right heart catheterisation was reproducible and viable in a representative range of participants.(25) The experiment outlined by Cournand et al. described the collection of exhaled gases using a Douglas bag and arterial and mixed venous blood sampling from the femoral artery and right atrium/ventricle, respectively. The sampling of blood was performed during the time that exhaled gas was collected. In general terms, except for the location of mixed venous blood collection, the experimental method would be considered acceptable in a modern-day setting.

Since the pioneering work of Cournand and others, right heart catheterisation has allowed for the wide utilisation of Fick cardiac output measurements in clinical and research environments. This has also led to the development of indirect Fick methods, where the term indirect indicates that one or more of the variables of the Fick equation is estimated.

The estimated variable used for indirect Fick cardiac output calculation in the clinical setting is usually $\dot{V}O_2$ given the difficulty in direct measurement in the clinical setting. Nomograms which take into account anthropometric and physiological factors are used.(20) The arterial content of O_2 in blood can also be estimated using pulse oximetry. Estimating either the mixed venous O_2 or CO_2 content is more complex and is discussed later in this chapter.

1.3.3 Early studies using tracer gases

In parallel with the work done in the early twentieth century to measure cardiac output by applying the direct Fick method, the idea that the measurement of the uptake of an exogenous gas by the lungs and circulation could also be used was under development. The appeal of this concept stemmed from the assumption that the starting mixed venous concentration of the exogenous gas was zero. This would negate the need for right heart catheterisation. Instead, the exogenous or 'tracer' gas in expired air could be measured once it had reached equilibrium within the lungs and systemic circulation but before it

had recirculated back to the lungs. The fractional volume of the expired tracer gas at this equilibrium and the difference in both tracer gas concentrations between the first and second gas samples was used to estimate cardiac output (or, more precisely, pulmonary blood flow).(27)

Krogh and Lindard were the first to use tracer gases for this purpose.(28) Their rationale for using nitrous oxide (N_2O) was that a gas soluble in the blood was required, having first, unsuccessfully, attempted to replicate the work of Adolf Bornstein, who used N_2.(28; 29) The insolubility of N_2 in blood resulted in significant measurement errors. Their experiment can be summarised as having a subject breathe a predetermined mixture of N_2O, O_2, and N_2, sampling the expired gas at 5 and 15 seconds, and calculating the difference in N_2O between the samples to determine the uptake in blood (using the blood-solubility of N_2O at 37 °C), and calculating cardiac output using this difference.

Subsequent to the foundational work of Krogh and Lindard and others, Arthur Grollman refined the experimental technique for using tracer gases. This included identifying acetylene (C_2H_2) as a more suitable gas than N_2O (difficulties with analysis), ethyl iodide (soluble in rubber), and ethylene (unpredictable solubility in blood due to lipophilicity). C_2H_2 was also better fit for purpose due to a greater solubility in blood compared to ethylene or N_2O, reducing measurement error and due to its similar aqueous and non-aqueous solubility.(27) He, along with Eli Marshall, also proposed a rebreathing method in which a rubber bag was filled with a tracer gas mixture of known volume and composition. This method was considered to be simpler than previously proposed ones.(30)

Using the C_2H_2 rebreathing method, Grollman was able to demonstrate reproducible estimates of cardiac output within 2%.(27) As he had noted in a previous publication, the use of tracer gases for the determination of cardiac output relied on the following assumptions(30):

- That gas sampling would take place when equilibrium was reached between both the

lungs and rebreathing bag and between alveolar air and the blood before recirculation occurred.

- The correct solubility of the tracer gas in blood was known.
- The mixed venous content of O_2 remained constant during the experiment.
- The absorption of the tracer gas in tissues such as the lung and upper respiratory tract was accounted for.

1.3.4 Advances in respiratory-based methods

Grollman's promising initial results with the C_2H_2 rebreathing method resulted in other researchers' interest in further tracer gas-based experiments. This included comparing the tracer gas technique with the direct Fick method. Noting that earlier studies compared the two methods in sequence, Chapman et al. were the first to simultaneously compare the direct Fick and C_2H_2 rebreathing method of measuring cardiac output.(31)

The key finding from the Chapman study was a direct Fick value which was consistently around 24% higher across participants compared to the C_2H_2 value. This was a result consistent with some of the earlier studies which had compared the methods in sequence.

Potential limitations of the tracer gas method and explanations for the discrepancy with direct Fick values for cardiac output included the possibility of recirculation before blood sampling had taken place, an incorrect solubility coefficient for C_2H_2 in blood being used, and an altered arteriovenous O_2 difference due to rebreathing. The arteriovenous difference was specifically thought to be at risk of overestimation (which would result in an underestimation of cardiac output) due to the potential for rebreathing to result in increased alveolar recruitment and consequently reducing the effect of any venous shunt within the pulmonary circulation.(31)

Chapman et al. discussed the error due to recirculation, an incorrectly high solubility coefficient for C_2H_2 in blood, and forced rebreathing causing an increased arteriovenous difference as being approximately 5% (greater with a higher true cardiac output), 7%, and 6%, respectively. Ascribing the underestimation of cardiac output when using the C_2H_2 method to multiple factors was an important conclusion, as it provided an avenue for each of the issues identified to be addressed in future studies, rather than representing an inherent issue with the principles of the technique.

The tracer gas method using exogenous gases (including but not limited to C_2H_2) was further refined to account for the solubility of gas in the lung and to use the measured uptake of the tracer gas in blood from semi-continuous respired gas analysis to estimate cardiac output.(32; 33) The effective lung tissue volume into which tracer gases dissolve was either assumed based on literature values or estimated experimentally. Sackner et al., for example, used a carbon monoxide isotope to determine lung tissue volume and subsequently how much of the initial C_2H_2 uptake was into tissue rather than blood.(33)

Although an exogenous tracer gas such as C_2H_2 has clear benefits, as discussed previously, CO_2 can also be used as an endogenous tracer gas. The following general principles apply when using CO_2 for this purpose: By using either a total or partial method of rebreathing, a mixed venous CO_2 content can be estimated. This is based on the assumption that the arterial content of CO_2 can be estimated if the end-tidal PCO_2 at rest is taken as a surrogate for arterial PCO_2. If the CO_2 production ($\dot{V}CO_2$) is also known, then the Fick equation can be applied to calculate a value for cardiac output. CO_2 rebreathing may be categorised as an indirect Fick method as the arteriovenous difference is estimated.(34)

The total rebreathing method for CO_2 did not gain traction as a viable clinical technique due to the risk of hypoxia and the impracticality of application in most patient populations. This method involved the participant rebreathing CO_2 until the end-tidal partial pressure of CO_2 plateaued, indicating that an equilibrium with mixed venous blood had been

reached. The partial rebreathing method instead requires deliberate and transient changes in ventilation to generate two sets of CO_2 partial pressure (used as a surrogate for arterial content) and production values. These values can then be applied to derive cardiac output in the following way(35):

$$\dot{Q} = \frac{\dot{V}CO_{2_1}}{c_{aCO_{2_1}} - c_{\bar{v}CO_{2_1}}} = \frac{\dot{V}CO_{2_2}}{c_{aCO_{2_2}} - c_{\bar{v}CO_{2_2}}} \tag{1.1}$$

Where $\dot{Q}$ is the cardiac output, $\dot{V}CO_2$ is the production of CO_2, and c_{aCO_2} and $c_{\bar{v}CO_2}$ are the arterial and mixed venous contents of CO_2 respectively. The subscripts 1 and 2 refer to the two measurement timepoints.

Equation 1.1 can be rearranged:

$$\dot{Q} = \frac{\dot{V}CO_{2_1} - \dot{V}CO_{2_2}}{(c_{aCO_{2_1}} - c_{aCO_{2_2}}) - (c_{\bar{v}CO_{2_1}} - c_{\bar{v}CO_{2_2}})} \tag{1.2}$$

The mixed venous content is assumed to stay constant between timepoints 1 and 2, giving $c_{\bar{v}CO_{2_1}} - c_{\bar{v}CO_{2_2}} = 0$. Therefore:

$$\dot{Q} = \frac{\dot{V}CO_{2_1} - \dot{V}CO_{2_2}}{c_{aCO_{2_1}} - c_{aCO_{2_2}}} \tag{1.3}$$

It is, therefore, possible to estimate cardiac output using the partial rebreathing method without knowing the mixed venous content of CO_2 (if the assumption is held that the

mixed venous content does not change between timepoints). Various methods have been discussed for generating the change in ventilation (and end-tidal CO_2).(34; 35)

1.4 Non-Respiratory Approaches to Measuring Cardiac Output

1.4.1 Thermodilution

The measurement of cardiac output by thermodilution, which requires insertion of a PAC, is considered the clinical reference standard. Thermodilution, like the direct Fick method, is a technique rooted in principles of mass balance. Unlike the direct Fick method, however, thermodilution is far more convenient to implement in various clinical settings.

Thermodilution involves the injection of an indicator substance (usually cold saline) of a known temperature and volume into the right atrium via a proximal port of the PAC. A sensor attached to the PAC in the pulmonary artery then detects the temperature of blood, which has mixed with the injectate.(36) The change in temperature over time is then used to calculate cardiac output ($\dot{Q}$) as shown with the modified Stewart-Hamilton equation(20):

$$\dot{Q} = \frac{A}{\int C(t)dt}$$

Where A is the amount of thermal indicator, C is the concentration of thermal indicator, and t is the time from injection to measurement in the pulmonary artery. The integral function in the denominator represents the area under the curve of the change in temperature with respect to time.

Thermodilution can either be performed as a bolus method or continuously. The bolus method requires multiple injections of thermal indicator in order to generate three measurements of cardiac output within 10% of each other. The continuous method replaces

the need for manual boluses by the use of a heated filament or continuous cold saline infusion in the PAC, proximal to the pulmonary artery, to effect a temperature change; as a result, a semi-continuous measure of cardiac output is possible.(37; 38)

The reliability of thermodilution-based cardiac output measurement can be affected by the following factors(20):

- Loss of indicator between the injection site and the temperature sensor in the pulmonary artery. Potential causes of loss of indicator include intracardiac shunt and a lower volume of injectate used than expected due to operator error. Similarly, an erroneously greater volume of injectate than expected will also result in an incorrect measurement.
- A transient bradycardic response to the cold injectate. This would potentially lower the cardiac output at the time of measurement.
- Cyclical changes in cardiac output due to mechanical ventilation will disproportionately affect the right side of the heart.
- Significant tricuspid regurgitation will result in underestimation of cardiac output.

While the scientific basis for cardiac output measurement using thermodilution is robust, the invasiveness of PAC insertion has seen a shift in practice to utilising alternative methods where possible.(39; 40; 41; 42) This is especially true in situations where the only PAC-derived parameter sought to guide diagnosis or management is cardiac output. The risks of PAC insertion include those that exist for the central venous line insertion, such as infection, bleeding, arterial puncture, and pneumothorax. Risks which are more PAC-specific include cardiac arrhythmias, valvular rupture, cardiac perforation, pulmonary infarction, and pulmonary artery rupture.(39; 40; 43)

A landmark study which was influential in shifting practice away from the widespread use of PACs in the ICU setting was the PAC-Man trial. This was a large multicentre study based in the United Kingdom examining the relationship between ICU mortality rates and

PAC insertion.(39) The overall findings showed no difference between PAC and non-PAC groups in terms of mortality and ICU and hospital length of stay. 10% of the PAC group also suffered complications directly attributed to PAC insertion.

It should be noted that while the study had many strengths, there were also significant flaws and features which make it difficult to draw specific conclusions. Notably, no sub-group analysis was conducted for patients with a diagnosis of decompensated heart failure, right heart failure or pulmonary hypertension, most PAC-related complications were those associated with central line insertion (haematoma at insertion site, arterial puncture etc), and patients with a PAC in-situ upon admission to the ICU were not eligible. These factors make conclusions about PAC use difficult to establish in specific patient populations, such as for those admitted from cardiac surgery (some of whom will already have a PAC in-situ) with acutely decompensated heart failure. Despite this, as noted by the authors of the PAC-man study in a later post hoc analysis, alternative methods of cardiac output measurement had already been fast-tracked without proper evaluation since publication, indicating the desire of clinicians to move away from using PACs.(44)

1.4.2 Non-pulmonary artery catheter-based methods

Most methods of cardiac output measurement that do not require pulmonary artery catheterisation may be classified as minimally invasive or non-invasive. Transpulmonary dilution methods are an exception to this due to the need for central venous and arterial access, although are still less invasive than a PAC. This alone makes these methods worthy of consideration over PAC-based ones. However, significant questions relating to accuracy, practicality, and applicability to critically ill patients exist.(42; 45) The main non-PAC-based methods, which are also not respiratory-based, are summarised below.

Pulse contour analysis

Pulse contour analysis is based on the principle that the morphology of the arterial waveform corresponds to left ventricular stroke volume. Cardiac output can therefore be

calculated if the heart rate is also known. A connection to an arterial line (a commonly utilised monitoring modality in an ICU patient) is required in order to detect the arterial waveform. Multiple commercially available models exist. All models follow the same general principle of transforming the arterial waveform to a pressure measurement and then to cardiac output, but differ on the technological approach.(38; 42; 45) A distinction can also be made between uncalibrated and calibrated pulse contour devices. Uncalibrated devices do not require calibration with a separate technique such as echocardiography or transpulmonary dilution.(42)

A sub-cohort of postoperative cardiac surgery patients discussed in the experimental chapters of this thesis had cardiac output measured for clinical purposes using the FloTrac (Edwards Lifesciences, CA, USA) system. In a survey of approximately 6000 cardiac anaesthetists across North America, Europe, Asia, Australia, New Zealand, and South America, the FloTrac was the most used alternative to a PAC for haemodynamic monitoring during cardiac surgery (excluding transesophageal echocardiography which is invariably used for monitoring during the perioperative course of a cardiac surgery patient).(46) For these reasons, the FloTrac is discussed in more detail below.

The FloTrac is an uncalibrated pulse contour device which is connected to the arterial line. Following connection, the pressure signal obtained from the arterial waveform is used along with the standard deviation of mean arterial pressure and a conversion factor to calculate a stroke volume.(38; 42; 45) The product of the stroke volume and heart rate is then used to calculate cardiac output. The exact derivation of the conversion factor is proprietary, however, characteristics of the arterial waveform- specifically, skewness and kurtosis- and demographic details are used to calculate an estimate for arterial compliance. Multiple updates to the algorithm have been released in order to better account for extremes of physiology. Noted limitations which have been accounted for in the fourth generation of updates include reduced accuracy and precision in patients with high or low systemic vascular resistance and in patients with a low cardiac output.(47; 48; 49)

Cine MRI

Cine magnetic resonance imaging (MRI) is considered a reference technique to measure cardiac output due to the high accuracy and precision associated with measurements.(50; 51) Given the non-invasive nature of the technique, it is very close to an ideal cardiac output monitor. The limiting factor of cine MRI is the lack of applicability to a significant percentage of patients who would benefit from cardiac output monitoring. This includes intensive care patients for whom the risks associated with transport to the MRI facility may outweigh the benefits of a single cardiac output measurement.(52)

Transpulmonary dilution

Transpulmonary dilution uses the same methodological principles as PAC-based thermodilution. A thermal or chemical indicator is injected into the venous system and the temperature or concentration change, respectively is measured via an arterial sample from a pre-existing arterial line. This differs from PAC-thermodilution where the injection is in the right atrium and the temperature sensor is in the pulmonary artery. As with PAC-thermodilution, the modified Stewart-Hamilton equation is applied to calculate cardiac output based on the temperature/concentration-time curve.(38; 53) The main commercially available models of transpulmonary dilution available are PiCCO (Pulsion Medical Systems, Germany), which uses intermittent thermodilution, and LiDCO, which uses a bolus of lithium as the chemical indicator. The added advantage of the LiDCO system is that central venous access is not required, as the lithium bolus may be delivered through a peripheral vein.

Transoesophageal Doppler

This technique allows for the continuous estimation of cardiac output using Doppler ultrasonography. An ultrasound probe is positioned and secured within the oesophagus, and aortic blood flow velocity is measured. The cross-sectional diameter of the aorta is then calculated, in conjunction with the measured velocity, to produce an estimate for

cardiac output. (38; 45)

Transthoracic/transoesophageal echocardiography

Both transthoracic and transoesophageal echocardiography may be used to measure the end-systolic and end-diastolic dimensions of the left ventricle. These dimensions can then be converted to a stroke volume and subsequently cardiac output using the heart rate in a similar fashion to cine MRI. (54)

Thoracic bioimpedance

Bioimpedance systems rely on the application of an electrical current of known frequency and amplitude across the thorax. The changes during a cardiac cycle are measured and correspond to variations in intrathoracic blood volume.(45) Due to concerns over signal loss with high lung water, newer bioimpedance systems instead measure phase shifts that occur when an oscillating current is passed through the thorax. These phase shifts occur due to pulsatile flow rather and are volume-independent.(55)

Other non-invasive methods

A select few non-invasive cardiac output measurement methods involve the application of a cuff to the distal upper limb (finger or wrist) to detect arterial pressure and volumetric changes.(45) The ClearSight system (Edwards Lifesciences, CA, USA) for example, uses a finger cuff to apply equal pressure to both sides of the artery to maintain a constant arterial volume. This process is repeated to generate a finger pressure waveform, which is then reconstructed to form an estimate of the brachial pressure waveform. This brachial waveform can then be used to estimate cardiac output in a manner similar to pulse contour analysis.(56; 57)

1.5 Limitations of Current Cardiac Output Measurement Methods

The broad categories of cardiac output measurement methods available clinically, which have been discussed, all have limitations. In general, there is an inverse relationship between accuracy and invasiveness of the technique used (cine MRI is an exception). Methods such as thermodilution and the direct Fick technique are considered to be the standards of reference for measuring cardiac output but rely on invasive pulmonary artery catheterisation. Conversely, less invasive methods lack accuracy and precision. Discussed in this section are the issues associated with cardiac output monitors currently in use.

Invasiveness

The risks of PAC insertion have previously been summarised. The most common complications are those which may occur in any procedure requiring central venous access such as infection, bleeding, perforation of the vessel, pneumothorax, and arterial puncture.(39; 40; 43) Virtually all of the complications reported in the PAC-man study were due to these complications.(39) It is because of the complications unique to PAC insertion, however, that there is a reluctance to utilise them for cardiac output monitoring. Despite this, a prospective observational study by Bossert et al. (2006) showed the rate of PAC-specific complications to be approximately 0.1% in their cohort of 3730.(58) In this study, the complications were specifically pulmonary arterial rupture, knotting of the catheter, and perforation of the right ventricle. While the complications relating to PAC insertion are potentially overemphasised, it should also be acknowledged that a significantly less invasive method with similar accuracy and precision would increase the proportion of patients who would receive cardiac output monitoring significantly.

Transpulmonary dilutional methods of measuring cardiac output such as PiCCO and LiDCO are classified as minimally invasive due to not requiring pulmonary artery catheterisation. It should be noted that there is still a degree of invasiveness, however, given that central venous (although peripheral venous access can also be used for LiDCO) and major

arterial access is required.(38; 53; 59)

Accuracy and precision

The reliability of cardiac output measurements varies significantly based on the method used. Within individual methods, it is also true that populations of patients with specifically deranged physiology, e.g. those with low cardiac output, high systemic vascular resistance etc. may not be suited for certain techniques. The levels of accuracy and precision for the various methods of measuring cardiac output are discussed below.

Cardiac output measured using thermodilution via a PAC is generally considered reliable with exceptions that are well documented. Specific pathologies, such as tricuspid valve regurgitation and intracardiac shunt render measurements significantly less reliable.(20)In cases where a patient has a low cardiac output, thermodilution measurements may overestimate the true value.(60; 61) This has been hypothesised to be due to the heat loss that occurs in low-output states.(61) Similarly, in states of high cardiac output, thermodilution may not be reliable.(60; 62) Possible reasons include increased sensitivity to intrathoracic pressure changes and larger variations in body temperature.(62) For the bolus method of thermodilution specifically, various operator-dependent factors can lead to error. These include the injectate being of incorrect volume or temperature, concurrent administration of intravenous fluids, injections not being synchronised with the respiratory cycle, and poor positioning of the catheter.(20; 63; 64)In terms of accuracy, continuous and bolus/intermittent thermodilution can be considered interchangeable.(65; 66)

Transpulmonary dilution methods such as LiDCO and PiCCO are inherently less reliable than PAC-based thermodilution due to the unpredictable loss of indicator which occurs across the pulmonary circulation. Recirculation of cold indicator is also a more significant consideration given the longer transit time of the indicator.(38; 53) Low cardiac output states render transpulmonary measurements unreliable due to the greater loss of injectate temperature when compared to pulmonary artery thermodilution.(53)

The accuracy of the indirect Fick technique is dependent on which of the components of the Fick equation is estimated. $\dot{V}O_2$ is often estimated, due to the difficulties around direct measurement in the clinical setting, using standard formulae such as those described by LaFarge and Miettinen and Bergstra.(67; 68) These formulae have been shown to be unreliable and resulting cardiac output values should be interpreted with significant caution.(69; 70)

Cardiac output measurement using other minimally invasive methods, such as pulse contour analysis, oesophageal Doppler, and thoracic bioimpedance, is becoming more common in the critical care setting.(46) Accuracy and trending ability over a variety of physiological states are lacking, however, and remain a significant barrier to using these results to guide clinical decision making.(38; 42; 45; 66)

Practicality

After taking into account the degree of invasiveness and accuracy of a monitoring device, the next most important consideration is the practicality of integrating it within the standard clinical setup. This setup will vary significantly depending on the disposition of the patient and the interventions they require. For example, cine MRI, a reference technique for cardiac output measurement which is also non-invasive, would be unlikely to be suitable for an unstable patient in the intensive care unit due to issues associated with transporting such patients to imaging facilities.(52) Another reference technique, the direct Fick is also rarely utilised clinically due to difficulties with $\dot{V}O_2$ measurement in the inpatient setting.

1.5.1 Conclusion

This chapter has introduced an assessment of the available options for cardiac output measurement. Their advantages and limitations have been described. It is clear that concerns of invasiveness, accuracy, and/or practicality limit all of these methods from widespread use.

The evolution of respiratory-based methods of measuring cardiac output has also been chronicled. The principle of conserving mass balance underpins these methods and makes them a promising avenue for further investigation.

The need for a form of cardiac output monitoring which is safe, applicable across a broad range of clinical settings, and accurate is clear. The findings in this thesis relate to the development and application of a novel and non-invasive technique for measuring cardiac output, computed cardiopulmonography (CCP).

CCP consists of a technological component, the molecular flow sensor (MFS) which allows for the highly accurate and precise measurement of respired gases, and an accompanying computational model of the cardiopulmonary system. CCP has previously been implemented primarily in characterising respiratory physiology and pathology. This thesis shifts the focus to a cardiac output-centred one but also explores aspects of respiratory physiology which have yet not been considered in the CCP computational model. Two variations of CCP for the purpose of cardiac output monitoring are presented, both of which are compared against the gold-standard technique for cardiac output determination. The two variations discussed were uniquely tailored to the cohorts they were implemented for, pulmonary hypertension patients undergoing right-heart catheterisation and mechanically ventilated patients in the ICU following cardiac surgery.

2 Computed Cardiopulmonography

Introduced in this chapter are the foundational concepts related to the molecular flow sensor (MFS) and computational model of the lungs and circulation, which together make up computed cardiopulmonography (CCP). The MFS provides a method for respired gas to be measured in an accurate and contemporaneous manner. This measured data is then used within the computational model to estimate cardiopulmonary parameters which reflect the subject's physiology.

The use of laser absorption spectroscopy and pneumotachography within the MFS is discussed, along with descriptions of how individual gas concentrations and environmental conditions are measured. The three sub-models which make up the CCP computational model are introduced, as is the integration of these sub-models to work as one larger model. Finally, a broad outline of the steps taken when undertaking a CCP protocol is given.

2.1 The Molecular Flow Sensor

2.1.1 Laser absorption spectroscopy

Absorption spectroscopy refers to the process of measuring the decrease in radiation intensity as it passes through an absorbing sample to determine the sample's concentration.(71) The technique has several advantages in the quantitative analysis of chemical concentrations. All atoms and molecules absorb EM radiation, making it wholly generalisable. Each species will also have a unique absorption spectrum, depending on wavelength. Along with this generality and specificity, the widespread use of absorption spectroscopy is made possible by the simplicity of both the experimental application and subsequent analysis of the technique.(72)

When an atom or molecule absorbs a photon, it transitions from a ground state to a higher energy level—an excited state. Depending on the frequency of the radiation, the higher energy level can be characterised by the motions or degrees of freedom within

the atom or molecule. These include rotational motion, vibrational motion, electronic motion, and nuclear and electron spin motion. The energy absorbed during the transition corresponds to the peak in the subject species' absorption spectrum.(73)

Laser absorption spectroscopy refers to an absorption spectroscopic method used for measuring gases in which a laser is used as the light source. The laser beam is transmitted along an optical path, and the reduction in beam intensity is measured after it has passed through the gas sample.(74)

The Beer-Lambert law underlies the basis for absorption spectroscopy. It describes the attenuation of light through an absorption species, and is expressed as follows(71):

$$I(v) = I_0(v) \exp^{-\sigma(v)[N]l} \tag{2.1}$$

Where $I(v)$ is the light intensity following transmission through the absorber, $I_0(v)$ is the incident intensity (i.e. intensity before passing through the absorber) of the light, $\sigma(v)$ is the absorption cross-section of the species at frequency v, $[N]$ is the concentration of the absorbing species, and l is the path length (i.e. distance the light travels through the absorber).

The absorption cross-section for a given frequency is unique to individual atoms or molecules in the absorbing sample, allowing for the concentration measurement of these individual species. To account for experimental conditions, it is necessary that the spectral line shape is factored into the analysis. This involves measurement of line broadening and line shifting mechanisms. For both mechanisms, pressure and Doppler shifts are the major factors of influence. Pressure broadening (also known as collision broadening) results in a homogeneous broadening of absorption lines, meaning that all species in a sample are affected in the same way. Essentially, a rise in pressure (causing an increase in collision frequency) will shorten the lifetime of a species in its excited state, and therefore increase the uncertainty associated with the frequency and contribute to homogeneous broadening of the spectral line. The increase in uncertainty as a result of excited state

lifetime shortening can be expressed as shown in equation 2.2.

$$\Delta v = \frac{1}{2\pi}(\frac{1}{\tau\prime} + \frac{1}{\tau\prime\prime}) \tag{2.2}$$

Where Δv is the frequency uncertainty and $\tau\prime$ and $\tau\prime\prime$ are the lifetimes in the excited and ground states, respectively.

Doppler broadening is the main inhomogeneous line broadening mechanism. If a molecule has a velocity component in the same direction as the radiation source, the photon absorption frequency shifts. Molecules can be classified into velocity classes, based on their distribution of random velocities, using the Maxwellian velocity distribution function. Based on the velocity class, the Doppler shift will vary.(75) Pressure broadening and Doppler broadening result in a Lorentzian and Gaussian line shape, respectively. The combination of these two mechanisms results in a mixed line shape, known as a Voigt profile.(76)

Line shifting is the process whereby the line shape is shifted in frequency. This can be due to pressure shift, where the shift is directly proportional to the pressure, or Doppler shift. With the latter mechanism, the Voigt profile is shifted based on the mean speed of the gas in the direction of the beam of radiation.(75)

Laser absorption spectroscopy in its most basic form, i.e. direct absorption spectroscopy, is limited by the need to measure a small change in light intensity variation against a comparatively large background of transmitted light intensity.(71; 72) Variations have been developed to counter this limitation. Among these variations is cavity enhanced absorption spectroscopy (CEAS), which greatly increases the sensitivity of the technique by enhancing the effective path length of the absorbing species by trapping light between two highly reflective mirrors. The mirrors create an optical cavity which allows for light to circulate. The effectiveness of CEAS relative to standard laser absorption spectroscopy

can be shown using the following equation(71):

$$\frac{I_0 - I(v)}{I(v)} = \frac{\sigma(v)[N]l}{1 - R} \tag{2.3}$$

Where R is the geometric mean of the reflectivity of the two cavity mirrors.

If no mirrors are used to enhance the path length, then R will be 0, and equation 2.3 can be transformed into equation 2.1. Conversely, if, for example, R=0.9999, it can be seen that the path length increases significantly, resulting in a much higher variation in light intensity. The MFS utilises both direct absorption and cavity enhanced absorption spectroscopy to obtain measurements of respired gas concentrations.

2.1.2 Molecular flow sensing

The technological approach to directly measure the five gases—CO_2, H_2O, O_2, CH_4 (methane), and C_2H_2 (acetylene)—of experimental interest varied due to the different physical properties of each gas. A summary of how each gas species was measured is presented below. Common to all gas species analysed was the estimation of the concentration; where a predicted line shape, using instantaneous sample temperature and pressure, sample composition from the previous 10 ms window, and line broadening parameters from the literature, was regressed.

Measurement of CO_2, H_2O, methane (CH_4), and acetylene (C_2H_2)

CO_2 and H_2O have similar transition strengths that are large enough that direct absorption spectroscopy may be used. Distributed feedback diode lasers are used as the EM radiation source. For both gases, rovibrational (rotational and vibration) transitions that were both of a large enough absorption cross-section (to use direct absorption spectroscopy) and specific enough to avoid the transitions of other gas species in the sample were selected.

Due to the similar transition strengths of CO_2 and H_2O, it was possible for both lasers to be housed in the MFS electronics module and connected to the measurement head via a

single optical cable. It was desirable to keep the measurement head itself as small and light as possible, an important consideration in clinical settings, especially where space around the head-end of the patient is limited. To help facilitate this aim, in addition to housing the lasers in the electronics module, a V-path system with an optical path of approximately 5 cm was installed within the head (panel A in figure 2.1). This served to functionally increase the path length using mirrors located on both ends of the cell.

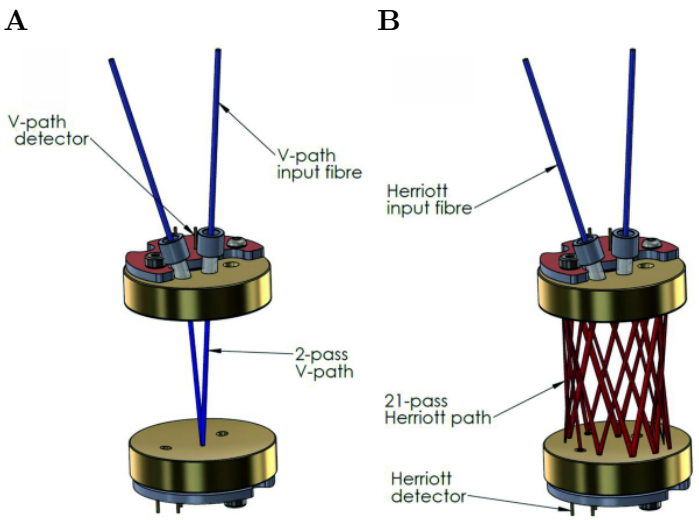

Figure 2.1: Panel A shows two highly reflective spherical mirrors separated by a V-path for the measurement of CO_2 and H_2O concentrations. The laser radiation is transmitted through the V-path input fibre on top of the cell before reflecting off the mirrors and coming through the V-path output fibre, also on top of the cell. Panel B shows the 21-pass system required for CH_4 and C_2H_2 concentration measurement. The 21-pass system increases the effective path length in the same way as the V-path system. Image courtesy of Smith et al.(77)

Direct absorption spectroscopy using the distributed feedback diode lasers was also used for CH_4 and C_2H_2. Due to the smaller absorption coefficients for these molecules and the low concentrations in which they are used in the experimental protocols discussed, the V-path system used for CO_2 and H_2O was not suitable. Instead, a Herriott cell was used to enhance the optical path length in a similar fashion to the V-path (panel B in figure 2.1).

Measurement of O_2

Compared to the other gas species directly measured using the MFS, the absorption cross-section of O_2 for rovibrational transitions that can be measured using readily available lasers is extremely small. For this reason, off-axis CEAS was utilised instead of direct

absorption spectroscopy. This system was contained in the MFS measurement head, and is shown in figure 2.2. With CEAS, the relationship between the O_2 concentration and absorption cross-section is given by the modified Beer-Lambert equation (described previously in equation 2.3) to take into account the reflectivity of the cavity mirrors.

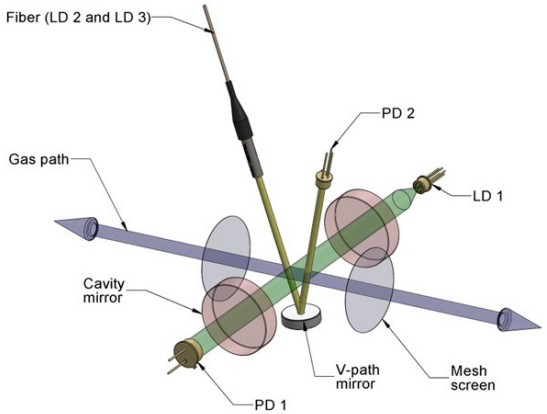

Figure 2.2: Schematic of the spectrometry setup within the MFS measurement head. Gas travels through the mesh screens (gray) along the blue path. LD1 and PD1 are the O_2 diode laser and photodiode, respectively. The former emits radiation through the optical cavity (green) created by the two highly-reflective mirrors (red) and the latter detects the radiation output. The configuration of the V-path system for measuring the other gases, including the mirror (white and gray), optical path (yellow), diode lasers (LD2 and LD3) and photodiode (PD2), is shown for context. Image courtesy of Ciaffoni et al.(78)

Measurement of temperature, pressure, and flow

The measurement of respired gas concentrations using laser absorption spectroscopy has been discussed above. Additionally, it is necessary to measure temperature, barometric pressure, and flow to contextualise these concentration measurements so that they reflect the dynamic nature of the respiratory cycle accurately and contemporaneously.

Temperature and barometric pressure are necessary for the measurements of gas concentrations and also for the spectroscopic line broadening parameters. The absolute pressure was sensed using a standard pressure sensor (HCA-BARO, Sensortechnics, UK) connected, with silicone tubing, to the airway pressure port, within the MFS measurement head (figure 2.3).

The temperature was monitored using four wire thermocouples, paired at either end of the MFS measurement cell. Within the pairs, one wire measures peripheral gas flow and the other protrudes further in to sample central gas flow. Positioning of the thermocouples

was determined by simulations run prior to manufacturing the device. The readings from the four thermocouples are averaged to obtain an estimate of gas flow temperature. Prior to experimental measurements being taken, the MFS is warmed to 36°C. This serves to minimise condensation, which would affect the reflectivity of the mirrors used, and also to provide a more stable spectroscopic environment, given that exhaled breath is close to this temperature.

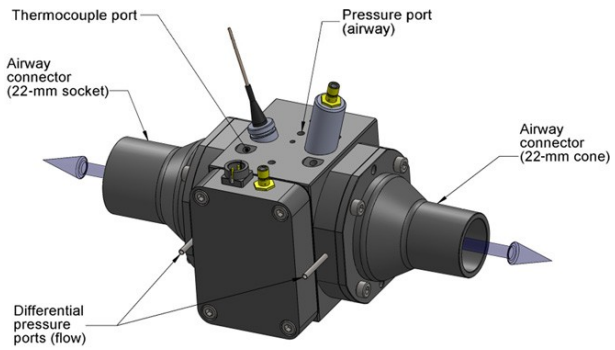

Figure 2.3: Schematic of the MFS measurement cell with the protective casing removed. Bidirectional gas flows through the openings in the airway connectors. The differential pressure ports on the outside of the mesh sheets are shown. Ports for the thermocouple and airway pressure port are located at the top of the cell. Image courtesy of Ciaffoni et al.(78)

For the measurement of flow, a modified Lilly-style pneumotachograph, where flow is measured by calculating the pressure drop through a mesh with a known resistance, is used. A standard Lilly-style pneumotachograph has multiple limitations which were necessary to overcome to achieve the accurate and time-aligned measurements required with the MFS. The initial factors to consider are that firstly, the relationship between pressure drop and flow is not necessarily linear, and secondly, differential pressure transducers are prone to drift, which results in incorrect readings at zero flow. The former factor was addressed using helical flow conditioners and wire meshes to ensure reproducible flow, independent of upstream geometry, across the measurement mesh. The issue of baseline drift was addressed with the installation of eight differential pressure sensors (HCLA, Sensortechnics, UK) to reduce the variability of readings at zero flow states. The eight sensors were split into two banks of four. Every five minutes, one of the banks is isolated for 20 seconds and a drift correction is performed; during this time, the other bank continues to measure the differential pressure to avoid breaks in data collection.

A more complicated and multifaceted consideration is that the need for accurate and contemporaneous flow measurements is affected by the respiratory cycle, in which gas composition, including viscosity and density, changes. Additionally, due to the variable and bidirectional nature of the flow passing through the MFS measurement cell, it is not laminar and therefore not linearly proportional to the pressure drop across the mesh membrane. As a result, it was necessary to develop a term for the pressure drop to account for the factors described. This was expressed in the following way:

$$\Delta P = \alpha\mu\dot{V} + \beta\rho\dot{V}^2 \tag{2.4}$$

Where ΔP is the pressure drop, α and β are parameters determined through calibration of the pneumotachograph, μ and ρ are the instantaneous viscosity and instantaneous density, respectively, and $\dot{V}$ is the rate of flow. The α and β parameters from equation 2.4 are determined by non-linearly regressing fit sets of integrated flows (obtained during calibration) to the known calibration pump volume.

Estimating cardiac output using MFS measurements

Smith et al. described the development of the MFS to measure these tracer gases by installing a Herriot cell and then used a non-invasive, MFS-based approach to estimate cardiac output by measuring the uptake of CH_4 and C_2H_2 in a group of healthy volunteers.(77) The use of C_2H_2 to estimate cardiac output was based on the principles of mass balance, in a conceptually similar way to that described by Grollman, as discussed in chapter 1.(30)

The cohort consisted of six men, between the ages of 21 and 40, with no significant cardiorespiratory comorbidities. Participants were required to breathe through the MFS in a two-stage protocol. For the first stage, participants breathed air for four minutes and then a mixture of CH_4, C_2H_2, 21% O_2, and balance N_2 at 30 L/min in an open-circuit configuration (thereby breathing in the mixture as it flowed past and exhaling into air) for a further four minutes. The second stage involved participants an exercise period, where participants pedalled on a bicycle ergometer and breathed air for three minutes and the same tracer gas mixture for 3 minutes at 60 L/min. To assess the reproducibil-

ity of these measurements, the participants underwent the protocol on five consecutive days.

An algorithm to estimate cardiac output based on the tracer gas uptake was written and is described in detail by Smith et al. To summarise, the tracer gas uptake was assumed to occur by equilibration in the lungs and uptake into the tissue and circulation. C_2H_2 is relatively soluble in blood, the uptake can therefore be used to predict cardiac output. CH_4 is relatively insoluble and will equilibrate in the lung without passing into the circulation, this allows for a lung volume estimate to be made using the calculated uptake in the breath. A cubic smoothing spline was fitted to the end-expiratory points for the total respired gas flow to estimate the functional residual capacity (FRC). The uptake of CH_4 and C_2H_2 at this estimated FRC were used in the cardiac output algorithm.

To estimate the cardiac output with the method described, some assumptions were necessary. Firstly, it was assumed that cardiac output and the lung gas volume were constant over the measurement period. Secondly, and related to the first assumption, was that the lung was homogeneous. This leads to further assumptions which need to be made related to gas mixing, including whether the tracer gases had enough time to equilibrate within the lung. To account for this, the first two breaths of the tracer gas breathing phase were excluded from the analysis. The final two assumptions were that the solubility of the tracer gases in the lung tissue was the same as the solubility in blood and that there was no recirculation. To minimise the chance of using breaths after tracer gas recirculation had taken place, breaths after the 10th tracer gas breath were excluded.

The results for this study showed a 7% test-to-test variability in cardiac output, highlighting the reproducible nature of the MFS measurements, especially given the likelihood of a natural variation in cardiac output on a day-to-day basis. Comparison with a reference method of cardiac output measurement, such as the direct Fick method or thermodilution, was not possible due to the ethics of performing pulmonary artery catheterisation on a healthy volunteer. Instead, comparison was made using regression relations between

cardiac output measured using the direct Fick method and O_2 consumption ($\dot{V}O_2$). This was possible as $\dot{V}O_2$ is directly measured using the MFS.

Summary

The core technologies, laser absorption spectroscopy and modified Lilly-pneumotachography, used in the MFS have been discussed. The unique requirements needed to interrogate the composition and flow of respired gas passing through the MFS in a contemporaneous and reliable manner have also been considered. The end result is a device which is capable of making direct measurements of molecular flow, which are clinically useful both in isolation and also for input into the CCP model.

2.2 Cardiopulmonary Modelling

The basis for CCP is that information relating to respiratory gas exchange, if measured accurately enough, can be reproduced using a cardiopulmonary model that conserves mass balance. In the MFS, a device with the required accuracy and contemporaneity exists. In the computational cardiopulmonary model, three sub-models—for the lungs, circulation, and blood—exist within it that run in parallel to optimise the fitting parameters to simulate the measured gas profiles. The lognormal lung model (LNL), recovers parameters relating to lung inhomogeneity and volume. The circulatory and body gas stores (CBGS) model simulates the uptake of gases across the circulation. The blood model describes the handling of respiratory gases in blood so as to constrain the LNL and CBGS model's simulation of gas exchange in a physicochemically consistent way.

The three CCP sub-models run within a nonlinear optimisation routine (lsqnonlin, MATLAB, Mathworks, USA).(79) The baseline characteristics of the participant are used, as the fitting parameters are iteratively altered to simulate measured expiratory gas profiles. Gases where the model has been set to simulate the expiratory profile (usually O_2, CO_2, and N_2) are compared against the measured profiles, and the squared difference between the true and simulated fractional flow is taken. An example of the measured and simulated

gas profiles is shown in figure 2.4. The squared difference for each gas is taken as a residual for the optimisation function. The fitting parameter values which minimise the sum of these residuals are taken as the best estimates. When a dataset is run through the CCP model, four separate fits are produced. Each fit uses different, randomised starting points for the fitting parameters. This is done to check the intra-dataset reproducibility of parameter estimates.

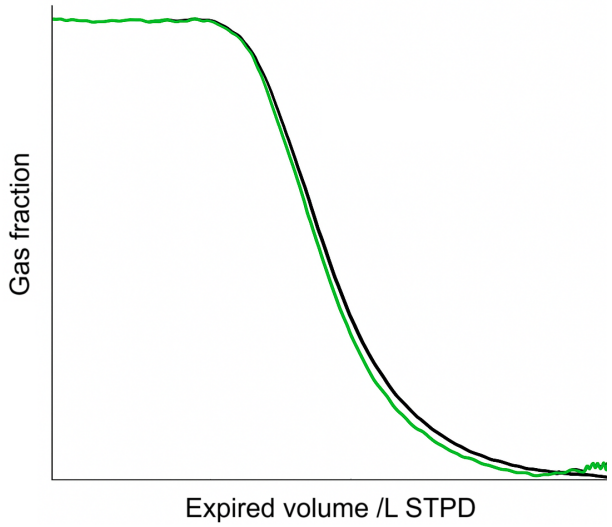

Figure 2.4: Example of an expiratory gas profile for O_2. The green plot is the measured expired gas profile for O_2. The black plot is the simulated gas profile. The overlap between measured and simulated gas profiles indicates a good model fit.

2.2.1 Lognormal lung model

The lognormal lung (LNL) model was first described by Mountain et al.(80) It serves to estimate lung parameters which relate to volume and inhomogeneity. Inhomogeneity within the lung occurs when there is a mismatch between ventilation ($\dot{V}$) and perfusion ($\dot{Q}$). LNL-specific CCP parameters are estimated with this concept of lung inhomogeneity as the core principle. Pure shunt ($\dot{V}/\dot{Q} = 0$) and alveolar dead space ($\dot{V}/\dot{Q} = \infty$) are not considered within the standard version of the model, although a version that accounts for the latter and the results of this change are discussed in subsequent chapters.

The fit parameters in the LNL model are as follows:

- $\boldsymbol{V_A}$: The alveolar volume, measured in litres (BTPS), at functional residual capacity (FRC).

- $\boldsymbol{V_D}$: The dead space volume, measured in litres (BTPS), at FRC. FRC is the sum of V_A and V_D.
- $\boldsymbol{C_{V_D}}$: The fractional expansion of dead space relative to the fractional expansion of the alveolar space.
- $\boldsymbol{\sigma V_D}$: The standard deviation of the standardised dead space.
- $\boldsymbol{\sigma C_L}$: The standard deviation for the natural logarithm of the standardised lung compliance.
- $\boldsymbol{\sigma Cd}$: The standard deviation for the natural logarithm of the standardised lung conductance. This is set to be 0.3 over σC_L based on previous investigations relating to CCP model parameter determination.

The model lung consists of 125 compartments, each of which receives an equal share of volume at FRC. For an individual lung compartment i, the volume is $V_{A,i} = \frac{V_A}{125}$. The lung tissue volume which gas can dissolve into is also the same across compartments, and is determined by the solubility of each gas species. To model inhomogeneity lung, each unit receives a differing fractional share of ventilation ($F_{C_L,i}$), perfusion ($F_{Cd,i}$), and anatomical dead space volume ($F_{\mathrm{DS},i}$). As ventilation and perfusion are affected by metabolic rate, compliance and pulmonary vascular conductance, respectively, are instead used. The ratios $F_{C_L,i} : V_{A,i}$ and $F_{Cd,i} : V_{A,i}$ are assumed to follow a bivariate lognormal distribution. This distribution is defined by the parameters σC_L, σCd (both of which have been described above), and ρ, which describes the correlation between σC_L and σCd. $F_{C_L,i}$ and $F_{Cd,i}$ are drawn from the distributions of standardised lung compliance and conductance, respectively. $F_{\mathrm{DS},i}$ is drawn from the standardised dead space distribution, which is assumed to be normally distributed. It is not expected that these distributions exactly match the real lung, but rather provide a scaffold for the fit parameters to accurately reflect the variance (inhomogeneity) within it.

Bidirectional gas flow and exchange is modelled contemporaneously, in a segmental fashion, with each MFS measurement (made every 10 ms). The delay between measurement and

modelling due to the transit of gas through the anatomical dead space is accounted for with a model of plug flow. Plug flow refers to the unaltered (no gas exchange) transit of gas through dead space.(81)

Gas exchange between the alveolus and pulmonary capillary is assumed to occur perfectly within each model compartment. Therefore, equilibrium between alveolar gas, blood, and the lung tissue is also assumed. Diffusion limitation, due to lung parenchymal damage, hypoxia, or other factors, is not modelled. Based on the assumption of gaseous equilibrium across phases, the gas concentration in each phase is iteratively adjusted until they are equal. As the end-capillary blood and alveolar partial pressure are equal, per-compartment gas exchange is determined by (per-compartment) blood flow and the mixed venous and end-capillary partial pressure difference.

2.2.2 Circulation and body gas stores model

The circulation and body gas stores (CBGS) model was originally described by Magor-Elliott et al.(82) The model uses anatomically viable compartments to estimate the composition of mixed venous gas (CO_2, O_2, and inert gas) from a known arterial composition of gas (as derived by the LNL model from inspired gas profiles). It is the CBGS sub-model within CCP that allows for the estimation of metabolic parameters by simulating the arteriovenous exchange of blood. The parameters fit by the CBGS model are as follows:

- $\boldsymbol{\dot{V}O_2}$: The metabolic rate of O_2 consumption at the tissue level, measured in L STPD/minute.
- $\boldsymbol{R}$: The respiratory quotient. This is the fraction of the metabolic production of CO_2 and consumption of O_2.
- $\mathbf{P}_i\boldsymbol{CO_2}$: The ideal partial pressure of CO_2. The ideal point refers to the point at which the alveolar and arterial partial pressures are equal in a lung with no inhomogeneity.(83)

Individual body compartments, each connected to the lung in independent, parallel pathways, are used; they are assigned perfusion parameters based on mass, density, vascular volume and transit time through systemic arteries. There are 11 such compartments, representing different major organs and tissue categories (skeletal muscle and adipose tissue), and an additional one for the volume of blood present in the large arteries and veins. Additionally, each compartment is assigned a solubility coefficient for the O_2, CO_2, N_2, CH_4, and C_2H_2. The model is initially based on the International Commission for Radiological Protection's report of the tissue sizes of a standard man; this reference man was a 25-year-old male, with a height and weight of 180 cm and 70 kg, respectively.(84; 85) The CBGS model can be scaled based on the age, height, and weight of the subject breathing through the MFS, by first calculating the fractional mass of fat (F_{fat}) and lean body mass (LBM) as shown below:

$$F_{fat} = \frac{1.2(\text{BMI}) + 0.23(\text{age}) - 10.8(\text{isMale}) - 5.4}{100} \tag{2.5}$$

Where BMI is the body mass index and isMale is set to 0 for females and 1 for males. The BMI is calculated as mass in kg divided by the squared height in metres.

$$\text{LBM} = \text{mass} - F_{fat}(\text{mass}) \tag{2.6}$$

Where mass is the total mass of the subject in kg.

To model gas exchange between the circulation and body tissues, it was first necessary to consider each gas separately. For CO_2 and O_2, it was also necessary to consider the interdependent exchange based on the Bohr and Haldane effects. The solubility coefficients of each gas in the different compartments of the CBGS model were established from literature values, as detailed by Magor-Elliott et al. The metabolic rates, again using literature values, then serve as a starting point, along with the known arterial blood gas contents, to simulate blood flow into the individual tissue compartments and the flow of venous blood out of the compartment. As fit parameters, R and $\dot{V}O_2$ are determined by this simulated exchange at the blood-tissue interface.

2.2.3 Blood model

The CCP blood sub-model, first described by O'Neill and Robbins, represents a mechanistic, physicochemically accurate representation of the carriage of CO_2 and O_2 in blood.(86) The process of constructing this model is detailed in their paper; the key points especially relevant to CCP modelling are detailed in this section.

The primary purpose of the blood model is to bridge the LNL and CBGS models by simulating the exchange of CO_2 and O_2 between the lungs and circulation. To do this, it is necessary to be able to convert a given pair of CO_2 and O_2 partial pressures and convert this to dissolved contents in the blood, and vice versa.

With the carriage of CO_2 in blood, multiple factors must be considered. CO_2 is soluble in blood, but will also react with proteins, including haemoglobin, to form carbamino compounds and react with water to form bicarbonate and protons via the formation of carbonic acid. The formation of carbamino compounds and bicarbonate contributes to the Haldane effect. The Haldane effect describes the increased affinity of deoxygenated haemoglobin to bind with CO_2. The binding of deoxygenated haemoglobin is also affected by the Hamburger effect, or chloride shift. This occurs due to the buffering of the protons, produced during the reactions with CO_2 and blood and water, by reactions with haemoglobin, albumin, and phosphates, but also with the bicarbonate ions, which are exchanged across the red cell membrane for chloride ions. These factors are all accounted for within the blood model.

For O_2, the major mode of transport in blood is by binding to haemoglobin, with a small amount also dissolved in blood. The oxygenated (relaxed) and deoxygenated (tense) forms of haemoglobin have different affinities for O_2. This, along with the Bohr effect, which describes the affinity of haemoglobin to bind or offload O_2 based on pH, CO_2 partial pressure, and 2,3-disphosphoglycerate (2,3-DPG), is information which is captured within the model to accurately simulate the carriage of O_2 in blood.

In addition to the specific considerations for each of CO_2 and O_2 outline above, the model was built with the physicochemical constants for albumin and relaxed and tense haemoglobin, as well as the physiological constraints of mass balance, electroneutrality, and a Gibbs-Donnan equilibrium (where a system containing an unequal distribution of permeant ions across a semi-permeable membrane exists). The model was validated with literature values and in a range of different physiological states, including hyperoxia, metabolic acidosis and alkalosis, anaemia and polycythaemia.

2.3 CCP Protocols

This chapter has thus far detailed the components of CCP, the MFS and the CCP model—made up of three sub-models. The studies described in this thesis have different experimental CCP protocols; however, they all share commonalities, which will be described in the following section. The unique aspects of the protocols will be discussed in their respective chapters.

2.3.1 Preparation

For the MFS to be ready for data collection, it must be warmed and calibrated. As discussed in section 2.1.2, the MFS is warmed to approximately 36°C to prevent condensation on the mirrors and to generate a spectroscopic environment similar to the one in which the subject's respired gas flow will create. The MFS is then calibrated using pure N_2 and then pure O_2 (both gas preparations are supplied by BOC Speciality Gases, UK). Following these steps, the MFS is allowed to run to ensure that the thermocouple temperatures are all consistent with one another and that there are no gross abnormalities with the absorbance spectra for individual gases.

In terms of preparing the subject for breathing through the MFS, the steps taken differ based on whether they are awake or sedated and breathing with the aid of a mechanical ventilator. If they are awake and able to follow instructions, the subject is first positioned

either seated and upright or supine. A nose clip is then placed, to ensure that all respired gas flow is through the MFS. The subject is then asked to breathe through the MFS via a mouthpiece and heat and moisture exchanger (HME) filter, as pictured in figure 2.5. During the first 30 seconds of breathing through the MFS, and before data collection begins, flow calibration takes place. For a mechanically ventilated subject, a nose clip is not necessary, given that all gas flow passes through an endotracheal tube (ETT). The other preparatory steps are similar to the awake subject.

Figure 2.5: Picture of a volunteer wearing a nose clip breathing through the MFS measurement head via a mouthpiece and heat and moisture exchanger (HME) filter.

The MFS unit consists of the measurement head (discussed earlier), in which the participant breathes through, which is connected to an electronics module placed on a trolley. The electronics module is connected to a laptop to facilitate data transfer and viewing, both in real-time and post-protocol. The MFS unit is shown in figure 2.6. The exact configuration of the MFS relative to the subject will vary slightly depending on the space and, whether the subject is awake or sedated and mechanically ventilated.

During the process of MFS-based data collection, the respired gas fractions and cumulative volume uptake of each gas are visible on-screen with the software used to run the device. An example of this is shown in figure 2.7. The cumulative volume of N_2 is of specific interest for all CCP protocols, as a balance of $\geq |\pm 50|$ mL/minute during the

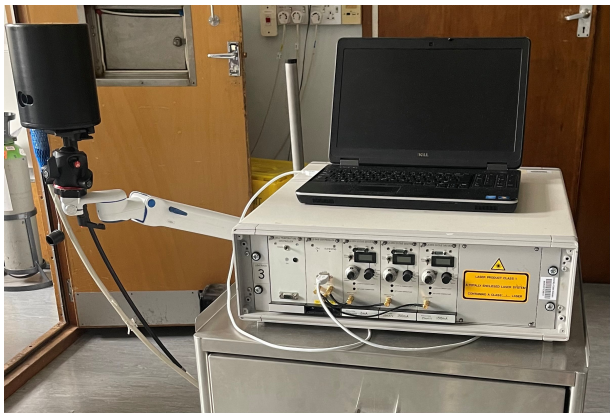

Figure 2.6: Picture of the MFS unit. The electronics module is placed on top of a trolley (partially visible in this picture). The laptop is connected via a USB cable to the electronics module. The MFS head is connected to the electronics module with an optical and power cable. The MFS head is secured with a movable arm, which is attached to the trolley.

phase when the subject is breathing in room air indicates a likely circuit leak.

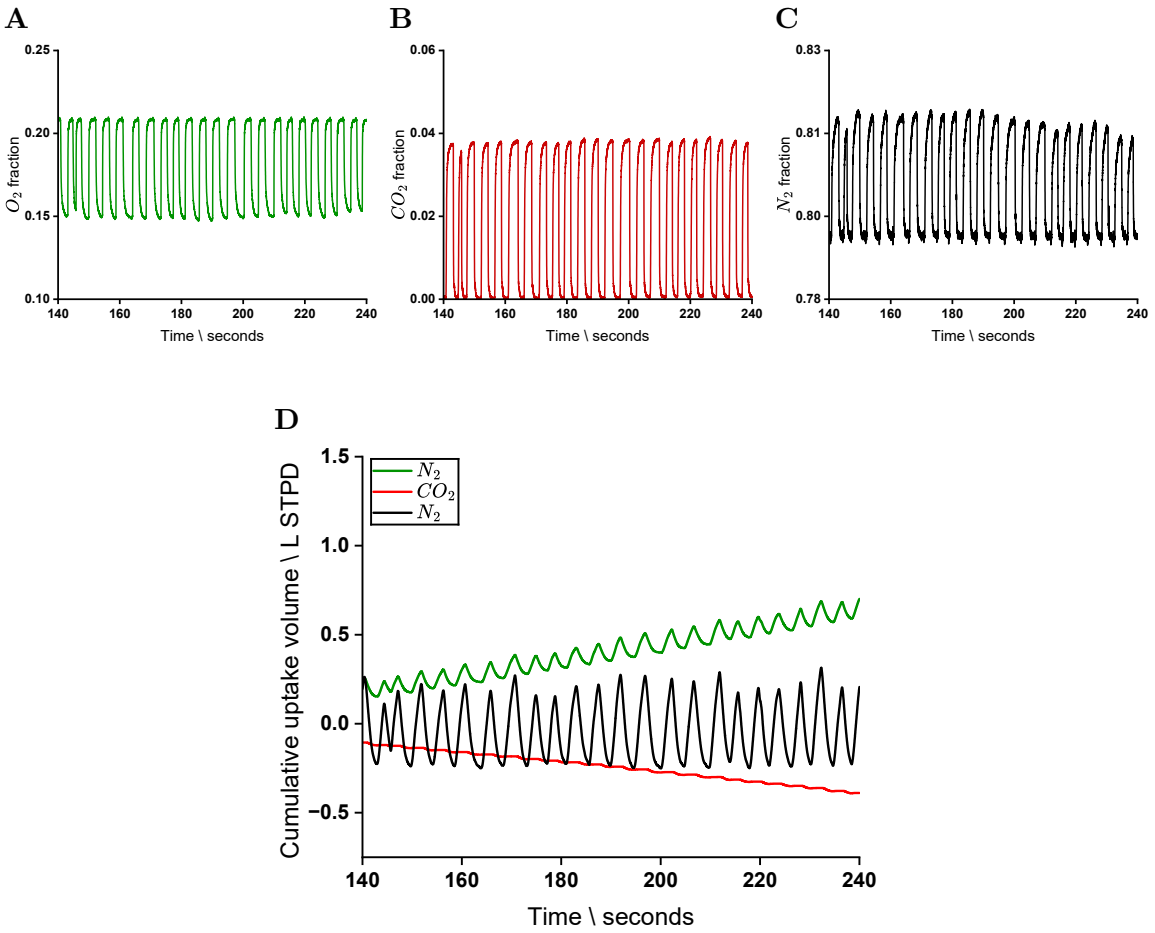

Figure 2.7: Panels A, B, and C show the respired gas fractions for O_2 (green), CO_2 (red), and N_2 (black), respectively. Panel D shows the same experimental dataset with the cumulative volumes over time for the same gases. The stable N_2 uptake, as seen in panel D, indicates a leak-free circuit during the experiment.

Prior to transferring the respired gas data from the MFS into the CCP model, a purpose-built graphical user interface (GUI) is used to process the data. This includes setting the

subject's age, sex, height, and weight. The apparatus dead space, which will differ for awake subjects compared to mechanically ventilated ones, and any available blood sample data is also entered at this time. The dataset itself is then examined using the GUI to determine the start and endpoint for modelling (useful if the subject does not immediately develop a steady breathing pattern on the device or if there is a leak at the end of the protocol) and to ensure the N_2 balance over the course of the experiment is sufficiently low, to rule out a circuit leak.

Depending on the objective of the protocol, the dataset will be processed (using the GUI) and modelled differently. The two main objectives of CCP modelling can be classified into deriving lung inhomogeneity and volume parameters and obtaining an estimate of cardiac output. If CH_4 and C_2H_2 are used as tracer gases, as in the pulmonary hypertension cohort discussed in chapter 3, then both objectives can be achieved within the same modelling run. CH_4, as a relatively insoluble gas, equilibrates with the lungs without being taken up in the pulmonary circulation and can be used to model lung inhomogeneity. C_2H_2 is comparatively soluble, and the uptake within the pulmonary circulation can be modelled to estimate cardiac output. For cases in which tracer gases are not used, but it is still necessary to model both inhomogeneity and cardiac output, such as in the cardiac surgery cohort discussed in chapter 5, it is currently necessary to split the dataset so that it can be modelled separately. Here, a full or partial N_2 washout is used for modelling lung inhomogeneity, and a ventilation-based adjustment of CO_2 is performed in order to monitor cardiac output. An example of a tracer gas wash-in and N_2 washout is shown in figure 2.8. The details related to the modelling and protocol of both the pulmonary hypertension and cardiac surgery cohorts have only been briefly summarised here, and are discussed in detail in their respective chapters.

2.4 Previous Applications of CCP

The applications of CCP to date have been primarily to estimate lung parameters and facilitate early detection of disease. As part of the development of the lognormal lung model,

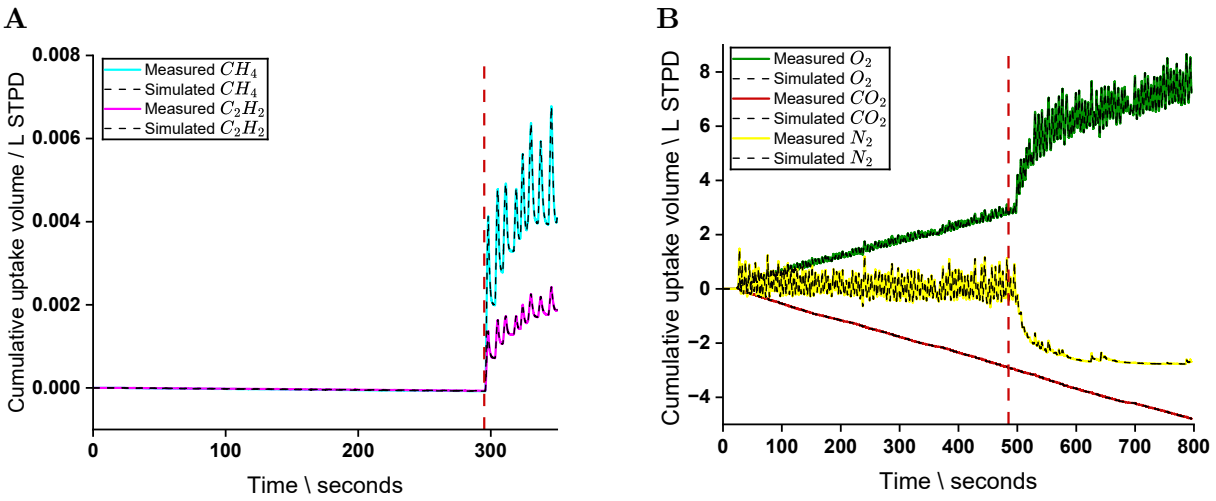

Figure 2.8: Examples of a tracer gas wash-in (panel A) and full N_2 washout (panel B). For both plots, the start of the wash-in/washout phase, preceded by the air-breathing phase, is indicated by the red, dashed line. The superimposed black, dashed lines represent the simulated uptake of the gases. In panel A, the measured uptake of CH_4 and C_2H_2 is seen by the cyan and magenta lines, respectively. CH_4 is seen to equilibrate between the reservoir bag and the lungs by the end of the rebreathing phase. This allows for an estimate of lung volume to be made. The progressive uptake of C_2H_2 is due to the gas' solubility in blood. An estimate of cardiac output can be made by measuring the rate of this uptake. In panel B, the measured uptake of O_2, CO_2, and N_2 is seen by the green, red, and black lines, respectively. The O_2 consumption can been seen to increase significantly from the start of the washout phase as pure O_2 is delivered to the participant. During the air-breathing phase, the N_2 slope is virtually flat as there is no uptake into the circulation. As the washout progresses, a production of N_2 is seen as it is displaced from the lungs for O_2. The volume of N_2 washed out can be used to calculate the lung volume. There is a consistent negative slope for CO_2, indicating a production, as it is unaffected by the N_2 washout.

Mountain et al. examined the reproducibility of the lung inhomogeneity parameters.(80) Three categories of participants were recruited: young and healthy, older and healthy, and those with mild-moderate chronic obstructive pulmonary disease (COPD). The fit parameter values recovered were highly repeatable between tests for participants, and varied with age and between healthy and COPD participants.

In participants with asthma, Smith et al. examined the CCP parameter, σC_L, and compared this with the percentage predicted forced expiratory volume over one second ($\text{FEV}_1\%_{\text{pred}}$) as a marker of disease severity.(87) Both σC_L and $\text{FEV}_1\%_{\text{pred}}$ were measured pre and post-bronchodilator administration. The values correlated to some extent, however, it was found that σC_L did not predict bronchodilator reversibility and could not be used interchangeably with $\text{FEV}_1\%_{\text{pred}}$. Subsequently, Alamoudi et al. examined a cohort of participants with severe asthma receiving biologic therapy, before and after therapy had commenced.(88) σC_L was found to be significantly reduced with bronchodilation and was

strongly correlated with a reduction in blood eosinophil count, a biomarker of asthma. It was also found that the cohort could be categorised based on the σC_L response following the commencement of biologics. Responders had improved symptoms, a lower $\text{FEV}_1\%_{\text{pred}}$, and were more likely to be in clinical remission a year after the baseline measurement.

Magor-Elliott et al. studied the impact of SARS-CoV-2 (COVID-19) infection on lung physiology in participants who had previously contracted the disease.(89) Participants were categorised based on the disease severity at the time of active infection: healthy controls, community-managed illness, admitted to a hospital ward, and admitted to an intensive care unit (ICU). A significant increase in anatomical dead space was seen in those who had been admitted to the ICU. The functional residual capacity was significantly lower, and σC_L significantly higher in participants who had been infected with COVID-19 compared to the healthy controls.

2.5 Conclusion

Computed cardiopulmonography combines a molecular flow sensor and computational model of the lungs and circulation system to characterise the cardiopulmonary physiology of an individual. The individual components and concepts related to the technology and modelling which make up CCP have been discussed in this chapter. The molecular flow sensing uses laser absorption spectroscopy and pneumotachography to generate in-airway concentration measurements and expired gas profiles of O_2, CO_2, H_2O, CH_4, and C_2H_2 every 10 ms. This data is then used within the CCP model to provide estimates of lung inhomogeneity, metabolism, and circulatory function, which are clinically useful. The lognormal lung, circulatory and body gas stores, and blood sub-models interact as one combined model to generate these estimates.

3 Pulmonary Hypertension Cohort Study

3.1 Introduction

This chapter presents the findings from a cohort of participants with pulmonary hypertension undergoing right heart catheterisation at the Hammersmith Hospital, London, UK. The central question to be answered within this study was whether cardiac output can be accurately estimated from respired gas analysis, and as such, builds on the previously published research of many others, as described in chapter 1. Described is the development of a technique which incorporates highly accurate and contemporaneous measurements of respired gas and uses these measurements to estimate cardiac output in a novel way.

In previous studies, such as those by Grollman and Chapman, cardiac output was estimated directly, such that it was the only parameter of interest which was solved for.(27; 30; 31) This limits the ability to allow for the many factors that influence the value, such as lung inhomogeneity and recirculation. An alternative approach is to solve the inverse problem. Here, there can be a more detailed model of lung inhomogeneity, recirculation, and cardiac output through an optimisation process involving estimates of parameters alongside cardiac output so as to predict the most likely value for cardiac output, allowing for these complex effects.

In the computed cardiopulmonography (CCP) protocol described in this chapter, an indirect estimate of cardiac output in the inverted manner described above is obtained through a comprehensive cardiopulmonary model and nonlinear optimisation, where several parameters relating to the lungs, circulation, and metabolism are fit. This approach has the advantage of incorporating the inhomogeneity of the lung, as well as recirculation of gases in a much more detailed and potentially accurate manner. Additionally, the potential influence of any previously unidentified dead space within the lung is also examined.

Smith et al. have previously shown that it is possible to generate reproducible estimates of

cardiac output using the MFS with an acetylene (C_2H_2) and methane (CH_4)-based tracer gas approach.(77) An open-circuit approach was taken, and cardiac output was calculated using a simple algorithmic approach. The study described in this chapter explores the feasibility of developing Smith et al.'s protocol by using a detailed modelling approach.

As discussed in chapter 1, the use of C_2H_2 as a tracer gas to estimate cardiac output is not new. C_2H_2 has the advantage of being predictably soluble in blood, not highly lipophilic, and safe for inhalation in the quantities required for analysis. CH_4 is relatively insoluble in blood and will therefore undergo equilibration between the gas source and lungs, in a manner dependent primarily on lung volume. With the highly accurate and contemporaneous measurements of the molecular flow sensor (MFS) and mass balance-based computational model, it is therefore possible to use C_2H_2 and CH_4 to estimate cardiac output and other relevant cardiopulmonary parameters. When C_2H_2 has equilibrated between the lungs and blood, the total pulmonary blood flow (equivalent to cardiac output in the absence of an intracardiac shunt) can be calculated. CH_4 is used for the purposes of estimating CCP lung model parameters and replaces the N_2 washout required in most CCP protocols, including the one discussed in this chapter.

3.1.1 Closed-circuit approach

Smith et al. argued for the benefits of an open-circuit experimental setup due to the issues of a closed/rebreathing-circuit potentially affecting cardiac output and the impracticality of most devices required for this approach. A rebreathing circuit with the MFS used to measure respired gases can feasibly be used to solve the latter problem, and is discussed later in this chapter. It is also true that for widespread clinical and research use, a small rebreathing bag which can be filled ahead of time would be more convenient than requiring cylinders filled with tracer gases in close proximity to the subject during the protocol.

The risk of affecting cardiac output due to the rebreathing can be mitigated by having a reservoir of sufficient volume, increasing the O_2 concentration within the reservoir to

reduce a chemoreceptor-triggered hyperventilatory response, and by keeping the rebreathing time sufficiently short.

3.1.2 Estimating cardiac output

Smith et al. used a simple algorithmic approach to estimate lung volume and cardiac output based on the early wash-in of tracer gases. Their method used data collected from the MFS, but did not use the CCP model. Instead, the tracer gas uptake was taken to be a function of equilibration of the gas in the lung and uptake into the lung tissue and blood. Several assumptions were made to circumvent the need for a comprehensive modelling approach, as discussed in section 2.1.2. The early wash-in data was specifically used to avoid recirculating gases, which was not accounted for within the algorithm. Additionally, the first two to three breaths were excluded to account for lung inhomogeneity causing imperfect gas mixing. For the study of the pulmonary hypertension cohort studied in this chapter, a full CCP protocol was used. In addition to being able to estimate all CCP parameters, using the full model has the advantage of accounting for lung inhomogeneity and recirculation.

3.1.3 Alveolar dead space

Alveolar dead space reduces the proportion of inhaled gas that participates in gas exchange with pulmonary capillary blood. The exact magnitude of alveolar dead space in healthy individuals is debated. One position holds that true alveolar dead space is negligible in the absence of respiratory disease, and that the main contribution arises from regions with high ventilation–perfusion ($\dot{V}/\dot{Q}$) ratios. Within the multiple inert gas elimination technique (MIGET), the logSDV parameter is used to quantify ventilation distribution, and values above 0.6 are considered abnormal. On this basis, Roca and Wagner estimated that V/Q mismatch contributes approximately 5% of tidal volume to alveolar dead space.(90)

However, other evidence indicates that total alveolar dead space may be substantially greater. Experimental and analytic studies suggest an end-tidal to arterial PCO_2 gradient

of 2.5 mmHg,(91) together with an alveolar to end-tidal gradient of 2 mmHg, giving an alveolar–arterial gradient of 4.5 mmHg.(92) This corresponds to a total alveolar dead space of 10%.(93) Recent data support this interpretation. Sandhu et al. reported a total alveolar dead space of 11.5% in convalescent COVID-19 subjects, of which only 5.5% could be attributed to $\dot{V}/\dot{Q}$ mismatch, the remainder likely reflecting other mechanisms.(94) Comparable findings have also been observed in recent studies.(95)

Standard compartmental models of gas exchange typically incorporate only the $\dot{V}/\dot{Q}$-related component of alveolar dead space. To test the potential importance of other sources, this chapter introduces an additional 6% alveolar dead space as a sensitivity analysis, in order to examine the effect on computed estimates of cardiac output and mixed venous oxygen saturation ($S_{\bar{v}}O_2$).

3.2 Methods

3.2.1 Experimental protocol

The ethics approval for this study was already in place as part of a broader set of studies which examine the use of CCP in both healthy volunteers and patients with respiratory disease. REC reference: 17/SC/0172. The experimental work was carried out in accordance with the general principles of the Declaration of Helsinki.

Participants were studied during their scheduled right heart catheterisation procedure. The aim was to have near-simultaneous direct Fick, thermodilution, and CCP cardiac output measurements for comparison. The preparation required prior to studying a participant involved multiple steps. Firstly, the MFS was switched on to allow warming to 36 °C to ensure a stable spectroscopic environment and minimise condensation on the mirrors; following this, the MFS was calibrated with pure O_2 and N_2, from calibration cylinders. Next, a 6 L anaesthetic reservoir bag was filled to approximately 75% of the participant's functional residual capacity (FRC). The FRC was obtained from lung function tests done as part of the clinical work-up for right heart catheterisation. If this was not available, the predicted FRC

was obtained using the Global Lung Initiative's (GLI) lung function calculator.(96) 75% of FRC was chosen as the reservoir volume to account for the participants' supine position during right heart catheterisation. FRC is known to decrease in the supine position.(97; 98)

The contents of the reservoir bag were 0.2% C_2H_2, 0.6% CH_4, 40% O_2, and balance N_2. A concentration of O_2 higher than room air was chosen to minimise the hyperventilatory chemoreceptor response caused by a progressively hypoxic and hypercapnic gas mixture due to rebreathing.(99) Once the reservoir bag was filled, it was connected to one port of a three-way tap. Of the remaining ports, one was connected to the non-participant end of the MFS, and the remaining one was open to air. The configuration of the MFS with the three-way tap and reservoir bag is shown in figure 3.1.

Figure 3.1: Picture of the reservoir bag attached, via a three-way tap, to the MFS head. The bag is attached to the opposite end of the participant end of the MFS head. The participant breathes through the MFS via a mouthpiece and heat and moisture exchanger (HME) filter. During the air-breathing phase, the three-way tap is open to the participant end and air; during the rebreathing phase, the tap is turned to allow the participant to respire into the bag.

With the participant lying supine, and after the pulmonary artery catheter (PAC) had been confirmed to be positioned within in the pulmonary artery, breathing through the MFS began. A nose clip was attached just prior to connection to ensure all respired gas flowed through the MFS. Once the participant had reached a steady state of breathing through the MFS (breathing through a mouthpiece and with a nose clip invariably alters the breathing), a mixed venous blood gas sample was taken. The blood gas sample was analysed using a point of care blood gas analyser (GEM Premier 5000, Instrumentation Laboratory, MA, USA). The steady state period lasted at least three minutes, during this time, the peripheral oxygen saturation as measured by a pulse oximeter (S_pO_2) was recorded. After the steady state phase, the three-way tap was turned so that the participant was rebreathing

into the reservoir bag. Where possible, the rebreathing phase, which lasted between 30 to 60 seconds, was synchronised with the bolus thermodilution measurements of cardiac output. After the rebreathing phase, the participant was disconnected from the MFS and MFS data collection was stopped. An example of an experimental dataset is shown in figure 3.2. It includes the measured and simulated (by CCP) uptakes of the tracer gases.

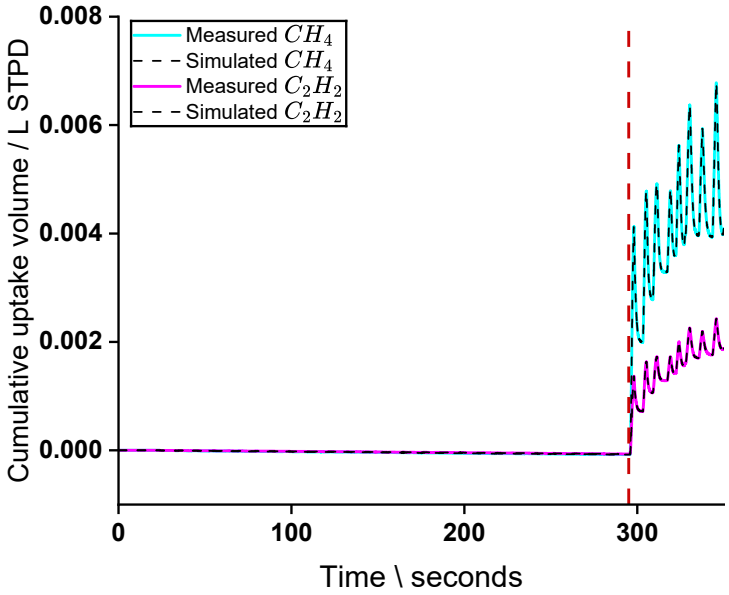

Figure 3.2: Example of a tracer gas rebreathing dataset. The start of the rebreathing phase, preceded by the air-breathing phase, is indicated by the red, dashed line. The measured uptake of CH_4 and C_2H_2 is seen by the cyan and magenta lines, respectively. The superimposed black, dashed lines represent the simulated uptake of the gases. CH_4 is seen to equilibrate between the reservoir bag and the lungs by the end of the rebreathing phase. This allows for an estimate of lung volume to be made. The progressive uptake of C_2H_2 is due to the gas' solubility in blood. An estimate of cardiac output can be made by measuring the rate of this uptake.

The direct Fick cardiac output was calculated using the mixed venous blood gas results, O_2 consumption ($\dot{V}O_2$) as measured with the MFS, and the S_pO_2 value recorded during the steady state phase. Further details pertaining to the direct Fick calculation are discussed in section 3.3.2. The respired gas data collected during the protocol from the MFS was processed through the CCP model using the University of Oxford Advanced Research Computing (ARC) cluster supercomputer.

When modelling the data, using an accurate solubility for C_2H_2 in blood and lung tissue was an important consideration as this would affect the cardiac output estimate. A range of solubility coefficients for C_2H_2 have been published in the literature. An Ostwald

(blood-gas partition) coefficient of 0.84 (equivalent to a Bunsen solubility coefficient of 0.74) was used in the CCP model. This value represented a reasonable midpoint in experimentally derived values at standard temperature and pressure.(100; 101)

3.2.2 Modelling

As the attempt to estimate cardiac output using a short, closed-circuit CCP protocol is novel, the results of the modelling were explored in detail. The CCP model utilises a nonlinear optimisation routine to fit parameters. Each time a dataset is run through the model, the fitting process is repeated four times from different, randomised starting points. Inconsistent results within the four repeated fits would indicate that a global minimum (a clear solution to the optimisation problem) has not been found, leading to unreliable values for individual fit parameters. Given the novelty of the protocol and the number of participants with significant respiratory disease (which affects modelling), a single run, with four outputs to compare, was not deemed sufficient to be confident of the estimated parameters. Instead, three different sets of optimisation parameters (specifically, tolerances) were used. All datasets were run three times each per set, giving 12 fits per set (as each run results in four different fits), and 36 fits in total. Details regarding the different sets of optimisation tolerances used, along with the conclusions gained from this analysis, are presented below.

A trust-region-reflective algorithm is used within the nonlinear least-squares solver. Using this algorithm, multiple tolerance types, namely, optimality, function, and step, can be set, which, if crossed, will stop the iterations of the solver. As such, they can be referred to as termination sensitivities. Optimality tolerance sets the first-order optimality measure, which describes how close a point x is to the optimal value based on the first derivative of the objective function, where x is the parameter value. Practically, the optimality tolerance helps to set the upper and lower bounds for fit parameters. Function tolerance sets the relative lower bound for the change in the objective function from one step to the next. If $|f(x_i) - f(x_{i+1})| <$ function tolerance $\times + |f(x_i|)$, where $f(x)$ is the objective

function of parameter x and i is the i^{th} iteration, then the solver stops. Step tolerance is also a relative lower bound that limits the size of a step in the parameter value, x. The iterations of the solver end when $|(x_i - x_{i+1}| <$ step tolerance $\times(1 + |x_i|)$.(102) A visual explanation of function and step tolerance is shown in figure 3.3.

The default values for the optimality, function, and step tolerances were 1×10^{-6}

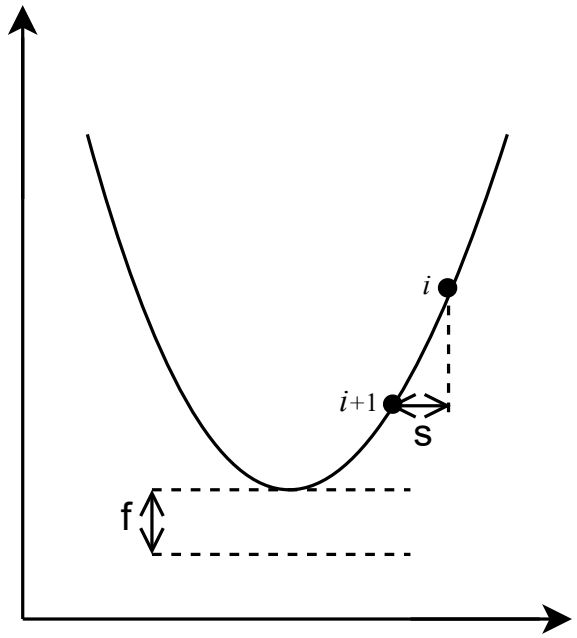

Figure 3.3: Visual depictions of function and step tolerance. If the next iteration of the objective function does not exceed the function tolerance, 'f', then the solver stops. A tighter function tolerance equates to a lower value for 'f'. If the difference between the $i{+}1^{th}$ and i^{th} iteration is less than the step tolerance, 's', then the solver will again stop. A tighter step tolerance equates to a lower value for 's'.

for previous CCP protocols. These tolerance values were used in addition to two progressively tighter sets of termination sensitivities, using tolerance values of 1×10^{-8} and 1×10^{-10}. The 36 fits (12 from each termination sensitivity) for each participant were examined primarily as a whole dataset. The results of this analysis are discussed in detail in section 3.3.3.

3.3 Results

3.3.1 Participants

47 participants were recruited to take part in the study, three participants were studied twice. 12 participants were excluded due to a high N_2 balance ($\geq \pm$ 50 mL), indicating a circuit leak. 38 datasets, including the three participants who were studied twice, were

used from 35 participants for the final analysis. Their baseline characteristics are shown in table 3.1. The repeat studies were treated as separate participants due to the time that had passed between measurements and changes in their physiology due to disease improvement or progression and/or pharmacological therapy. The cohort identification (ID) numbers for those studied twice were 3 and 27, 5 and 29, and 26 and 35.

Table 3.1: Per-person baseline characteristics of the pulmonary hypertension cohort

Cohort ID	Age / years	Sex	BMI / kg m^{-2}	PH class.	Cardiovascular disease	Respiratory disease	Smoking status	Smoking pack years	S_pO_2 / %	L-R shunt	WHO func. class.
1	31	Male	26	1	-	-	Never smoked	0	94	-	3
2	47	Male	33	4	Autoimmune myocarditis	PE	Ex-smoker	19	97	-	3
3	59	Female	26	1	-	Asthma	Ex-smoker	6	92	-	1
4	24	Male	17	1	Congenital heart disease	-	Never smoked	0	97	Yes	3
5	38	Female	24	1	-	-	Ex-smoker	5	98	-	2
6	62	Male	25	1	-	-	Never smoked	0	93	-	3
7	54	Female	36	2	-	-	Never smoked	0	99	-	3
8	42	Female	29	1	-	-	Never smoked	0	96	-	3
9	70	Male	27	4	-	PE	Ex-smoker	15	92	-	1
10	20	Female	20	1	Atrial septostomy	Restrictive lung disease	Never smoked	0	95	-	3
11	59	Female	32	0 (no PH)	-	-	Never smoked	0	98	-	2
12	55	Female	49	1	-	OSA	Never smoked	0	88	-	3
13	54	Male	29	1	Hypertension	-	Never smoked	0	99	-	1
14	78	Male	27	1	Hypertension		Ex-smoker	4	78	-	4
15	34	Female	21	1	ASD with L-R shunt	-	Never smoked	0	98	Yes	2
16	60	Male	26	4	-	PE, asthma, bronchiectasis	Never smoked	0	96	-	2
17	69	Female	27	2	IHD	Acute unilateral pleural effusion	Never smoked	0	99	-	2
18	51	Male	27	1	-	-	Current smoker	10	99	-	2
19	76	Male	29	4	SSS, IHD, hypertension	PE, COPD (non-smoker)	Never smoked	0	96	-	2
20	57	Female	41	1	ASD (L-R shunt)	Asthma	Never smoked	0	96	Yes	3
21	53	Female	36	4	Hypertension	PE	Never smoked	0	96	-	3
22	72	Male	25	4	IHD	PE, COPD	Ex-smoker	50	95	-	3
23	73	Male	31	1	IHD	-	Ex-smoker	35	91	-	3
24	66	Female	26	1	Hypertension	Asthma	Never smoked	0	95	-	3
25	87	Male	34	4	AF, hypertension, IHD	PE	Ex-smoker	30	94	-	3
26	55	Female	27	1	Hypertension	-	Ex-smoker	20	100	-	4
27	60	Female	26	1	-	Asthma	Ex-smoker	6	97	-	2
28	64	Female	25	3	Hypertension	COPD	Ex-smoker	15	94	-	3
29	38	Female	24	1	-	-	Ex-smoker	5	99	-	2
30	29	Female	29	1	Flow regulator*	-	Never smoked	0	82	-	3
31	48	Female	30	4	-	PE	Current smoker	12	98	-	3
32	67	Female	32	3	-	PE, ILD	Never smoked	0	97	-	2
33	22	Female	21	1	ASD	-	Never smoked	0	97	-	3
34	80	Male	27	1	AF	ILD	Never smoked	0	99	-	3
35	55	Female	26	1	Hypertension	-	Ex-smoker	20	99	Yes	4
36	41	Male	32	4	-	PE	Ex-smoker	2	92	-	3
37	38	Male	27	1	-	-	Never smoked	0	94	-	2
38	78	Male	22	4	-	PE	Ex-smoker	18	95	-	3

ID, identification number. BMI, body mass index. PH class., World Health Organisation pulmonary hypertension classification. S_pO_2, pulse oximeter measured peripheral oxygen saturation. L-R, left-to-right intracardiac shunt. WHO func. class., World Health Organisation functional classification. ASD, atrial septal defect. IHD, ischaemic heart disease. SSS, sick sinus syndrome. AF, atrial fibrillation. HIV, human immunodeficiency virus. PE, pulmonary embolism. OSA, obstructive sleep apnoea. COPD, chronic obstructive pulmonary disease. ILD, interstitial lung disease. *:In this participant's case, the flow regulator was implanted to offload pressure in the right heart.

3.3.2 Direct Fick cardiac output

The direct Fick cardiac output ($\dot{Q}_{DF}$) can be calculated if the consumption or production ($\dot{V}_x$) and arteriovenous difference ($c_a x - c_{\bar{v}} x$) of gas x is known:

$$\dot{Q}_{DF} = \frac{\dot{V}_x}{c_a x - c_{\bar{v}} x} \tag{3.1}$$

Given that the direct Fick cardiac output was considered the reference value with which the experimentally derived cardiac output was compared, it was necessary to ensure all components of the direct Fick calculation were as accurate as possible. This was especially true for the O_2 consumption ($\dot{V}O_2$), which was measured directly using the MFS.

All participants had a mixed venous blood gas taken at the time of MFS connection. This allowed for modelled estimation of a mixed venous O_2 content ($c_{\bar{v}}O_2$) value that was contemporaneous with MFS breath-by-breath data acquisition. For participant 3, a satisfactory mixed venous blood sample was not obtained. Arterial blood gases were taken when clinically indicated for some participants, but never during the time of MFS connection, given the likelihood of arterial puncture disturbing ventilation. Therefore, arterial O_2 saturation from pulse oximetry readings at the time of MFS connection were used to calculate arterial O_2 content. The following standard formula was applied:

$$c_a O_2 = \mathrm{Hb}_v \times 0.1 \times 1.39 \times (1 - \mathrm{COHb}_v - \mathrm{MetHb}_v) \times (S_p O_2/100) \tag{3.2}$$

Where Hb_v, $COHb_v$, and $MetHb_v$ are the haemoglobin in g/L, carboxyhaemoglobin fraction, and methaemoglobin fraction from the mixed venous blood gas sample respectively, 1.39 is Hufner's constant in mL O_2/ g Hb (103), and $\mathrm{S}_p O_2$ is the arterial O_2 saturation percentage from pulse oximetry.

An initial $\dot{V}O_2$ value was obtained from the air-breathing phase of the experiment. This value required correcting for potential fractional changes in O_2 due to changing lung stores.

The cumulative end-expiratory volumes were also regressed to account for the change in lung stores (figure 3.4).

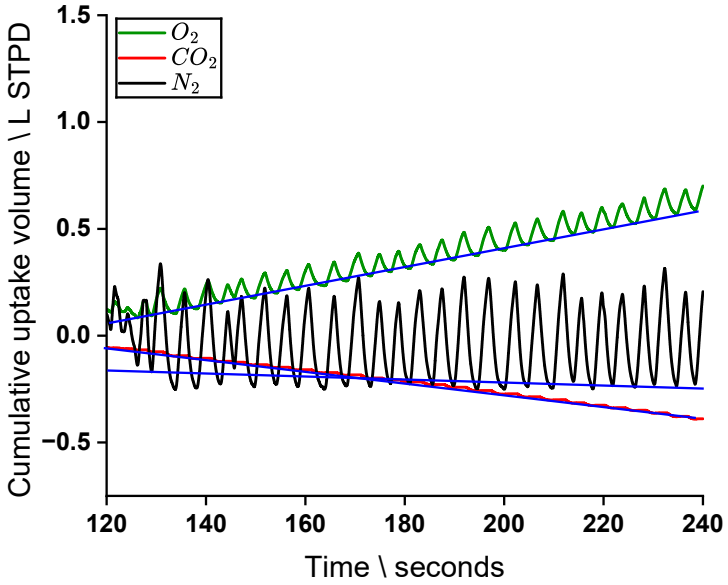

Figure 3.4: An example of a section of an experimental dataset, which shows the regression line (blue) applied to the end-expiratory uptake volumes. O_2 is in green, N_2 is in black, and CO_2 is in red (partially visible due to the superimposed regression line).

The corrected $\dot{V}O_2$ ($\dot{V}O_{2_c}$) in mL/minute was calculated in the following way:

$$\dot{V}O_{2_c} = \dot{V}O_2 - 1000(\text{FRC} \times \dot{F}O_2) \tag{3.3}$$

Where FRC is the functional residual capacity in L STPD and $\dot{F}O_2$ is the fractional end-tidal change in O_2 over the air-breathing phase per minute.

The corrections applied to the $\dot{V}O_2$ measurements did not significantly alter the data (figure 3.5). All subsequent analysis and discussion in this and later chapters use the corrected $\dot{V}O_2$, $\dot{V}O_{2_c}$ values unless otherwise stated.

A full list of values used for the direct Fick calculation, including the final direct Fick cardiac output, is shown in table 3.2. The direct Fick value for participant 3 was not calculated due to the spurious mixed venous blood sample that was collected.

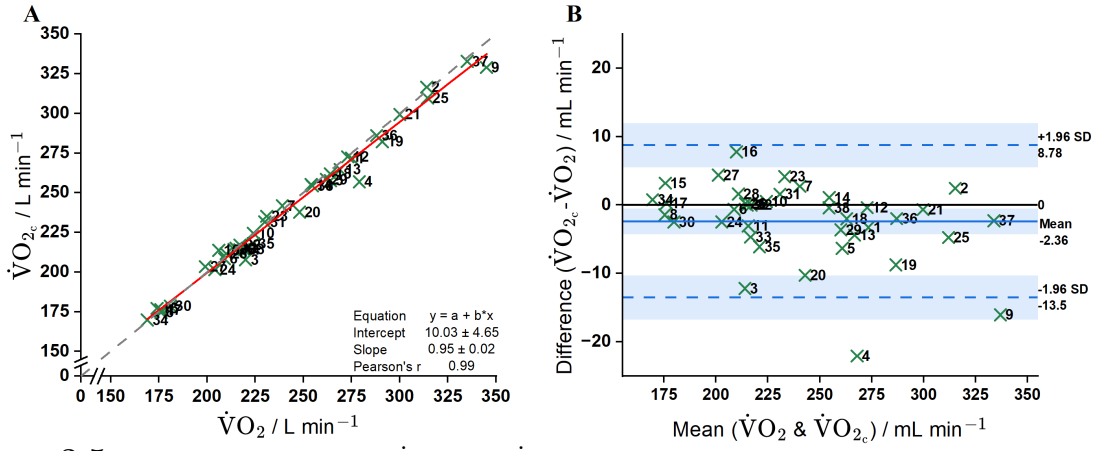

Figure 3.5: Comparison between $\dot{V}O_2$ and $\dot{V}O_{2_c}$. In panel A, the solid red line is the result of a linear fit between the two values. The equation for this line is shown along with the confidence intervals for the intercept and slope, and Pearson correlation coefficient (r). Panel B shows a Bland-Altman plot with the difference between uncorrected and corrected VO_2 measurements against the mean of the two measurements; the mean and limits of agreement are shown with confidence intervals. Numbers next to the datapoints represent the cohort ID numbers.

Table 3.2: Values used for the calculation of the direct Fick cardiac output

Cohort ID	$\dot{V}O_2$ / mL min^{-1}	$\dot{V}N_2$ / mL min^{-1}	$\dot{F}O_2$ / min^{-1}	FRC / L BTPS	$\dot{V}O_{2_c}$ / mL min^{-1}	S_pO_2 / %	$S_{\bar{v}}O_2$ / %	Hb / g L^{-1}	COHb / %	MetHb / %	$\dot{Q}_{\mathrm{DF}}$ / L min^{-1}
1	275	-12	0.003	1.4	272	94	74	155	1	0.6	6.4
2	314	33	-0.001	2.3	316	97	68	119	1.9	0.4	6.8
3†	220	4	0.005	3.2	208	92	-	136	1.9	0.3	-
4*	279	-28	0.008	3.5	257	97	90	175	1.1	0.3	-
5	264	0	0.003	3.0	258	98	64	128	0.9	0.8	4.3
6	209	-40	0.000	3.8	208	93	60	159	1.1	0.6	2.9
7	239	-27	-0.003	1.2	242	99	69	142	1.1	0.7	4.2
8	176	-6	0.002	1.1	175	96	68	133	1	0.6	3.4
9	345	3	0.003	7.5	329	92	69	123	1.1	1.2	8.5
10	224	-36	-0.001	1.2	225	95	70	143	1	0.6	4.7
11	217	21	0.002	1.9	214	98	77	120	1.6	0.7	6.4
12	273	-28	0.000	1.2	273	88	64	143	1.2	0.7	5.9
13	269	-14	0.002	2.9	265	99	77	160	1.1	0.5	5.6
14	254	-75	-0.001	2.6	255	78	43	118	1.5	0.6	4.5
15*	174	-33	-0.002	1.8	177	98	73	117	0.9	0.7	4.3
16	206	-32	-0.002	5.5	214	96	71	148	1.3	0.5	4.3
17	176	-15	0.000	1.0	176	99	68	112	1.5	0.7	3.7
18	264	-27	0.001	2.1	262	99	69	131	3.7	0.8	5.0
19	291	-35	0.003	3.4	282	96	69	149	1.3	0.5	5.1
20	248	-29	0.003	4.0	238	96	79	116	1.4	0.8	8.8
21	300	-2	0.000	2.0	299	96	75	138	1.3	0.5	7.7
22	217	-45	0.000	4.5	217	95	59	140	1.5	0.6	3.2
23	231	-24	-0.002	2.5	235	91	58	149	1.5	0.7	3.5
24	204	-40	0.002	2.0	202	95	70	121	1.2	0.8	4.9
25	314	-32	0.003	2.1	310	94	68	135	1.3	0.7	6.6
26	214	-19	0.000	2.2	214	100	77	135	1.2	0.7	5.0
27	199	-36	-0.002	3.0	203	97	75	140	2.3	0.5	4.9
28	210	3	-0.001	3.9	212	94	70	152	1.6	0.6	4.3
29	262	-22	0.002	2.5	258	99	68	131	1.1	0.6	4.7
30	181	-36	0.002	1.4	179	82	46	200	1.3	0.5	1.8
31	230	-5	-0.001	2.4	232	98	69	131	1.7	0.6	4.6
32	215	-7	0.000	1.6	215	97	75	138	1.3	0.5	5.3
33	219	-17	0.003	2.3	214	97	70	143	1.1	0.7	4.1
34	169	-15	0.000	3.1	170	99	52	88	1.5	0.8	3.0
35*	224	-9	0.004	2.0	218	99	83	117	1	0.7	8.6
36	288	-62	0.001	1.9	286	92	59	148	0.9	0.6	4.3
37	335	-50	0.001	2.1	333	94	38	167	0.9	0.6	2.6
38	255	-47	0.000	4.9	254	95	65	150	1.3	0.5	4.1
Mean	242±46	-22±21	0 ±0.002	2.2 ±1.1	239 ±44	95 ±5	68 ±11	138 ±20	1.4 ±0.5	0.6 ±0.2	6.3 ±8.6

Mean ± standard deviation. $\dot{V}O_2$, O_2 consumption. $\dot{V}N_2$, N_2 consumption. $\dot{F}O_2$, fractional O_2 change. FRC, functional residual capacity. $\dot{V}O_{2_c}$, O_2 consumption corrected for $\dot{F}O_2$. S_pO_2, pulse oximeter measured peripheral O_2 saturation. $S_{\bar{v}}O_2$, mixed venous O_2 saturation. The mixed venous blood gas sample measurement was used for $S_{\bar{v}}O_2$, Hb, COHb, and MetHb. Hb, haemoglobin. COHb, carboxyhaemoglobin. MetHb, methemoglobin. $\dot{Q}_{\mathrm{DF}}$, direct Fick cardiac output. †: No valid mixed venous blood gas sample available. *: Left-to-right intracardiac shunt.

Estimation of error in the direct Fick measurement

The calculation of the direct Fick cardiac output, including the process for correcting $\dot{V}O_2$ was discussed in section 3.3.2. With all components of the direct Fick equation, shown below, a degree of variance will be present and contribute to an overall variance for the direct Fick cardiac output.

$$\dot{Q}_{DF} = \frac{\dot{V}O_2}{k \times \mathrm{Hb}_v \times (S_pO_2 - S_{\bar{v}}O_2)} \tag{3.4}$$

Where $k = 0.1 \times 1.39 \times (1 - \text{COHb}_v - \text{MetHb}_v)$ and S_pO_2 and $S_{\bar{v}}O_2$ are given as fractional terms.

If the standard deviations of these components are known, an overall variance can be calculated by using a variance propagation equation. The variance propagation equation for the direct Fick cardiac output can be given as:

$$\begin{aligned}\text{Var}(\dot{Q}) = \left(\frac{1}{\text{Diff}_{AV}}\right)^2 \text{Var}(\dot{V}_{O_2}) + \left(\frac{\partial \dot{Q}}{\partial \text{Hb}_v}\right)^2 \text{Var}(\text{Hb}_v) + \\ + \left(\frac{\partial \dot{Q}}{\partial S_pO_2}\right)^2 \text{Var}(S_pO_2) + \left(\frac{\partial \dot{Q}}{\partial S_{\bar{v}}O_2}\right)^2 \text{Var}(S_{\bar{v}}O_2)\end{aligned} \tag{3.5}$$

Where Diff_{AV} is the arteriovenous difference, given as: $k \times \text{Hb}_v \times (S_pO_2 - S_{\bar{v}}O_2)$, in mL/L.

The standard deviations used to calculate the variances of the Hb_v and $S_{\bar{v}}O_2$ were taken from values reported in the literature for the GEM Premier 5000 blood gas analyser.(104). These values were 0.3 g/L for Hb_v and 0.01% for $S_{\bar{v}}O_2$. An error of approximately ±2% has been reported for pulse oximetry.(105) This was used to calculate a standard deviation of approximately 1%. The standard deviation of $\dot{V}O_2$ was considered to be roughly proportional to the N_2 balance. As the N_2 balance reflects the total change of the dataset during the airbreathing period, this was divided by four to obtain an approximate standard deviation for $\dot{V}O_2$. The effects of COHb_v and MetHb_v on the overall cardiac output variance were considered sufficiently small that their variances were not included in the equation. The partial derivatives for the individual components given in equation 5.13 are as follows:

$$\frac{\partial \dot{Q}_{\text{DF}}}{\partial \dot{V}O_2} = \frac{1}{\text{Diff}_{AV}} \tag{3.6}$$

$$\frac{\partial \dot{Q}_{\text{DF}}}{\partial \text{Hb}_v} = -\frac{\dot{V}_{O_2}}{(\text{Diff}_{AV})^2} \times k \times (S_pO_2 - S_{\bar{v}}O_2) \tag{3.7}$$

$$\frac{\partial \dot{Q}_{\text{DF}}}{\partial S_pO_2} = -\frac{\dot{V}O_2}{(\text{Diff}_{AV})^2} \times k \times \text{Hb}_v \tag{3.8}$$

$$\frac{\partial \dot{Q}_{\text{DF}}}{\partial S_{\bar{v}}O_2} = -\frac{\partial \dot{Q}_{\text{DF}}}{\partial S_pO_2} \tag{3.9}$$

The calculated standard deviations for the direct Fick cardiac outputs for all participants are given in table 3.3. Overall, these calculations suggest that a standard deviation of approximately 6% applies to cardiac output measurements made by the gold standard direct Fick approach.

Table 3.3: Direct Fick cardiac output and variance values for all participants

Cohort ID	$\dot{Q}_{\mathrm{DF}}$ / L min^{-1}	SD / %
1	6.4	5.1
2	6.8	4.3
3†	-	-
4*	-	-
5	4.3	2.9
6	2.9	5.7
7	4.2	3.4
8	3.4	3.7
9	8.5	4.3
10	4.7	5.7
11	6.4	5.4
12	5.9	4.9
13	5.6	4.8
14	4.5	7.9
15*	4.3	6.1
16	4.3	5.5
17	3.7	3.9
18	5.0	4.2
19	5.1	4.8
20	8.8	6.6
21	7.7	4.8
22	3.2	5.9
23	3.5	3.9
24	4.9	6.4
25	6.6	4.7
26	5.0	4.8
27	4.9	6.4
28	4.3	4.2
29	4.7	3.9
30	1.8	5.7
31	4.6	3.5
32	5.3	4.7
33	4.1	4.2
34	3.0	3.1
35*	8.6	6.4
36	4.3	6.2
37	4.1	5.7
38	2.6	4.2
Mean	6.3± 8.6	6.2± 7.9

Mean ± standard deviation. SD, standard deviation. †: No valid mixed venous blood gas sample available. *: Left-to-right intracardiac shunt.

3.3.3 Modelling

As discussed earlier in this chapter, three different sets of termination sensitivities were used to fit the CCP parameters for each participant. This process resulted in 36 total

fits per participant (three termination sensitivities, each run three times, with each run yielding four fits from different, randomised starting points). To assess the reliability of the fitting routine for each participants modelled data, two parameters in particular were identified as particularly instructive. Firstly, the sum of squared residuals (referred to as the residual from here on) for each fit was compared and the coefficient of variation (CV) calculated. A high CV would indicate an inability for the solver to converge on a single best solution, using the data available. Similarly, and for the same reason, the cardiac output scaling (to modelled metabolic rate, height, weight, and sex; mean = 1) coefficient of variation (referred to as $\dot{Q}$ CV from here on) was examined in this way.

Figure 3.6 compares the CVs for residuals and cardiac output for the different termination sensitivities. A Friedman test, a non-parametric statistical test to compare three or more paired groups, was used to confirm that there were no differences between the termination sensitivities for residual ($\chi^2(2)$=1.041, p=0.594) and $\dot{Q}$ ($\chi^2(2)$=1.421, p=0.491) CVs.

Given the lack of significant difference between the different sets of termination sensitivities, the results were combined into one dataset of 36 fits per participant (figure 3.8). From analysis of this dataset, it was clear that for some participants, the $\dot{Q}$ CV was larger than would be expected for a single minimum value. It was also apparent that there was far more variability in $\dot{Q}$ scaling values than expected with any of the tolerance settings used. This can be explained using the analogy of a footprint in sand. An overall minimum (for cardiac output in this case) exists and is the footprint. If the footprint is magnified, gaps are seen between the grains of sand; the magnification is analogous to the tolerance settings, where even at the lowest sensitivity (1×10^{-6} in this case), a level of detail which is not physiologically and/or clinically useful is captured; a further illustration of this is shown in figure 3.7.

Prior to calculating the final $\dot{Q}$ CV, a single outlier deletion was permitted if there was a standardised value which was greater than (or less than if negative) or equal to $\pm$ 2.5, to account for fitting aberrations. Subsequent to this process, 10 participants were

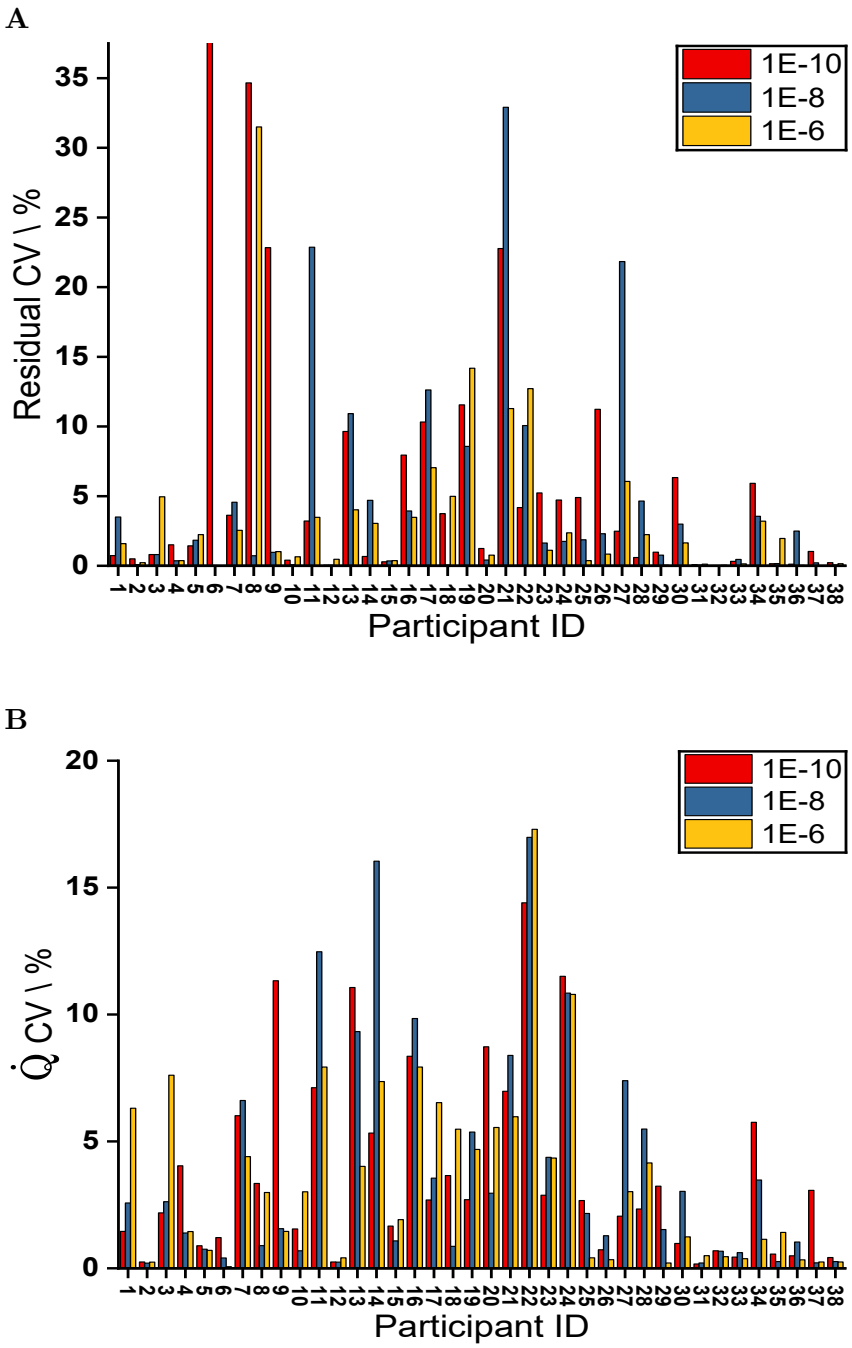

Figure 3.6: Comparison of CVs for the three termination sensitivities for residuals and cardiac output ($\dot{Q}$). Panel A shows the residual CVs against the individual participant datasets. The termination sensitivities are shown from most sensitive to least. Panel B shows the $\dot{Q}$ CVs in an identical format. In panel A, the 1×10^{-10} (red) column for participant 6 is cut off at the y-axis; the CV was 45%. In both panels, any columns not visible are due to scale, and indicate a CV of close to 0.

flagged as exceeding the cutoff value, which was set to be a $\dot{Q}$ CV of 5% (panel B in figure 3.8). Participants who were at or above this cutoff value were flagged as having an unreliable modelled cardiac output. One of these participants, 20, had previously been flagged due to having a left-to-right cardiac shunt.

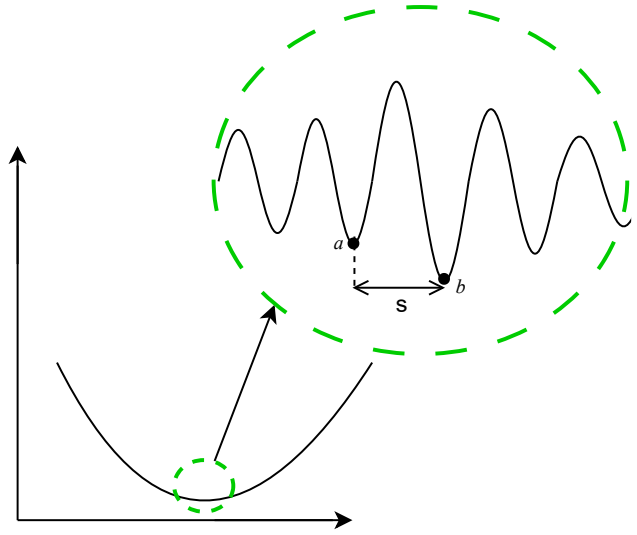

Figure 3.7: Visual depiction of the process of finding a global minimum value. The base of the function, where the global minimum exists, is seen in the green circle with the dashed circumferential line and is magnified. There is a local minimum at 'a' and a global minimum at 'b'. The step tolerance, at any termination sensitivity setting, is smaller than 's', which is the distance between 'a' and 'b'. This indicates that the variability between possible values of cardiac output is of a greater magnitude and, therefore, not necessarily affected by different termination sensitivities.

As discussed in section 3.3.1, the heterogeneity of the cohort's cardiorespiratory physiological characteristics warranted the partitioning into subgroups for analysis in addition to analysing the cohort as a whole. Firstly, it was necessary to acknowledge that the participants who had been flagged due to having a left-to-right intracardiac shunt should be considered separately. With CCP, the cardiac output is estimated by measuring the uptake of tracer gases by the pulmonary circulation via the lung. This means that a left-to-right shunt is not ordinarily accounted for as the shunt is bypassed, unlike for the direct Fick measurement, where the arteriovenous content difference of the measured gas will narrow correspondingly to the magnitude of the shunt. Secondly, in terms of subgroups, the cohort was divided into two based on the S_pO_2 during the air-breathing phase of the experiment; these groups were S_pO_2 <95% and $S_pO_2 \geq 95\%$. Participants flagged due to a $\dot{Q}$ CV of $\geq 5\%$ are highlighted in any results they are included in in this section. Finally, participant 3, who did not have a reliable mixed venous blood sample, was excluded from the analysis. Other possible reasons for the variability in $\dot{Q}$ CV between participants, such as smoking status and pulmonary hypertension diagnosis and classification, were considered; however, no patterns were readily apparent.

Individuals with a higher S_pO_2 are unlikely to have clinically significant impairments to gas exchange, which would then potentially affect respiratory measurements of cardiac output. For those with S_pO_2 values of less than <95%, a pure shunt would dissociate the

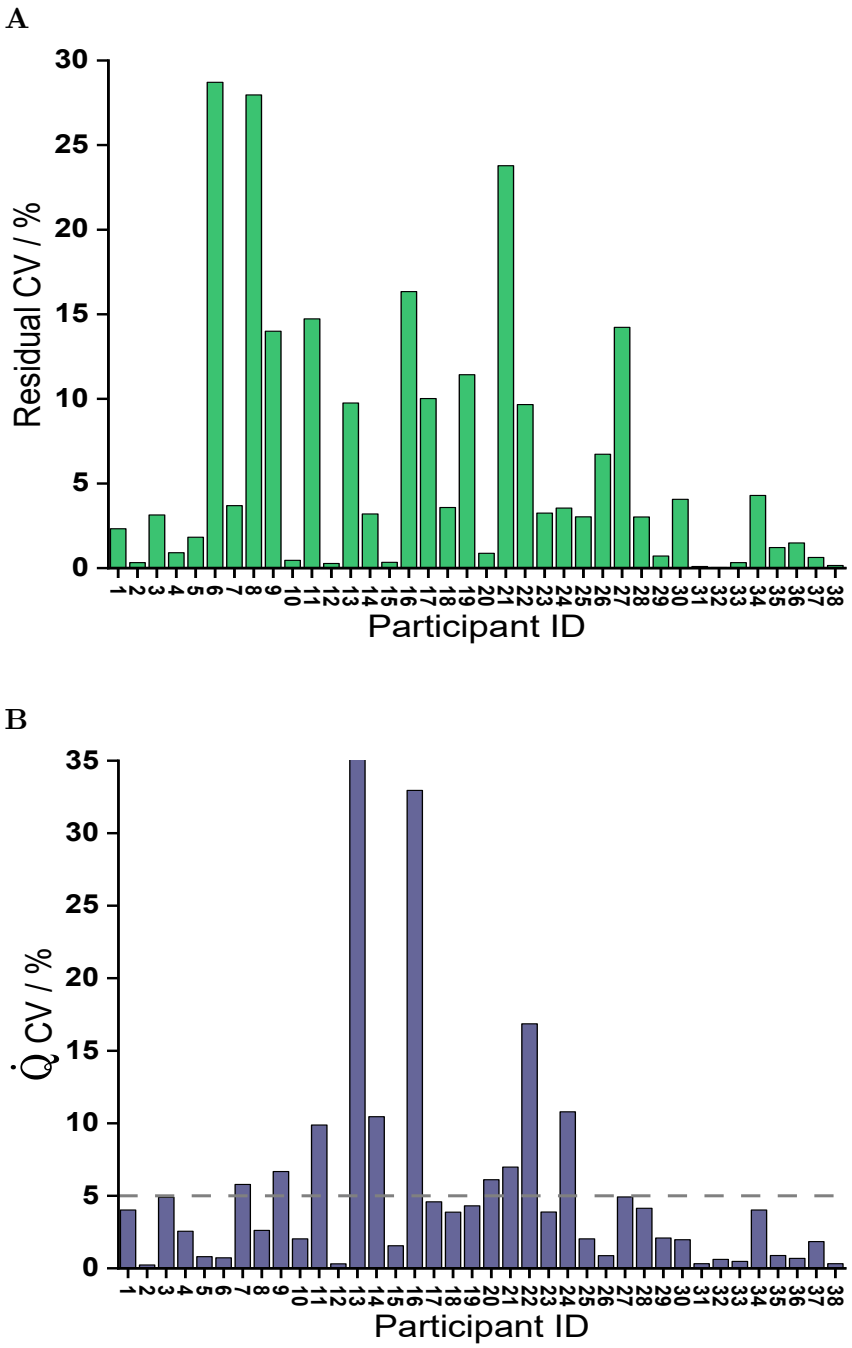

Figure 3.8: The residual (panel A) and $\dot{Q}$ (panel B) CVs for the combined termination sensitivity datasets for each participant. Some datasets had one outlying fit deleted if the standardised value for $\dot{Q}$ scaling was greater than or equal to $|\pm 2.5|$. In panel B, the dashed grey line indicates the 5% cutoff value at which the fit was deemed unreliable.

values for the direct Fick from the indirect Fick. For the direct Fick, the shunt narrows the arteriovenous O_2 differences, and this is included in the cardiac output measurement. For the indirect Fick, the CCP estimate in this case, the C_2H_2 is not included in the shunt. Therefore, this may be a reason to exclude participants with low S_pO_2, as done for participants with a left-to-right intracardiac shunt. However, true right-to-left shunting is

rare, and these participants were included in the analysis as they may still have yielded useful data for the direct and indirect Fick comparison.

Another reason for dividing participants based on S_pO_2 measurements was that hypoxia is a major driver of diffusion limitation in alveolar gas exchange in a similar way to the effects of high altitude.(106; 107) The CCP model does not account for diffusion limitation in this way. Further to this, hypoxic individuals are more likely to have their respiratory physiology represented by a multimodal $\dot{V}/\dot{Q}$ distribution. When used for respiratory disease, CCP is primarily intended as an early detection modality. The CCP model uses a unimodal distribution for $\dot{V}/\dot{Q}$ and may not be able to accurately fit lung inhomogeneity and volume parameters in patients with moderate to severe lung disease who are more likely to have a multimodal $\dot{V}/\dot{Q}$ distribution.

The CCP-estimated parameters are presented in table 3.4. Out of the combined termination sensitivity dataset of 36 fits per participant, the fit with the median $\dot{Q}$ was chosen as the reference set of parameters for each participant. All results presented, including in table 3.4 were from this reference parameter set.

Table 3.4: Fit parameter values from the CCP model for all participants

Cohort ID	V_A / L BTPS	V_D / L BTPS	C_{V_D}	σV_D	σC_L	P_iCO_2 / kPa	$\dot{V}O_2$ / mL min^{-1}	RQ	$\dot{Q}$ / L min^{-1}	$S_{\bar{v}}O_2$ / %
1	1.28	0.09	0.52	0.36	0.79	3.85	279	0.70	6.0	77
2	1.99	0.18	0.62	0.40	0.81	4.61	317	0.89	5.5	64
3	2.90	0.18	0.00	0.71	1.30	4.89	190	0.82	5.2	77
4	3.36	0.15	0.00	0.53	0.69	2.69	270	0.70	3.9	71
5	3.02	0.10	1.00	0.46	1.05	3.89	242	0.81	4.3	67
6	3.63	0.17	0.74	0.44	0.84	3.38	218	0.79	3.9	74
7	1.16	0.09	0.57	0.22	0.81	4.02	251	1.00	4.4	71
8	1.01	0.06	0.60	0.32	0.87	3.93	169	0.71	2.5	62
9	7.44	0.47	0.00	0.71	1.33	3.27	285	0.92	10.4	83
10	1.15	0.10	1.00	0.41	0.79	4.63	232	0.92	3.5	66
11	1.61	0.28	0.08	0.49	0.85	4.84	201	0.96	7.9	83
12	1.09	0.08	0.49	0.36	0.83	3.75	275	0.80	3.7	62
13	2.57	0.14	0.48	0.33	0.96	3.19	273	0.87	2.9	57
14	2.48	0.17	0.54	0.24	0.94	4.05	262	0.72	4.3	61
15	1.68	0.08	0.98	0.38	0.72	4.06	187	0.83	4.1	71
16	4.30	0.22	0.00	0.53	1.15	5.29	246	0.86	3.9	64
17	0.95	0.10	0.00	0.57	1.05	4.60	177	0.86	3.0	60
18	1.88	0.18	0.00	0.54	0.92	4.43	265	0.92	5.3	71
19	3.36	0.13	0.72	0.38	1.05	4.25	268	0.86	4.1	65
20	3.80	0.13	0.40	0.71	0.93	6.17	278	0.78	8.0	73
21	1.99	0.14	0.31	0.34	0.84	4.93	298	1.00	5.2	69
22	4.00	0.27	0.79	0.53	0.98	3.58	213	0.90	2.6	55
23	2.44	0.13	0.59	0.37	0.90	3.89	249	0.93	3.0	59
24	1.94	0.14	0.78	0.58	0.84	3.63	204	0.92	2.6	52
25	1.90	0.14	0.36	0.28	0.68	3.95	314	0.77	5.4	68
26	2.13	0.10	0.57	0.35	0.97	4.15	218	0.83	4.1	70
27	2.72	0.18	0.00	0.66	1.31	4.71	204	0.86	5.3	77
28	3.68	0.23	0.36	0.63	1.45	5.43	212	0.88	4.4	71
29	2.38	0.08	0.80	0.58	0.89	4.05	255	0.72	4.0	63
30	1.29	0.08	0.20	0.52	0.82	2.96	186	0.84	1.4	51
31	2.29	0.10	0.02	0.65	1.16	4.75	231	0.76	4.5	68
32	1.51	0.10	0.99	0.63	1.01	5.10	221	0.94	5.3	76
33	2.15	0.09	1.00	0.54	0.73	4.67	213	0.73	3.5	67
34	2.50	0.40	0.11	0.54	1.27	4.01	154	0.94	3.9	65
35	1.88	0.10	0.40	0.41	0.88	4.59	210	0.77	5.8	76
36	1.76	0.09	0.46	0.46	0.90	3.31	288	0.83	3.0	52
37	1.99	0.11	0.46	0.50	0.77	2.87	353	0.79	2.3	32
38	4.61	0.37	0.43	0.47	1.30	2.66	244	0.99	3.5	66

V_A, alveolar volume. V_D, dead space volume at functional residual capacity. C_{V_D}, fractional expansion of dead space relative to the fractional expansion of the alveolar space. σV_D, standard deviation of the standardised dead space. σC_L, standard deviation for the natural logarithm of the standardised lung vascular compliance. P_iCO_2, ideal partial pressure of CO_2. RQ, respiratory quotient. σCd, standard deviation for the natural logarithm of the standardised lung vascular conductance, is not shown in this table, but is equal to σC_L+0.3.

The results for cardiac output and $S_{\bar{v}}O_2$ for all participants (including those flagged) are shown in figure 3.9. The comparison between the CCP estimated and direct Fick cardiac output is shown in panels A and B, whilst the comparison between the CCP estimated and mixed venous blood sample $S_{\bar{v}}O_2$ is shown in panels C and D. CCP estimates for both cardiac output and $S_{\bar{v}}O_2$ strongly correlate with the invasive reference values. The cardiac output estimates are biased towards underestimating cardiac output, this becomes more pronounced at higher flow states. Notably, most outliers nearing or exceeding the limits of agreement were participants flagged due to a high $\dot{Q}$ CV. For $S_{\bar{v}}O_2$, there is less overall bias, however the limits of agreement were broad, indicating a lack of agreement between methods.

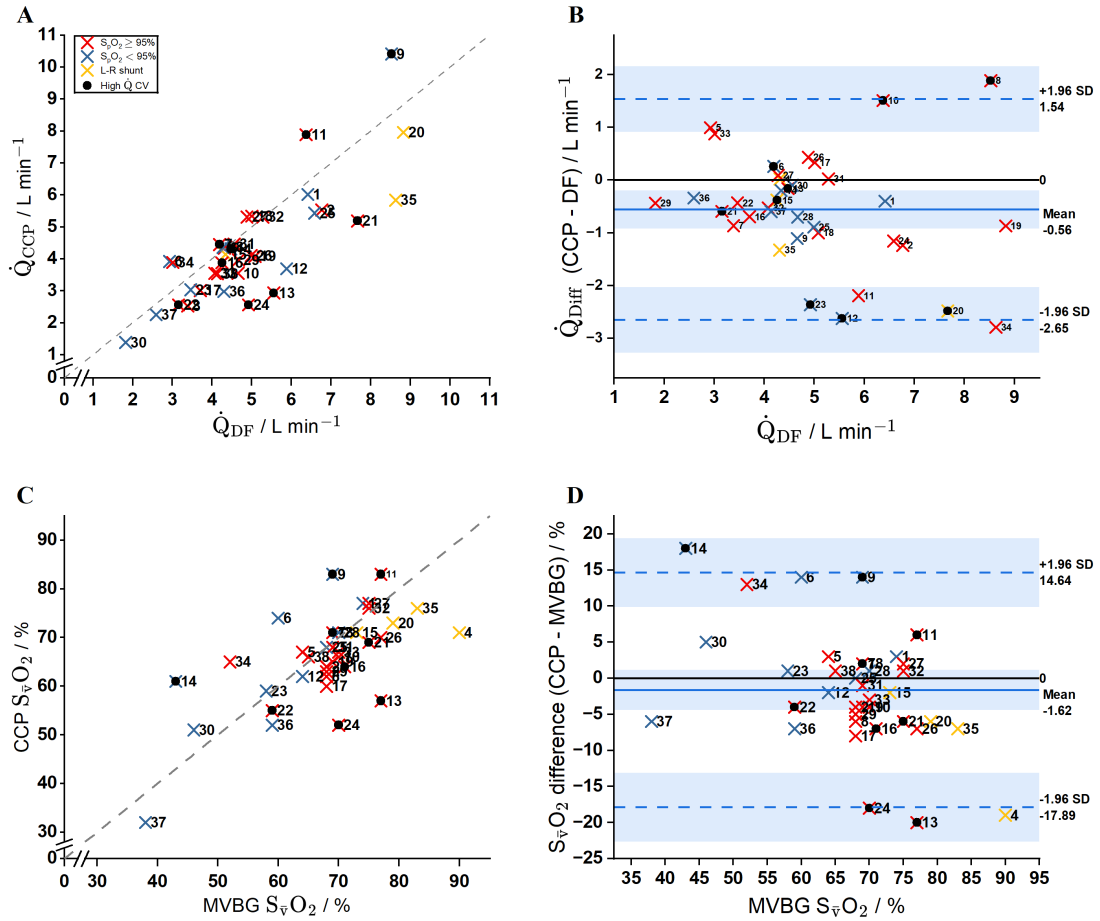

Figure 3.9: Comparison between computed cardiopulmonography (CCP) estimates of cardiac output and $S_{\bar{v}}O_2$ against the direct Fick (DF) and mixed venous (MVBG) measurements, respectively. Panels A and B compare cardiac output values. Panel A shows the correlation between the direct Fick cardiac output and the CCP estimate. Panel B shows the CCP and direct Fick cardiac output values against the reference direct Fick value. $\dot{Q}_{\text{diff}}$ is the difference between values. The mean and limits of agreement for the difference in values is shown with confidence intervals. Panels C and D show similar comparisons for $S_{\bar{v}}O_2$, using the MVBG $S_{\bar{v}}O_2$ as the reference. In panels A and C, the dashed grey line is the line of identity.

3.3.4 S_pO_2-based subgroup analysis

For the analysis of participants based on the measured S_pO_2, those flagged due to a high $\dot{Q}$ CV or left-to-right intracardiac shunt were not included.

$S_pO_2 \geq 95\%$ subgroup

The results for cardiac output and $S_{\bar{v}}O_2$ for participants with an $S_pO_2 \geq 95\%$ are shown in figure 3.10. For cardiac output, there was a strong correlation between the direct Fick and CCP values. A significant bias towards underestimating cardiac output is still seen, however, with most estimates being lower than the corresponding direct Fick measurement. For $S_{\bar{v}}O_2$, the correlation is much weaker. The notable outlier, participant 34, skews the correlation significantly, and also partially masks the bias of CCP underestimating $S_{\bar{v}}O_2$. A possible explanation for this participant being an outlier for both $S_{\bar{v}}O_2$ and cardiac output (where they breach the upper limit of agreement) is their severe interstitial lung disease (lung function tests revealed airways obstruction and reduced carbon monoxide diffusing capacity). This level of lung inhomogeneity could feasibly have caused problems with CCP modelling.

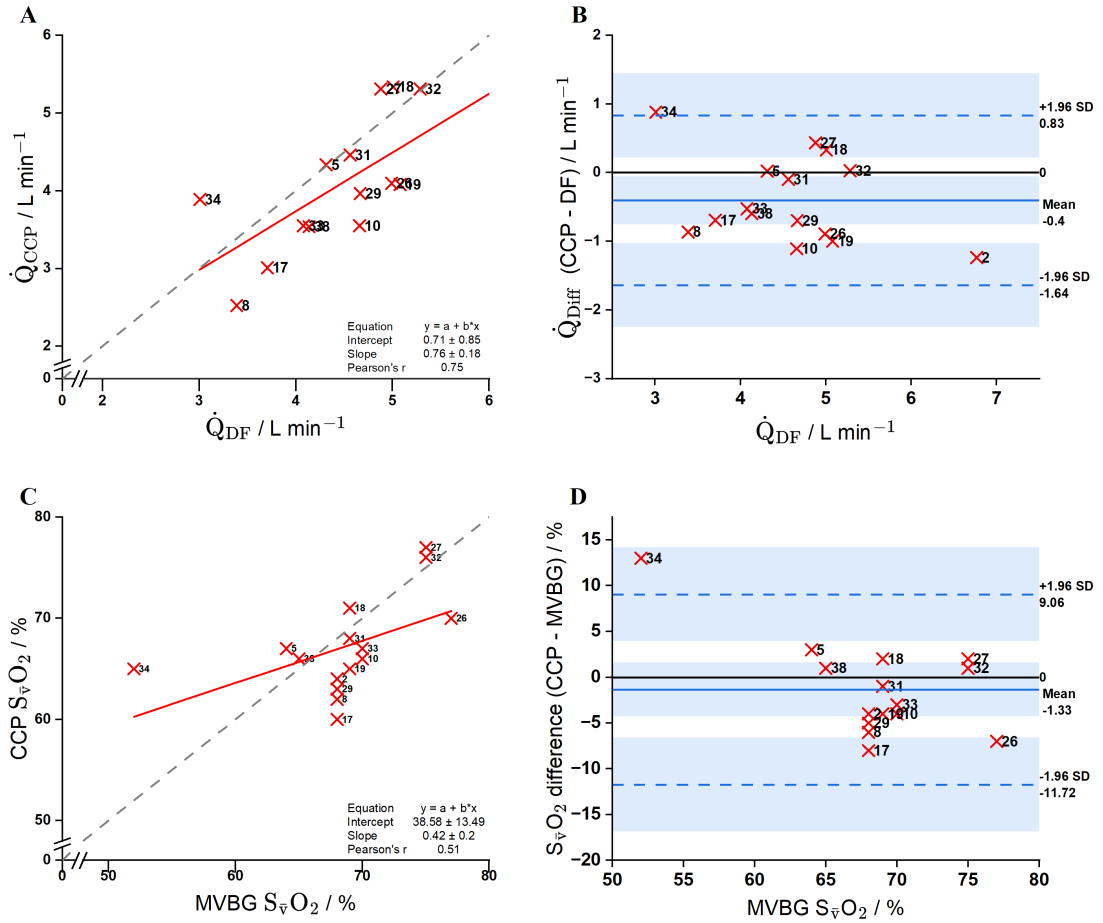

Figure 3.10: Comparison between CCP-estimated cardiac output and $S_{\bar{v}}O_2$ and the invasive reference measurements for the $S_pO_2 \geq 95\%$ subgroup. Panels A and B compare the cardiac output values and panels C and D compare the $S_{\bar{v}}O_2$ values. In panels A and C, the solid red line is the linear fit between values. The equation for this line, along with confidence intervals for the slope and intercept, and the Pearson correlation coefficient (r), is shown. Grey, dashed line, line of identity.

$S_pO_2 < 95\%$ subgroup

The results for cardiac output and $S_{\bar{v}}O_2$ for participants with an $S_pO_2 < 95\%$ are shown in figure 3.11. Unlike for the $S_pO_2 \geq 95\%$ participants, both cardiac output and $S_{\bar{v}}O_2$ estimates correlate strongly with the invasive reference measurements. There is a similar pattern of underestimation for cardiac output, although the limits of agreement are wider than for the $S_pO_2 \geq 95\%$ group. Limits of agreement and mean bias for $S_{\bar{v}}O_2$ are comparable with the $S_pO_2 \geq 95\%$ group.

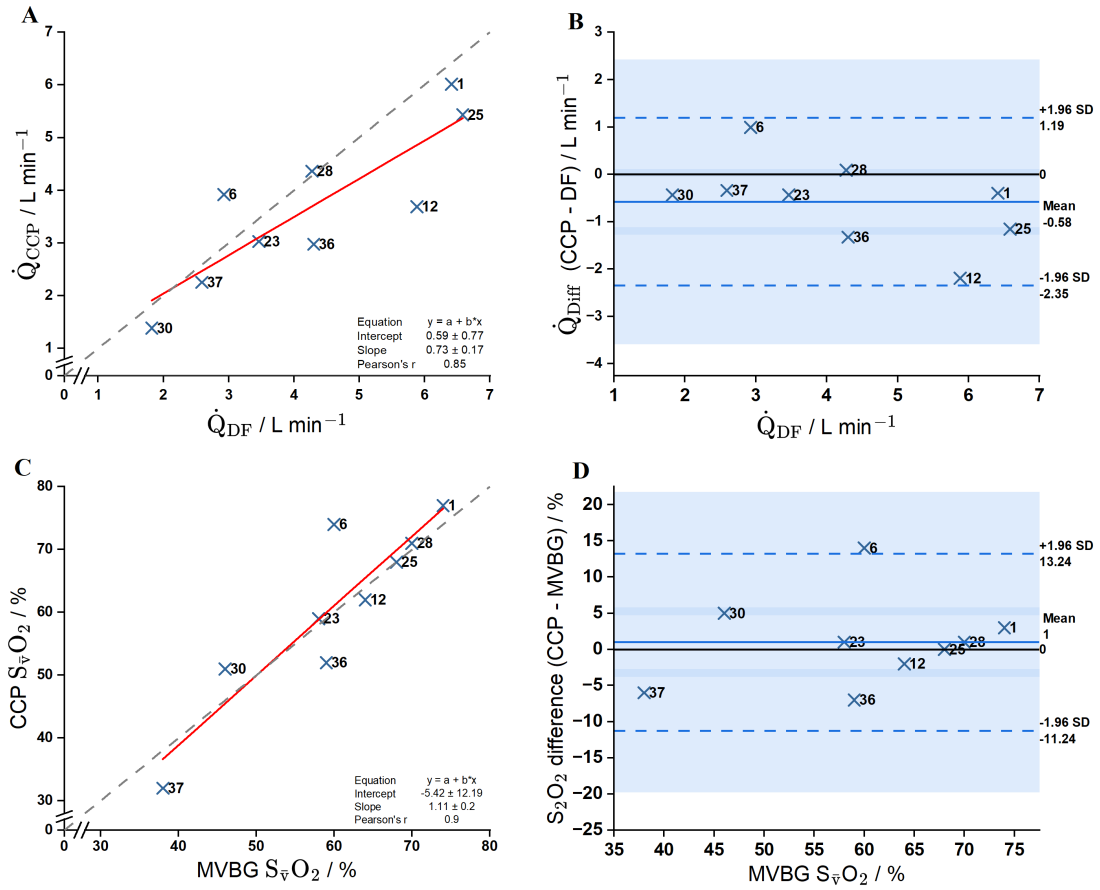

Figure 3.11: Comparison between CCP-estimated cardiac output and $S_{\bar{v}}O_2$ and the invasive reference measurements for the $S_pO_2 < 95\%$ subgroup. Panels A and B compare cardiac output values and panels C and D compare $S_{\bar{v}}O_2$ values. Grey, dashed line, line of identity; red line, regression line; b, regression slope; a, regression intercept.

Overall comparison

The combined results for non-flagged participants from both subgroups are shown in figure 3.12. Both $S_{\bar{v}}O_2$ and cardiac output estimates correlate strongly with invasive reference values. For cardiac output, the underestimation of cardiac output with a progressive increase in difference as the direct Fick value increases is again evident. For $S_{\bar{v}}O_2$ the overall dataset is not biased, although both high and low outliers mean that the limits of agreement are wider than would be acceptable.

$S_{\bar{v}}O_2$ correction

The estimation of cardiac output by CCP with this experimental protocol is done by measuring the uptake of C_2H_2 into the blood from the alveolar spaces. $S_{\bar{v}}O_2$, in general terms, is estimated using the Fick principle, with the measured tracer gas uptake and the

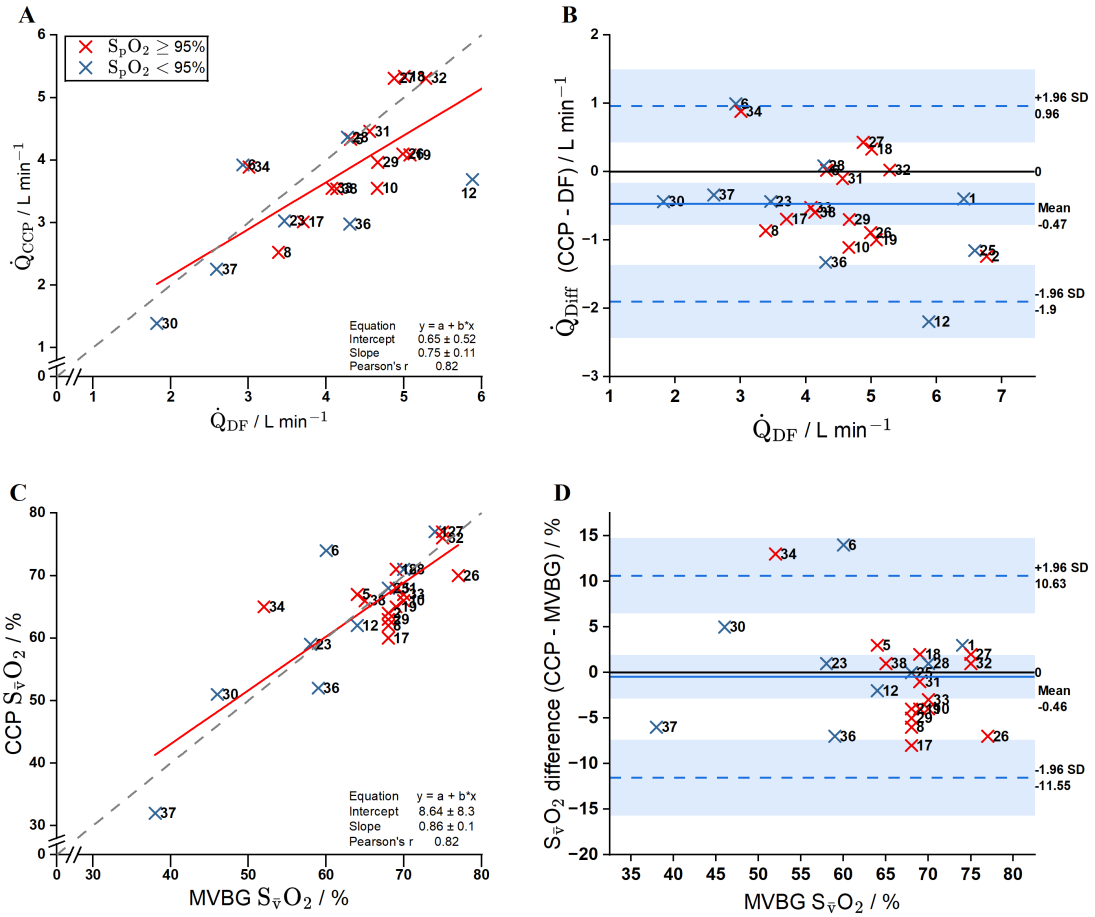

Figure 3.12: Comparison between CCP-estimated cardiac output and $S_{\bar{v}}O_2$ and the invasive reference measurements for all non-flagged participants. Panels A and B compare cardiac output values, and panels C and D compare $S_{\bar{v}}O_2$ values. Grey, dashed line, line of identity; red line, regression line; b, regression slope; a, regression intercept. The red and blue crosses indicate an S_pO_2 of $\geq 95\%$ and $<95\%$, respectively.

modelled arterial oxygen saturation ($S_a^mO_2$). It is therefore possible that an inaccurately estimated $S_a^mO_2$ would lead to a follow-on error with the estimated $S_{\bar{v}}O_2$. This would be particularly relevant in participants with a low S_pO_2 given the discussed limitations of modelling diffusion limitation. For this reason, a corrected CCP $S_{\bar{v}}O_2$ ($S_{\bar{v}}^cO_2$) was calculated which would, in effect, use the pulse oximeter arterial O_2 saturation instead of $S_a^mO_2$:

$$S_{\bar{v}}^cO_2 = S_{\bar{v}}^mO_2 - (S_a^mO_2 - S_pO_2) \tag{3.10}$$

Where $S_{\bar{v}}^mO_2$ is the initial, uncorrected CCP $S_{\bar{v}}O_2$ estimate.

The potential margin for error with pulse oximetry was also considered.(105; 108) A further method of correction, which involved taking the mean of $S_{\bar{v}}^mO_2$ and $S_{\bar{v}}^cO_2$ to give $S_{\bar{v}}^\mu O_2$ was therefore calculated. The results of the comparison for $S_{\bar{v}}^cO_2$ and $S_{\bar{v}}^\mu O_2$ against

the mixed venous blood sample mixed venous O_2 saturation ($S\bar{v}O_2$) are shown in figure 3.13. Compared to the non-corrected estimates (panels C and D, figure 3.12, both $S^c_{\bar{v}}O_2$ and $S^{\mu}_{\bar{v}}O_2$ are slightly less biased towards underestimating the mixed venous sample's O_2 saturation, but are similarly correlated and have broadly similar limits of agreement.

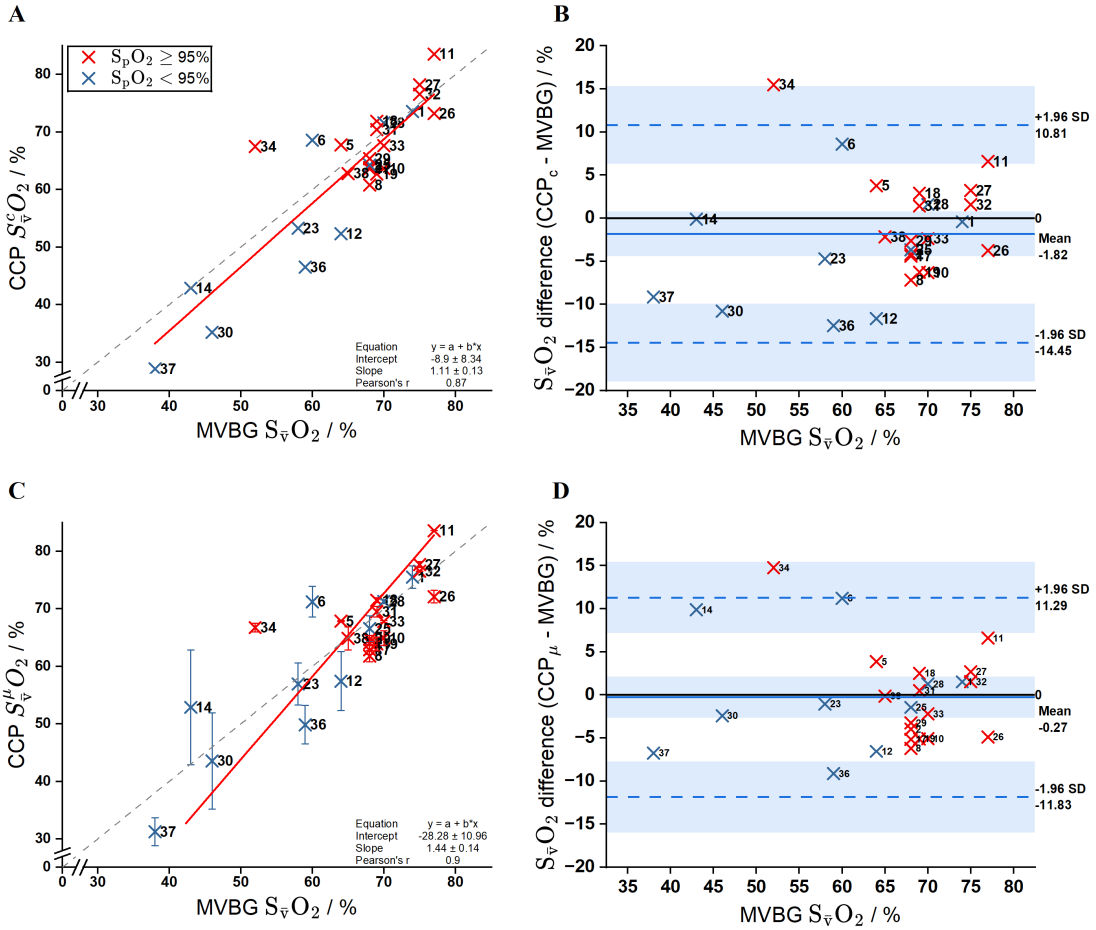

Figure 3.13: Comparison between the corrected (panels A and B) and averaged (panels C and D) CCP-estimated $S_{\bar{v}}O_2$ the mixed venous blood gas measurement for all non-flagged participants. The vertical error bars indicate the range between the uncorrected and corrected ($S^c_{\bar{v}}O_2$) CCP $S_{\bar{v}}O_2$ estimates. CCP_c is $S^c_{\bar{v}}O_2$ and CCP_{μ} is $S^{\mu}_{\bar{v}}O_2$. Grey, dashed line, line of identity; red line, regression line; b, regression slope; a, regression intercept. The red and blue crosses indicate an S_pO_2 of $\geq 95\%$ and $<95\%$, respectively.

3.3.5 Alveolar dead space

The process of producing 36 fits for each participant based on the three different termination sensitivities was repeated following the addition of 6% pure alveolar dead space to the CCP model. Participants flagged for having a high $\dot{Q}$ CV were the same except for

participants 11 and 14, who were included in this set of results, having previously been flagged with the non-alveolar dead space modelling.

The presence of alveolar dead space may, at least in part, explain the underestimation of cardiac output using respiratory-based measurements, which has been present historically, and also with the results presented earlier in this section. Presented below are the results of adding 6% alveolar dead space to the CCP model lung. The results are again presented within the measured S_pO_2 subgroups and then shown as an overall cohort.

$S_pO_2 \geq 95\%$ subgroup

The results for cardiac output and $S_{\bar{v}}O_2$ for participants with an $S_pO_2 \geq 95\%$ for the 6% alveolar dead space fits (referred to as 6% AD from here on) are shown in figure 3.14. For cardiac output, the bias improved from an underestimate of 400 mL/minute to 130 mL/minute. The correlation and limits of agreement were broadly comparable between regular and 6% AD fits for this subgroup. For $S_{\bar{v}}O_2$, there was minimal difference between the correlation, bias, and limits of agreement between regular and 6% AD fits.

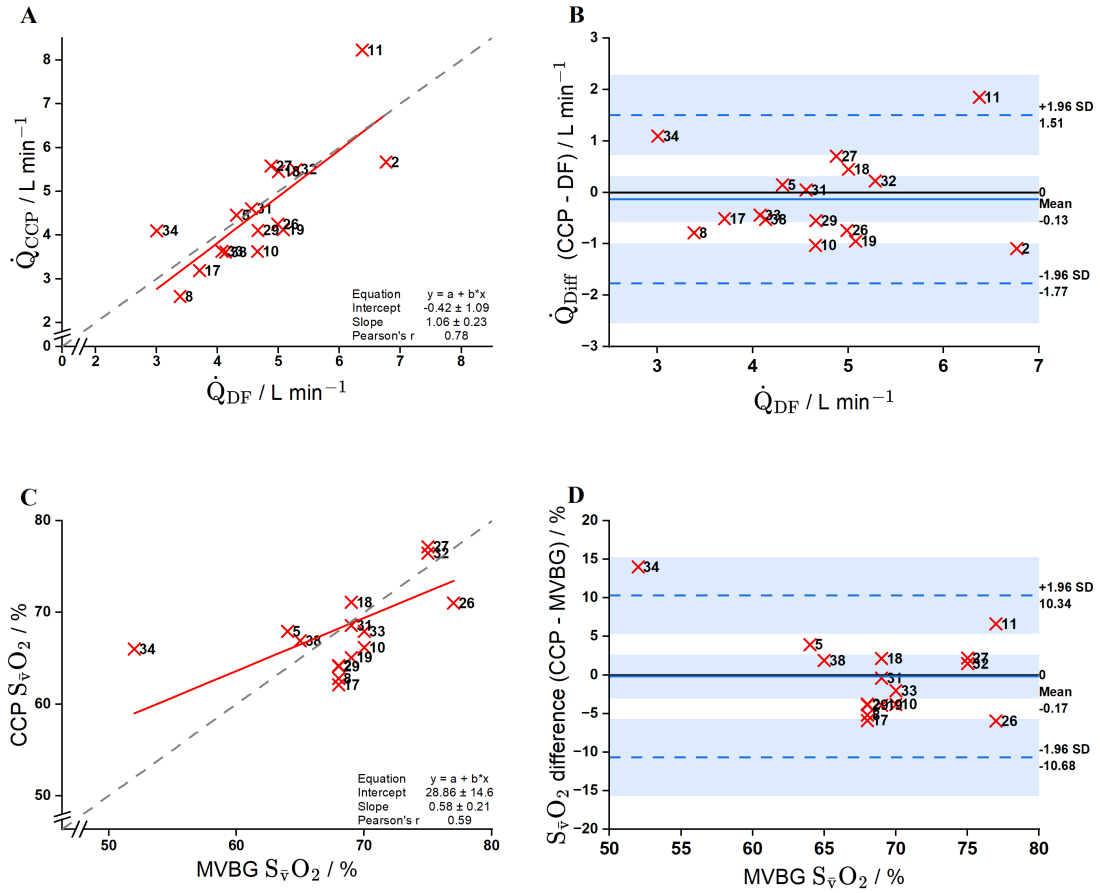

Figure 3.14: Comparison between CCP-estimated cardiac output and $S_{\bar{v}}O_2$ with 6% alveolar dead space added and the invasive reference measurements for the $S_pO_2 \geq 95\%$ subgroup. Panels A and B compare cardiac output values, and panels C and D compare $S_{\bar{v}}O_2$ values. Grey, dashed line, line of identity; red line, regression line; b, regression slope; a, regression intercept.

$S_pO_2 < 95\%$ subgroup

The results for cardiac output and $S_{\bar{v}}O_2$ for participants with an $S_pO_2 < 95\%$ are shown in figure 3.15. For cardiac output, the results between regular and 6% AD fits are similar. For $S_{\bar{v}}O_2$, the addition of participant 14, where the saturation is significantly overestimated, to the 6% AD results skews the results so that the upper limit of agreement is much higher when compared to the same subgroup's regular results.

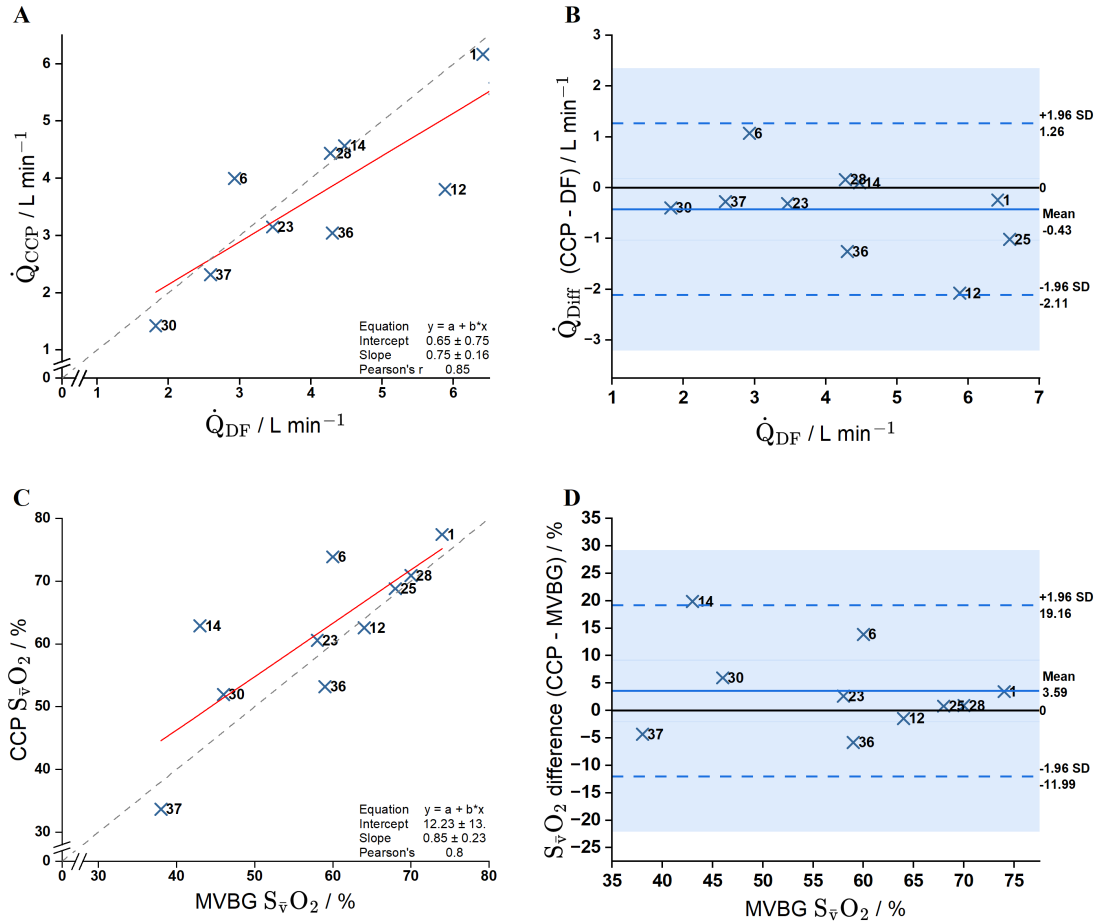

Figure 3.15: Comparison between CCP-estimated cardiac output and $S_{\bar{v}}O_2$ with 6% alveolar dead space added and the invasive reference measurements for the $S_pO_2 < 95\%$ subgroup. Panels A and B compare cardiac output values, and panels C and D compare $S_{\bar{v}}O_2$ values. Grey, dashed line, line of identity; red line, regression line; b, regression slope; a, regression intercept.

Overall comparison

The combined results for non-flagged participants from both subgroups are shown in figure 3.16. Both $S_{\bar{v}}O_2$ and cardiac output estimates correlate strongly with invasive reference values. For cardiac output, the underestimation of the direct Fick cardiac output is less compared to the regular fit with no added dead space (panel B in figure 3.12). For $S_{\bar{v}}O_2$ the overall dataset is not biased, although the limits of agreement are still wide.

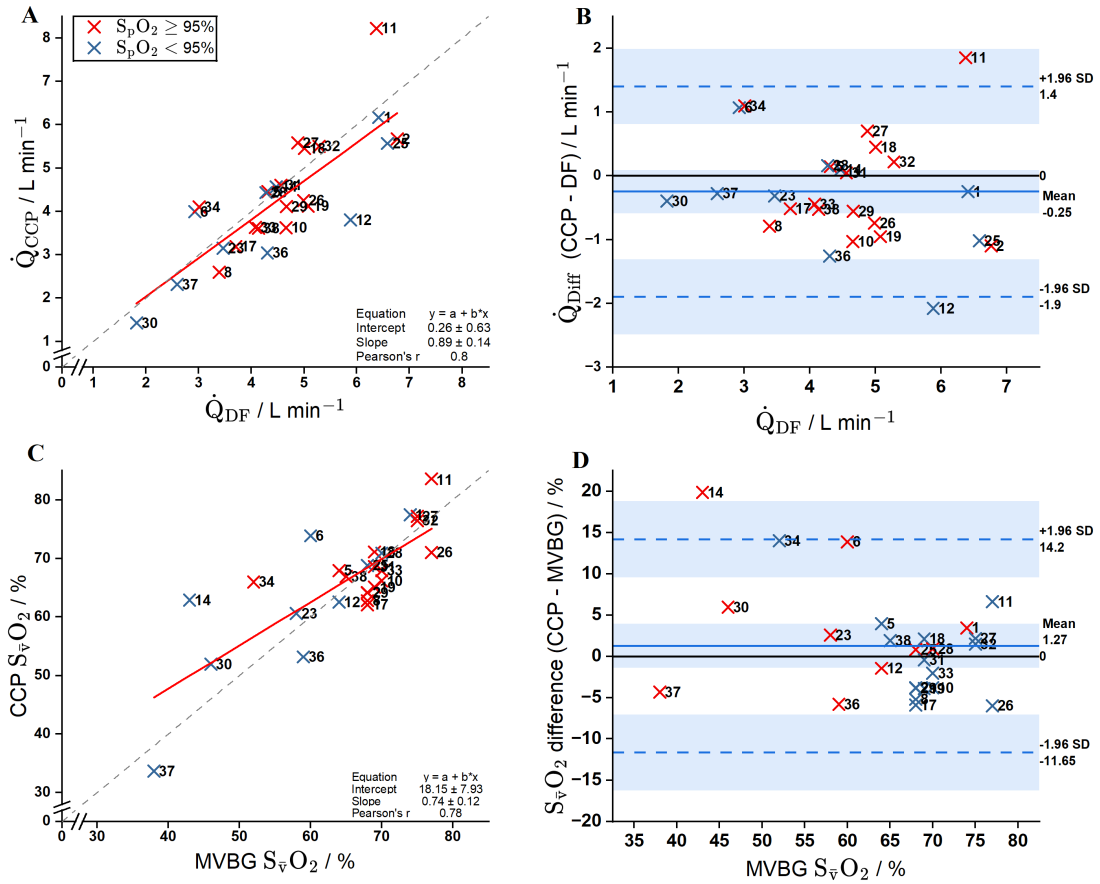

Figure 3.16: Comparison between CCP-estimated cardiac output and $S_{\bar{v}}O_2$ with 6% AD added and the invasive reference measurements for all non-flagged participants. Panels A and B compare cardiac output values, and panels C and D compare $S_{\bar{v}}O_2$ values. Grey, dashed line, line of identity; red line, regression line; b, regression slope; a, regression intercept. The red and blue crosses indicate an S_pO_2 of $\geq 95\%$ and $<95\%$, respectively.

$S_{\bar{v}}O_2$ correction

The results of the comparison for $S^c_{\bar{v}}O_2$ and $S^{\mu}_{\bar{v}}O_2$ with 6% AD added against the mixed venous blood sample $S\bar{v}O_2$ are shown in figure 3.17. Compared to the results for the non-corrected CCP $S\bar{v}O_2$ (panels C and D, figure 3.16), $S^c_{\bar{v}}O_2$ and $S^{\mu}_{\bar{v}}O_2$ values correlate better with the MVBG $S\bar{v}O_2$ measurements. The $S^{\mu}_{\bar{v}}O_2$ values are also less biased. Compared to the results for the non-6% AD fitting (panels C and D, figure 3.13), both $S^c_{\bar{v}}O_2$ and $S^{\mu}_{\bar{v}}O_2$ are similarly correlated and also have similar limits of agreement.

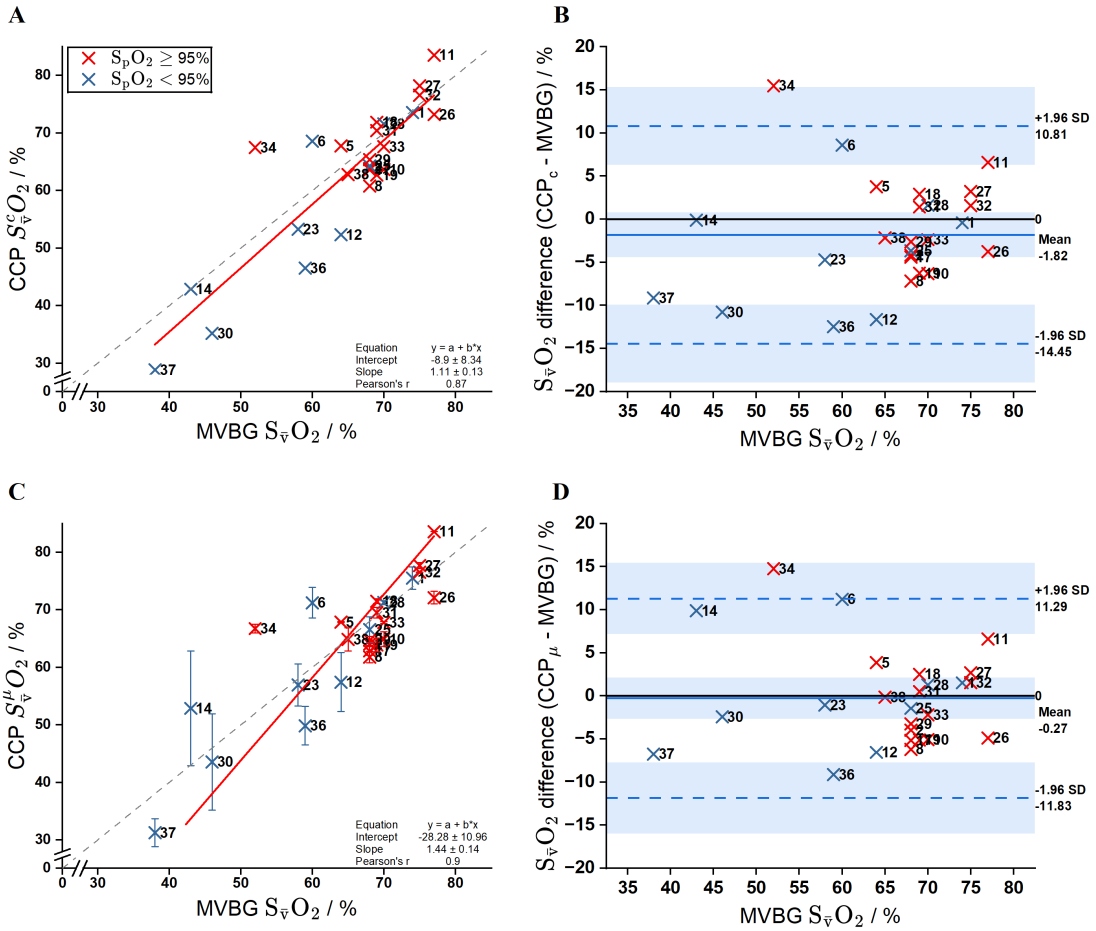

Figure 3.17: Comparison between the corrected (panels A and B) and averaged (panels C and D) CCP-estimated $S_{\bar{v}}O_2$ with 6% alveolar dead space added and the mixed venous blood gas measurement for all non-flagged participants. Grey, dashed line, line of identity; red line, regression line; b, regression slope; a, regression intercept. The red and blue crosses indicate an S_pO_2 of $\geq$ 95% and <95%, respectively. The vertical error bars indicate the range between the uncorrected $S_{\bar{v}}O_2$ ($S^m_{\bar{v}}O_2$) and corrected ($S^c_{\bar{v}}O_2$) CCP $S_{\bar{v}}O_2$ estimates.

3.3.6 Comparison with thermodilution

All recruited participants had cardiac output measured using thermodilution as part of their routine clinical workup in the cardiac catheterisation laboratory. Participant 30's thermodilution cardiac output measurement was not interpretable due to a right-to-left intracardiac shunt. Given that these measurements were used by the treating clinicians when forming an overall conclusion of their patient's physiological state, a comparison was made with the direct Fick cardiac output. This comparison is included in figure 3.18 along with the comparison of 6% AD and non-6% AD cardiac output estimates for all non-flagged participants against the direct Fick cardiac output. The CCP estimates of cardiac output correlates significantly better with the direct Fick measurement than thermodilution-based

values. Both thermodilution and 6% AD cardiac output values slightly underestimate the direct Fick cardiac output and have comparable limits of agreement.

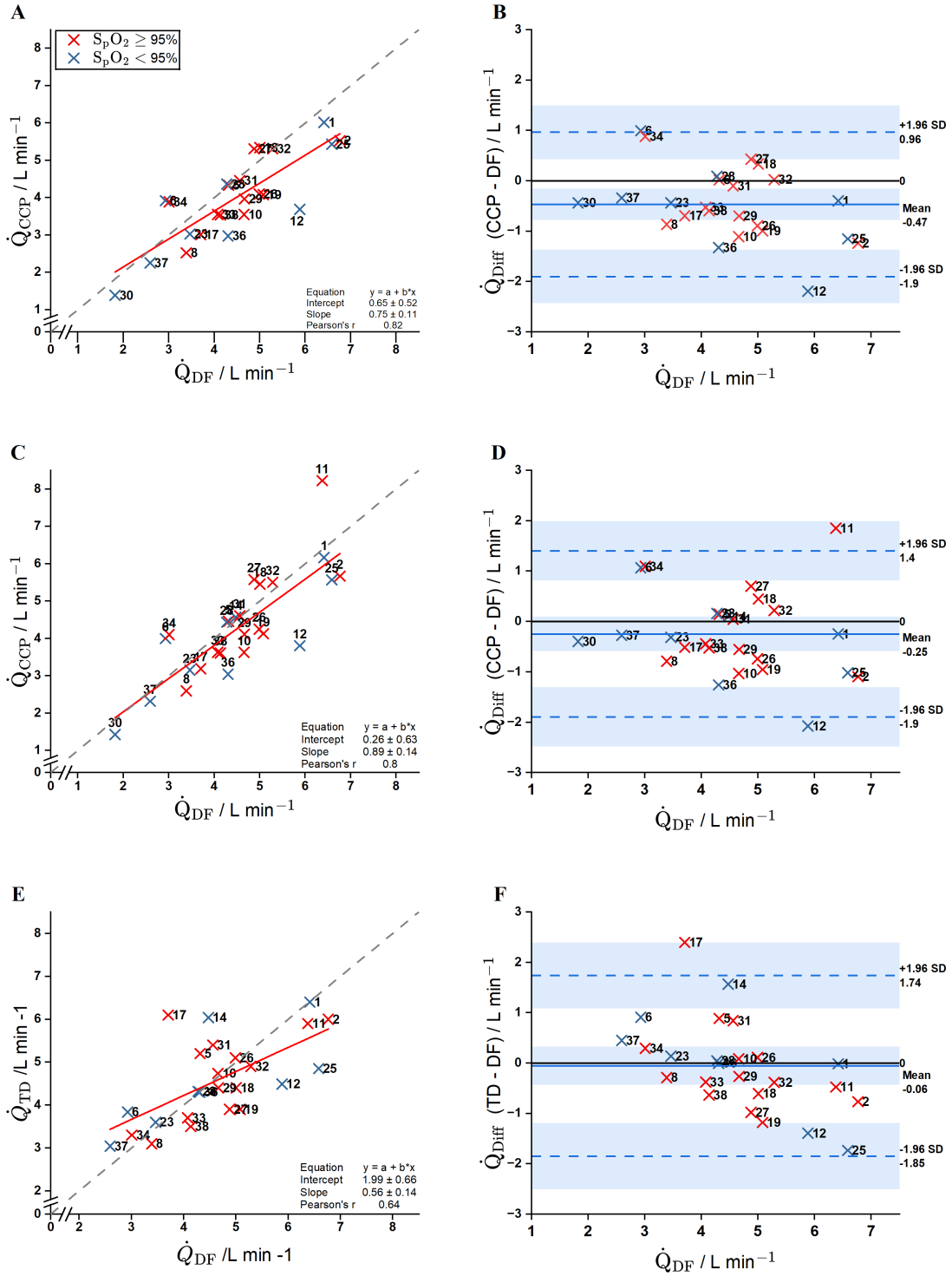

Figure 3.18: Comparison between CCP-estimated (with and without 6% alveolar dead space added) and thermodilution-based cardiac output ($\dot{Q}_{TD}$) with the direct Fick measurement for all non-flagged participants. Panels A, B, C, and D show the comparison between CCP and direct Fick cardiac output. Panels A and B are without 6% alveolar dead space added and panels C and D include the added dead space. Panels E and F show the comparison between thermodilution and direct Fick cardiac output. Grey, dashed line, line of identity; red line, regression line; b, regression slope; a, regression intercept. The red and blue crosses indicate an S_pO_2 of $\geq$ 95% and <95%, respectively.

3.4 Discussion

In this chapter, a novel method for the estimation of cardiac output and $S_{\bar{v}}O_2$ has been discussed. The combination of a highly accurate device with which to measure respired gases and a computational model of the lungs and circulation is used to recover these, along with other, relevant cardiopulmonary parameters. Considered in this section are factors relating to the overall methodology of the study, including strengths, weaknesses, and the feasibility and applicability of the protocol in future studies.

3.4.1 Protocol feasibility

Experimental setup

A short, usually less than five minutes, protocol with a closed-circuit setup has been introduced in this chapter. The development of this protocol builds upon the foundational work done by Smith et al., who demonstrated the promise of using the MFS to estimate cardiac output. Here, the MFS was used similarly to obtain accurate and contemporaneous measurements of respired gases. These measurements were then processed in the CCP model to retrieve an indirect estimate of cardiac output and $S_{\bar{v}}O_2$.

The length of the protocol should be noted. In busy clinical and research settings, a long protocol would reduce the motivation to conduct it in the first place and may also lessen the likelihood of patients or participants consenting to partake. In the current study, the protocol barely interrupted the clinical workflow. It was also noted that some participants were more willing to consent to the study after being informed of the length of time they would be required to breathe through the MFS. The closed-circuit setup was trialled as an alternative to an open-circuit one for convenience and efficiency. The reservoir bag was prefilled either ahead of the participant entering the catheterisation laboratory or while the right heart catheterisation procedure was taking place, highlighting the flexibility of this approach. The option to not have the tracer gas cylinders in the room was also advantageous. It was also sometimes necessary for the procedure to take place in an alternative, smaller laboratory. In these rooms, space for additional equipment

was extremely limited and therefore, the tracer gas cylinders were left outside. In an open-circuit protocol, with the cylinders directly connected to the MFS, this would not have been possible.

Another methodological strength of the study was the clinical setting. For over 90% of the participants recruited, the same clinician performed the right heart catheterisation, minimising the risk of unreliable thermodilution cardiac output measurements due to operator error. For participants where this clinician did not perform the procedure, one other comparably experienced clinician did so instead. For all participants, bolus thermodilution measurements were made until three values within 10% of each other were obtained; these measurements were then averaged to calculate a final thermodilution cardiac output value.

MFS data is currently modelled using the University's supercomputer. While multiple estimates of cardiac output and $S_{\bar{v}}O_2$ can be generated (the frequency of which depends on the specific protocol) in less than one hour, the supercomputer queue times are highly variable, ranging from no queue time to days. For population-based studies where single measurements of cardiac output and $S_{\bar{v}}O_2$ may be taken once every few months or years, this is not an issue. If used for clinical monitoring, where results are required every few hours or less, a version of the model would need to be available either locally or on a private server. As discussed above, the protocol described in this chapter is short and simple enough to implement for both the experimental operator and participant, that performing the experiment multiple times a day to obtain these estimates would not pose a significant challenge.

Modelling

The final results for CCP estimated parameters were presented after flagging participants for a high $\dot{Q}$ CV. The cutoff value of 5% was chosen based on literature data pertaining to the variation of cardiac output in stable patients, where values of between 4.4% to 7.7% were reported.(109; 110)

An alternative to using the $\dot{Q}$ CV to flag participants would have been to use the residual CV instead. The residual value indicates how close the simulated expired gas profiles are to the measured ones. Therefore, the residual values reflect the fit parameters, including respiratory ones, as a whole. The short, rebreathing protocol used in this study is not necessarily optimised to fit the respiratory parameters, compared to other CCP protocols which use a full N_2 washout or longer tracer gas wash-in (or both). As cardiac output was the main fit parameter of interest, it was considered appropriate to use the $\dot{Q}$ CV to identify participants to flag. In the case of future studies where a protocol which is more optimised for recovering respiratory parameters is used, it would be reasonable to consider using the residual CV as a cutoff instead.

This is the first CCP study where the effects of termination sensitivities have been examined in detail. It was decided that all three sets of termination sensitivities would be used for two reasons. Firstly, the termination sensitivities are smaller than the variations for the estimated parameters, and as such, may not make a difference to the optimisation process. Related to the first point, is that secondly, as there was no difference between termination sensitivities for $\dot{Q}$ and residual CVs for this cohort, interpreting the results of 36 datapoints per participant was seen as a more robust way of analysing the data obtained from a protocol optimised for duration and portability. In future studies, it is likely that only one termination sensitivity setting will be used, given these findings.

3.4.2 Accuracy of CCP-estimated parameters

Cardiac output

The CCP estimates, without 6% AD added, of cardiac output for non-flagged participants correlated well with the direct Fick measurements, although there was a clear bias towards underestimating the direct Fick cardiac output. The mean underestimation bias for this cohort was 9%, however, which represents an improvement over Chapman's study, where the cardiac output using a C_2H_2 method was closer to 25%.(31) Chapman discussed the

potential sources of error as possibly being due to recirculation, an incorrect solubility coefficient for C_2H_2, and an altered arteriovenous O_2 difference due to rebreathing. In the current study, the latter factor is not applicable due to a difference in methodology. The rationale behind choosing the solubility coefficient for C_2H_2 used in this study was discussed in section 3.2.1, and barring any new additions to the literature, would not be altered within the CCP model. It is possible that the recirculation may not have been modelled accurately in our study. To explore this further, more work around the validation of the CBGS sub-model would need to be conducted. The potential influence of alveolar dead space affecting the measured uptake of C_2H_2, and causing an underestimation of cardiac output, is discussed in the section 4.4.3.

The error associated with the direct Fick cardiac output measurements was discussed in section 3.3.2. An estimate of approximately 5% or 250 mL/minute was made for the standard deviation of the reference method ($\dot{Q}_{\mathrm{DF}}$) for non-flagged participants (table 3.3). When considering the variance of the difference between the experimental ($\dot{Q}_{\mathrm{CCP}}$), the function, f, of the random variables $\dot{Q}_{\mathrm{CCP}}$ and $\dot{Q}_{\mathrm{DF}}$ is:

$$f = \dot{Q}_{\mathrm{DF}} - \dot{Q}_{\mathrm{CCP}} \tag{3.11}$$

The partial derivatives are therefore $df/\dot{Q}_{\mathrm{DF}} = 1$ and $df/\dot{Q}_{\mathrm{CCP}} = -1$. The variance function becomes:

$$\mathrm{Var}(\dot{Q}_{\mathrm{DF}} - \dot{Q}_{\mathrm{CCP}}) = (1)^2\mathrm{var}(\dot{Q}_{\mathrm{DF}}) + (-1)^2\mathrm{var}(\dot{Q}_{\mathrm{CCP}}) \tag{3.12}$$

From the standard deviation calculated in section 3.3.2 of 250 mL/minute (non-flagged participants) and from the standard deviation for $\dot{Q}_{\mathrm{CCP}} - \dot{Q}_{\mathrm{DF}}$ of approximately 750 mL/minute, calculated from the limits of agreement from panel B of figure 3.12:

$$\begin{aligned}\text{var}(\dot{Q}_{\text{CCP}}) &= \text{Var}(\dot{Q}_{\text{DF}} - \dot{Q}_{\text{CCP}}) - \text{var}(\dot{Q}_{\text{DF}}) \\ &= 750^2 - 250^2 \\ &= 500000\end{aligned}$$

Therefore, the standard deviation for $\text{var}(\dot{Q}_{\text{CCP}})$ is $\sqrt{500000} \approx 707$ mL/minute- significantly higher than the direct Fick standard deviation. Given that the former is the estimate obtained from an optimisation algorithm, and the latter is calculated from direct measurements, this is to be expected, however.

$S_{\bar{v}}O_2$

The estimation of $S_{\bar{v}}O_2$ in this study has been promising, but the wide confidence intervals for CCP values compared to the mixed venous sample values indicate that further work is required. It is important to note, however, that the uncertainty associated with the arterial O_2 saturation greatly affected these results. The excellent correlation when this is accounted for support this claim. For future studies or clinical situations where an arterial blood gas sample is taken, the blood gas arterial O_2 saturation may be used. In the current study, some participants did require arterial gas sampling for clinical reasons. These results were not used to ensure the consistency of method application between participants. Further, these arterial blood gases were taken after the CCP protocol. Ideally, they would be taken during the air-breathing phase of the protocol, as the mixed venous gas sample was, and from a pre-existing arterial line, so as not to disturb ventilation.

Multi-visit participants

For the three participants who were studied twice, it would have been reasonable to compare the results of their invasive, reference measurements and CCP-estimates for cardiac output and $S_{\bar{v}}O_2$ from the first visit to the second. However, for one participant (ID 3 and 27), the mixed venous blood gas sample taken during their first procedure was

considered a spurious one, and for another (ID 26 and 35), they had developed a left-to-right intracardiac shunt following a change to their pulmonary hypertension medication after the first procedure as the right heart pressures had reduced sufficiently to 'reactivate' the shunt. The medication change had worked well in that the pulmonary pressures, and therefore right heart pressures, were reduced; however, this allowed blood to be shunted from the left to right heart via a patent foramen ovale. For the remaining participant (ID 5 and 29), the mixed venous $S_{\bar{v}}O_2$ went from 64% to 68%, the corresponding (uncorrected) CCP estimates were 67% to 63% with no added alveolar dead space and 68% to 65% with 6%AD. The direct Fick cardiac output went from 4.3 L/min to 4.7 L/min, the corresponding CCP estimates were 4.3 L/min to 4 L/min with no added alveolar dead space and 4.5 L/min to 4.1 L/min with 6%AD.

3.4.3 Alveolar dead space

A key finding discussed in this chapter is the effect of alveolar dead space. The concept of a proportion of total ventilation flowing into alveolar dead space in the healthy lung is not one that is established within the current understanding of respiratory physiology. However, this has been shown to be a possibility and may serve to at least partially explain the underestimation of cardiac output, both with CCP and for conceptually similar techniques such as those described by Grollman and Chapman.(30; 31) Based on Sandhu et al.'s work, the total dead space in the lung was calculated to be approximately 11.5%, with roughly half of this being due to $\dot{V}/\dot{Q}$ mismatch and the other half potentially being due to pure or apparent alveolar dead space.(94) It is possible that, instead of half of this total dead space being due to alveolar dead space, it is another process driving this observation. One such possibility is that water in the lung airways absorbs C_2H_2 during inspiration and releases it back during expiration. This would mean that a fraction of C_2H_2 would not reach the level of the alveolus, and therefore, the C_2H_2 available to be taken up by the pulmonary capillary would be less. It is not certain whether the magnitude of underestimation (if any) of cardiac output with this mechanism would be the same as if it were due to alveolar dead space.

Another factor to consider is that the alveolar dead space calculated by Sandhu et al. may not manifest in the same way for C_2H_2 as it does for CO_2. It is possible that there is a delay in the equilibration of CO_2 with blood. There are many factors which affect the carriage of CO_2 in blood, as briefly discussed in section 2.2.3. A major determinant of this carriage is the Haldane effect, which in turn is dependent on the loading and unloading of O_2 to haemoglobin. Richardson et al. have shown that inefficiencies in gas exchange by red blood cells, specifically diffusion-limited O_2 unloading, may result in these processes of O_2 (and by extension, CO_2 exchange) to be slower than previously thought.(111) In future iterations of the CCP model, the uptake of gases in lung water and the alveolar dead space for C_2H_2 specifically will be explored.

The CCP cardiac output estimates with 6% AD were 4% lower, on average, than the direct Fick measurements. This represents an improvement over the non-6% AD fits, where the direct Fick cardiac output was underestimated by 9%, on average. It should be highlighted that two extra participants were included in the 6% AD results due to having a $\dot{Q}$ CV of <5%. One of these participants, 11, was a high outlier, with the CCP value being almost 2 L/minute higher than the direct Fick measurement. However, even when this outlier is removed, the 6% AD underestimation is approximately 5.5%, indicating the possible influence of dead space affecting the uptake of C_2H_2.

3.4.4 Limitations

12 participants out of the 47 recruited were excluded due to a high N_2 balance when breathing through the MFS, indicating a circuit leak. While this rate is high, there were factors which indicate that there is significant room for improvement with future studies. Firstly, most exclusions occurred early in the recruitment phase. Participants are more likely to have a circuit leak when lying supine due to the increased likelihood of the mouthpiece becoming malpositioned. As recruitment progressed, the experimental operator (this author) became better at preventing circuit leaks by instructing participants more effectively and being able to identify and prevent malpositioning before it occurred.

Some participants who were not fluent in English (although still able to provide informed consent), had more difficulty following instructions, which increased the likelihood of a leak. In rare cases where a degree of pharmacological sedation was required, a leak was more likely to occur due to the need to actively 'stay on' the mouthpiece, especially in the supine position. In one case, the participant's nose shape was such that the nose clip did not occlude the nostrils adequately; in future, this could be addressed by using nostril plugs instead.

From the 38 datasets from the 35 participants remaining, seven participants from the 6% AD fitting and nine participants from the non-6% AD fitting were flagged as having a high $\dot{Q}$ CV. Proportionally, this is a high number of participants to exclude, and is likely due to the pathophysiological characteristics of the participants in this cohort and the CCP protocol. As previously discussed, CCP, even in protocols optimised to recover respiratory parameters, is designed for the early detection of disease. This, along with the fact that the protocol described in this chapter was designed to be as short and convenient to execute as possible, will inevitably result in fitting failures, defined here as a high $\dot{Q}$ CV. To test this, a comparison with this protocol and a longer and/or open-circuit protocol would be required. Increasing the time for the air-breathing phase is unlikely to be of benefit. To increase the rebreathing time, a CO_2 absorber could be used.

While the number of participants flagged for a high $\dot{Q}$ CV was high, it is a success of the protocol that participants with a low S_pO_2 had CCP estimates of cardiac output and $S\bar{v}_{O2}$ that were largely comparable to those with S_pO_2 values of $\geq$95%. Given these findings, it is likely that stratification based on participant S_pO_2 is not required for CCP protocols, although the small sample sizes of the two subgroups in this cohort make it difficult to make a definitive conclusion.

3.4.5 Thermodilution measurements

In this cohort, the thermodilution measurements taken during right heart catheterisation show a tendency for overestimation of low true cardiac outputs and underestimation of high true cardiac outputs. This is in keeping with findings published in the literature. Figure 3.19 shows plots published by Baylor and Narang et al., where the globular pattern of the datapoints demonstrated in panel F of figure 3.18 can be appreciated as a result of this two-way bias.(36; 60) The proposed mechanism for underestimation is that rapid temperature changes occurring in high-flow states can result in cardiac output underestimation due to the limited sensitivity of the PAC-thermistor to such changes.(112). In low-flow states, it is possible that the heat loss that occurs causes thermodilution-based overestimation of cardiac output measurements.(61) Both Narang et al. and Baylor's studies included taking the average of three (in Narang et al.'s case, three to five) thermodilution measurements. Baylor also specified that only the measurements where the thermodilution curve appeared satisfactory (Narang et al. did not comment on this). Therefore, the quality control measures for thermodilution are largely comparable to the study discussed in this chapter.

As the thermodilution to direct Fick bias is bidirectional, depending on the direct Fick value, it is not helpful to compare the mean difference when comparing the results to CCP-estimates. This is highlighted by the fact that the mean difference for thermodilution when compared to the direct Fick cardiac output is 1%, despite the limits of agreement being wider and the correlation being poorer than CCP-estimated cardiac output (with or without 6% AD).

Given the above results, CCP appears to be the superior method over thermodilution for a single estimate of cardiac output. This is further supported by the comparative invasiveness of the two methods, where pulmonary artery catheterisation has well-documented risks compared to what is a non-invasive method in CCP.(39; 40; 43) The small sample size of the cohort and the significant number of excluded and flagged participants, however, do not make this conclusion a definitive one. These limitations can be addressed in future

studies, as previously discussed.

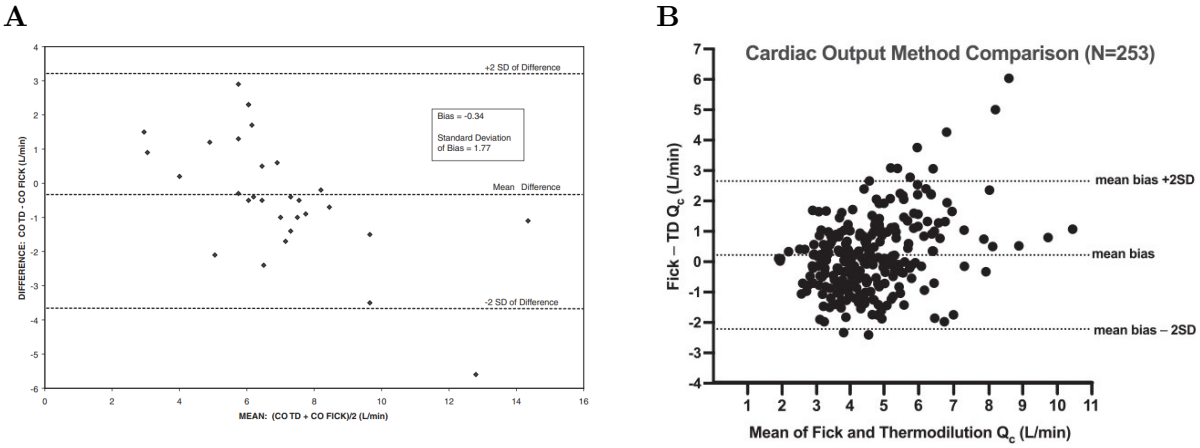

Figure 3.19: Comparison of thermodilution and direct Fick cardiac output measurements from two separate studies. Panel A shows the results from Baylor, and panel B shows the results from Narang et al. Note that for both figures, the x-axis shows the mean of thermodilution and direct Fick measurements, rather than using the direct Fick value as the reference. In panel B, the y-axis difference is direct Fick − thermodilution, rather than thermodilution − direct Fick as is the case for panel A and the results presented in this chapter.

3.4.6 Direct Fick cardiac output

The error associated with the direct Fick calculation was discussed in section 3.3.2. This calculated variance should be accounted for when considering the comparison of CCP estimates with the direct Fick cardiac output.

Using table 3.3 as a reference, the mean direct Fick cardiac output standard deviation was 6.2%, equivalent to 284 mL/minute for all participants. The approximate standard deviations derived from limits of agreement for both non-6% AD and 6% AD CCP-estimates of cardiac output (panels B and D in figure 3.18) were 720 mL/minute and 830 mL/min, respectively. Clearly, these standard deviations for CCP are wider than desirable. However, they still compare favourably compared to the thermodilution standard deviation of 900 mL/minute (panel F in figure 3.18). When considering the underestimation bias of CCP, it is possible that the magnitude of this is not as great as first thought, when the direct Fick standard deviation is accounted for.

3.5 Conclusion

The results of an observational study, examining non-invasively acquired cardiopulmonary parameters in pulmonary hypertension patients undergoing right heart catheterisation, have been discussed. Specifically, CCP estimates of cardiac output and $S_{\bar{v}}O_2$ have been compared against the invasive reference standards, the direct Fick method and mixed venous blood gas analysis, respectively. With cardiac output, an additional point of comparison with thermodilution, the clinical reference standard, was possible. CCP has been shown to be comparable, and potentially superior, to thermodilution for a single measure of cardiac output. Given the difference in invasiveness between thermodilution, where right heart catheterisation is required, and CCP, these findings represent a significant advancement in the progress of a technique for a respiratory-based measurement of cardiac output.

From a modelling standpoint, the effects of different termination sensitivities on CCP output parameters have been explored in detail. These findings have allowed for a greater degree of confidence in both identifying problematic datasets and interpreting CCP estimates. As such, it is likely that a similar approach to the process described will be carried forward to other studies where CCP is used.

This study has limitations which should be acknowledged. Primarily, the sample size of participants included in the final analysis, excluding flagged participants, was small. While this is the case, it is still possible to comment on the clear promise of CCP-estimated cardiac output and $S_{\bar{v}}O_2$ and that larger-scale studies are warranted given the initial results. The other limitations of this study relate more to factors inherent to CCP as a technique. Breathing through the mouthpiece and with a nose clip requires a degree of cooperation from the subject, which is not always possible. It is necessary for the tracer gases, in their appropriate concentrations, to be available in advance, although a closed-circuit protocol where the rebreathing gas mixture can be prepared in advance is a good step towards addressing the overall practicality of the technique.

To conclude, the results of this study show that in CCP, a non-invasive method of measuring cardiac output has been developed that is comparable to the invasive, clinical reference standard, pulmonary artery catheter-based thermodilution. It has also been shown that CCP-based $S_{\bar{v}}O_2$ mixed venous estimates may also have current utility in clinical and research settings, with further optimisation possible. The overall findings highlight the potential for the use of CCP-based cardiac output measurement in population-based studies. Examples of this include, but are not limited to, examining cardiac output as a long-term predictor of cardiac morbidity and mortality, and the use of cardiac output measurement to guide therapy in clinical settings where right heart catheterisation is inappropriately invasive.

4 Healthy Volunteer Study

4.1 Introduction

This chapter presents the findings from a cohort of healthy volunteers who were recruited to undertake a series of computed cardiopulmonography (CCP)-based experiments. The estimation of cardiac output and mixed venous O_2 saturation ($S_{\bar{v}}O_2$) using respired gas analysis were the primary outcomes of interest. In addition to using the exogenous tracer gases, methane (CH_4) and acetylene (C_2H_2), as described in the pulmonary hypertension cohort study in chapter 3, an endogenous tracer gas-based method, using CO_2, is introduced. The overarching objective in this study was to determine whether an endogenous gas such as CO_2 could feasibly be used in place of exogenous tracer gases to accurately and non-invasively estimate cardiac output and $S_{\bar{v}}O_2$, among other cardiopulmonary parameters.

4.1.1 CO_2 as a tracer gas

The appeal of using CO_2 as a tracer gas stems from the fact that it will be more readily available compared to a CH_4 and C_2H_2 mixture, in both research and clinical settings. For mechanically ventilated patients, especially, where it would be exceedingly difficult to load a ventilatory circuit with exogenous gases, an approach using CO_2 may be the only viable approach for the estimation of cardiac output using a respiratory gas-based technique.

The manipulation and analysis of CO_2 for the estimation of cardiac output using Fick principles has been described in the literature before and was discussed in chapter 1.(35) The novelty of the method introduced in this chapter stems from the use of integrated use of CCP, which consists of a highly accurate device for respired gas analysis with excellent time-resolution and a comprehensive model of the lungs and circulation, within a closed-circuit setup. The closed-circuit setup was described in chapter 3, but was initially developed during this study with healthy volunteers, and has the benefits of being easy to implement and brief in duration.

4.1.2 Computed cardiopulmonography (CCP)

The CCP-based approach to estimating cardiac output in this study remains broadly similar to that described in the pulmonary hypertension cohort. The respired gas data that is obtained from the molecular flow sensor (MFS) is passed through the cardiopulmonary model. Here, parameters relating to the lungs, circulation, and metabolism are fit. This approach allows for the inhomogeneity of the lung and any recirculation of gases to be accounted for in the nonlinear optimisation routine when estimating values for cardiac output and $S_{\bar{v}}O_2$.

The approach to modelling data obtained from CCP protocols has been simplified and refined from the pulmonary hypertension cohort study (chapter 3). This is discussed in detail later in the chapter, but the conclusions related to setting termination sensitivities within the model and examining the variances of fit parameters as a way of determining the quality of results are incorporated into this study.

Alveolar dead space

In recently published work, Sandhu et al. raised the possibility that a fraction of lung ventilation is distributed into regions of pure alveolar dead space, even in healthy individuals.(94) This leads to a higher overall proportion of alveolar dead space, in addition to apparent alveolar dead space arising as a result of $\dot{V}/\dot{Q}$ and other mechanisms. The effects of taking this possibility into account within the cardiopulmonary model are examined via a sensitivity analysis. The differences in these effects between protocols using endogenous (CO_2) and exogenous (CH_4 and C_2H_2) were also of interest, and discussed in this chapter.

4.1.3 Protocol comparison

As this study involved the recruitment of healthy volunteers, no invasive reference measurement of cardiac output or $S_{\bar{v}}O_2$ was possible due to reasons of ethical permissibility. Instead, comparisons were made between the different protocols. Specifically, the bias and precision of the protocols relative to each other were examined using a statistical

process, which is detailed. This process serves as an indicator of the potential feasibility for various research and clinical applications, where comparisons of results made with reference techniques can be made.

4.2 Methods

4.2.1 Experimental protocol

The ethics approval for this study was in place under a broader set of studies which utilise CCP to estimate cardiopulmonary parameters in healthy volunteers and patients with respiratory disease. REC reference 17/SC/1072. The experimental work was carried out in accordance with the general principles of the Declaration of Helsinki.

Healthy volunteers, i.e. with no significant comorbidities of a cardiac or respiratory nature, were recruited for the study at a research facility in the Department of Physiology, Anatomy and Genetics at the University of Oxford. Each participant underwent four CCP protocols. The reproducibility between the CCP cardiac output and $S_{\bar{v}}O_2$ estimates for each of the different protocols was analysed for each participant.

In order, the four protocols were a rebreathing exogenous tracer gas protocol where participants underwent a period of rebreathing into a reservoir bag filled with a mixture of CH_4 and C_2H_2 in air, two identical rebreathing protocols where the exogenous tracer gases were replaced with a high concentration of CO_2 (to serve as an endogenous tracer gas), and finally an open-circuit protocol where a period of breathing a CH_4 and C_2H_2 mixture took place, followed by a period of breathing only CH_4 (at the same concentration). The order of the protocols was kept the same across participants to minimise C_2H_2 loading by keeping the two exogenous tracer gas protocols as far apart as possible and to maintain experimental consistency. Regarding the latter reason, it was acknowledged that not randomising the order may introduce bias related to the order of the protocols, however.

For the closed- and open-circuit exogenous tracer gas protocols, cardiac output is es-

timated by measuring the uptake of C_2H_2, which is soluble in blood. The lung parameters are estimated from the equilibration of CH_4—which is far less soluble in blood than C_2H_2—between the lung and circuit. For the CO_2 rebreathing protocol, CO_2 acts as an endogenous tracer gas. As CO_2 is soluble in blood, its uptake in the circulation from the lungs can be used to estimate cardiac output in a similar way to how C_2H_2 is used. Modelling the parameters of lung inhomogeneity is primarily estimated by a combination of extrapolating the partial washout of N_2 (by inhaling 93% O_2 in the reservoir bag) and examining the equilibration of gases between the lung and reservoir bag.

The contents of the reservoir bag for the exogenous tracer gas protocol were 0.3% C_2H_2, 0.9% CH_4, 21% O_2, and balance N_2, these concentrations were the same for the open-circuit protocol. This mixture contained slightly higher concentrations of tracer gases than the pulmonary hypertension cohort. The mixture for the endogenous tracer gas protocol consisted of 7% CO_2 and balance O_2.

The configuration of the MFS and reservoir bag for the rebreathing protocols was the same as for the pulmonary hypertension cohort study. The pre-filled reservoir bag was connected to one port of a three-way tap. The second port was connected to the non-participant end of the MFS and the remaining port was open to air. The open-circuit protocol was configured so that gas flowed between a mass flow controller (MFC) and tubing open to air at a rate of 40–60 L/minute. Connected to the non-participant end of the MFS, and between the MFC and tubing was a T-piece connector for the participant to breathe in from the gas flow passing across and to expire through the expiratory tubing. The open-circuit configuration is shown in figure 4.1. The concentrations of exogenous tracer gases for the open-circuit protocol were the same as for the rebreathing protocol. Schematics of the three different protocols are shown in figure 4.2.

Participants were seated in an upright position when breathing through the MFS, with a nose clip attached. For the rebreathing protocols, a steady state phase of at least three minutes in which the participant breathed air was completed prior to the three-way tap

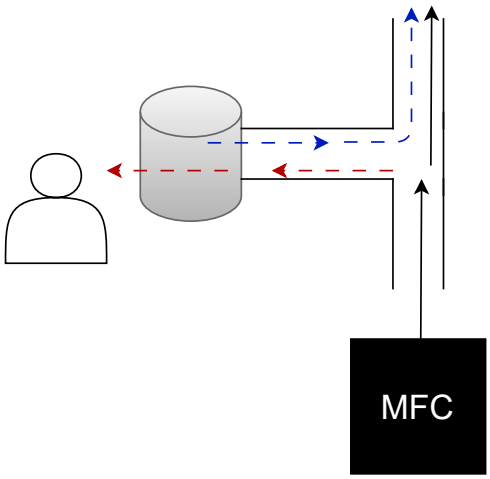

Figure 4.1: Simplified diagram of the open-circuit configuration. Gas from the MFC (black square) flows within a tubing circuit. It can be inspired by the participant via the MFS head (grey cylinder) in a path shown by the red, dashed arrows or flow across (black arrows) through the expiratory tubing, which is open to air. The participant's expired gas (blue, dashed arrows) also flows through the expiratory tubing. Not to scale.

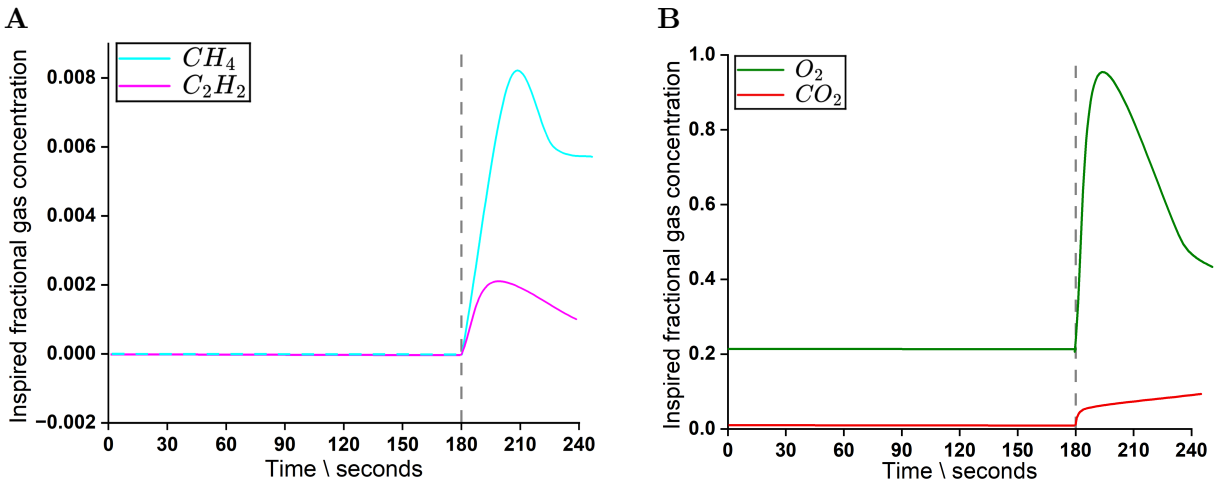

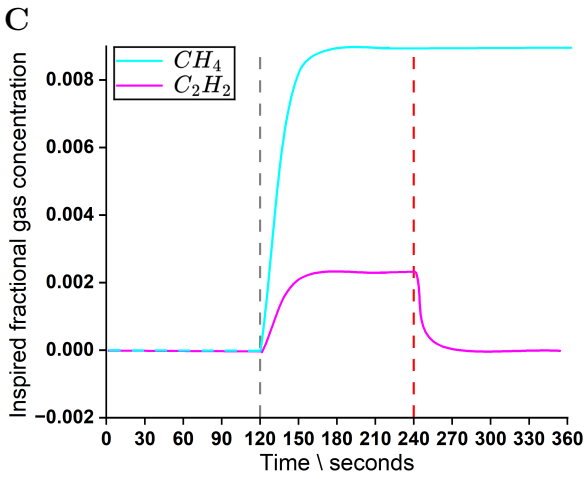

Figure 4.2: Schematics of the three experimental protocols. In panel A, the closed-circuit exogenous tracer gas protocol is shown, with the respired fractional gas concentrations of CH_4 in cyan and C_2H_2 in magenta. In panel B, the CO_2 rebreathing protocol is shown, with the respired fractional gas concentrations for CO_2 (red) and O_2 (green), respectively. In panels A and B, the grey, dashed line indicates the turning of the three-way valve to the reservoir bag, having initially been open to air, so that rebreathing can commence. In panel C, the open-circuit exogenous tracer gas protocol is shown, with the respired fractional gas concentrations of CH_4 in cyan and C_2H_2 in magenta. CH_4 and C_2H_2 are delivered via the mass flow controller between the periods marked by the grey and red, dashed lines. After this, the delivery of C_2H_2 is ceased, while the flow of CH_4 continues.

being turned in the direction of the reservoir bag for a one-minute rebreathing phase. For the open-circuit protocol, the air-breathing phase was two minutes long, followed by C_2H_2 and CH_4 breathing for two minutes, and finally, CH_4 without C_2H_2 for a further two

minutes.

All four protocols took place over a single day for each participant, a minimum of 10 minutes was taken between protocols to allow for any residual tracer gases to wash out of from the circulation. Before the first protocol for each participant, the MFS was warmed to 36°C and calibrated with pure O_2 and N_2, following the standard procedure for all CCP experiments. The reservoir bag was filled to the participant's predicted FRC for the three rebreathing protocols using the Global Lung Initiative lung function calculator.(96) The full FRC was used instead of a fraction as the participants were seated upright for these protocols.

Following the completion of the four protocols, a blood sample was taken to measure the haemoglobin. Participants were given the option of having a venous or capillary sample taken. The sample was then processed using a point-of-care system (HemoCue Hb 201+, HemoCue AB, Sweden). The blood sample was taken after all the protocols to ensure that the cardiac output was as stable as possible during measurements and not affected by a sympathetic nervous system response to the blood draw.

4.2.2 Modelling

The approach to CCP modelling for the healthy volunteer cohort was guided by the results of the pulmonary hypertension cohort. Only one termination sensitivity, the least sensitive (optimality, function, and step tolerances of 1×10^{-6}), was chosen for modelling. The rationale for this was discussed in detail in chapter 3, but briefly, the variations in the fit parameters of interest were greater than the differences that would be seen if they were due to the termination sensitivities. For each protocol, a total of 12 fits were obtained for each protocol. The process was then repeated for fits with 6% alveolar dead space (6% AD) added. Here, 6% of the ventilation to the CCP model lung was apportioned to a region of pure alveolar dead space. For each dataset, outliers were identified by examining the cardiac output scaling coefficient of variation ($\dot{Q}$ CV). The results of the modelling

are discussed in section 4.3.

4.2.3 Bias and precision

In the absence of a set of results from a reference method, the relative bias and precision of the three different protocols were compared. Correlation and Bland-Altman plots were inspected for visually apparent patterns of bias, followed by statistical analysis with a nonparametric method.

The assessment of the relative precision of the cardiac output and $S_{\bar{v}}O_2$ estimates obtained from the different protocols used here is based around the concept of an intraclass correlation coefficient (ICC).(113) In very general terms it may be written as:

$$\begin{aligned} \text{ICC} &= \frac{\text{variance of interest}}{\text{total variance}} \\ &= \frac{\text{variance of interest}}{\text{variance of interest } + \text{ unwanted variance}} \end{aligned}$$

The denominator is very simply the measured variance across individuals, where for method x:

$$\text{Var}(x) = \text{Var(q)} + \text{Var}(\epsilon_x) \tag{4.1}$$

Where Var(q) is the variance of interest and $\text{Var}(\epsilon_x)$ is the unwanted variance for protocol x.

To calculate the ICC, it is also necessary to estimate Var(q). Here, a simple model for the bias and noise for each protocol can be written, that this may be estimated by the covariance between two methods. Taking the cardiac outputs of the closed- (TG_c) and open-circuit (TG_o) exogenous tracer gas protocols as an example, the covariance is given by:

$$\text{Covar}(\text{TG}_\text{c}, \text{TG}_\text{o}) = \frac{1}{(\text{n}-1)} \sum \left[(\dot{Q}_{\text{TG}_{\text{c,i}}} - \bar{Q}_{\text{TG}_\text{c}})(\dot{Q}_{\text{TG}_{\text{o,i}}} - \bar{Q}_{\text{TG}_\text{o}}) \right] \tag{4.2}$$

Where the $\frac{1}{(\text{n}-1)}$ term refers to the degrees of freedom, $\dot{Q}_{\text{TG}_{\text{c,i}}}$ and $\dot{Q}_{\text{TG}_{\text{o,i}}}$ are the cardiac outputs for the i^{th} participants for the respective protocols, and $\bar{Q}_{\text{TG}_\text{c}}$ and $\bar{Q}_{\text{TG}_\text{o}}$ are the mean cardiac outputs for the

respective protocols.

A model term for $\dot{Q}_{\mathrm{TG_{c,i}}}$ can be expressed as:

$$\dot{Q}_{\mathrm{TG_{c,i}}} = \mathrm{q_i} + \mathrm{b_{TG_c}} + \epsilon_{\mathrm{TG_{c,i}}} \tag{4.3}$$

Where $\mathrm{q_i}$ is the true cardiac output value for the i^{th} participant, $\mathrm{b_{TG_c}}$ is the protocol specific bias, and $\epsilon_{\mathrm{TG_{c,i}}}$ is the error of the method for the i^{th} participant.

Here, $\mathrm{q_i}$ is assumed to be the same across protocols for each participant, $\mathrm{b_{TG_c}}$ is constant across participants for the specific method, and $\epsilon_{\mathrm{TG_c}}$ is the error without the influence of bias (which has been addressed with the $\mathrm{b_{TG_c}}$ term). $\dot{Q}_{\mathrm{TG_{o,i}}}$ can be expressed similarly. The model term for both protocols can then be substituted back into equation 4.2:

$$\mathrm{Covar}(\mathrm{TG_c}, \mathrm{TG_o}) = \frac{1}{(\mathrm{n}-1)} \sum \left[(\mathrm{q_i} + \mathrm{b_{TG_c}} + \epsilon_{\mathrm{TG_{c,i}}} - \bar{Q}_{\mathrm{TG_c}})(\mathrm{q_i} + \mathrm{b_{TG_o}} + \epsilon_{\mathrm{TG_{o,i}}} - \bar{Q}_{\mathrm{TG_o}}) \right] \tag{4.4}$$

Equation 4.4 can be partially expanded by multiplying both protocol terms by the error terms of the other protocol:

$$\begin{aligned} \mathrm{Covar}(\mathrm{TG_c}, \mathrm{TG_o}) = \frac{1}{(\mathrm{n}-1)} \sum \Big[& (\mathrm{q}_i + \mathrm{b_{TG_c}} - \bar{Q}_{\mathrm{TG_c}})(\mathrm{q}_i + \mathrm{b_{TG_o}} - \bar{Q}_{\mathrm{TG_o}}) \\ & + \epsilon_{\mathrm{TG_{o,i}}}(\mathrm{q}_i + \mathrm{b_{TG_c}} - \bar{Q}_{\mathrm{TG_c}}) + \epsilon_{\mathrm{TG_{c,i}}}(\mathrm{q}_i + \mathrm{b_{TG_o}} - \bar{Q}_{\mathrm{TG_o}}) \\ & + \epsilon_{\mathrm{TG_{c,i}}} \cdot \epsilon_{\mathrm{TG_{o,i}}} \Big] \end{aligned} \tag{4.5}$$

The expected values can then be taken. The mean term for both protocols can be expected to be the sum of the true cardiac output mean ($\bar{Q}$) and the protocol bias. The error terms ($\epsilon_{\mathrm{TG_{c,i}}}$ and $\epsilon_{\mathrm{TG_{o,i}}}$) each have a mean of zero and are uncorrelated with any of the terms for

which they are multipliers. The expression for the expected covariance becomes:

$$\begin{aligned}\mathrm{Covar}(\mathrm{TG_c}, \mathrm{TG_o}) &= \mathbb{E}\Big[\sum\Big[(\mathrm{q}_i + \mathrm{b}_{\mathrm{TG_c}} - (\bar{\mathrm{q}} + \mathrm{b}_{\mathrm{TG_c}}))(\mathrm{q}_i + \mathrm{b}_{\mathrm{TG_o}} - (\bar{\mathrm{q}} + \mathrm{b}_{\mathrm{TG_o}}))\Big]\Big] \\ &= \mathbb{E}\Big[\sum\Big[(\mathrm{q}_i - \bar{\mathrm{q}})(\mathrm{q}_i - \bar{\mathrm{q}})\Big]\Big] \\ &= \mathrm{Var}(\mathrm{q})\end{aligned} \tag{4.6}$$

There are two assumptions made in the set of equations listed above that have been mentioned, but require highlighting. Firstly, an assumption is made that the model term for the cardiac output, e.g. $\dot{Q}_{\mathrm{TG_{c,i}}}$ can be expressed in terms of a bias and error as outlined in equation 4.3. Secondly, it is assumed that the true cardiac output for each participant, q_i, is constant across all four protocols.

As the Pearson correlation coefficient is given by:

$$r = \frac{\mathrm{Covar}(\mathrm{TG_c}, \mathrm{TG_o})}{\sqrt{\mathrm{Var}(\mathrm{TG_c}) \cdot \mathrm{Var}(\mathrm{TG_o})}} \tag{4.7}$$

It follows that the ICCs for $\mathrm{TG_c}$ relative to $\mathrm{TG_o}$ and vice versa are:

$$\mathrm{ICC}_{\mathrm{TG_c}} = \frac{r \times \sqrt{\mathrm{Var}(\mathrm{TG_c}) \cdot \mathrm{Var}(\mathrm{TG_o})}}{\mathrm{Var}(\mathrm{TG_c})} \tag{4.8}$$

$$\mathrm{ICC}_{\mathrm{TG_o}} = \frac{r \times \sqrt{\mathrm{Var}(\mathrm{TG_o}) \cdot \mathrm{Var}(\mathrm{TG_c})}}{\mathrm{Var}(\mathrm{TG_o})} \tag{4.9}$$

Given there are four protocols, there will be three estimates of ICC for each protocol from the three correlations. These may be averaged to give an overall estimate of the ICC for each protocol.

4.3 Results

4.3.1 Participants

14 participants were recruited to take part in the study. One participant was only able to tolerate the first of four protocols and was therefore excluded from the final analysis. None of the participants had any cardiovascular or respiratory diseases of note. There were no smokers in the cohort. Their baseline characteristics are shown in table 4.1. A high N_2 balance was observed with participant 3's TG_o dataset, due to a presumed circuit leak, therefore warranting exclusion from the analysis.

Table 4.1: Per-person baseline characteristics of the healthy volunteer cohort

Cohort ID	Age / years	Sex	Height / m	BMI / kg m^{-2}	S_pO_2 / %	Hb / g L^{-1}
1	20	Female	1.72	21	100	118
2	20	Male	1.88	27	97	147
3	20	Female	1.72	22	97	124
4	22	Male	1.87	23	98	147
5	20	Male	1.78	20	98	142
6	20	Female	1.63	21	99	142
7	19	Female	1.73	24	97	137
8	20	Male	1.80	23	98	147
9	20	Male	1.86	23	97	151
10	19	Female	1.68	19	96	133
11	20	Female	1.58	22	95	136
12	20	Female	1.71	22	98	134
13	25	Male	1.84	27	98	151

ID, identification number. BMI, body mass index. S_pO_2, pulse oximeter measured peripheral oxygen saturation. Hb, haemoglobin concentration.

4.3.2 Modelling

Examples of the airway gas compositions and of the tidal flows for each protocol, along with their CCP model predictions, for the three types of protocols are shown in figure 4.4.

The $\dot{Q}$ CVs for each protocol without and with 6% AD are shown in figure 4.5. A coefficient of variation of 5% or greater following the deletion of up to one outlier was used to flag potentially unreliable datasets; this was the same procedure applied that

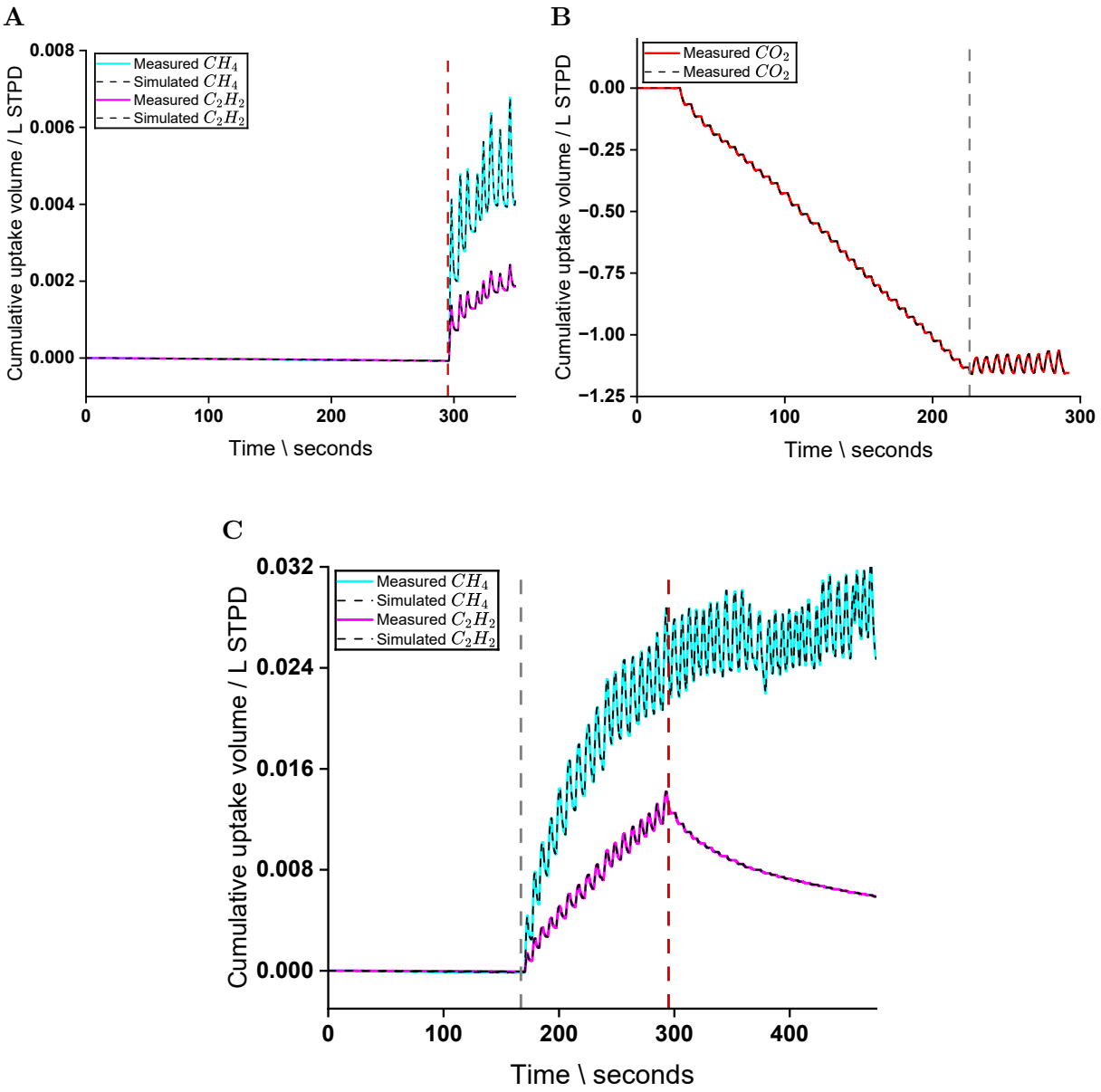

Figure 4.4: Examples of the exogenous closed-circuit (panel A) and open-circuit (panel C) and CO_2 rebreathing protocols (panel B). In panel A, the start of the rebreathing phase, preceded by the air-breathing phase, is indicated by the red, dashed line. For panels A and C, the measured uptake of CH_4 and C_2H_2 is seen by the cyan and magenta lines, respectively. In panel B, the start of the rebreathing phase, preceded by the air-breathing phase, is indicated by the grey, dashed line. The measured uptake of CO_2 can be seen by the red, dashed line. The negative trend prior to rebreathing represents a production of CO_2. Rebreathing through the reservoir bag results in the consumption of CO_2. In panel C, the start of the CH_4 and C_2H_2 breathing phase is indicated by the grey, dashed line; the delivery of C_2H_2 is stopped after two minutes, as indicated by the red, dashed line; the delivery of CH_4 is stopped two minutes after this. For all panels, the superimposed black, dashed lines represent the simulated uptake of the gases.

was used in the pulmonary hypertension cohort study. Following this, the dataset with the median cardiac output value for each of the participants' four protocols was used for further analysis. For ease of reference, the closed-circuit approach using exogenous tracer gases in the reservoir bag, two CO_2 rebreathing protocols, and open-circuit exogenous

tracer gas protocol, will be abbreviated as TG_c, CO_2 #1, CO_2 #2, and TG_o, respectively. For both non-6% AD and 6% AD runs, fits were not obtained for the TG_c protocols for participant 13, likely due to issues that arose during the air-breathing phase related to highly variable tidal breaths.

A Friedman test revealed a statistically significant difference in the $\dot{Q}$ CV across the different protocols ($\chi^2(3) = 17.945$, $p < 0.001$). A post hoc analysis with a Wilcoxon signed-rank test was conducted with a Bonferroni correction applied, resulting in a significance level set at $p < 0.0125$, to examine the specific differences between protocols. The second CO_2 protocol showed a significantly higher $\dot{Q}$ CV than the TG_c protocol (Z=-2.589, p=0.01). The first (Z=-3.059, p=0.002) and second (Z=-3.059, p=0.002) CO_2 protocols also had significantly higher $\dot{Q}$ CVs than the TG_o protocol. No statistically significant difference was found between the TG_c and TG_o protocols.

The CCP-estimated parameters for the exogenous tracer gas and CO_2 protocols are shown in tables 4.2 and 4.3, respectively.

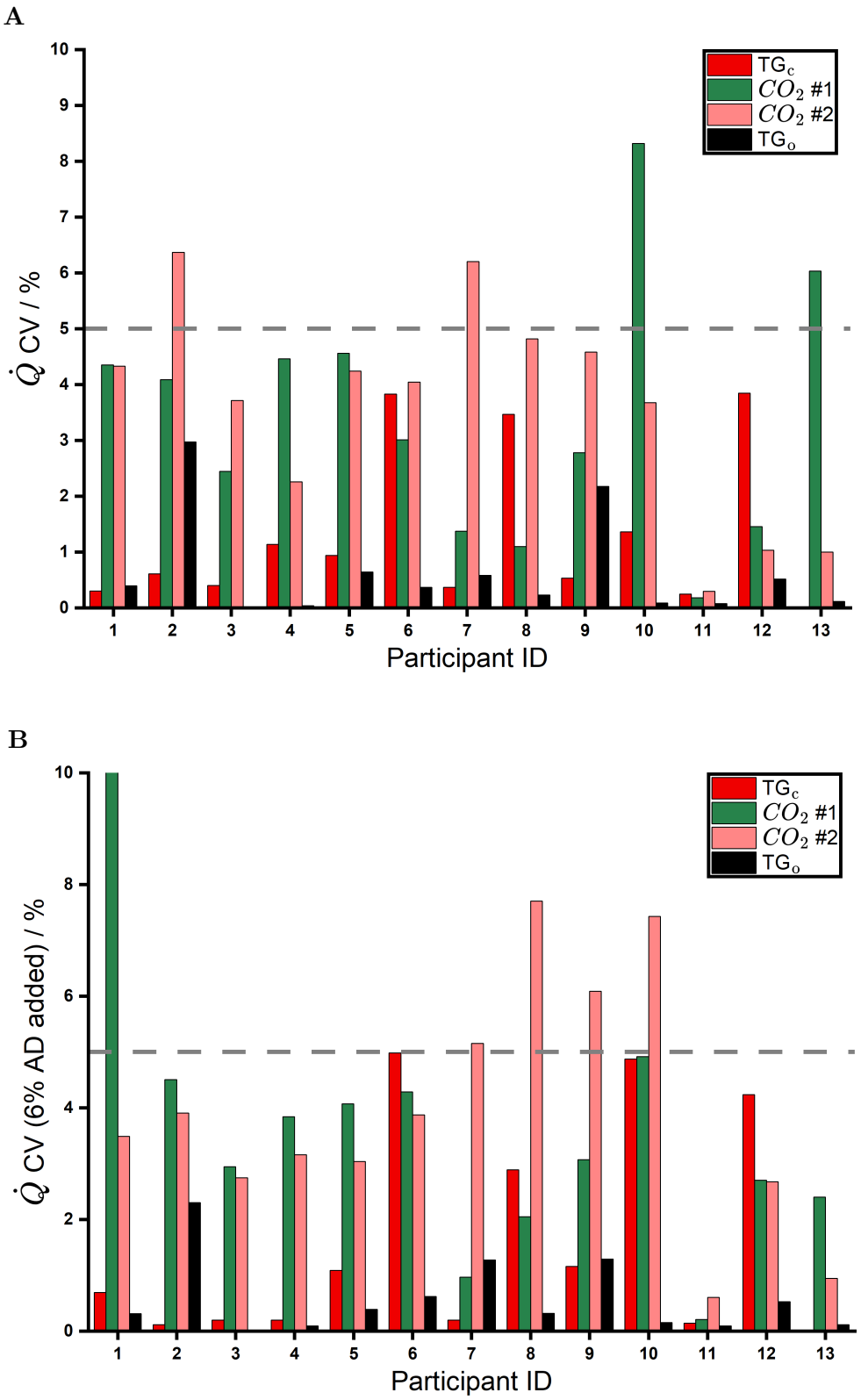

Figure 4.5: Comparison of the $\dot{Q}$ CVs for the four experimental protocols. Panel A shows the $\dot{Q}$ CVs for the non-6% AD fits. Panel B shows the $\dot{Q}$ CVs for the 6% AD fits. In panel A, the TG_o (black) column is not visible due to scale for participant 4; the CV was 0.04%. In panel B, the CO_2 #1 (green) column is cut off at the y-axis; the CV was 10.56%. The dashed grey line in both panels indicates the 5% cutoff value at which fits were deemed potentially unreliable.

Table 4.2: Fit parameter values from the exogenous tracer gas fits for all participants

Cohort ID	Protocol	V_A / L BTPS	V_D / L BTPS	C_{V_D}	σV_D	σC_L	P_iCO_2 / kPa	$\dot{V}O_2$ / mL min^{-1}	RQ	$\dot{Q}$ / L min^{-1}	$S_{\bar{v}}O_2$ / %
1	TG_c	3.44	0.09	0.11	0.34	0.55	4.74	313	0.77	5.7	65
2	TG_c	3.72	0.15	0.51	0.33	0.43	5.23	436	0.91	10.2	77
3	TG_c	2.96	0.13	0.00	0.31	0.46	4.20	324	0.95	6.0	68
4	TG_c	5.09	0.13	0.99	0.37	0.62	5.42	412	0.79	6.7	67
5	TG_c	3.98	0.12	1.00	0.30	0.45	4.93	393	0.72	7.5	72
6	TG_c	2.41	0.08	0.00	0.31	0.50	5.75	298	0.70	6.3	72
7	TG_c	2.46	0.08	1.00	0.32	0.50	4.41	375	0.87	5.7	64
8	TG_c	3.05	0.15	0.25	0.26	0.49	5.22	416	0.71	9.2	76
9	TG_c	3.65	0.18	0.12	0.11	0.49	4.84	420	0.78	6.2	66
10	TG_c	3.54	0.09	1.00	0.47	0.65	5.01	189	0.72	3.2	65
11	TG_c	2.67	0.06	0.00	0.47	0.51	4.30	298	0.82	5.2	69
12	TG_c	3.19	0.07	0.78	0.19	0.62	4.88	302	1.00	3.8	56
13	TG_c	-	-	-	-	-	-	-	-	-	-
Mean		3.33 ± 0.72	0.11 ± 0.03	0.41 ± 0.40	0.33 ± 0.10	0.53 ± 0.07	4.90 ± 0.45	332 ± 71	0.83 ± 0.10	6.2 ± 1.9	68 ± 6
1	TG_o	3.47	0.08	0.94	0.39	0.57	4.50	260	0.74	4.7	65
2	TG_o	3.60	0.12	1.00	0.45	0.41	4.98	424	0.74	8.3	73
3	TG_o	-	-	-	-	-	-	-	-	-	-
4	TG_o	4.52	0.11	1.00	0.27	0.59	5.33	388	0.81	6.8	70
5	TG_o	3.87	0.11	1.00	0.27	0.46	4.89	343	0.74	5.5	66
6	TG_o	2.44	0.08	0.43	0.26	0.54	5.61	232	0.75	3.2	59
7	TG_o	2.35	0.09	0.38	0.29	0.51	4.27	299	0.97	4.9	67
8	TG_o	3.38	0.13	0.16	0.22	0.50	4.74	374	0.91	7.4	74
9	TG_o	3.88	0.14	0.77	0.29	0.42	4.87	353	0.90	5.0	65
10	TG_o	3.20	0.08	1.00	0.47	0.53	4.79	181	0.74	2.7	62
11	TG_o	2.70	0.06	0.00	0.67	0.63	4.34	279	0.85	3.9	61
12	TG_o	2.95	0.07	0.16	0.27	0.49	5.15	240	0.89	3.7	63
13	TG_o	3.23	0.13	0.31	0.39	0.61	3.76	352	0.88	5.7	70
Mean		3.31 ± 0.60	0.10 ± 0.03	0.59 ± 0.35	0.36 ± 0.13	0.53 ± 0.07	4.71 ± 0.46	309 ± 69	0.82 ± 0.09	4.9 ± 1.7	66 ± 5

Mean ± standard deviation. V_A, alveolar volume. V_D, dead space volume at functional residual capacity. C_{V_D}, fractional expansion of dead space relative to the fractional expansion of the alveolar space. σV_D, standard deviation of the standardised dead space. σC_L, standard deviation for the natural logarithm of the standardised lung vascular compliance. P_iCO_2, ideal partial pressure of CO_2. RQ, respiratory quotient. σCd, standard deviation for the natural logarithm of the standardised lung vascular conductance, is not shown in this table, but is equal to σC_L+0.3.

Table 4.3: Fit parameter values from the CO_2 fits for all participants

Cohort ID	Protocol	V_A / L BTPS	V_D / L BTPS	C_{V_D}	σV_D	σC_L	P_iCO_2 / kPa	$\dot{V}O_2$ / mL min^{-1}	RQ	$\dot{Q}$ / L min^{-1}	$S_{\bar{v}}O_2$ / %
1	CO_2 #1	3.63	0.08	0.50	0.36	0.56	4.54	303	0.70	7.6	75
2	CO_2 #1	3.81	0.14	0.35	0.34	0.40	5.24	433	0.72	7.1	68
3	CO_2 #1	3.07	0.10	1.00	0.28	0.48	4.08	314	0.93	5.1	64
4	CO_2 #1	4.85	0.10	0.98	0.29	0.58	5.39	413	0.74	7.8	72
5	CO_2 #1	4.21	0.11	0.66	0.28	0.46	5.00	377	0.70	7.4	72
6	CO_2 #1	2.61	0.07	0.10	0.34	0.53	5.53	248	0.70	3.5	61
7	CO_2 #1	2.47	0.08	0.38	0.35	0.43	4.59	370	0.83	4.3	54
8	CO_2 #1	3.46	0.11	0.84	0.32	0.47	5.19	399	0.91	7.5	72
9	CO_2 #1	3.83	0.15	0.49	0.26	0.40	5.28	406	0.88	6.6	69
10	CO_2 #1	3.88	0.10	1.00	0.41	0.65	4.97	183	0.77	2.1	51
11	CO_2 #1	2.86	0.06	0.04	0.28	0.53	4.29	309	0.82	3.5	52
12	CO_2 #1	2.95	0.08	0.47	0.26	0.58	4.96	269	0.95	4.1	63
13	CO_2 #1	3.39	0.16	0.05	0.44	0.57	4.05	375	0.96	5.4	67
Mean		3.47 ± 0.64	0.10 ± 0.03	0.52 ± 0.34	0.32 ± 0.06	0.51 ± 0.07	4.91 ± 0.45	339 ± 60	0.81 ± 0.10	5.5 ± 1.8	65 ± 8
1	CO_2 #2	3.88	0.09	0.51	0.26	0.64	4.60	306	0.70	7.7	74
2	CO_2 #2	3.91	0.15	0.07	0.27	0.40	5.00	416	0.70	6.2	65
3	CO_2 #2	3.09	0.11	0.70	0.31	0.51	4.27	333	0.70	5.1	61
4	CO_2 #2	4.90	0.10	0.98	0.32	0.65	5.41	408	0.77	6.3	66
5	CO_2 #2	4.31	0.11	0.67	0.38	0.41	4.92	362	0.70	4.7	59
6	CO_2 #2	2.60	0.07	0.18	0.32	0.53	5.58	258	0.76	3.3	57
7	CO_2 #2	2.59	0.08	0.00	0.32	0.41	4.69	382	0.70	5.5	62
8	CO_2 #2	3.51	0.15	0.00	0.22	0.51	5.26	397	0.83	7.2	71
9	CO_2 #2	3.97	0.16	0.45	0.22	0.47	5.31	406	0.96	6.1	67
10	CO_2 #2	3.76	0.10	1.00	0.29	0.67	5.03	186	0.77	2.8	62
11	CO_2 #2	2.93	0.06	0.00	0.63	0.53	4.40	320	0.76	3.3	47
12	CO_2 #2	2.87	0.07	0.15	0.19	0.57	5.28	267	0.85	3.6	58
13	CO_2 #2	3.13	0.18	0.02	0.41	0.59	3.98	377	0.85	6.2	70
Mean		3.49 ± 0.66	0.11 ± 0.04	0.31 ± 0.35	0.31 ± 0.12	0.52 ± 0.08	4.96 ± 0.43	333 ± 64	0.77 ± 0.08	5.2 ± 1.5	63 ± 8

Mean ± standard deviation. V_A, alveolar volume. V_D, dead space volume at functional residual capacity. C_{V_D}, fractional expansion of dead space relative to the fractional expansion of the alveolar space. σV_D, standard deviation of the standardised dead space. σC_L, standard deviation for the natural logarithm of the standardised lung vascular compliance. P_iCO_2, ideal partial pressure of CO_2. RQ, respiratory quotient. σCd, standard deviation for the natural logarithm of the standardised lung vascular conductance, is not shown in this table, but is equal to σC_L+0.3.

4.3.3 Inter-protocol comparison

This section outlines the stepwise process for examining the CCP estimates for cardiac output and $S_{\bar{v}}O_2$. The relative bias and precisions between protocols are presented; the derivation processes of which were described in the Methods section (section 4.2).

Statistical comparisons of respiratory parameters

As a preliminary step, the fit respiratory parameters across protocols (tables 4.2 and 4.3) were compared. Variability of these parameters across the protocols may cause differences in cardiac output and as such, they were compared for statistically significant differences. Friedman tests were conducted for each of the respiratory parameters, with only V_A being significantly different across groups ($\chi^2(3) = 14.229$, $p = 0.003$). A post hoc Wilcoxon signed-rank test with a Bonferroni correction (significance level set at $p < 0.0125$) for V_A showed a significant difference between the CO_2#1 and TG_o (Z=-2.851, p=0.004) and CO_2#2 and TG_o (Z=-2.746, p=0.006) protocols. Here, the CO_2 protocols estimated smaller alveolar volumes than the TG_o protocol.

General comparisons of cardiac output

The CCP-estimated parameters for each protocol, including cardiac output, were shown in tables 4.2 and 4.3. The median cardiac output estimates for each protocol were: 6.1 ± 2 L/minute for TG_c, 5.3 ± 1.9 L/minute for CO_2 #1, 5.3 ± 1.4 L/minute for CO_2 #2, and 5 ± 1.8 L/minute for TG_o.

Cardiac output bias

When comparing the results of the experimental protocols against each other, the first stage of analysis was to look for patterns of relative bias. Firstly, the cardiac outputs of the two identical CO_2 protocols were compared against each other, as shown in figure 4.6. In general, there was good correlation between these protocols. The positive bias of 310 mL/minute towards the first CO_2 protocol relative the second CO_2 one is mostly explained by the large difference for participant 5's results.

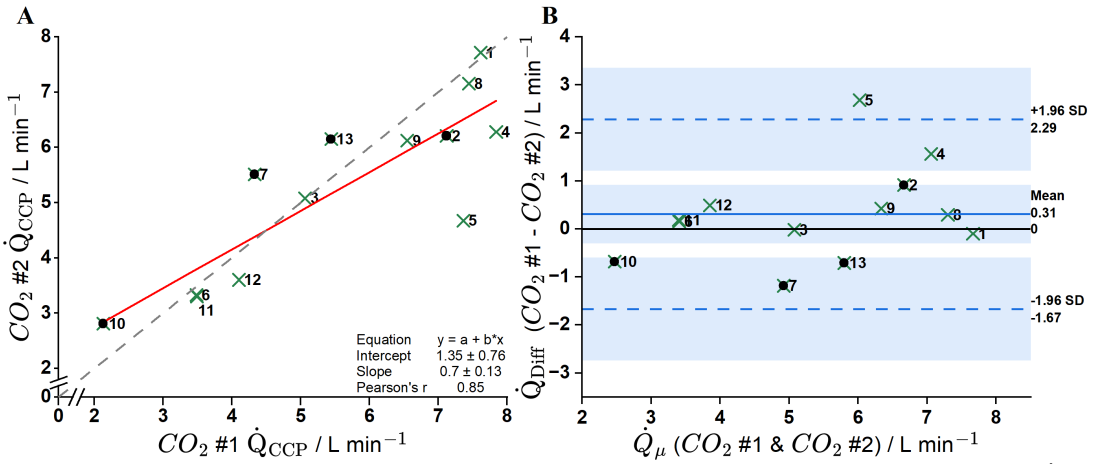

Figure 4.6: Comparisons for CCP cardiac output estimates for the two CO_2 protocols. $\dot{Q}_{\mu}$ is the mean of the cardiac outputs. $\dot{Q}_{diff}$ is the difference between values. Flagged datasets based on the 5% $\dot{Q}$ CV cutoff are marked with black dots. Grey, dashed line, line of identity; red line, regression line; b, regression slope; a, regression intercept.

Similarly, figure 4.7 shows the cardiac output comparisons for the two CO_2 protocols individually against the mean of the two exogenous tracer gas protocols (TG_{μ}). A greater degree of bias can be seen for the CO_2 #2 protocol, where the cardiac output is underestimated by 500 mL/minute compared to the exogenous tracer gas cardiac output. A poorer correlation than for the CO_2 #1 protocol is also seen.

Finally, the two exogenous tracer gas protocols were assessed for differences, the comparison plots are shown in figure 4.8. While there is a clear bias towards higher cardiac output values for the TG_c protocol, the excellent correlation between the protocols suggests a significant degree of proportional reproducibility.

The cardiac output values between protocols were examined for statistically significant differences. A Friedman test revealed a statistically significant difference ($\chi^2(3) = 11.073$, $p = 0.011$). A post hoc Wilcoxon signed-rank test with a Bonferroni correction (significance level set at $p < 0.0125$) for cardiac output showed a significant difference only between the TG_o and TG_c (Z=-2.845, p=0.004).

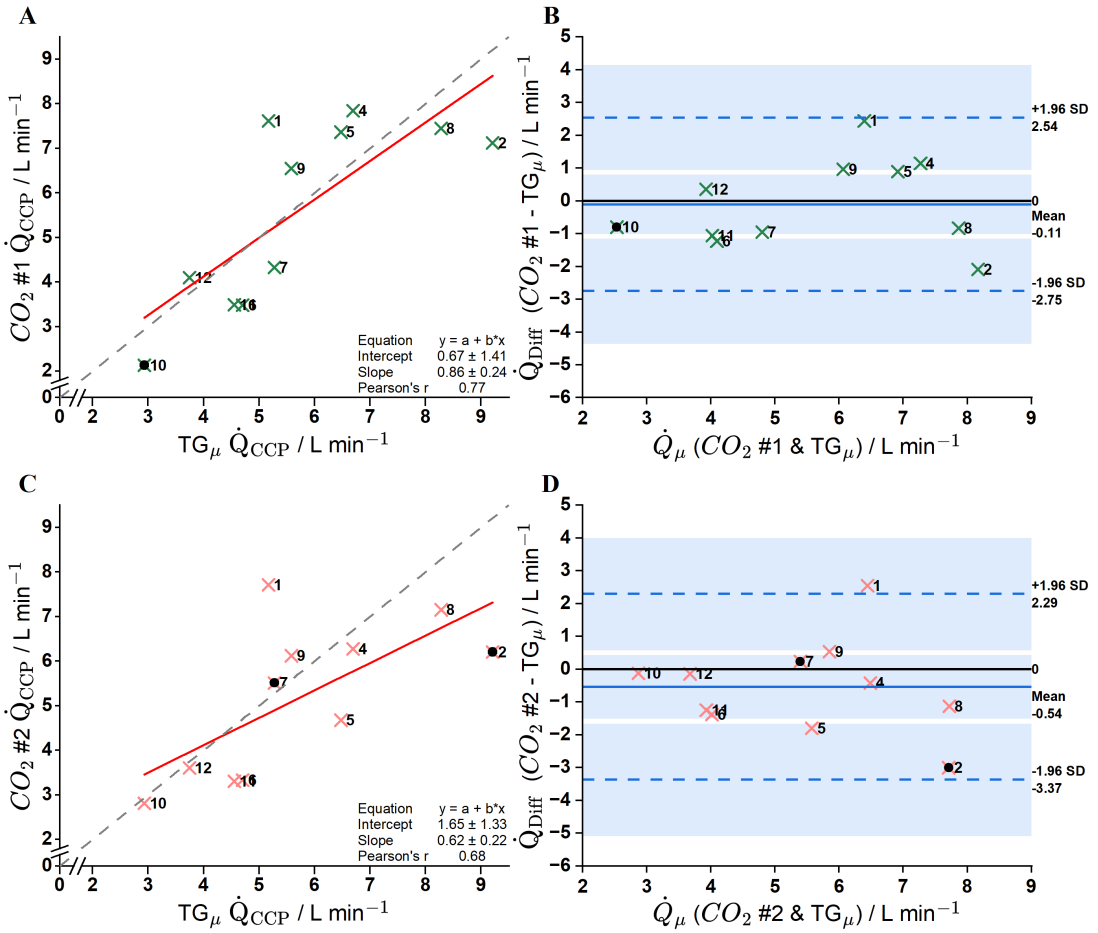

Figure 4.7: Comparisons for CCP cardiac output estimates for the CO_2 protocols against the mean of the exogenous tracer gas protocols. Panels A and B compare the CO_2 #1 protocol against the mean cardiac output of the TG_c and TG_o protocols (TG_μ). Panels C and D compare the same for the CO_2 #2 protocol. Participants 3 and 13 were excluded as both had missing exogenous tracer gas values. Grey, dashed line, line of identity; red line, regression line; b, regression slope; a, regression intercept.

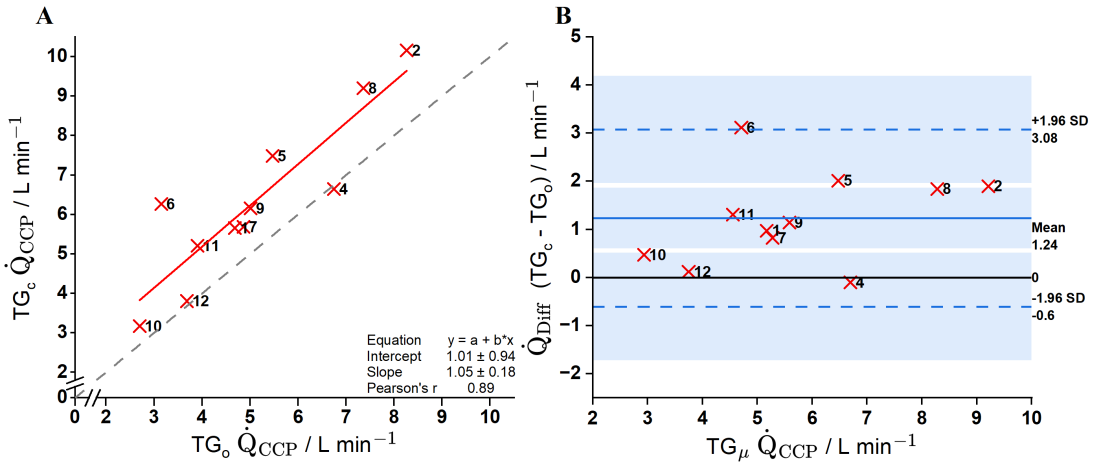

Figure 4.8: Comparisons for CCP cardiac output estimates for the two exogenous tracer gas protocols. Participants 3 and 13 were excluded as both had missing exogenous tracer gas values. Flagged datasets based on the 5% $\dot{Q}$ CV cutoff are marked with black dots. Grey, dashed line, line of identity; red line, regression line; b, regression slope; a, regression intercept.

Cardiac output variance, correlation, and precision

As discussed in section 4.2.3, the relative precision of the cardiac output (and $S_{\bar{v}}O_2$) CCP estimates for the different protocols may be assessed using the intraclass correlation coefficient (ICC). For each protocol, three ICC estimates may be calculated from the correlations with the other three protocols as shown in equations 4.8 and 4.9. An overall estimate of the ICC for each protocol can then be given by taking the mean of the three calculated estimates. The calculated correlation coefficients and variances for cardiac output, including the Var(q) values, are given in table 4.4.

Table 4.4: Protocol correlation coefficients and variances for cardiac output

Correlation coefficient (r)	TG_c	CO_2#1	CO_2#2	TG_o
TG_c	-	0.70	0.60	0.89
CO_2#1	-	-	0.85	0.80
CO_2#2	-	-	-	0.73
Protocol variance / (L min^{-1})^2	3.91	3.66	2.48	2.87
Var(q) / (L min^{-1})^2				
TG_c	-	2.65	1.87	2.98
CO_2#1	-	-	2.56	2.59
CO_2#2	-	-	-	2.09
Mean ICC	0.64	0.71	0.86	0.87

The values for the TG_c and first CO_2 protocols are indicative of moderate reliability, while the values for the second CO_2 and TG_o indicate good to excellent reliability.(114)

General comparisons for $S_{\bar{v}}O_2$

The median $S_{\bar{v}}O_2$ estimates for each protocol were: 68 ± 6 % for TG_c, 65 ± 8 % for CO_2 #1, 62 ± 6 % for CO_2 #2, and 66 ± 5 % for TG_o.

$S_{\bar{v}}O_2$ bias

The CCP estimates of $S_{\bar{v}}O_2$ for the two CO_2 protocols are shown in figure 4.9. Moderate correlation was seen between the two protocols, with the three datasets in particular seen to be outlying (participants 5, 7, and 10), two of whom were flagged due to a high $\dot{Q}$ CV. There was minimal bias, as shown by the mean difference of 1.5 % in the Bland-Altman plot in panel B of figure 4.9.

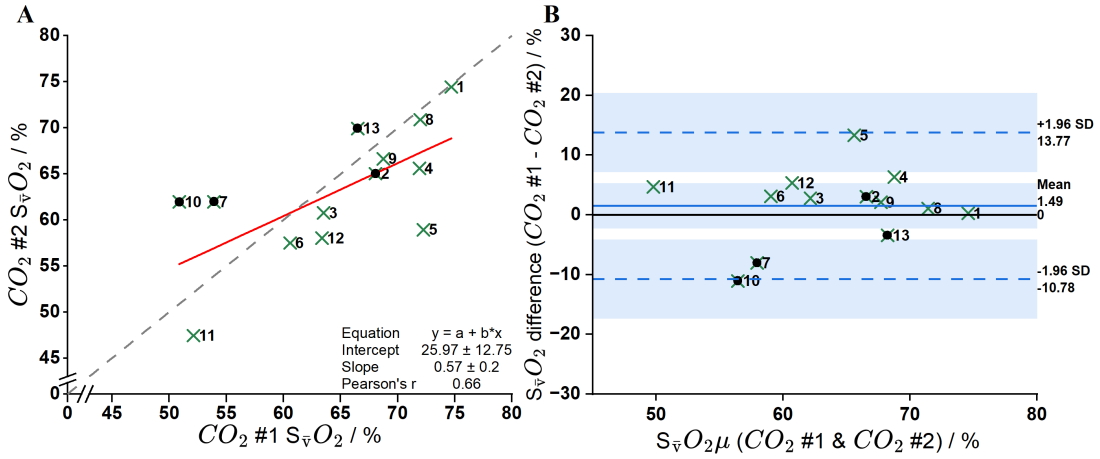

Figure 4.9: Comparisons for CCP $S_{\bar{v}}O_2$ estimates for the two CO_2 protocols. $S\bar{v}O_2\mu$ is the mean of the cardiac outputs. Flagged datasets based on the 5% $\dot{Q}$ CV cutoff are marked with black dots. Grey, dashed line, line of identity; red line, regression line; b, regression slope; a, regression intercept.

The comparisons for the individual CO_2 protocols against the mean $S_{\bar{v}}O_2$ of the two exogenous protocols is shown in figure 4.7. The correlation for both comparisons was relatively weak. A slight degree of bias towards a lower CO_2 protocol-estimated $S_{\bar{v}}O_2$ is also observed, this bias was not significantly different between protocols. The limits of agreement were also similar in comparison.

The comparison between the two exogenous tracer gas protocols is shown in figure 4.11. A moderate correlation is observed. The data was not overly biased, however, most datasets had higher TG_c estimates of $S_{\bar{v}}O_2$.

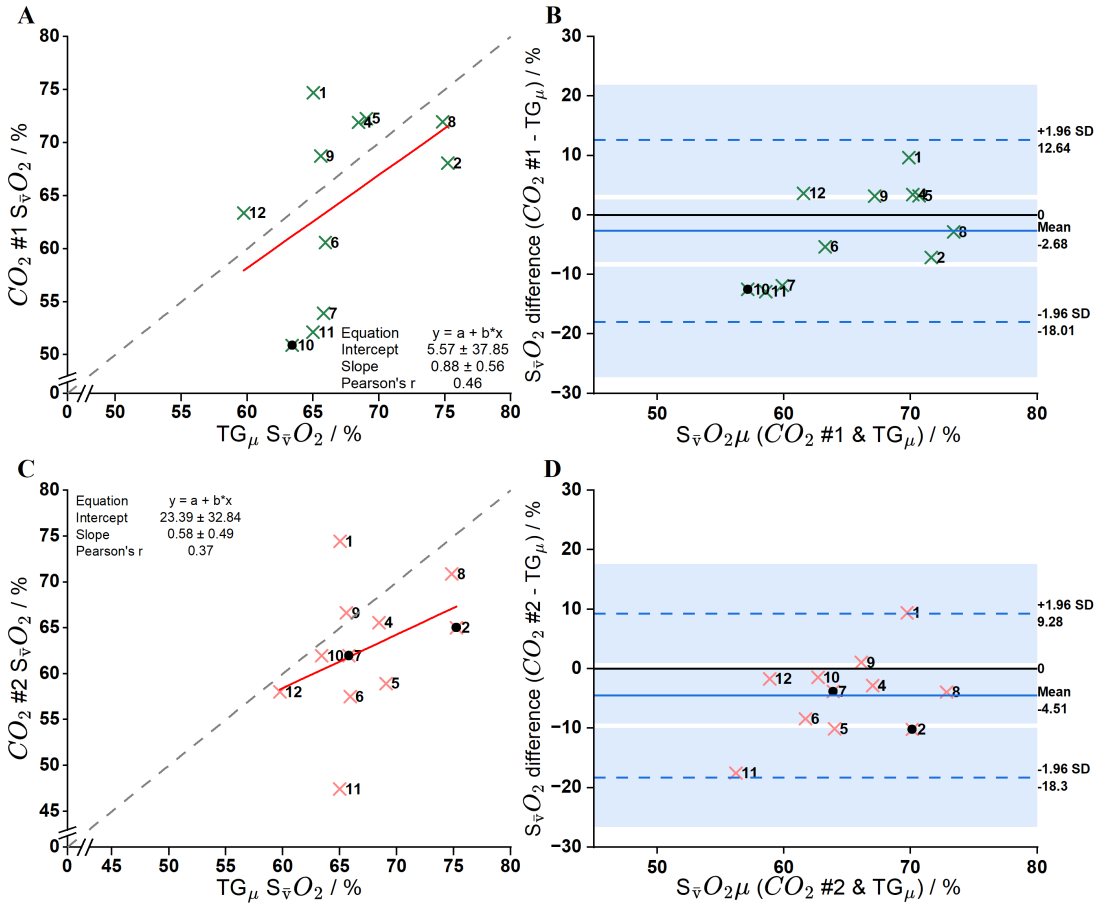

Figure 4.10: Comparisons for CCP $S_{\bar{v}}O_2$ estimates for the CO_2 protocols against the mean of the exogenous tracer gas protocols. Panels A and B compare the CO_2 #1 protocol against the mean $S_{\bar{v}}O_2$ of the TG_c and TG_o protocols. Panels C and D compare the same for the CO_2 #2 protocol. Participants 3 and 13 were excluded as both had missing exogenous tracer gas values. Grey, dashed line, line of identity; red line, regression line; b, regression slope; a, regression intercept.

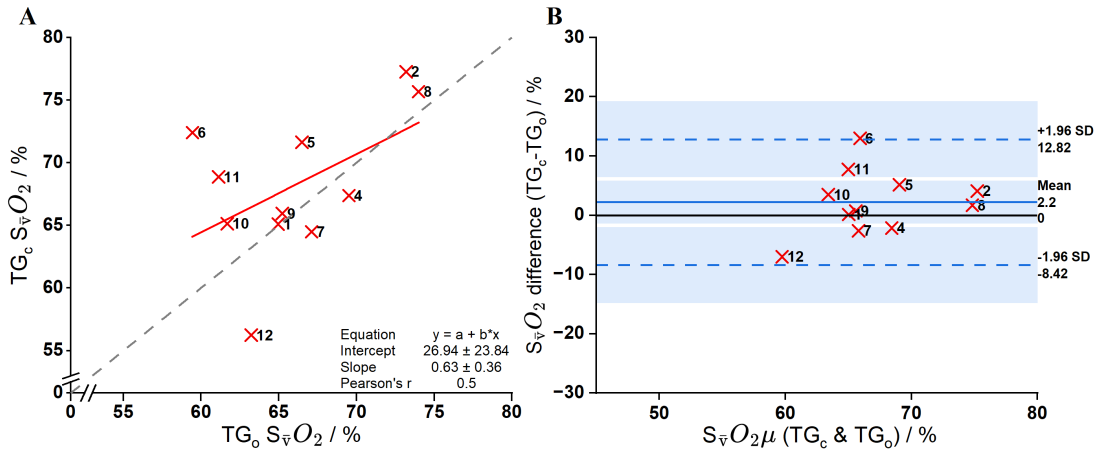

Figure 4.11: Comparisons for CCP cardiac output estimates for the two exogenous tracer gas protocols. Participants 3 and 13 were excluded as both had missing exogenous tracer gas values. Flagged datasets based on the 5% $\dot{Q}$ CV cutoff are marked with black dots. Grey, dashed line, line of identity; red line, regression line; b, regression slope; a, regression intercept.

A Friedman test for the $S_{\bar{v}}O_2$ CCP estimates revealed no statistical differences ($\chi^2(3) = 5.509$, $p = 0.138$). Therefore, no statistical tests within protocol pairs were indicated.

$S_{\bar{v}}O_2$ variance, correlation, and precision

The same calculations for variance and correlation made for cardiac output can be repeated for $S_{\bar{v}}O_2$. Table 4.5 shows the correlation coefficients and variances for $S_{\bar{v}}O_2$.

Table 4.5: Protocol correlation coefficients and variances for $S_{\bar{v}}O_2$

Correlation coefficient (r)	TG_c	CO_2#1	CO_2#2	TG_o
TG_c	-	0.61	0.12	0.50
CO_2#1	-	-	0.29	0.41
CO_2#2	-	-	-	0.60
Protocol variance / (%)²	32	65	49	22
Var(q) (%)²				
TG_c	-	28	5	13
CO_2#1	-	-	16	15
CO_2#2	-	-	-	13
Mean ICC	0.48	0.31	0.28	0.70

The ICCs were expectedly worse than those for cardiac output. As Koo and Li indicate, values with a lower variability among sampled subjects will result in a lower ICC value.(114) In this case, $S_{\bar{v}}O_2$ values across participants will vary less than for estimates of cardiac output, which are influenced by factors such as body surface area. For the $S_{\bar{v}}O_2$ estimates, compared to the cardiac output estimates, the TG_o was indicative of greater reliability than the other protocols.

Alveolar dead space

With one exception (participant 6 for the TG_c protocol) across the protocols, the cardiac output estimates increased in a roughly linear way following the addition of alveolar dead space to the model. The magnitude of this change was significantly greater for the CO_2 protocols than the exogenous tracer gas ones.

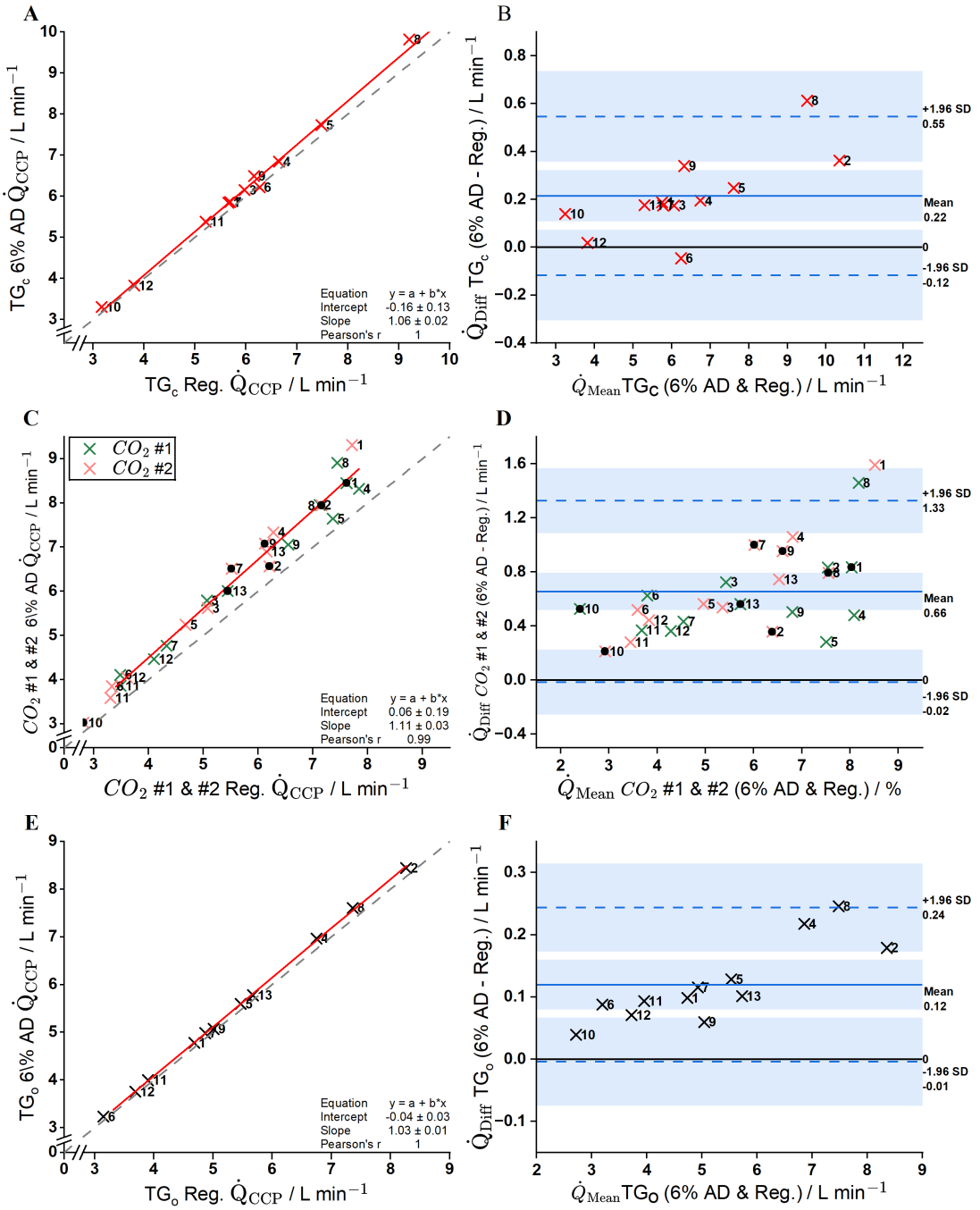

Figure 4.12: Comparisons for cardiac output between the 6% AD and regular (reg.) fits for each protocol. Panels A and B compare the TG_c fits, C and D compare the combined CO_2 protocol fits, and E and F compare the TG_o fits. $\dot{Q}_{Mean}$ is the mean of the 6% AD and regular cardiac output estimates. The black dots indicate datasets which were flagged due to a high $\dot{Q}$ CV for either or both of the 6% AD and regular fits. Grey, dashed line, line of identity; red line, regression line; b, regression slope; a, regression intercept.

The results of adding alveolar dead space to $S_{\bar{v}}O_2$ are shown in figure 4.13. For most datasets, the $S_{\bar{v}}O_2$ was slightly higher following the addition of alveolar dead space to the model. For the cardiac output estimates, the CO_2 datasets were the most affected by the addition of dead space.

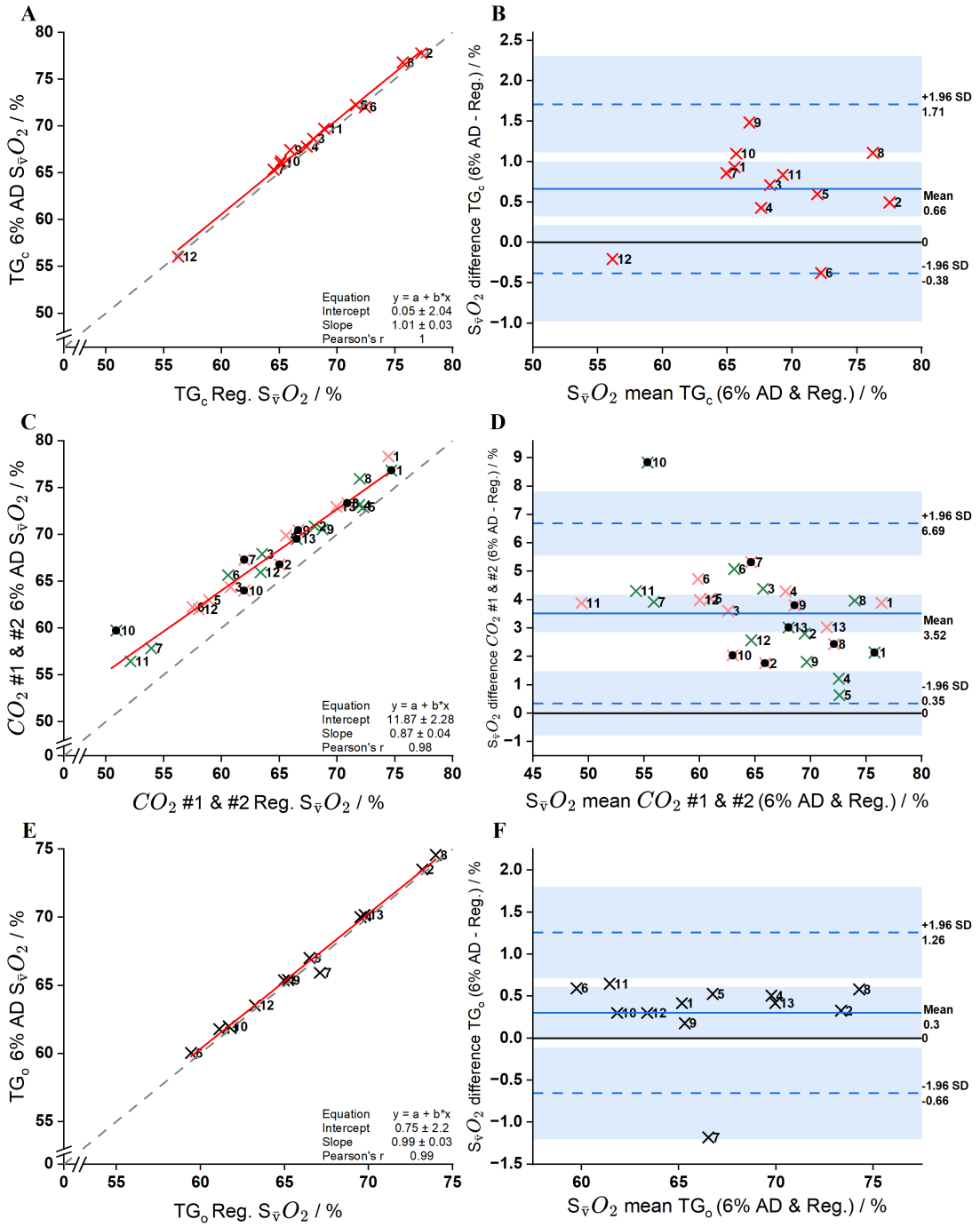

Figure 4.13: Comparisons for $S_{\bar{v}}O_2$ between the 6% AD and regular (reg.) fits for each protocol. Panels A and B compare the TG_c fits, C and D compare the combined CO_2 protocol fits, and E and F compare the TG_o fits. The black dots indicate datasets which were flagged due to a high $\dot{Q}$ CV for either or both of the 6% AD and regular fits. Grey, dashed line, line of identity; red line, regression line; b, regression slope; a, regression intercept.

4.4 Discussion

4.4.1 Protocol feasibility

The potential benefits of a closed-circuit approach, as used for the TG_c and CO_2 protocols, were discussed in chapter 3. Briefly, the short length of the protocol (around four minutes) and flexibility to fill the reservoir bag ahead of time make it easier to implement in clinical and research settings. The four protocols were conducted on the same day, primarily to enable fair comparison. However, this also demonstrated that these CCP protocols may be repeated without issue. In general, participants were willing and comfortable completing the full series of protocols in relatively quick succession. One participant withdrew from the study after the first protocol, citing respiratory discomfort when breathing through the MFS. This was likely related to anxiety in the context of having an underlying psychiatric history, and not an issue commonly seen with volunteers or patients breathing on the device.

For the TG_c protocol, the gas mixture in the reservoir bag was made up to approximately 21% and not 40% O_2 as it had been for the pulmonary hypertension cohort. This was due to the fact that the healthy volunteer study was conducted before recruitment for the pulmonary hypertension cohort had begun. Reducing hyperventilation during the rebreathing period by increasing the starting concentration of O_2 was only proposed following the conclusion of the former study.

To estimate cardiac output using CCP, a measured haemoglobin value is required. For all other biochemical parameters, which are usually input during the data processing stage (prior to modelling), such as electrolytes and O_2 and CO_2 partial pressures, standard values may be used to construct the blood sub-model. To avoid the requirement for laboratory processing of blood samples and to give participants the choice of a capillary draw instead of a venous one, only haemoglobin was measured, using the HemoCue Hb 201+ point-of-care device. As this cohort consisted only of relatively young and healthy participants, it is unlikely that estimating the other blood values would have significantly affected the accuracy of CCP-estimated parameters.

As a gas which is endogenous to the body, CO_2 is an attractive alternative to the exogenous tracer gases used for the other protocols. As discussed in section 1.3.4, indirect Fick methods which utilise CO_2 in this way have been described in the literature. Haryadi et al. compared their partial rebreathing CO_2 method against bolus thermodilution measurements of cardiac output in six canine subjects. Their experimental method correlated and agreed relatively well with thermodilution.(35) For this study, with healthy volunteers, a concentration of 7% was chosen based on previous preliminary experiments as one in which alveolar and arterial CO_2 levels would rise quickly (within the rebreathing period) and to a magnitude where the signal far exceeds the noise. All participants noted the taste associated with breathing in this high concentration of CO_2, however, none found it intolerable.

4.4.2 Modelling

The modelling approach was largely guided by the results of the pulmonary hypertension cohort. The main deviation from this was to use one termination sensitivity instead of three. Outlying datasets were again identified and flagged if the $\dot{Q}$ CV was $\geq 5\%$. Only the CO_2 protocols had outliers, suggesting a weakness with this particular protocol. Specifically, it is possible that a longer rebreathing time is required for a more definitive estimate of cardiac output when using CO_2 as a tracer gas and/or that the difficulty of recovering lung parameters affected the cardiac output estimates. Regarding the latter factor, the lung parameters would have primarily been estimated from the partial N_2 washout which occurs following the inhalation of the rebreathing mixture containing 93% O_2. In comparison, for regular CCP protocols, a full N_2 washout is performed by having the subject breathe 100% O_2 for five minutes. However, with reference to tables 4.2 and 4.3, which show the fit parameter values for each protocol, the fit respiratory parameters were only different for the two CO_2 protocols when compared to the TG_o protocol, where the former estimates were less than the latter's. This highlights that compared to a CH_4 based approach for estimating lung parameters, the CO_2 approach is partially, but not

wholly, comparable.

The $\dot{Q}$ CVs between protocols were compared using non-parametric tests and discussed in section 4.3.2. Compared to both CO_2 protocols, the $\dot{Q}$ CV for the TG_o protocol was significantly lower. While the two exogenous tracer gas protocols were not different, it is possible that with a larger sample size, the TG_o $\dot{Q}$ CV would have also been significantly lower than for the TG_c protocol. In future studies, this would ideally be tested with a larger sample size, as a lower $\dot{Q}$ CV would increase the strength of argument for using an open-circuit over a closed-circuit approach.

4.4.3 Inter-protocol comparison

Cardiac output bias

The analysis of relative bias between the cardiac output estimates of each protocol was discussed in section 4.3.3. The first comparison made was between the two CO_2 protocols (figure 4.6), to assess the reproducibility of the method over a short space of time. The two sets of results were strongly correlated, with some (310 mL/minute) bias towards a higher cardiac output with the CO_2 #1 protocol. As most participants had mean cardiac output estimates of over 4 L/minute, this equates to a less than 10% mean difference in the values. Of uncertain significance is that three of the four flagged datasets underestimated the CO_2 #1 cardiac output relative to CO_2 #2; only one other dataset had a lower CO_2 #1 cardiac output estimate than CO_2 #2.

The difference between the two CO_2 protocols is made more evident when comparing each of them to the mean cardiac output estimates for the exogenous tracer gas protocols (TG_μ), as shown in figure 4.7. Here, the CO_2 #1 protocol estimates correlate better with the TG_μ estimates than the CO_2 #2 and TG_μ pair. There is also a greater magnitude of bias with the latter comparison, although both comparisons yield higher TG_μ cardiac output values on average. The reason for the higher estimates with the exogenous tracer gases may potentially be due to CCP modelling factors. Particularly, it is possible estimating

cardiac output using C_2H_2, where the starting concentration in the body is zero, lends to a higher value, than for CO_2, even at a high inspired concentration.

The most notable aspect of the comparison between the two exogenous tracer gas protocols (figure 4.8) is the significant positive bias, of over 1 L/minute, with the TG_c cardiac output estimates. Despite this, the results are strongly correlated, with the overestimation of the TG_c relative to the TG_o protocol corresponding to a rise in the mean cardiac output. A consideration here is that the observation may be partially true, in that the open-circuit method results in a lower true cardiac output than rebreathing into a reservoir bag. To assess whether this is true, or if it is simply a case that one method over- or underestimates the true cardiac output (both may also be true), a measurement of cardiac output using a reference method would need to be taken at the time of both protocols.

In clinical situations where cardiac output monitoring is utilised, the trend over time is often more relevant than the absolute values. Therefore, the excellent correlation seen between the TG_c and TG_o protocols (panel A in figure 4.8), between the two CO_2 protocols (panel A in figure 4.6), and potentially also between the CO_2 #1 and mean of the exogenous tracer gas protocols (panel A in figure 4.7) suggest that the techniques in their current form could be serviceable as as trending monitor, even if the absolute estimated values are different to the true cardiac output values.

Cardiac output precision

The calculation of the intraclass correlation coefficient (ICC) was used to evaluate the relative precision of the four protocols. The ICC reflects both the degree of correlation and agreement between measurements.(114) As such, it was chosen as an alternative to comparing the estimates against a reference measurement standard of cardiac output and $S_{\bar{v}}O_2$.

The reason for the significant difference between the ICCs for the two CO_2 protocols is unclear, although likely related to the low sample size. Another possibility is that

participants were more comfortable rebreathing into the reservoir bag for the repeat study, resulting in a cardiac output closer to a resting state. This is somewhat supported by the decreasing variance of the three rebreathing protocols in the order of which they were performed.

The higher ICC with the TG_o compared to the TG_c protocol suggests that the former is more reliable when generating reliable cardiac output estimates. Although if the results from chapter 3 are considered, where the CCP-estimates of the TG_c protocol underestimated the reference method (direct Fick), the underestimation of the open-circuit protocol relative to the closed-circuit one may indicate greater reproducibility with less accuracy.

An assumption made when calculating the ICC for each protocol is that the true cardiac output for each participant remains constant across the four protocols. This was a necessary assumption to proceed with the inter-protocol comparison of cardiac output and $S_{\bar{v}}O_2$, but may not be true. A small amount of variation may occur, even when external conditions and factors are kept constant, however, it is also a possibility that rebreathing into a reservoir bag as opposed to an open circuit or rebreathing CO_2 instead of CH_4 and C_2H_2 was more stimulating, leading to a higher circulatory flow state.

$S_{\bar{v}}O_2$ bias

The comparison of the $S_{\bar{v}}O_2$ estimates from the two CO_2 protocols (figure 4.9) shows moderately correlated results, with a low mean difference, indicating little bias. While the mean difference was low, it is potentially of note that only flagged datasets had lower CO_2 #1 than CO_2 #2 values.

For the comparison of the individual CO_2 protocols with the exogenous tracer gas protocol mean, both sets of results showed poor to moderate correlation. There was minimal bias when comparing the CO_2 #1 and TG_μ values. The bias was slightly higher for the CO_2

#2 protocol, which was in part due to a significant outlier (participant 11), although most datasets had lower values for CO_2 #2 than for TG_μ.

The comparison between the two exogenous tracer gas protocols showed results which were moderately correlated and minimally biased. The limits of agreement were also slightly tighter than for the CO_2 comparisons made above.

In general, the lack of bias for the comparisons made with the different $S_{\bar{v}}O_2$ estimates is encouraging. It is also a reflection of the fact that natural variation in $S_{\bar{v}}O_2$ is likely to be less than for cardiac output, with the expected values for the former also occupying a tighter normal range across participants than the latter.

$S_{\bar{v}}O_2$ precision

As discussed in section 4.3.3, the ICCs for $S_{\bar{v}}O_2$ were lower than for cardiac output. While this was an expected result due to the lower variability between participants of $S_{\bar{v}}O_2$ compared to cardiac output, it is also a reflection of the difficulty with obtaining CCP-estimates of $S_{\bar{v}}O_2$. The wide limits of agreement when examining the Bland-Altman plots in figures 4.9, 4.10, and 4.11 of between 21 to 31% (to give approximate standard deviations between 5 and 8%), underscore this. As discussed in chapter 3, the CCP estimate of $S_{\bar{v}}O_2$ is dependent on the cardiac output and modelled arterial saturation, as it is conceptually the arteriovenous difference which is estimated. This is in contrast to the more direct way of estimating cardiac output with CCP, where the uptake of the tracer gas from the lung and into the circulation is modelled.

Alveolar dead space

The rationale for adding a fraction of pure alveolar dead space (6% AD) to the modelled ventilation was discussed in chapter 3, and relates to findings made by Sandhu et al.(94) For cardiac output, physiologically negligible changes were seen when adding 6% AD to the exogenous tracer gas datasets. While all of these datasets, except for one (participant

6–TG_c protocol), had higher cardiac output estimates with the 6% AD fits, the mean difference of between 120 to 220 mL/minute for participants with mean cardiac outputs mostly greater than 4 L/minute indicates that the uptake of C_2H_2 was not overly affected by the change. This was not the case for the CO_2 protocols, where the 6% AD estimates gave significantly higher estimates of cardiac output, with effects proportional to the total cardiac output mean.

Discussed in section of chapter 3 was the possibility of a difference between the calculated alveolar dead space for CO_2 and C_2H_2. The complexities associated with the carriage of CO_2 in blood, including the linked exchange of CO_2 with O_2 through the Haldane effect, may cause this difference.(111) From the comparison of cardiac output estimates presented in section 4.3.3, it can be seen that CO_2 is more sensitive to the addition of alveolar dead space than C_2H_2. This may be due to an apparent effect of the dead space, due to a mechanism such as incomplete CO_2 exchange. More probably, it may be a true effect, where the arteriovenous pressure difference of CO_2 is relatively small, such that a 6% increase (equating to roughly 2 $mmHg$) in the arterial-alveolar CO_2 pressure gradient is significant in relation to this. In comparison, a 6% change in the arterial value for C_2H_2 is much less significant due to a large arteriovenous pressure gradient, given that the mixed venous pressure is 0.

The sensitivity of the uptake of CO_2 to adding alveolar dead space is further supported by the $S_{\bar{v}}O_2$ estimate comparison. Again, the differences for the exogenous tracer gas datasets were physiologically insignificant, with a few clear outliers. For the CO_2 datasets, there was a slight but notable increase in $S_{\bar{v}}O_2$ estimates following the addition of 6% AD. This was an expected result, as the increase in the CCP cardiac output would result in an increased $S_{\bar{v}}O_2$ to reduce the arteriovenous difference in O_2.

4.4.4 Limitations and other considerations

This study was primarily limited by a small sample size and lack of a reference standard of measurement by which to compare CCP estimates of cardiac output and $S_{\bar{v}}O_2$. The former obscures conclusions that can be made relating to the inter-protocol comparisons of the fit CCP parameters and the coefficient of variation of cardiac output scaling. While the lack of reference measurement for either cardiac output or $S_{\bar{v}}O_2$ means that it is impossible to determine the accuracy of any of the three different protocols discussed, some degree of association can be made by using the results from the pulmonary hypertension cohort results, and examining the results of the TG_c protocol with direct Fick and mixed venous blood gas measurements as discussed above in section 4.4.3.

Beyond the number of participants, a point can be made that these participants were also not representative of those who would require cardiac output and/or $S_{\bar{v}}O_2$ monitoring. The response to this is twofold. Firstly, the estimation of parameters of lung inhomogeneity with CCP is optimised for those with, at most, mild respiratory disease. As an accurate characterisation of lung inhomogeneity is required to estimate cardiac output and $S_{\bar{v}}O_2$, via the nonlinear optimisation process, studying healthy volunteers, who are unlikely to have overly inhomogeneous lungs, is a logical starting point. With these participants, the estimation of lung parameters is less of an unknown variable, in comparison to one such as the pulmonary hypertension cohort used in chapter 3, where participants almost invariably had some degree of respiratory disease. Secondly, a long-term objective with CCP is to examine trends in cardiac output and $S_{\bar{v}}O_2$ in population-based studies, in participants where such measurements are currently not possible due to the invasive or questionable accuracy of the available techniques. Therefore, studying a cohort of healthy volunteers such as this one represents a preview of what can be extended into much larger studies.

Blood sampling

As the study described in this chapter employed a convenience sampling method of healthy volunteers, and because a measurement of haemoglobin was essential for the estimation

of cardiac output, the participants were given the choice between a venous and capillary blood sample. In a study comparing capillary and venous haemoglobin values with the same device (HemoCue Hb 201+) used in the present study, it was shown that the capillary values were 5.9 g/L higher than the venous values.(115) Most participants were amenable to having a venous sample taken, but the non-standardised approach to blood sampling is a minor weakness of this study.

Protocol order

The four protocols were ordered in such a way as to avoid the excessive loading of the exogenous tracer gases between consecutive protocols with those gases. As discussed in section 4.3.3, however, a slight trend was noticed with a reduction in cardiac output related to the protocol order, with the first protocol (TG_c) resulting in the highest and last protocol (TG_o) resulting in the lowest cardiac output estimate. As most of these participants had not undergone a CCP experiment before, it is possible that they became more relaxed as the study progressed, resulting in a reduction of cardiac output back to a normal baseline. In future studies with multiple protocols, the order can be randomised, with longer breaks between experiments to address the concerns of residual tracer gases being present in the circulation from previous protocols.

4.5 Conclusion

The results of an observational study, examining the estimates of cardiac output and $S_{\bar{v}}O_2$ across protocols using endogenous and exogenous tracer gases in healthy volunteers have been discussed. The primary objective, to explore the feasibility of using CO_2 for the purposes of estimating cardiac output using a respiratory gas-based approach was partially achieved. The variability of the CO_2 protocols compared to the exogenous tracer gas ones indicates that there are still questions to be answered on how best to use CO_2 as a tracer gas. However, the differences between the CO_2 rebreathing protocols and the exogenous tracer gas protocols were not so stark as to suggest that the former would not be viable even with adjustments to the protocol and modelling.

While the nature of this study was such that invasive reference measurements of these parameters for comparison were not possible, examining the relative bias and precision of the protocols yielded insight into how viable these techniques would be for use in patients or other subjects. The generally good correlation of cardiac output between types of protocols, suggests that future studies comparing these protocols against reference techniques would be worthwhile.

The quantification of precision using intraclass correlation coefficients for cardiac output revealed that the open-circuit tracer gas may be more reliable than the closed-circuit alternatives discussed, although clearly, future work comparing the protocols against reference techniques such as the direct Fick method or even thermodilution (as a clinical standard of reference) is required.

The sub-analysis of fits using added alveolar dead space was significant in that differences in the values for cardiac output and $S_{\bar{v}}O_2$ were greater for the CO_2 protocols than for the exogenous tracer gas protocols. The physiological implications of this are not yet completely clear, as further validatory work is required to ensure the modelling is accurate, and these observations reflect real physiology.

The limitations of this study have been discussed in detail. To summarise, they primarily include a small sample size, lack of reference measurements for comparison, and slight inconsistencies in the haemoglobin measurements. It is important to note, however, that this study was executed as a proof-of-concept study to then apply these or similar CCP protocols to populations undergoing invasive cardiac output monitoring. As such, while it is difficult to draw definitive conclusions from the results of this study due to the stated weaknesses of the study, enough information was obtained to achieve the initial purposes for which the study was designed.

The use of CCP as a technique for the noninvasive estimation of cardiopulmonary parameters, using CO_2 in a closed-circuit configuration and CH_4 and C_2H_2 in both open- and closed-circuit configurations, has been introduced. These different protocols are currently not wholly comparable, with varying differences between them. Overall, however, the promise of these techniques in future, larger studies can be seen. In these future studies, the comparisons of estimated parameters with their corresponding reference measurements will help answer questions related to the current validity of these protocols and applied concepts.

5 Cardiac Surgery Cohort

5.1 Introduction

This chapter presents the findings from a cohort of patients studied upon their admission to the cardiothoracic intensive care unit (ICU) following cardiac surgery. The primary outcomes observed in the study were the computed cardiopulmonography (CCP)-based estimation of cardiac output and mixed venous O_2 saturation $S_{\bar{v}}O_2$ using CO_2 as an endogenous tracer gas. The use of CO_2 as a tracer gas was introduced in chapter 4, where the results of a study involving healthy volunteers were discussed. With the cardiac surgery cohort, the process and challenges of using the same conceptual approach with participants who were sedated and mechanically ventilated are discussed, along with the results of the study.

5.1.1 Participants

This was one of the first CCP studies involving mechanically ventilated patients, and the first to attempt the estimation of cardiac output and $S_{\bar{v}}O_2$ in this population. These estimates were compared with the pulmonary artery catheter (PAC)-based invasive reference measurements, the direct Fick method and mixed venous blood gas analysis, respectively.

As this study was observational in nature, it was not ethically permissible for PACs to be inserted purely for research purposes. This, combined with the institutional preference for avoiding the use of PACs where possible, made it apparent that recruitment would be exceedingly slow. Due to the low sample size and novelty of the CCP protocol, for the reasons mentioned above, the inclusion criteria were later widened to include a small group of participants where cardiac output was monitored using a minimally invasive method. This group was recruited primarily for the purpose of protocol evaluation and optimisation.

5.1.2 Positive pressure ventilation

The positive pressure ventilation system used for mechanically ventilated patients in ICU had not been extensively tested with CCP prior to this study. During the course of the study, issues related to CCP data collection via the molecular flow sensor (MFS) were identified and attributed, at least in part, to the differences in mechanical ventilation compared to spontaneous breathing. For this reason, a thorough investigation of specific potential causes and solutions was conducted. This included considering factors such as the machinery within the MFS and other factors unique to this cohort, including residual volatile anaesthetic gases in the circulation. A detailed description of this investigative process, including the subsequent fixes implemented, is provided later in this chapter.

5.1.3 Computed cardiopulmonography

Cardiac output and $S_{\bar{v}}O_2$

The estimation of cardiac output and $S_{\bar{v}}O_2$ using CCP in this cohort required the design of a novel protocol to account for the fact that gases cannot be easily added to a mechanical ventilator circuit. This ruled out the possibility of using exogenous tracer gases as described in chapters 3 and 4, but also using endogenous gases in high concentrations, as done with CO_2 in chapter 4. Instead, the minute ventilation was adjusted to effect a brief change in end-tidal CO_2 ($P_{ET}CO_2$).

The fitting of MFS-recorded data with the cardiopulmonary model is largely as described for the healthy volunteer and pulmonary hypertension cohorts. A notable difference is the segmenting of the protocol into various stages to recover lung, blood, and metabolic parameters separately. The reasons and process for this are detailed in section 5.2.

Alveolar dead space

The possibility that the fraction of alveolar dead space in the wider population is underestimated has been discussed in chapters 3 and 4. This possibility was considered on the basis of work done by Sandhu et al.(94) Within this cohort, all participants (including

those without PACs), had arterial blood gas samples taken during MFS data collection. It was therefore possible to estimate the total fraction of alveolar dead space, including that arising from mechanisms other than $\dot{V}/\dot{Q}$ mismatch, for each participant using CCP. These dead space values were then used when estimating cardiac output and $S_{\bar{v}}O_2$.

5.2 Methods

5.2.1 Experimental protocol

The ethics approval for this study was granted by the West Midlands – Black Country Research Ethics Committee in May 2022. REC reference: 22/WM/0094. The experimental work was carried out in accordance with the general principles of the Declaration of Helsinki.

Participants scheduled to undergo elective mitral valve, multi-valve, or otherwise complex cardiac surgery were identified and handed participant information sheets during their cardiac surgery preadmission clinic. This population was identified as having the highest likelihood of having a PAC placed during the perioperative period. These clinic visits usually took place between a week to several months before the surgery, depending on the clinical condition of the patients. Potential participants were approached upon their admission to hospital to discuss consent to participate in the study.

Participants were initially eligible for recruitment if they had given written consent to take part in the study prior to their surgery, were aged 18 years or older, were receiving mechanical ventilation via an endotracheal tube (ETT) post-surgery in the intensive care unit (ICU), and if they had a PAC in situ in the ICU. Due to difficulties with recruitment, an amendment to this criteria was made so that participants with a minimally/non-invasive cardiac output monitoring device were also eligible even without a PAC. These participants had cardiac output continuously monitored with a pulse contour system, the FloTrac (Edwards Lifesciences). This was the institutional preference for minimally invasive cardiac output monitoring.

Recruited participants had their clinical cardiac output measurements, either with continuous thermodilution (requires a PAC) or a FloTrac, recorded during the period of time the MFS was connected to their ventilatory circuit. The direct Fick cardiac output for participants with a PAC was calculated after data collection, along with a single CCP estimate of cardiac output.

The MFS was connected to the participant's ventilatory circuit upon their postoperative admission to the cardiac ICU. Prior to connection, the MFS had been warmed to 36°C and calibrated with pure O_2 and N_2, in line with the standard operating procedure for CCP protocols. The experimental configuration for this study required adjustments due to the need to integrate the MFS with the ventilatory circuit instead of having an awake participant able to breathe through the MFS via a mouthpiece. The MFS electronics module was situated at the foot-end of the participant's bed, with the MFS measurement head supported by a purpose-built, adjustable arm at the head-end of the bed. The measurement head was connected to the participant's ETT via a catheter mount and heat and moisture exchanger (HME) filter; the ventilatory tubing was connected to the non-participant end of the measurement head. The configuration of the measurement head and ventilatory circuit is shown in figure 5.1.

Figure 5.1: Photograph of the MFS measurement head connected to a mechanically ventilated participant in the ICU. The ETT is connected to the MFS measurement head via a catheter mount, end-tidal CO_2 sensor, and HME filter. Both the inspiratory and expiratory limbs of the ventilatory tubing connect to the non-participant end of the MFS head. The MFS head is supported by an adjustable arm; the adjustable arm in turn is connected to a pole attached to the hospital bed (not in picture). Photo courtesy of Dr Jessica Luiz, Department of Physiology, Anatomy and Genetics, University of Oxford.

The data collection for this protocol was split into four main stages. Firstly, a steady state of at least five minutes allows for the initial quality control checks to take place, including

to check for circuit leaks, which would manifest as a high N_2 balance. The steady state also provides the baseline for the second stage, the partial N_2 washout, to take place. In this stage, the fraction of inspired O_2 (F_iO_2) was increased to 20% above the initial value for five minutes. For example, if the initial F_iO_2 was 50%, then it would be increased to 70%. The N_2 washout stage allows for the CCP lung inhomogeneity parameters to be recovered. A partial instead of a full N_2 washout was chosen due to the risk of absorption atelectasis.(116)

Following the washout, the F_iO_2 was reduced to its initial value and a second steady state of at least five minutes was conducted to allow for O_2 levels in the lung to return to baseline. The final stage involved a deliberate change in minute ventilation, either by adjusting the respiratory rate, tidal volume or both, to effect a change in CO_2 levels for at most one minute. This was guided by using the $P_{ET}CO_2$ displayed on the clinical monitoring screen. By effecting a change in CO_2 over a relatively short period of time, CO_2 was used as an endogenous tracer gas in a similar way to described in chapter 4 with the cohort of healthy volunteers, where the solubility of CO_2 in blood allows for the uptake in the circulation to be measured and used to estimate cardiac output. A change of approximately 1 kPa was thought to be sufficient for modelling purposes.

To facilitate the calculation of the direct Fick cardiac output, paired arterial and mixed venous blood gas samples were taken during one of the two steady state phases. Examples of the partial N_2 washout and CO_2 change stage are shown in figure 5.2.

Over the course of data collection, any clinical events, such as changes in therapy (ino/chronotropic infusions etc.) and postoperative complications, were recorded.

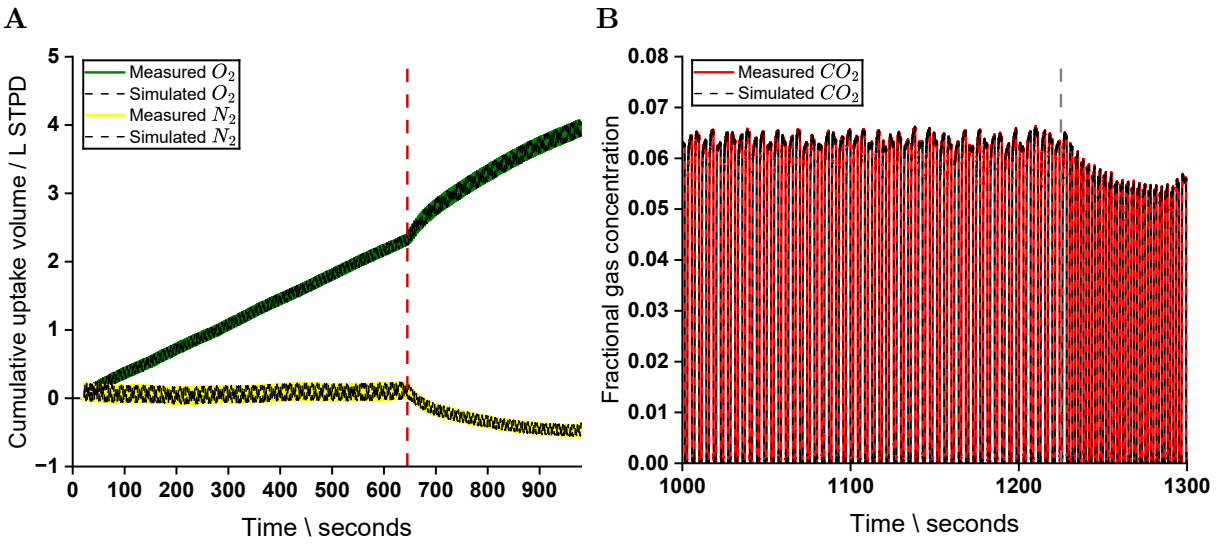

Figure 5.2: Examples of the partial N_2 washout (panel A) and CO_2 change (panel B) stages. In panel A, the start of the partial washout, where the F_iO_2 is increased, is indicated by the red, dashed line. The measured uptake of O_2 and CO_2 can be seen by the green and yellow lines, respectively. The black, dashed lines represent the simulated uptake of both gases. In panel B, the fractional gas concentration is shown against time. In this example, the participant was hyperventilated by increasing the minute ventilation and respiratory rate. The start of the hyperventilation period is indicated by the grey, dashed line. The measured fractional gas concentration of CO_2 can be seen by the red lines. The black, dashed lines represent the simulated fractional concentration of CO_2.

5.2.2 N_2 balance

For CCP protocols, the N_2 balance is a quality control indicator. It is observable while data collection is taking place and during the data processing stage. A N_2 balance of, or close to, zero will be seen as a flat line. Panel A of figure 5.2 shows a dataset where the N_2 balance is close to zero.

In the cardiac surgery cohort, it was observed that the N_2 balance was consistently negative, indicating a production of N_2. At times, the negative N_2 balance approached or exceeded 50 mL/minute. This was significant as a dataset with a ± 50 mL/minute N_2 balance has previously been established as a criterion for exclusion for CCP protocols of this length. As participants were ventilated with relatively low tidal volumes, in keeping with modern intensive care unit practices of 'lung protective ventilation', N_2 balances of this magnitude were more concerning than they would have been with non-ventilated participants with a higher minute ventilation. The investigative approach taken to identifying the cause of large negative N_2 balances and the measures implemented to address each

possible cause are discussed below.

General considerations

As with non-ventilated, spontaneously breathing participants, the first and most important cause of a high N_2 balance to rule out is a circuit leak. This was done systematically by first ensuring a secure connection of the endotracheal tube's catheter mount and the ventilatory tubing to either end of the MFS. Following that, all accessory items, including the mainstream end-tidal CO_2 sensor and HME filters, were double-checked for fit. Finally, the endotracheal tube cuff pressure was checked to rule out the possibility of air flowing around the cuff and bypassing the MFS. The ventilator display was also checked to ensure that inspiratory and expiratory tidal volumes were roughly equal. A significantly higher inspiratory, i.e. delivered volume would be indicative of a circuit leak. It should also be noted, however, that a circuit leak would manifest as a consumption of N_2 (positive balance), rather than a production as observed in this cohort. Nevertheless, the above steps were implemented as standard quality control checks when connecting participants to the MFS for this study.

Technical issues with the MFS head and electronics module were also considered. Any major problems were largely ruled out by conducting breathing tests with the same MFS using a non-ventilated participant, where the N_2 balance was observed to be negligible.

Volatile anaesthesia

A unique characteristic of the cardiac surgery cohort compared to other previously studied groups using CCP was that these participants potentially had residual volatile anaesthesia in their systemic circulation. Given that the standard three-gas MFS used for the cohort measures O_2, H_2O vapour, and CO_2 with the balance assumed to be N_2, it was possible that participants were exhaling volatile anaesthetic gas not accounted for in the MFS readings and therefore manifesting as a large N_2 production.

All participants were maintained under general anaesthesia with isoflurane, the institutional preference for an inhalational anaesthetic agent during cardiac surgery. For a minimum anaesthesia time of over four hours, including time on cardiopulmonary bypass, the participants were given a minimum alveolar concentration (MAC) between 0.7-1.2 of isoflurane. Following transfer from surgery to the cardiac intensive care unit, participants were usually connected to the MFS around one to two hours after they had last been exposed to isoflurane. With no practical way of measuring the isoflurane MAC at the point of MFS connection, it was necessary to estimate this using literature values. Shown in figure 5.3, from Miller's Anesthesia, 9th edition, are the washout curves for isoflurane based on inhalation time and MAC.(1) The dashed purple and orange lines depict the washout of isoflurane after four hours of delivery at a MAC of 1.2 and best represent this cohort. While the graph ends at 60 minutes, it was considered a reasonable possibility that there was between 0.1-0.2 MAC of residual isoflurane at the time of MFS connection.

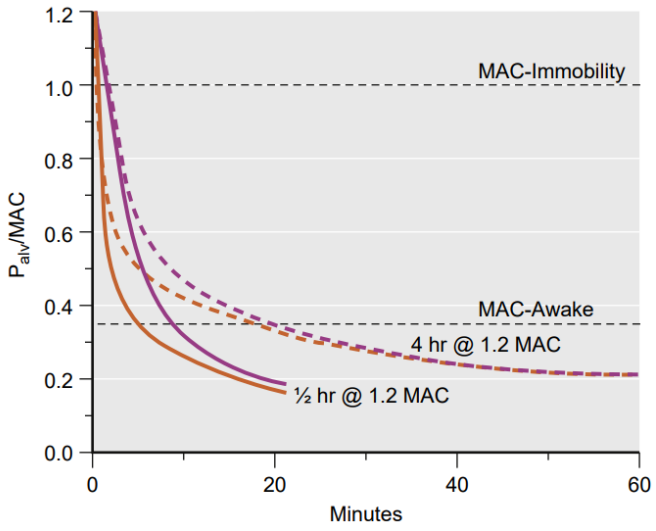

Figure 5.3: Graph showing the modelled washout of isoflurane, as alveolar partial pressure normalised to MAC, with respect to time. The solid and dashed lines represent 30 minutes and four hours of isoflurane delivery at 1.2 MAC. The orange and purple lines indicate the alveolar and central nervous system partial pressure of isoflurane, respectively. Image from Chapter 20 of Miller's Anesthesia, 9th Edition, Elsevier.

Based on this possibility, a method for processing MFS breath-by-breath data accounting for isoflurane was developed. 1 MAC of isoflurane is equivalent to an alveolar concentration of 1.5%, subject to other factors such as age. Therefore, 0.1-0.2 MAC of isoflurane would be approximately equivalent to 0.15-0.3% in the lung. As discussed in section 2.1.2, the pressure drop by which flow is calculated requires measurements of instantaneous density and viscosity. Therefore, to quantify the effects of volatile agent passing through the

MFS, it is necessary to calculate the viscosity and density of isoflurane. Habre et al. experimentally calculated the viscosity of isoflurane at varying concentrations in different carrier gases. The mean viscosity and density for 1 MAC of isoflurane in 50% O_2 was given as 1.8927 Pa s$\times$ 10^{-5} and 1.172 kg/m^3, respectively. (117) These values, along with the others published by Habre et al., were used as a starting point to calculate the viscosity and density of any isoflurane passing through the MFS.

A program was developed to examine the effects of varying concentrations of the volatile agent. This program accounted for the viscosity and density of isoflurane, as discussed above, and also the volume present in the composite gas mixture. Based on the washout curves discussed earlier, it was likely that participants would have no more than 0.1-0.2 MAC of isoflurane in their system at the time of MFS connection. The last ten participants to be recruited for the study were reanalysed at isoflurane MACs of 0.1, 0.2 and 0.3. The results of this analysis are shown in table 5.1.

Table 5.1: N_2 balance for different MACs of isoflurane

Study order	0 MAC: $\dot{V}N_2$ / mL min^{-1}	0.1 MAC: $\dot{V}N_2$ / mL min^{-1}	0.2 MAC: $\dot{V}N_2$ / mL min^{-1}	0.3 MAC: $\dot{V}N_2$ / mL min^{-1}
25	-55	-51	-45	-40
24	-42	-38	-31	-25
23	-71	-67	-62	-56
22	-41	-38	-32	-27
21	-48	-44	-39	-34
20	-40	-35	-28	-21
19	-39	-34	-29	-24
18	-41	-38	-31	-24
17	-34	-32	-29	-25
16	-38	-33	-29	-24
15	-31	-24	-16	-8

$\dot{V}N_2$, N_2 production. Participants were sorted based on time of recruitment, starting from the most recent. 0 MAC indicates the original, uncorrected N_2 balance.

As seen in table 5.1, a uniform decrease in the magnitude of the N_2 balance was observed

with increasing MACs of isoflurane. Also evident, however, was that respired isoflurane did not account for the majority of the negative N_2 balance in any of the individual datasets. This was true even at a MAC of 0.3, a concentration of isoflurane unlikely to have been present in any of the participants at the time of MFS connection.

Based on these results, it was concluded that residual isoflurane within the participants' circulation was unlikely to be significant factor in the large N_2 balances observed. To avoid over-processing the MFS measurement data, the isoflurane correction was not used in the final version of datasets run through the CCP model, and the remaining participant datasets were not run through the isoflurane correction program. The uncertainty of the exact isoflurane MAC in each participant at the time of MFS connection also contributed to this decision.

Positive pressure ventilation

The MFS has been used in numerous studies to assess cardiopulmonary parameters in awake, spontaneously breathing participants. Less data exists for intubated participants receiving positive pressure ventilation. Given the non-physiological nature of positive pressure ventilation, where there is a progressive inspiratory pressure rise followed by a sharp return to baseline on expiration, it was thought that this could potentially result in an incorrect cumulative inert gas balance calculation.

An experiment was conducted to examine the effects of positive pressure ventilation on the MFS data recordings in the Department of Physiology, Anatomy and Genetics, University of Oxford. Here, the same MFS used for the study was connected to a ventilator on one side and an anaesthetic reservoir bag on the other side. The reservoir bag simulated the inflation and deflation of a lung. The cumulative uptake of N_2 was measured over a range of different ventilator modes and settings. Invariably, an N_2 production, similar to that observed during the actual study, was observed. Repeat experiments with a spontaneously breathing volunteer instead of a ventilator resulted in N_2 balances of close

to zero. An example record with the ventilator and reservoir bag configuration is shown in figure 5.4.

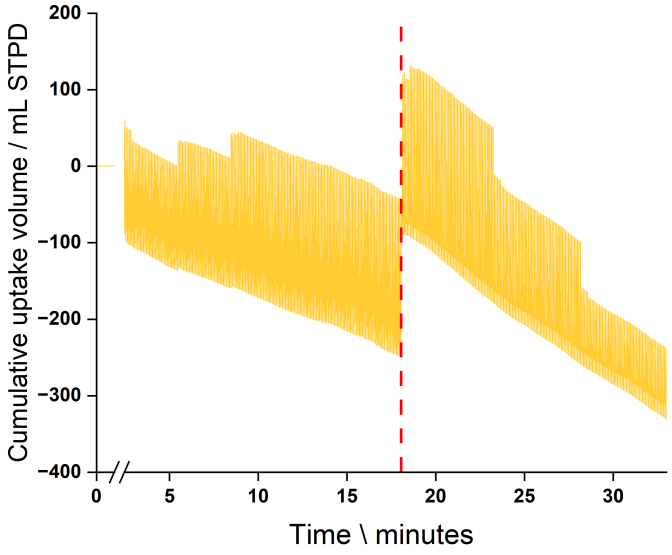

Figure 5.4: Example record of the cumulative uptake of N_2 (yellow lines) over time of a test conducted with the ventilator and anaesthetic reservoir bag. The ventilator was set to continuous mandatory ventilation (CMV) with a starting positive-end expiratory pressure (PEEP) of 0 cmH_2O, with tidal volumes stepping up from 200 to 250 to 300 mL. The red, dashed line indicates the increase of the PEEP to 5 cmH_2O, with volumes stepping down from 300 to 200 to 100 mL. A negative uptake volume indicates a production of N_2.

A subsequent experiment was conducted to examine the pressure effects on flow using the MFS employed in the study. A syringe pump was attached to the participant side of the MFS, with the non-participant side sealed off with a plug. In this configuration, the pump movement would pressurise and depressurise the MFS measurement cell (figure 5.5). The pump was programmed to move 10 mm towards the MFS, then back to its original position, and finally 10 mm away from the MFS. It was observed that the transient flow, and therefore volume, was always in the direction of the increasing or decreasing pressure. Experimental recordings of this are shown in figure 5.6. The conclusion from this was that virtually all measured flow was driven by a pressure change, which would lead to a cumulatively high inert gas balance.

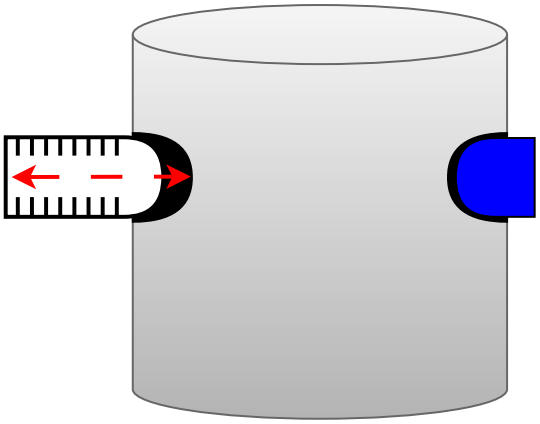

Figure 5.5: Simplified diagram of the syringe pump experiment's configuration. The syringe pump, shown on the left, can move in and out of the MFS (grey cylinder) in the path shown by the red, dashed arrows. On the right side of the MFS, the non-participant side, the port is sealed with a plug (blue shape). Not to scale.

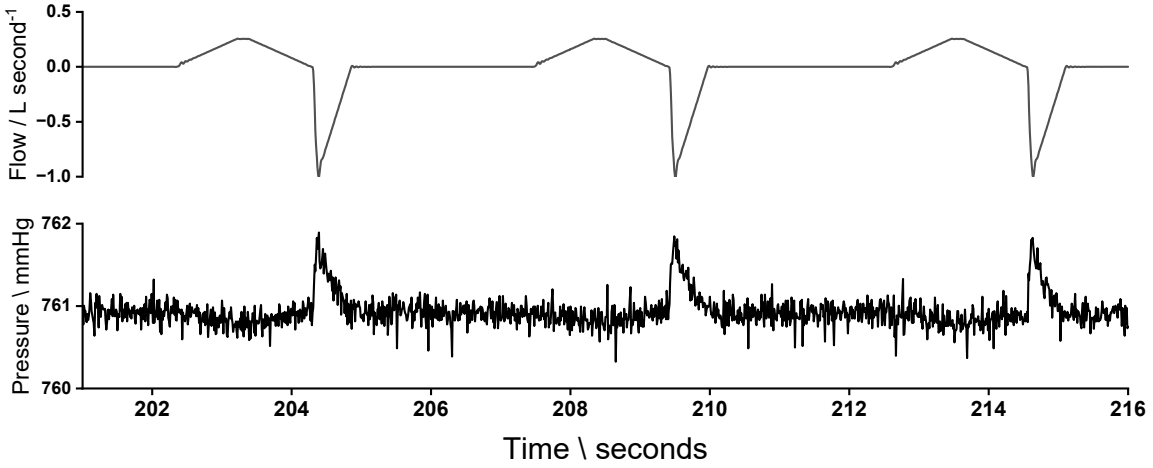

Figure 5.6: Example record of the flow and barometric pressure from the MFS during a syringe pump experiment. In this example, pressurising the system can be seen to cause a corresponding change in flow, which is then recorded as a change in volume.

Depending on the mode of mechanical ventilation, the ramp speed of the inspiratory pressure delivered varies. It was not believed, however, that the ramp speed of inspiratory pressure contributed to the false inert gas balance. This can be shown mathematically within the context of the syringe pump experiment:

From time $(t) = 0$ and at pressure $(p) = 0$, i.e. atmospheric pressure, there is a pressure ramp to $p = P$ at $t = T$. If the flow transients at the beginning and end of this ramp are discounted, pressure may be written as:

$$p = mt \tag{5.1}$$

Therefore, $m = P/T$.

Within the MFS, the pressure inside the two limbs of the pneumotachograph can be expressed as:

$$\text{Limb}_1 : p_1 = m(t - \tau_1) \tag{5.2}$$

$$\text{Limb}_2 : p_2 = m(t - \tau_2) \tag{5.3}$$

Where τ_1 and τ_2 are the time constants for Limb_1 and Limb_2 respectively.

Given the differential pressure applied by the syringe pump is proportional to the fictitious volume, it can be expressed as:

$$p_1 – p_2 = m(\tau_1 – \tau_2) \tag{5.4}$$

Integrating this over the period of the ramp time will yield a value that is proportional to the fictitious volume (V):

$$V \propto mT(\tau_1 – \tau_2) \tag{5.5}$$

Substituting for $m = \frac{P}{T}$ yields:

$$V \propto P(\tau_1 – \tau_2) \tag{5.6}$$

V is therefore shown to be independent of the speed of the ramp increase in pressure. Figure 5.7 shows the relationship between pressure and time, as presented in the above series of equations, graphically.

Given the significantly asymmetric flow patterns during inhalation and exhalation through a ventilator, the syringe pump configuration was used to ensure the MFS was capable of making accurate measurements across a wide range of values. First MFS recordings were made with a normal pump action. Following this, the pump was set to simulate the

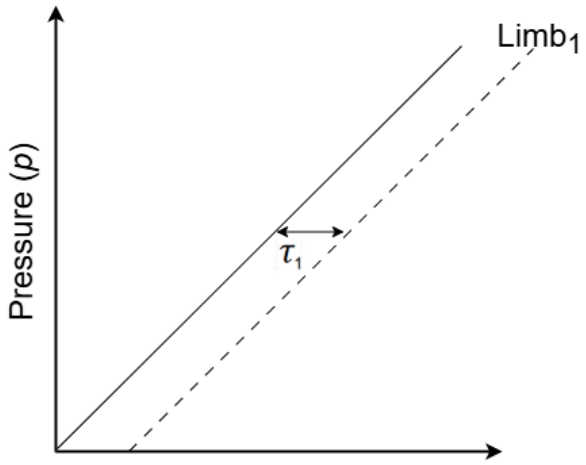

Figure 5.7: Schematic of the relationship between pressure (p) and time (t). There is a ramp in pressure over time, with a gradient m, represented by the solid line. Here, the flow transients at the beginning and end of the ramp in pressure are not shown. For the pneumotachograph limbs , the first order solution for p is given by $p1 = m(t - \tau_1)$ and $p2 = m(t - \tau_2)$ for limbs 1 and 2 (limb 2 not shown here for image clarity), respectively.

flow pattern of a ventilator, with a slow inhalation and rapid exhalation. No significant differences were seen between the two sets of experimental recordings (figure 5.8).

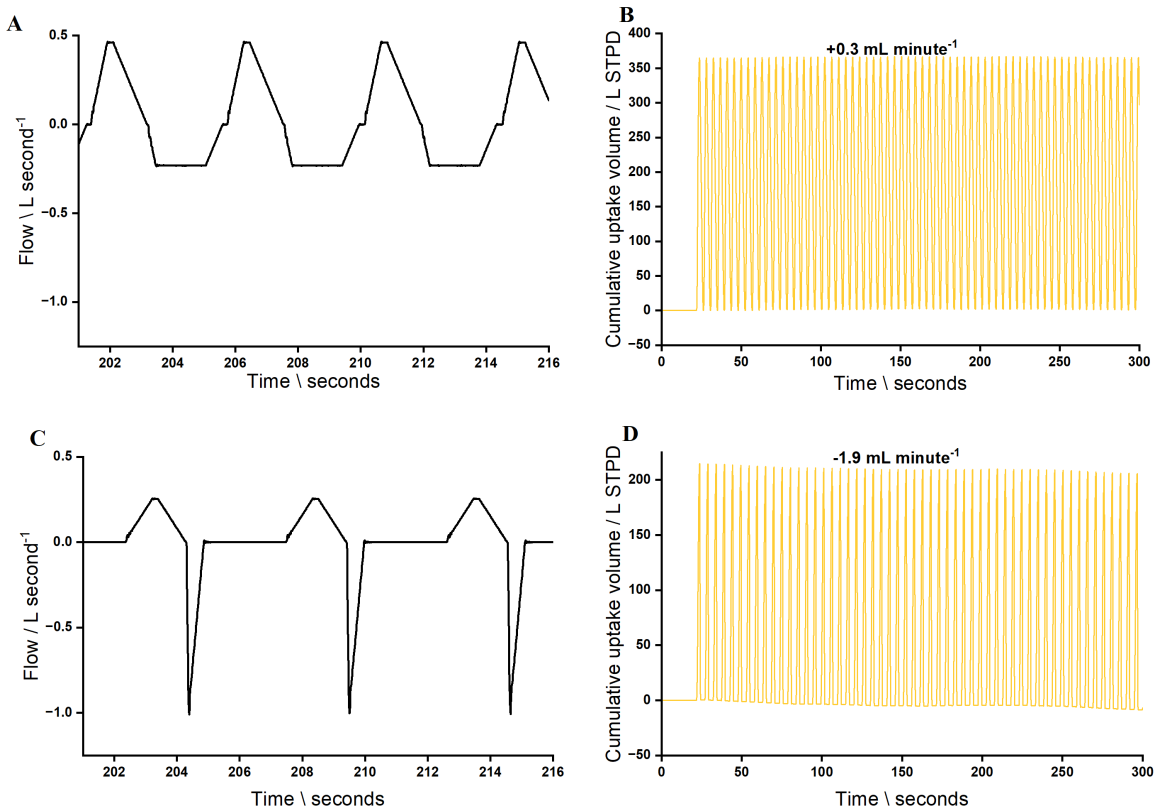

Figure 5.8: Comparison between the normal syringe pump action (panels A and B) and the ventilator-like action (panels C and D). Panels A and C show three syringe pump-delivered 'breaths' each. In panel C, the gradual inspiration followed by the sharp release for expiration can be observed. Panels B and D show the cumulative volume uptake for N_2 (yellow lines) over time. The N_2 balances are shown on top of the plotted data.

Differential pressure sensors

As part of a series of upgrades to the MFS, new differential pressure sensors were installed

midway through the recruitment of the cardiac surgery cohort study. With the old sensors (HCLA, Sensortechnics) it was found that the measurements taken at a constant flow over a 5- 10 minute period were not stable. This had been initially accounted for by using the average of eight sensors, split into two banks of four, as described in section 2.1.2. The new sensors (SM9336, TE Connectivity) were comparatively more stable, however, they had a slower response time. While this slower response time is not significant for spontaneously breathing participants, the fast transitions during the respiratory cycle in mechanically ventilated participants potentially caused a degree of inaccuracy, seen as an incorrect N_2 balance.

Using the ventilator and reservoir bag setup described above, a comparison was made between the two sets of sensors. The results of this comparison are shown in figure 5.9.

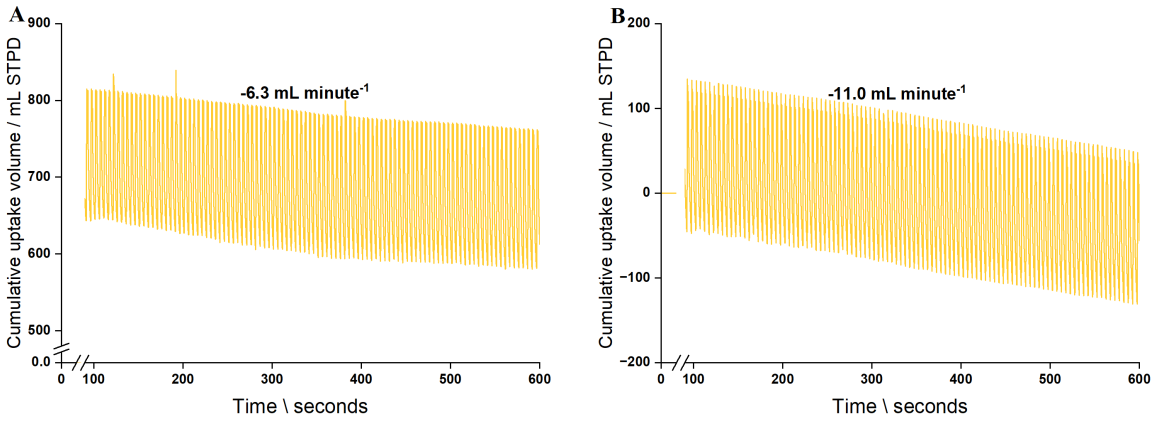

Figure 5.9: Comparison between the old (panel A) and new (panel B) differential pressure sensors. The cumulative uptake volume for N_2 is shown in yellow. The N_2 balances are shown on top of the plotted data.

Flow correction

To account for the fictitious volume registered due to the potential interaction between differential pressure sensing and mechanical ventilation, a routine to correct the datasets was developed. The nature of this correction first requires the manual identification of a window in which the N_2 balance is expected to be close to zero. Two such periods exist in this protocol, the steady state stages before and after the partial N_2 washout. The pre-washout stages occurs from the time of MFS connection to the ventilator circuit

to just before the F_iO_2 is increased for the partial N_2 washout. Datasets were initially corrected using the pre-washout window for the washout fit and the post-washout window for the cardiac output fit. To avoid the complication of having two separately corrected fits, however, it was decided that the correction window would be between the start of the pre-washout stage and the end of the post-washout stage. An example of a corrected dataset is shown in figure 5.10.

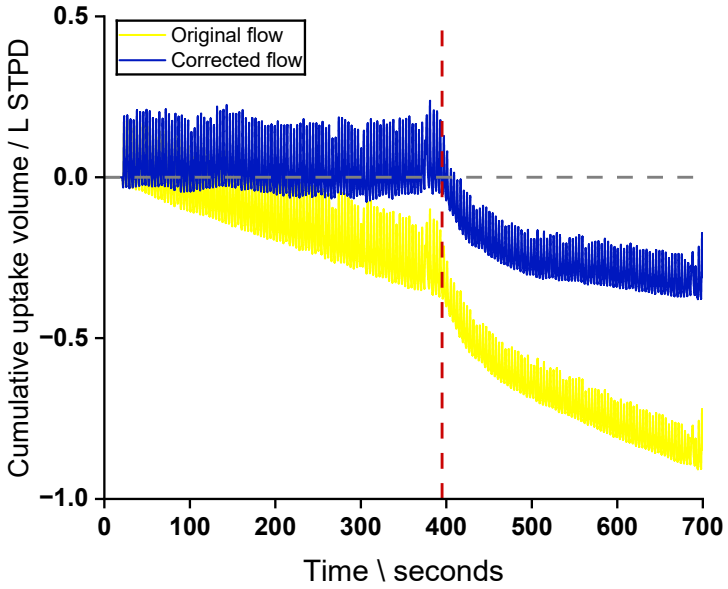

Figure 5.10: Example of a dataset before and after flow correction. The cumulative uptake of N_2 during the partial N_2 washout stage and preceding steady state is shown. The original dataset is in yellow and the flow corrected dataset is in blue. The horizontal, grey, dashed line is at 0 L uptake, for reference. The vertical, red, dashed line indicates the start of the partial N_2 washout stage.

Within the chosen correction window, a correction coefficient for flow, k, is calculated, which minimises the absolute cumulative N_2 volume. The flow correction function from which k is derived is fit with a non-linear least squares routine, specifically the Levenberg-Marquardt algorithm. No constraints are set for k. The function is expressed as:

$$F^* = F\big(1 \pm (k \times dP)\big)$$

Where F^* is the corrected flow, F is the uncorrected flow, and dP is the rate of airway pressure change over the window.

Due to the varying degrees of N_2 production in each dataset, a common value for k was not found. Given the process of manually selecting the minimisation window for k for

each dataset and the different pressure sensors used for part of the cohort, this was an expected outcome. The pre-washout phase N_2 balances before and after flow correction are shown in table 5.2.

Table 5.2: Original and corrected $\dot{V}N_2$ values

Study order	Original $\dot{V}N_2$ / mL min^{-1}	Corrected $\dot{V}N_2$ / mL min^{-1}
1	-21	12
2	-7	26
3	-28	-9
4	-13	8
5	-44	35
6	-18	6
7	-23	39
8	-36	-22
9	-31	1
10	-27	5
11	-31	29
12	-39	13
13	-46	-14
14	-31	10
15	-52	17
16	-34	-7
17	-37	2
18	-39	40
19	-40	21
20	-48	-7
21	–	37
22	-41	13
23	-71	16
24	-42	13
25	-55	-6
Median	-37 ± 15	12 ± 20

Median ± interquartile range. Comparison of original and flow corrected pre-washout N_2 balances. A negative value indicates a production of N_2. For the 21st participant (ID: 11), the data was not viable for fitting until it had been corrected for flow.

Conclusion

The issue causing incorrect N_2 balances for participant datasets in this study has not been definitively identified or resolved. It is a strong possibility, however, that the newly installed differential pressure sensors were less suitable than the old ones for the sharp transitions between inspiration and expiration in mechanically ventilated individuals. The small sample size of participants studied with either sensor type limits the certainty of this conclusion.

The impact of isoflurane was examined in a subset of participants, selected based on the chronology of their recruitment into the study, but all with high N_2 balances. It is unlikely that any residual isoflurane would contribute significantly to the N_2 balance.

A method of correcting acquired MFS data has been discussed. This method was used to correct all data collected before it was put through the cardiopulmonary model. For participants with low N_2 balances studied with the old differential pressure sensors, the correction was still applied to ensure all participants were treated equally.

5.2.3 Modelling

In preparation for CCP modelling, all datasets were corrected for flow as described previously to account for incorrectly recorded N_2 balances. Following this, a segmented approach was required to process the data through the CCP model. The current version of CCP is such that a protocol with discrete stages to estimate lung parameters, blood chemistry, and cardiac output requires modelling of these stages separately. This was the case for the cardiac surgery cohort study, where a partial N_2 washout was used to estimate lung parameters and a hyper/hypoventilation manoeuvre was used to estimate the cardiac output. In contrast, the studies using closed-circuit configurations with anaesthetic reservoir bags described in chapters 3 and 4, achieved both modelling objectives during the rebreathing phase. Similarly, the open-circuit protocol using the exogenous tracer gases CH_4 and C_2H_2 described in chapter 4 could be modelled as one dataset.

For the cardiac output fitting, 12 separate fits were obtained for each participant's dataset. This was the approach used for the healthy volunteer cohort, which in turn was guided by the results from the pulmonary hypertension cohort. As with the healthy volunteer cohort, only one set of optimality, function, and step tolerances was used (1×10^{-6}). This process was then repeated after the addition of alveolar dead space (AD) to the model lung. Unlike for the two previous cohorts, the dead space was estimated for each participant using CCP. The modelling approach for this is discussed below. For each dataset, outliers were identified by examining the cardiac output coefficient of variation ($\dot{Q}$ CV).

Lung parameters

The first segment to be modelled is the washout stage. It is at this stage that alveolar volume (V_A) and the parameter for quantifying the distribution of lung compliance (σC_L) are estimated, and thereafter set as fixed parameters for the subsequent segments of modelling. The other CCP parameters, with the exception of cardiac output, are also fit during the partial washout phase, but are not carried forward to the other modelling segments. This is primarily due to the assumption that these other parameters, such as $\dot{V}O_2$, the ideal CO_2 point (P_iCO_2), dead space distributions etc, may change during the other protocol stages.

Cardiac output

Using the fixed estimates of V_A and σC_L, cardiac output is estimated by using data acquired during the time of the change in minute ventilation and the steady state prior. The perturbation of CO_2 caused by the change in minute ventilation allows for the difference in uptake of CO_2 in the circulation before and after the change to be used to estimate the cardiac output. This can be further expanded upon by considering the Fick relation with CO_2 as the subject gas:

$$\dot{Q} = \frac{\dot{V}CO_2}{c_{\bar{v}CO_2} - c_{aCO_2}} \tag{5.7}$$

Where $\dot{Q}$ is the cardiac output, $\dot{V}CO_2$ is the production of CO_2, and c_{aCO_2} and $c_{\bar{v}CO_2}$ are the arterial

and mixed venous contents of CO_2 respectively.

In the first instance, $\dot{V}CO_2$ may be estimated from the CO_2 exchange at the mouth and c_{aCO_2} may be estimated from the end-tidal CO_2 partial pressure. $\dot{Q}$ and $c_{\bar{v}CO_2}$ remain unknown, however. A potential theoretical solution to solving these unknowns would be to change c_{aCO_2} instantaneously, thus causing a change in $\dot{V}CO_2$, but with $\dot{Q}$ and $c_{\bar{v}CO_2}$ remaining unchanged. This would yield a second equation, to then solve for the two unknowns simultaneously. In this situation, however, it would not be possible to change c_{aCO_2} to a fixed unchanging value without considering the effects of recirculation and the change in production of CO_2 at the mouth, which will initially be buffered by the lung volume. To deal with these issues of transience, a more detailed version of the Fick relation can be used:

$$\dot{Q} = \frac{\int_{T_1}^{T_2} \dot{V}_{CO_2}(t)\,dt - (V_{L,T_2} \cdot F_{A,CO_2,T_2} - V_{L,T_1} \cdot F_{A,CO_2,T_1})}{\int_{T_1}^{T_2} c_{\bar{v}CO_2}(t)\,dt - \int_{T_1}^{T_2} c_{aCO_2}(t)\,dt} \tag{5.8}$$

Where T_1 and T_2 are the two timepoints over which this equation is considered, V_L is the volume in the lung with respect to time and F_{A,CO_2} is the fractional alveolar concentration of CO_2 with respect to time.

The $\int_{T_1}^{T_2} \dot{V}_{CO_2}(t)\,dt$ term gives the integrated production of CO_2 at the mouth over the specified time period, between T_1 and T_2. The remaining terms in the numerator account for the exchange of CO_2 across the pulmonary capillary at T_1 and accumulated CO_2 in the lung at T_2. The denominator accounts for the change in $c_{\bar{v}CO_2}$ due to recirculation as c_{aCO_2} changes between the time period of T_1 to T_2. Conceptually, it is in this way that the deliberate perturbations in CO_2 generate the information for the CCP model fitting to estimate cardiac output.

Blood chemistry parameters and alveolar dead space

All participants in the cohort had an arterial blood gas sample taken during a steady state phase of the protocol. Additionally, those with a PAC in situ also had a mixed venous blood gas sample taken, usually during the same steady state stage. To model estimates

of the arterial and mixed venous O_2 and CO_2 partial pressures in blood, a window of approximately one minute before and after the blood gas sample(s) is used. This window was chosen to facilitate a direct comparison with the sampled blood gas values, where the MFS-measured values for $\dot{V}O_2$ and $\dot{V}CO_2$ from the 30-second period immediately prior to blood sampling gave a value for the respiratory exchange ratio (RER) associated with the sample(s). For this modelling segment, V_A and σC_L are again fixed.

Using the same steady state stage window, the proportion of ventilation that is distributed to alveolar dead space can be estimated. This process can be represented with an R-line diagram (figure 5.11). Using the RER 30 seconds before blood sampling (specifically arterial in this case, in case the mixed venous sample was taken at a different steady state), a blood R-line is constructed through the modelled arterial point, $\mathrm{P_a}O_2$ and $\mathrm{P_a}CO_2$. The CCP blood sub-model is used to construct the remainder of the line, where the measured haemoglobin and other blood gas parameters are incorporated. The second line plotted is the gas R-line. Here, the simulated alveolar point, $\mathrm{P_A}O_2$ and $\mathrm{P_A}CO_2$, is used with the same RER to construct the line based on the alveolar gas equation.(118) The intersection of the blood and gas R-lines is the ideal point, P_iO_2 and P_iCO_2. The ideal point represents both the arterial and alveolar partial pressures of O_2 and CO_2 if there was no inhomogeneity present in the lung.(83)

Estimation of the ideal point allows for an iterative modelling process, whereby the alveolar dead space fraction can be adjusted from zero to a value at which the modelled arterial $\mathrm{P_a}O_2$ and $\mathrm{P_a}CO_2$ falls on the blood R-line. To facilitate this iterative modelling approach, a further 125 model lung compartments that match the properties of the initial 125 lung compartments in the CCP model are added. These additional compartments are only different in that they have no blood flow. The inspired gas flow is then gradually diverted to these compartments until the condition of the modelled arterial point intersecting with the blood R-line is met.

Alveolar dead space can arise as both pure alveolar dead space and apparent alveolar dead space. The latter is caused by significant $\dot{V}/\dot{Q}$ inequalities. In order to estimate total alveolar space entirely though pure alveolar deadspace, it is first necessary to effectively eliminate the V/Q inhomogeneity normally present in the CCP model. This was done by the following means:

- σCd, which is the standard deviation for the natural logarithm of the standardised lung conductance, is usually set to be 0.3 over σC_L (the standard deviation for the natural logarithm of the standardised lung compliance). Instead, σCd was set to equal σC_L.

- The correlation coefficient between σCd and σC_L, ρ, which can be thought of as the correlation between ventilation and blood flow, is usually fixed at 0.87. In this homogenised version of the model lung, ρ was set at 0.98.

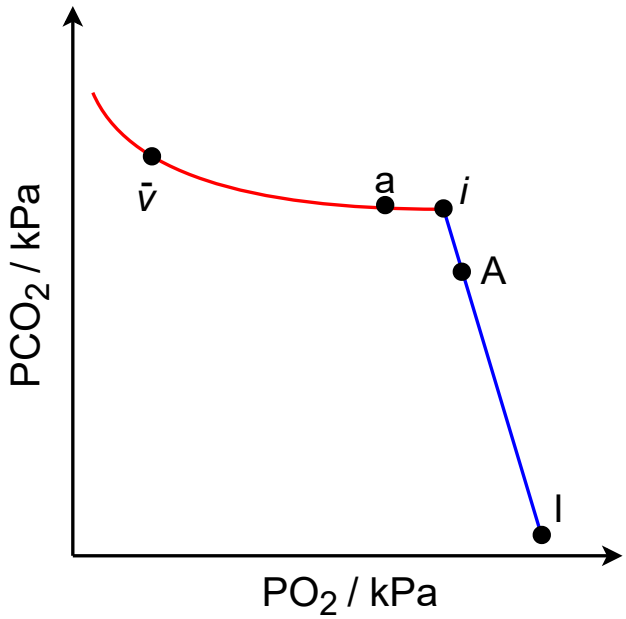

Figure 5.11: Schematic of the R-line diagram. The x- and y-axis are the partial pressures of O_2 and CO_2, respectively. The blood R-line is in red and the gas R-line is in blue. $\bar{v}$ is the modelled mixed venous point, a is the modelled arterial point (using the arterial blood gas sample), i is the ideal point, A is the alveolar point, and I is the inspired point. As alveolar dead space is added, A will move up the gas R-line, due to the reduced efficiency in gas exchange.

5.3 Results

5.3.1 Participants

The difficulty in recruiting participants with a PAC was primarily due to the clinical preference for avoiding insertion where possible, due to the lack of perceived benefit-to-risk ratio. From September 2022 to November 2024, nearly all patients undergoing mitral valve, multi-valve, or otherwise complex cardiac surgery in the John Radcliffe Hospital, Oxford were handed participant information sheets during their preadmission clinic visit. Figure 5.12 shows the outcome of recruitment during this period.

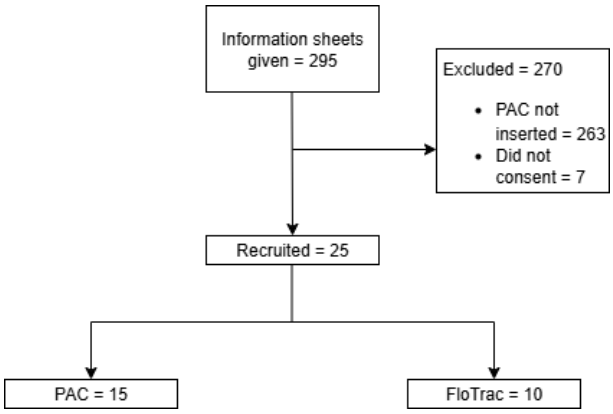

Figure 5.12: Flow diagram of participant recruitment to the cardiac surgery cohort study. In most cases, it was possible to ascertain whether patients would be subject to PAC insertion before consenting them for the study. The number that did not consent includes those who had a PAC inserted, but also those where the consent discussion took place prior to discussing the possibility of PAC insertion with the treating anaesthetist/intensivist.

15 participants with PACs in situ were recruited to take part in the study, their characteristics are shown in table 5.3. Due to the major issues with recruitment, participants with FloTrac-monitored cardiac output were recruited. The FloTrac participants were considered separately where possible, given the lack of a validated cardiac output measurement in this group. Their characteristics are shown in table 5.4. For ease of reference, the cohort identification numbers have been assigned such that those with invasive reference measurements were given numbers between 1 and 15, and those without were given numbers between 16 and 25. Within these groups, the numbers reflect the chronology of recruitment to the study.

Table 5.3: Per-person baseline characteristics of the PAC cardiac surgical cohort

Cohort ID	Age / years	Sex	BMI / kg m^{-2}	Surgery	Cardiovascular disease	Respiratory disease	Smoking status	Smoking pack years
1	52	Female	22	Re-do AVR, AA and hemiarch replacement	Hypertension, previous AVR	-	Never smoked	0
2	71	Male	26	AVR, MVr	CVA, infective endocarditis, hypertension	Asthma	Never smoked	0
3	78	Female	31	MVr, TVr, LAAO	AF	-	Never smoked	0
4	71	Male	23	MVr, AVR, CABG	Hypertension	-	Never smoked	0
5	59	Male	25	MVr, AVR, AF ablation, LAA excision	AF	-	Never smoked	0
6	66	Male	29	AVR, MVR	Hypertension, CVA	-	Never smoked	0
7	78	Male	28	MVr, TVr	AF	-	Never smoked	0
8	62	Male	27	MVr, TVr, AVR	AF, hypertension	-	Never smoked	0
9	71	Female	22	Re-do MVR, ASD closure	IHD, previous MVr and CABG, AF, hypertension	-	Ex-smoker	5
10	65	Male	23	MVr, TVr, LAAO, AF ablation	AF	-	Current smoker	8
11	69	Male	34	MVr, TVr, CABG	Hypertension, AF	-	Current smoker	10
12	84	Male	21	MVR	CMC	-	Never smoked	0
13	80	Male	23	MVr, LAAO	AF	-	Never smoked	0
14	63	Male	21	MVr, TVr, LAAO	AF	-	Ex-smoker	18
15	75	Male	27	MVr, PFO closure	-	-	Ex-smoker	3

ID, identification number. BMI, body mass index. AA, ascending aorta. AVR, aortic valve replacement. MVr, mitral valve repair. MVR, mitral valve replacement. TVr, tricuspid valve repair. LAAO, left atrial appendage occlusion. LAA, left atrial appendage. CABG, coronary artery bypass graft. AF, atrial fibrillation. CVA, cerebrovascular accident. IHD, ischaemic heart disease. ASD, atrial septal defect. CMC, closed mitral commissurotomy. PFO, patent foramen ovale.

Table 5.4: Per-person baseline characteristics of the FloTrac cardiac surgical cohort

Cohort ID	Age / years	Sex	BMI / kg m^{-2}	Surgery	Cardiovascular disease	Respiratory disease	Smoking status	Smoking pack years
16	42	Male	32	MVr	Hypertension	Asthma	Never smoked	0
17	77	Male	27	MVr, TVr, LAAO	AF	-	Ex-smoker	2
18	44	Male	22	MVr	Infective endocarditis	-	Current smoker	2
19	80	Female	18	MVr, TVr	Hypertension	-	Never smoked	0
20	71	Male	25	MVr, TVr	AF, hypertension	-	Never smoked	0
21	48	Male	25	MVr	AF	-	Current smoker	15
22	71	Female	26	MVr	-	Asthma	Never smoked	0
23	63	Female	29	MVr, TVr	Hypertension	-	Never smoked	0
24	72	Female	17	MVr	Hypertension	COPD	Never smoked	0
25	66	Male	29	MVr	Hypertension	-	Never smoked	0

ID, identification number. BMI, body mass index. MVr, mitral valve repair. TVr, tricuspid valve repair. LAAO, left atrial appendage occlusion. AF, atrial fibrillation. COPD, chronic obstructive pulmonary disease.

5.3.2 Direct Fick cardiac output

For participants recruited with a PAC in situ, the direct Fick cardiac output was calculated and used as a reference measurement by which to compare the CCP estimates. In this

study, the direct Fick cardiac output ($\dot{Q}_{\mathrm{DF}}$)was calculated using O_2 as the subject gas:

$$\dot{Q}_{\mathrm{DF}} = \frac{\dot{V}O_2}{c_aO_2 - c_{\bar{v}}O_2} \tag{5.9}$$

A similar stepwise approach to the one described in section 3.3.2 of chapter 3 for the pulmonary hypertension cohort was taken to ensure the accuracy of all measured components of the direct Fick calculation. Arterial and mixed venous blood gas samples were taken during the steady state stages of the protocol, and were usually paired. The same formula was applied to calculate both the arterial and mixed venous O_2 contents. This formula is shown for the calculation of c_aO_2 below:

$$c_aO_2 = \mathrm{Hb}_a \times 0.1 \times 1.39 \times (1 - \mathrm{COHb}_a - \mathrm{MetHb}_a) \times (S_aO_2/100) + 0.0031 \times \mathrm{P}_aO_2 \times 7.50062 \tag{5.10}$$

Where Hb_a, $COHb_a$, and $MetHb_a$ are the haemoglobin in g/L, carboxyhaemoglobin fraction, and methaemoglobin fraction from the arterial blood gas sample respectively, 1.39 is Hufner's constant in mL O_2/ g Hb(103), P_aO_2 is the arterial O_2 partial pressure in kPa, 0.0031 is the solubility coefficient for O_2 in plasma, and 7.50062 is the conversion factor for kPa to mmHg. To note is that the arterial values for Hb, $COHb$, and $MetHb$ were used for the calculation of the mixed venous O_2 content for consistency.

The $\dot{V}O_2$ values used were from the steady state stage at which the blood gases were taken. The datasets were first corrected for flow, as discussed in section 5.2.2. The $\dot{V}O_2$ values were then corrected for any fractional changes in O_2 due to the change in lung stores. This was the same approach used for the pulmonary hypertension cohort (section 3.3.2). The corrected $\dot{V}O_2$ ($\dot{V}O_{2_c}$) in mL/minute is given as:

$$\dot{V}O_{2_c} = \dot{V}O_2 - 1000(\mathrm{FRC} \times \dot{F}O_2) \tag{5.11}$$

Where FRC is the functional residual capacity in L STPD and $\dot{F}O_2$ is the fractional end-tidal change in O_2 over the air-breathing phase per minute.

All references to $\dot{V}O_2$ herein refer to the $\dot{V}O_{2_c}$ value unless otherwise stated. The full list of values used for the direct Fick calculation for participants with a PAC is shown in table 5.5.

Table 5.5: Values used for the calculation of the direct Fick cardiac output (updated with arterial and mixed venous oxygen partial pressures)

Cohort ID	$\dot{V}O_2$ / mL min^{-1}	$\dot{V}N_2$ / mL min^{-1}	$\dot{F}O_2$ / min^{-1}	FRC / L BTPS	$\dot{V}O_{2_c}$ / mL min^{-1}	S_aO_2 / %	P_aO_2 / kPa	$S_{\bar{v}}O_2$ / %	$P_{\bar{v}}O_2$ / kPa	Hb g/L^{-1}	COHb / %	MetHb / %	$\dot{Q}_{DF}$ / L min^{-1}
1	221	23	-0.002	2.0	224	99	30.8	77	5.4	105	0.5	1.5	6.0
2	270	-42	-0.001	1.7	272	98	14.5	68	5.4	108	1.2	1.4	5.8
3	176	-22	0.004	1.3	171	99	18.7	74	5.7	105	1.8	0.8	4.4
4	215	17	-0.003	2.6	221	100	17.1	50	3.4	77	1.5	1.6	4.1
5	357	-18	-0.004	1.7	363	99	16.8	75	5.7	131	1.5	1.5	8.1
6	277	25	-0.006	1.6	285	97	14.2	77	6.8	116	1.8	1.4	8.5
7	240	29	-0.002	3.2	245	100	24.6	77	5.9	120	1.9	1.7	6.0
8	289	-29	0.001	2.3	287	98	13.3	72	5.3	99	1.7	1.9	7.9
9	272	17	-0.003	2.0	277	98	13.4	61	4.6	91	2.3	1.6	5.8
10	277	-7	-0.001	2.7	278	95	10.9	67	5.5	132	1.7	1.7	5.6
11	251	37	0.001	3.4	248	97	13.6	73	6.1	129	1.7	1.6	5.7
12	281	13	0.000	2.2	281	99	16.4	60	3.8	76	1.6	1.2	6.5
13	354	16	0.000	2.7	354	99	18.4	72	5.3	83	1.3	0.9	10.4
14	259	13	0.000	3.6	260	98	14.7	78	6.3	145	2.8	0.2	6.4
15	293	-6	0.001	1.5	293	97	15.3	73	5.7	114	0.8	1.6	7.5
Mean	263 ±41	4 ±25	0.000 ±0.002	2.3 ±0.7	265 ±45	98.2 ±1.4	17.2 ±5.0	5.3 ±0.8	69.6 ±6.8	109 ±20	1.6 ±0.5	1.4 ±0.4	6.4 ±1.5

Mean ± standard deviation. $\dot{V}O_2$, O_2 consumption. $\dot{V}N_2$, N_2 consumption. $\dot{F}O_2$, fractional O_2 change. FRC, functional residual capacity. $\dot{V}O_{2_c}$, O_2 consumption corrected for $\dot{F}O_2$. S_aO_2, arterial O_2 saturation. P_aO_2, arterial O_2 partial pressure. $P_{\bar{v}}O_2$, mixed venous O_2 partial pressure. $S_{\bar{v}}O_2$, mixed venous O_2 saturation. Hb, haemoglobin, COHb, carboxyhaemoglobin, MetHb, methemoglobin; all three of these parameters came from the arterial blood gas sample. $\dot{Q}_{DF}$, direct Fick cardiac output.

Estimation of error in the direct Fick measurement

The error associated with the calculation of the direct Fick cardiac output due to the variance with the individual components of the calculation was also discussed in section 3.3.2 of chapter 3. The Fick equation, using O_2 as the subject gas, may be given as:

$$\dot{Q}_{\mathrm{DF}} = \frac{\dot{V}O_2}{k \times \mathrm{Hb_a} \times (S_aO_2 - S_{\bar{v}}O_2)} \tag{5.12}$$

Where $k = 0.1 \times 1.39 \times (1 - \mathrm{COHb}_a - \mathrm{MetHb}_a)$ and S_aO_2 and $S_{\bar{v}}O_2$ are given as fractional terms.

The variance propagation equation for the direct Fick cardiac output is:

$$\begin{aligned}\mathrm{Var}(\dot{Q}) = &\left(\frac{1}{\mathrm{Diff}_{AV}}\right)^2 \mathrm{Var}(\dot{V}_{O_2}) + \left(\frac{\partial \dot{Q}}{\partial \mathrm{Hb}_v}\right)^2 \mathrm{Var}(\mathrm{Hb}_v) + \\ &+ \left(\frac{\partial \dot{Q}}{\partial S_pO_2}\right)^2 \mathrm{Var}(S_pO_2) + \left(\frac{\partial \dot{Q}}{\partial S_{\bar{v}}O_2}\right)^2 \mathrm{Var}(S_{\bar{v}}O_2)\end{aligned} \tag{5.13}$$

Where $\mathrm{Diff_{AV}}$ is the arteriovenous difference, given as: $k \times \mathrm{Hb_a} \times (S_aO_2 - S_{\bar{v}}O_2)$, in mL/L.

The standard deviations used to calculate the variances of the haemoglobin and O_2 saturation for arterial and mixed venous blood were taken from the values reported in the manual for the device used, the ABL800 Flex (Radiometer, Denmark), where reference had also been made to the previous generation's device for certain performance characteristics which had not changed.(119; 120) The standard deviations for haemoglobin and the saturations were 1 g/L and 0.3%, respectively. The standard deviation for $\dot{V}O_2$ was calculated from the N_2 balance, as these two values were considered roughly proportional. The N_2 balance value for each participant was divided by four to give an approximate standard deviation for $\dot{V}O_2$. The effects of COHb, MetHb, and the O_2 dissolved in blood were considered sufficiently small that their variances were not included in the equation. The partial derivatives for the individual components in the direct Fick variance propagation

equation were:

$$\frac{\partial \dot{Q}_{\mathrm{DF}}}{\partial \dot{V}O_2} = \frac{1}{\mathrm{Diff}_{AV}} \tag{5.14}$$

$$\frac{\partial \dot{Q}_{\mathrm{DF}}}{\partial \mathrm{Hb}_a} = -\frac{\dot{VO}_2}{(\mathrm{Diff}_{AV})^2} \times k \times (S_aO_2 - S_{\bar{v}}O_2) \tag{5.15}$$

$$\frac{\partial \dot{Q}_{\mathrm{DF}}}{\partial S_aO_2} = -\frac{\dot{VO}_2}{(\mathrm{Diff}_{AV})^2} \times k \times \mathrm{Hb}_a \tag{5.16}$$

$$\frac{\partial \dot{Q}_{\mathrm{DF}}}{\partial S_{\bar{v}}O_2} = -\frac{\partial \dot{Q}_{\mathrm{DF}}}{\partial S_aO_2} \tag{5.17}$$

The calculated standard deviations for the direct Fick cardiac outputs for all participants with a PAC are given in table 5.6.

Table 5.6: Direct Fick cardiac output and variance values for PAC participants

Cohort ID	$\dot{Q}_{\mathrm{DF}}$ / L min^{-1}	SD / %
1	6.0	3.1
2	5.8	4.1
3	4.4	3.6
4	4.1	2.5
5	8.1	2.2
6	8.5	3.0
11	6.0	3.4
14	7.9	3.1
15	5.8	2.1
20	5.6	1.8
21	5.7	4.2
22	6.5	2.0
23	10.4	2.1
24	6.4	2.5
25	7.5	1.9
Mean	6.3± 1.6	2.8± 0.8

Mean ± standard deviation. SD, standard deviation.

5.3.3 N_2 balance

The issues relating to the N_2 balances with the datasets acquired from the cardiac surgery cohort were discussed in section 5.2.2. In this section, the change in differential pressure sensors during recruitment was discussed as possibly exacerbating these issues. Figure

5.13 shows the N_2 balance comparisons before and after the new sensors were installed. Based on these findings, the old sensors were reinstalled. However, no further participants were recruited to the study following this change. A Mann-Whitney U test was conducted

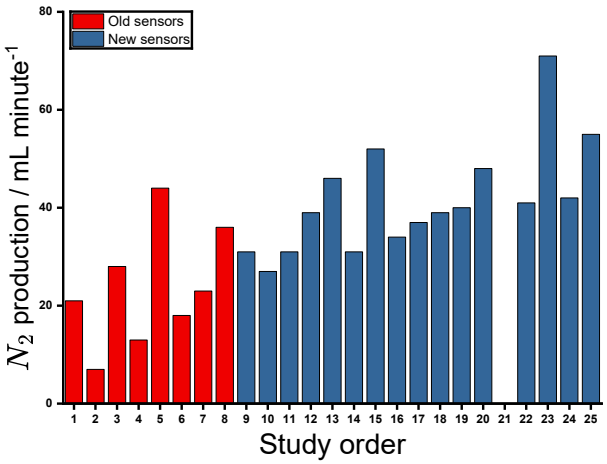

Figure 5.13: Pre-washout stage N_2 balances (given as productions) of the cardiac surgery cohort (PAC and non-PAC) participants. The x-axis gives the chronological order of recruitment. The first eight participants (red columns) were studied with the old differential pressure sensors. For the 21st participant (ID: 11), the data was not viable for fitting until it had been corrected for flow.

to determine if there were differences in the N_2 balance between participants studied with the old and new sensors. The group studied with new sensors had an N_2 production significantly higher than those studied with old sensors (U= 111, p=0.003).

5.3.4 Modelling

The $\dot{Q}$ CVs for each participant's 12 cardiac output fits (using the data collected during the ventilation stage) with and without added alveolar dead space (AD) are shown in figure 5.14. A coefficient of variation of 5% or greater following the deletion of up to one outlier was used to flag potentially unreliable datasets. Following this, the dataset with the median cardiac output value was used for further analysis. For the 15th and 21st participants for both AD and non-AD runs, and the AD run for the 22nd participant, fits were not obtained for reasons that were not completely clear, although were potentially related to the N_2 balance.

Given the findings discussed in section that the N_2 balance was significantly worse in participants studied with the new differential pressure sensor, a Mann Whitney U test

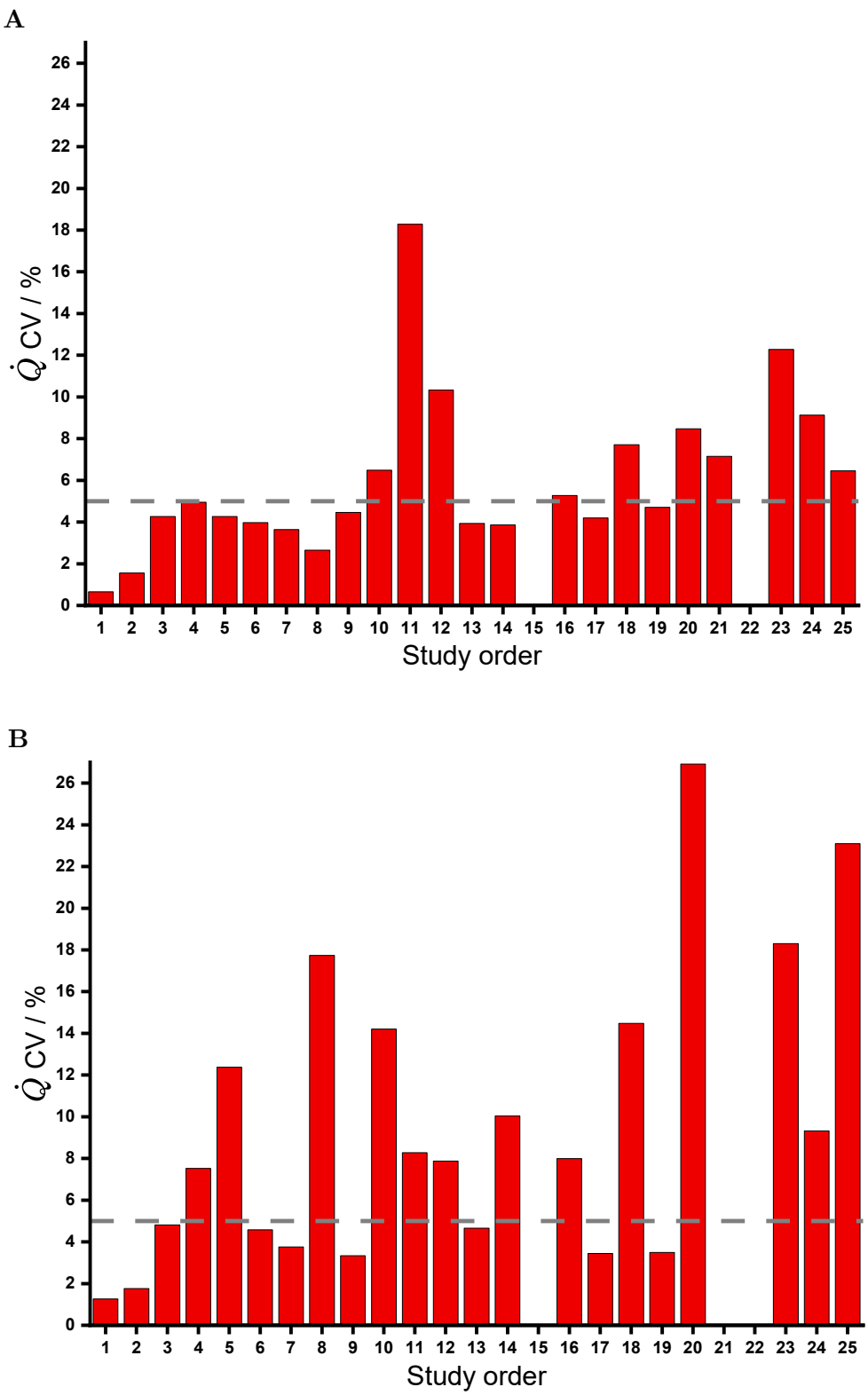

Figure 5.14: Comparison of the $\dot{Q}$ CVs for the cardiac output fits. Panel A shows the $\dot{Q}$ CVs for the fits without added dead space. Panel B shows the $\dot{Q}$ CVs for the fits with dead space added. Missing columns indicate a modelling failure for that particular dataset. The dashed grey line in both panels indicates the 5% cutoff value at which fits were deemed potentially unreliable.

was conducted to assess the difference in $\dot{Q}$ CV between participants studied with the old and new sensors. Here, the $\dot{Q}$ CV was significantly higher in participants studied with the

new sensors (U=107, p=0.001).

The CCP-estimated parameters from the different fitting segments are shown in tables 5.7 and 5.8 for the participants with a PAC in situ. Tables 5.9 and 5.10 show the same parameters for participants who did not have a PAC inserted.

Table 5.7: Fit parameter values from the CCP model during the washout stage for PAC participants

Cohort ID	V_A / L BTPS	V_D / L BTPS	C_{V_D}	σC_D	σC_L	P$_i CO_2$ / kPa	AD* / %
1	1.96	0.03	1.00	0.10	1.02	5.49	22
2	1.62	0.04	1.00	0.69	0.73	5.42	9
3	1.26	0.07	0.92	0.16	0.49	4.66	24
4	2.49	0.21	0.99	0.21	2.06	6.54	0
5	1.61	0.06	1.00	0.45	0.40	5.98	16
6	1.48	0.06	1.00	0.45	0.49	6.15	17
7	3.15	0.04	0.93	0.62	0.88	5.10	24
8	2.22	0.07	1.00	0.47	0.52	5.48	18
9	1.62	0.05	1.00	0.10	0.92	4.86	18
10	2.59	0.10	1.00	0.10	0.74	5.22	36
11	3.26	0.13	0.05	0.26	1.53	6.66	21
12	2.12	0.07	1.00	0.19	0.60	4.75	27
13	2.55	0.16	1.00	0.22	0.44	6.17	30
14	3.52	0.10	0.97	0.47	0.47	6.14	3
15	1.47	0.10	0.56	0.47	1.04	5.40	16

V_A, alveolar volume. V_D, dead space volume. C_{V_D}, relative expansion of dead space. σC_D, standard deviation of the standardised dead space. σC_L, standard deviation of the natural logarithm of lung vascular compliance. P$_i CO_2$, ideal partial pressure of CO_2. AD, alveolar dead space. *:The alveolar dead space value was estimated by fitting the steady state stage where the arterial blood gas was taken. σCd, standard deviation for the natural logarithm of the standardised lung vascular conductance, is not shown in this table, but is equal to σC_L+0.3.

Table 5.8: Fit parameter values from the CCP model during the ventilation change stage for PAC participants

Cohort ID	$\dot{V}O_2$ / mL min^{-1}	RQ	$\dot{Q}$ / L min^{-1}	$S_{\bar{v}}O_2$ / %
1	220	0.75	2.5	43
2	314	0.72	5.9	72
3	189	0.84	3.6	68
4	190	0.96	4.2	59
5	358	0.63	6.6	72
6	290	0.62	5.7	72
7	240	0.66	4.2	67
8	280	0.63	7.3	74
9	-	-	-	-
10	284	0.62	2.3	36
11	194	1.00	2.6	58
12	-	-	-	-
13	334	0.59	3.9	32
14	249	0.64	3.6	66
15	290	0.78	3.2	46

$\dot{V}O_2$, oxygen consumption. RQ, respiratory quotient. $\dot{Q}$, cardiac output. $S_{\bar{v}}O_2$, mixed venous oxygen saturation.

Table 5.9: Fit parameter values from the CCP model during the washout stage for FloTrac participants

Cohort ID	V_A / L BTPS	V_D / L BTPS	C_{V_D}	σV_D	σC_L	P_iCO_2 / kPa	AD* / %
16	1.47	0.08	1.00	0.20	0.73	5.30	6
17	1.99	0.08	0.61	0.22	0.55	6.40	24
18	1.93	0.07	0.91	0.32	0.51	5.66	1
19	2.21	0.06	1.00	0.25	0.52	6.86	3
20	1.43	0.04	0.96	0.58	0.84	5.88	17
21	2.80	0.10	0.09	0.44	1.10	4.39	23
22	2.58	0.11	1.00	0.10	0.51	4.58	33
23	2.15	0.10	0.40	0.10	0.49	5.09	10
24	2.75	0.19	0.41	0.30	0.29	5.88	33
25	2.29	0.12	0.53	0.20	0.75	5.74	16

V_A, alveolar volume. V_D, dead space volume. C_{V_D}, relative expansion of dead space. σV_D, standard deviation of the standardised dead space. σC_L, standard deviation of the natural logarithm of lung vascular compliance. P_iCO_2, ideal partial pressure of CO_2. AlvDS*, alveolar dead space estimated by fitting the steady state stage where the arterial blood gas was taken.

Table 5.10: Fit parameter values from the CCP model during the ventilation change stage for FloTrac participants

Cohort ID	$\dot{V}O_2$ / mL min^{-1}	RQ	$\dot{Q}$ / L min^{-1}	$S_{\bar{v}}O_2$ / %
16	354	0.78	4.8	63
17	225	0.54	6.5	81
18	260	0.71	4.3	68
19	197	0.72	2.6	45
20	194	0.92	3.2	72
21	214	0.96	2.3	53
22	226	0.66	2.6	45
23	265	0.89	3.4	54
24	183	0.99	1.7	41
25	338	0.80	6.6	73

$\dot{V}O_2$, oxygen consumption. RQ, respiratory quotient. $\dot{Q}$, cardiac output. $S_{\bar{v}}O_2$, mixed venous oxygen saturation.

5.3.5 PAC participant comparison

The primary group of participants studied were those who had PAC-based invasive reference measurements of cardiac output and $S_{\bar{v}}O_2$ available for comparison against the corresponding CCP estimates. This section examines the results of participants with PACs. Important to note is that no postoperative complications (beyond expected postoperative changes such as basal atelectasis etc.) were encountered during data collection that may have significantly affected the modelled results.

Cardiac output

Figure 5.15 shows the results of the comparison between CCP estimates and the direct Fick measurements of cardiac output. The CCP estimates underestimate the direct Fick measurements, and there is a poor correlation between the two sets of values. The flagged datasets appear to have a significant effect on these results, with the CCP − direct Fick difference ($\dot{Q}_{\text{diff}}$) being below the mean for all of these datasets except for one (participant 7). A Mann-Whitney U test was conducted to examine $\dot{Q}_{\text{diff}}$ values between flagged and non-flagged participants. The test showed that the $\dot{Q}_{\text{diff}}$ was significantly larger (more

negative) for flagged participants (U=5, p=0.02).

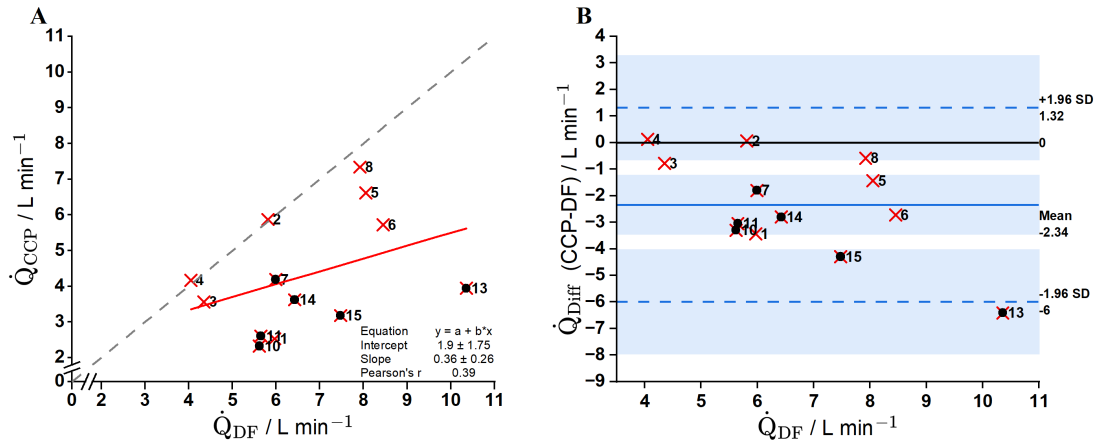

Figure 5.15: Comparison between CCP-estimated cardiac output and the invasive reference measurement from the direct Fick method. $\dot{Q}_{diff}$ is the difference between values. Flagged datasets based on the 5% $\dot{Q}$ CV cutoff are marked with black dots. Grey, dashed line, line of identity; red line, regression line; b, regression slope; a, regression intercept.

As there were more flagged participants with the new differential pressure sensors than the old, and because the N_2 balance was worse with the new sensors, it was considered a possibility that datasets with an initially worse N_2 balance (before correcting the dataset as described in section 5.2.2) yielded poorer cardiac output estimates. The relationship between the N_2 production and $\dot{Q}_{diff}$ was therefore examined to investigate this, and is shown in Figure 5.16. There was a strong negative correlation between the N_2 production and $\dot{Q}_{diff}$. r(10) = -0.79, p $<$ 0.0025.

Finally, a Mann Whitney U test was conducted to examine the differences in $\dot{Q}_{diff}$ between participants studied with the old and new differential pressure sensors. Here, the difference was not significant (U=9, p=0.086), indicating that a poor initial N_2 balance was more likely to be predictive of a poor CCP cardiac output estimate than the flow sensors themselves. This should, however, be taken with the context that the new flow sensors were more likely to yield worse N_2 balances, as shown in section 5.3.4.

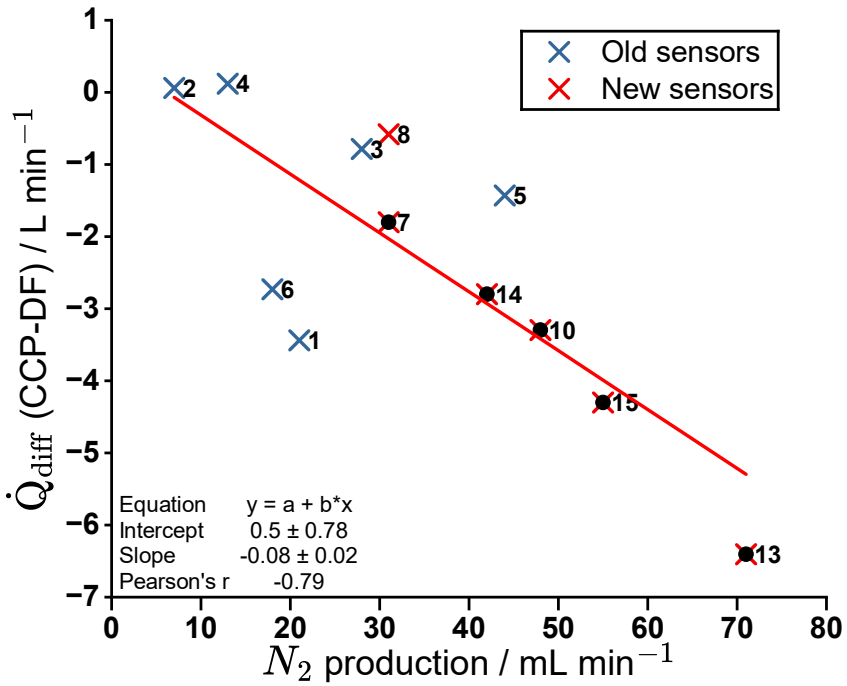

Figure 5.16: Comparison between $\dot{Q}_{\text{diff}}$ and the N_2 production. Flagged datasets based on the 5% $\dot{Q}$ CV cutoff are marked with black dots. Grey, dashed line, line of identity; red line, regression line; b, regression slope; a, regression intercept.

$S_{\bar{v}}O_2$

The comparison of CCP-estimates of $S_{\bar{v}}O_2$ and the values obtained from the mixed venous blood gas sample are shown in figure 5.17. The CCP estimates underestimate the true $S_{\bar{v}}O_2$ values, with the flagged datasets contributing significantly to this. The one non-flagged participant–1, where the $S_{\bar{v}}O_2$ was significantly underestimated, an issue at the point of data collection or modelling was likely, given that the cardiac output was also grossly underestimated (figure 5.15).

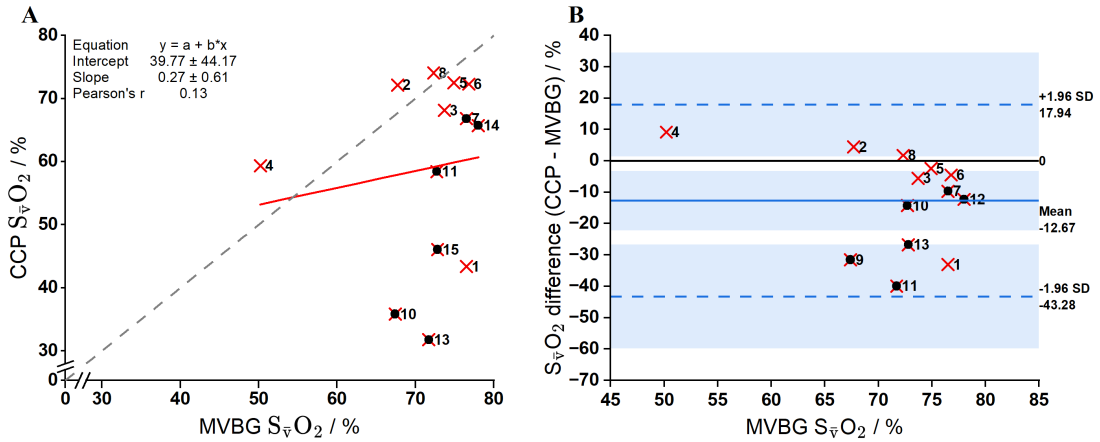

Figure 5.17: Comparison between CCP-estimated $S_{\bar{v}}O_2$ and the invasive reference measurement from the mixed venous blood gas sample. Flagged datasets based on the 5% $\dot{Q}$ CV cutoff are marked with black dots. Grey, dashed line, line of identity; red line, regression line; b, regression slope; a, regression intercept.

Alveolar dead space

The process of producing 12 cardiac output fits for each participant was repeated after the personalised alveolar dead space (AD) had been calculated. More participants were flagged due to having a high $\dot{Q}$ CV than for the runs without added dead space. Participants 7, 10, 13, 14, and 15 were flagged to both groups. Participants 4, 5, and 8 were flagged only for the AD fits. Participant 11 was flagged for the non-AD fit but not for the AD fit.

The comparisons for CCP estimates of cardiac output and $S_{\bar{v}}O_2$ with the invasive reference measurements is shown in figure 5.18. For cardiac output, apart from a minor improvement in the correlation between values when compared to fits without added dead space, the CCP estimates still underestimated the direct Fick measurements. These results were again skewed by outlying data from primarily flagged datasets. For $S_{\bar{v}}O_2$, the limits of agreement and correlation were improved when compared to non-AD fits.

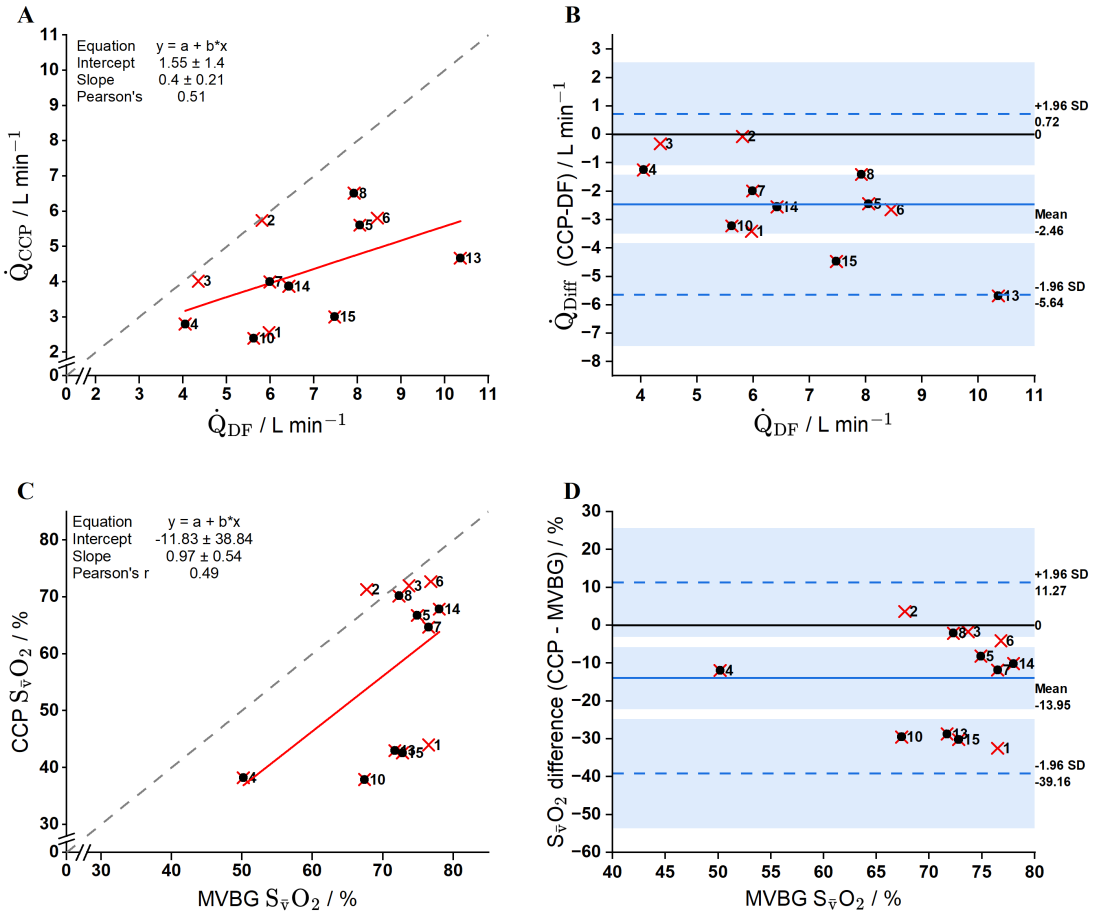

Figure 5.18: Comparison between CCP-estimated cardiac output with added alveolar dead space and the invasive reference measurement from the direct Fick method. Panels A and B compare the cardiac output values, and panels C and D compare $S_{\bar{v}}O_2$ values. Flagged datasets based on the 5% $\dot{Q}$ CV cutoff are marked with black dots. Grey, dashed line, line of identity; red line, regression line; b, regression slope; a, regression intercept.

Comparison with thermodilution

For participants with a PAC, clinical monitoring of cardiac output was made with continuous thermodilution, except for one participant–9, where a PAC without continuous monitoring functionality was used due to a supply shortage. A comparison was made between these thermodilution measurements and the direct Fick measurements. Figure 5.19 shows this comparison along with the comparison of CCP estimates (with AD) of cardiac output against the direct Fick measurements. Both thermodilution and CCP-based values underestimate the direct Fick cardiac output.

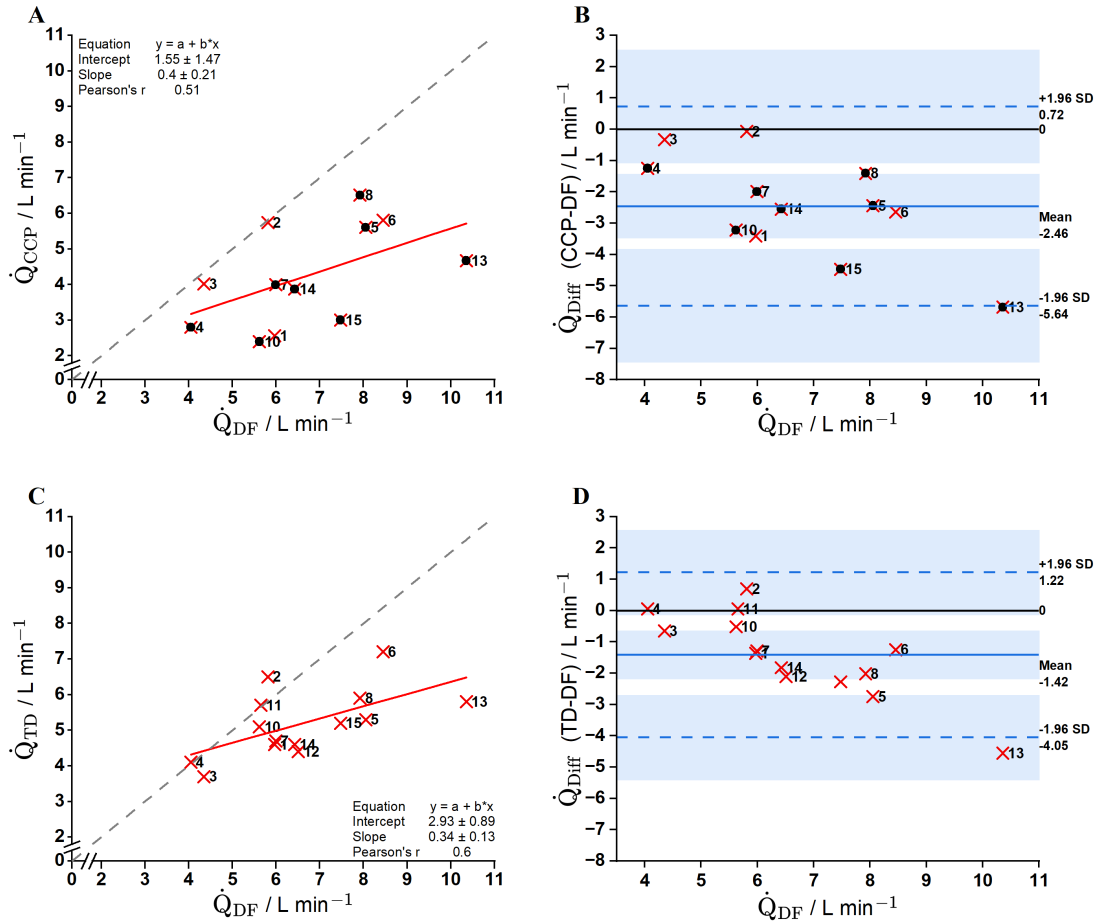

Figure 5.19: Comparison between CCP-estimated cardiac output with added alveolar dead space and thermodilution-based (TD) cardiac output (with the direct Fick measurement. Panels A and B show the comparison between CCP and direct Fick cardiac output. Panels C and D show the comparison between thermodilution and direct Fick cardiac output. Flagged datasets based on the 5% $\dot{Q}$ CV cutoff are marked with black dots. Grey, dashed line, line of identity; red line, regression line; b, regression slope; a, regression intercept.

5.3.6 Non-PAC participant comparison

As discussed in section 1.4.2 of chapter 1, there are questions over the accuracy and precision of FloTrac-based cardiac output values across a broad range of patient groups.(47; 48; 49) As such, without a reliable reference measurement of cardiac output, it is not possible to evaluate the accuracy of the CCP estimates. These participants were primarily recruited for the ongoing evaluation and optimisation of the protocol, especially the ventilation change stage. Acknowledging these points, the comparison between FloTrac and CCP estimates of cardiac output are shown in figure 5.20. Here, the CCP estimates underestimated the FloTrac values and were poorly correlated.

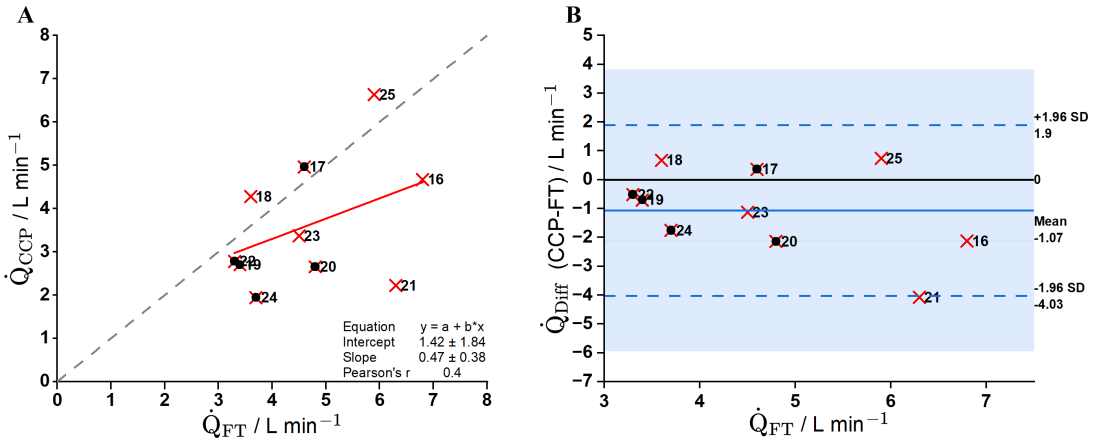

Figure 5.20: Comparison between CCP-estimated cardiac output with added alveolar dead space and FloTrac-based (FT) cardiac output. Flagged datasets based on the 5% $\dot{Q}$ CV cutoff are marked with black dots. Grey, dashed line, line of identity; red line, regression line; b, regression slope; a, regression intercept.

5.4 Discussion

5.4.1 Protocol feasibility

Experimental setup

When considering the experimental setup of the cardiac surgery cohort study, the main challenge to overcome was developing a CCP protocol which could be used to estimate cardiac output in the mechanically ventilated patient. The MFS has previously been integrated into a ventilatory circuit, as described by Ciaffoni et al., where data was collected from a participant undergoing an aortic aneurysm repair.(78) Unlike for the pulmonary hypertension and healthy volunteer cohort studies (chapters 3 and 4, respectively), it was not possible to introduce an exogenous tracer gas, such as C_2H_2, or a pre-prepared endogenous gas mixture into the ventilatory circuit.

The solution, to make brief changes to the minute ventilation, appears to be a feasible one. Due to operator inexperience with this approach, there were certain participants for whom the magnitude of the end-tidal CO_2 change was not close enough to the target of 1 kPa, as the minute ventilation adjustments were too conservative. It also became apparent that hyperventilating was preferable to hypoventilating for modelling and safety purposes. As the optimisation algorithm at the core of the CCP model aims to minimise the difference between the simulated and measured expired breaths, having more breaths

for the model to use (as is the case with hyperventilating) seemed to yield better model fits. Regarding safety, to hypoventilate the participant enough to effect a large enough change in end-tidal CO_2 in less than a minute required a period resembling an end-expiratory breath hold interspersed with two or three breaths with the potential for desaturation.

The size of the full MFS unit, including the head and trolley-mounted electronics module (figures 2.3 and 2.6 shown in chapter 2), was also a factor when planning the experiment. With critically ill patients, space around the bed, and especially the head-end, is limited. As the MFS is still in a state of constant redesign and development, there is a significant amount of space in the electronics module and, to a lesser extent, the head that can be reduced in the future.

Modelling

The sequential nature of the experimental protocol, where the partial N_2 washout stage was conducted at a separate time from the ventilation change stage, required a correspondingly segmented modelling approach. This is in contrast to the pulmonary hypertension and healthy volunteer cohort studies, including the open-circuit protocol conducted with the latter. In this study, the parameters of lung inhomogeneity recovered from the N_2 washout stage were then used for the metabolic parameter fitting. While this approach would not have affected the results, future studies, or indeed clinical applications, would benefit from a more streamlined approach where all modelling segments could be performed sequentially in the same run.

A potential source of modelling difficulty with the pulmonary hypertension cohort was the inhomogeneity of their lungs, due to factors such as a significant smoking history and previous thromboembolic disease. This would also have been true for this cohort, given the well-documented pulmonary complications of cardiac surgery in the early postoperative period. Common complications include pleural effusions and atelectasis, and others such as an increased pulmonary shunt fraction and a reduction in static and dynamic lung

compliance.(121)

5.4.2 N_2 balance

The problems relating to the N_2 balance were a major and unexpected limitation of the study. While significant work was done to diagnose and address the potential causes, as detailed in section 5.2.2, it is also clear that more work is required. This is especially true given the strong negative correlation between $\dot{Q}_{\text{diff}}$ (CCP cardiac output - direct Fick cardiac output value) and the uncorrected pre-washout N_2, which suggests that a poor N_2 balance affects the recovery of CCP parameters.

Isoflurane

The possible influence of expired isoflurane being measured incorrectly as an inert gas and being the main cause of the N_2 balance issue was effectively ruled out. While there was likely to be a percentage of isoflurane in each of the participants at the time of MFS connection, this was shown to be too small to affect the N_2 balance significantly. In future studies where a subject is connected to the MFS while anaesthetised with a volatile gas, either a post-hoc correction such as the one discussed in section 5.2.2 for isoflurane, or a hardware adjustment for the detection of the gas is required.

Positive pressure ventilation

An unresolved issue from the wider N_2 balance problem stems from the inability of the differential pressure sensors to accurately account for the rapid changes in flow with positive pressure ventilation. In an effort to optimise the datasets acquired in this study, a flow correction was applied. However, this did not appear to have the desired effect, as datasets with a worse initial N_2 balance were more likely to underestimate the corresponding direct Fick cardiac output (figure 5.16).

Future work to address this issue will revolve around finding an appropriately configured differential pressure sensor and possibly also adjusting the geometry of the flow path

within the MFS head. The new sensors installed midway through recruitment were more stable than the ones they replaced, but at the expense of response time. As seen in figure 5.13, this likely caused a worsening of the N_2 balance. Since the conclusion of the study, a third set of differential pressure sensors aimed at striking a better balance between the response time and stability will be trialled in upcoming studies.

The current pressure sensing system with the MFS is such that the pressure is sampled circumferentially at multiple points in a grid formed by the differential pressure sensors. With the rapid transience of positive pressure ventilation, it is possible that sampling pressure at the circumference does not adequately reflect the flow through the centre of the flow path. Therefore, altering the geometry of the MFS head for a central sampling of pressure may help with addressing this issue.

5.4.3 Accuracy of CCP-estimated parameters

Cardiac output

The CCP estimates, without dead space added, correlate relatively poorly with the direct Fick measurements, with a clear bias towards underestimating the direct Fick cardiac output. These results were clearly affected by the poor N_2 balances, as discussed above, and make it difficult to comment on the overall validity of the protocol and modelling aspects of the experiment.

A further consideration when considering the comparison between CCP estimates and the direct Fick cardiac output is that datasets flagged for having a high $\dot{Q}$ CV were included. This is in contrast to the results presented for the pulmonary hypertension cohort, and was considered necessary due to the small sample size. When considering only the non-flagged participants in the comparison plots in figure 5.15, the low $\dot{Q}_{\text{diff}}$ for most of these participants shows that further studies with this experimental method, where the limitations of this current study are addressed, would be worthwhile.

$S_{\bar{v}}O_2$

The CCP estimates of $S_{\bar{v}}O_2$ were poorly correlated with the mixed venous blood gas sample results (figure 5.17). Given the results for the cardiac output estimates, as discussed directly above, this is unsurprising. The CCP estimate of $S_{\bar{v}}O_2$ is reliant on the cardiac output estimate, as it is the uptake of the tracer gas (CO_2 in this study) that is modelled. Therefore, a poorly estimated cardiac output will inevitably result in a poorly estimated $S_{\bar{v}}O_2$. This can be seen when examining the comparison plots for cardiac output and $S_{\bar{v}}O_2$ (panel B in figures 5.15 and 5.17), where participants 2, 3, 4, 5, 6, and 8 have estimates for both parameters which are relatively close to the invasive reference measurements. It is also clear that the outlying datasets form the majority of the poor estimates.

Alveolar dead space

As all participants recruited had arterial blood gas measurements taken during their time connected to the MFS, it was possible to obtain an estimate of the alveolar dead space fraction (AD). In work that has been referenced in chapters 3 and 4, Sandhu et al. showed that the total fraction of alveolar dead space in healthy individuals may be greater than originally thought, at approximately 11.5%.(94) This was also shown in experimental data from Farrow et al.(95) As seen in tables 5.7 and 5.9, for most participants, the alveolar dead space values were much higher than the 11.5% figure that Sandhu et al. showed was present, on average, for healthy individuals. This is an expected finding given the changes to the lung in the immediate postoperative period.(121) Dixon et al. also discussed the effect of postoperative inflammatory changes triggering microvascular thromboses in the lung as a mechanism of an acute increase in dead space fraction.(122)

The addition of this estimated dead space to the metabolic stage of the modelling had the effect of slightly improving the CCP-estimated cardiac output and $S_{\bar{v}}O_2$, relative to the invasive reference measurements. For both parameters, the correlation and confidence intervals improved (figure 5.18) relative to the invasive measurements when compared to the fits with no added dead space. Importantly, not all AD estimates were higher than

the corresponding non-AD estimates. It is not clear whether this is an observation which stems from the previously stated issues of poor model fitting due to N_2 balance problems or a real finding. In the healthy volunteer cohort, all CO_2-based estimates of cardiac output were higher with added dead space (figure 4.12).

FloTrac participants

The recruitment of participants with a minimally-invasive FloTrac cardiac output monitoring was due to the previously discussed difficulties in recruiting participants with PACs. With these participants, the emphasis was on developing and fine tuning the experimental protocol. The scientific basis for pulse contour devices, and the FloTrac especially, was discussed in chapter 1. Briefly, the FloTrac is connected to a pre-existing arterial line. Here, the pressure signal from the arterial line is converted to a stroke volume and then used to give a cardiac output by multiplying this with the heart rate.(38; 42; 45) Multiple studies have highlighted the limitations of the FloTrac, especially in abnormal physiological states.(47; 48; 49) As such, the FloTrac cardiac output values were not considered to be true reference values for this study.

5.4.4 Limitations

The two major limitations of this study, recruitment and N_2 balance have been discussed extensively in this chapter. The latter will not be discussed here again. With the former, the difficulties in recruitment (figure 5.12), indicate the institutional, and likely regional, aversion to inserting PACs. Studies such as PAC-man have no doubt influenced this, although the previously discussed (section 1.5) caveats to the conclusions from this study and others, such as Bossert et al. indicate that PAC use may have fallen out of favour unfairly.(39; 58) Whether the reluctance to insert PACs is justified or not, however, any further studies examining this CCP protocol against PAC-based measurements (including the direct Fick method for mixed venous O_2 sampling), should be done in areas or institutions where the threshold for insertion is lower.

There are other limitations to this study which should be discussed. These include, protocol specific ones, especially relating to the ventilation change stage, and the modelling failures for certain participants, where cardiac output and $S_{\bar{v}}O_2$ estimates were not obtained.

Protocol

Most cardiac surgery patients admitted to the ICU in the study's institution were scheduled for extubation within four hours of admission, if they were clinically stable. This left a limited window of time to conduct what was a relatively lengthy (necessarily so) CCP protocol of between 20 to 30 minutes, before weaning from sedation and the ventilator had begun, but after the steps to properly admit the patient to the ICU had been completed. As a result, only one ventilation change stage and N_2 washout per participant was conducted. Apart from time considerations, however, there would be no reason why multiple such stages could not be conducted to examine the reproducibility of the fit parameters.

Regarding the ventilation change, during the early recruitment stage, the changes to minute ventilation often fell well below the target of a $\pm$ 1 kPa change with the end-tidal CO_2. This was primarily due to patient safety considerations, especially when hypoventilating the participant. It is possible that aiming for such a high magnitude of change is not necessary, given the highly precise measurements made with the MFS, however, it would be beneficial to examine the effect of this change relative to the accuracy of the estimated cardiac output. Another factor to consider is that the ventilation change stage was strictly kept to a minute at most, to avoid excessive recirculation and potential modelling difficulties. The circulation sub-model is currently being examined, with the view to improve how recirculation is modelled. It may be that this allows for a longer ventilation change stage, which could enable better model fitting.

Modelling

For two participants (9 and 12), estimates of cardiac output and $S_{\bar{v}}O_2$ were not recovered due to modelling failures. This was identified as likely being due to a disparity between

the true and modelled cardiac output. Here, the O_2 consumption would be the same in both cases (as it is measured), however, with the model attempting to fit a low cardiac output, the delivered O_2 would be too low to meet the metabolic demands. Machinery within the CCP model exists to protect against this, but only to a certain extent. As with most of the datasets obtained in this study, it may be that the N_2 balance affected the data and subsequently the modelling, rather than the issue being with the modelling itself, however.

5.4.5 Thermodilution measurements

The two-way bias of thermodilution-based cardiac output, where true low cardiac outputs are overestimated and vice-versa, has been discussed previously (section 1.5 and 3.4.5). This pattern is again seen with the cardiac surgery cohort, where higher direct Fick cardiac output values are progressively underestimated to a greater extent.

In this cohort, thermodilution is clearly superior to the CCP estimates. However, as discussed above, the significant technical limitations with the CCP protocol in this study warrant a repeat of this comparison once these limitations are addressed.

5.4.6 Direct Fick cardiac output

The direct Fick cardiac output measurements taken in this study were reliable from a methodological standpoint. In most cases, the arterial and mixed venous blood gases were taken during the same steady state. The $\dot{V}O_2$ values used were corrected as discussed in section 5.3.2. The reliability of the reference measurements is further reflected in the low variance (table 5.6) when the individual components of the direct Fick calculation are accounted for.

5.5 Conclusion

The results of an observational study, examining non-invasively acquired cardiopulmonary parameters in patients post-cardiac surgery, have been discussed. Specifically, CCP es-

timates of cardiac output and $S_{\bar{v}}O_2$ have been compared against the invasive reference standards, the direct Fick method and mixed venous blood gas analysis, respectively. It was also possible to compare the relative performance of thermodilution-based cardiac output compared to the direct Fick method.

Significant limitations in the study, primarily related to difficulties in recruiting appropriate participants and molecular flow sensing in the context of positive pressure ventilation, make it difficult to comment on the validity of this CCP protocol. With the small number of participants where the technical difficulties with N_2 balance were less pronounced, the CCP-estimated parameters compare favourably with the invasive reference measurements. This indicates that repeating the study, with more favourable recruitment conditions and once the technical difficulties have been solved, would be worthwhile.

This study has also highlighted the need for a less invasive alternative to PAC-based cardiac output and mixed venous O_2 measurement. The reluctance to insert PACs due to safety concerns meant that a relatively unvalidated alternative in the FloTrac was used when monitoring of cardiac output monitoring was clinically indicated. It is also evident that thermodilution is not completely reliable for single measurements of cardiac output, especially in situations of low or high output states.

A novel methodology for the CCP-based estimation of lung inhomogeneity and metabolic parameters in the mechanically ventilated patient has been presented in this chapter. While the difficulties encountered mean that a direct comparison of the estimated parameters against the reference measurements is not helpful in drawing conclusions, this study has set a foundation for future studies, including clear areas of improvement which can and are being addressed.

6 Conclusion and Future Work

Presented in this thesis is work centred around the development and application of computed cardiopulmonography (CCP) for estimating cardiopulmonary parameters. The primary parameters of interest were cardiac output and mixed venous O_2 saturation ($S_{\bar{v}}O_2$). CCP combines a technological aspect, the molecular flow sensor (MFS), with a computational model of the cardiopulmonary system. The MFS allows for highly accurate and frequent (every 10 ms) measurements of O_2, CO_2, H_2O vapour, CH_4, and C_2H_2 to be made. This is done using laser absorption spectroscopy and pneumotachography. A particular advantage of the MFS system is that all gas analysis occurs in the mainstream gas flow contemporaneously with the gas flow measurement. This avoids the uncertain delays associated with sidestream analysers, it avoids changes away from the physicochemical conditions under which flow is measured, and allows for the rapid estimation of viscosity and density to ensure an accurate translation of the pressure drop recorded by the pneumotachograph into a corresponding measurement of respiratory flow. The computational model utilises three sub-models: the lognormal lung, circulatory and body gas stores, and physicochemical blood models to simulate the physiology of gas exchange from the lung to the circulation. The parameters of the cardiopulmonary model are then fit to the measured gas profiles from the MFS in order to estimate the lung inhomogeneity and metabolic parameters using a nonlinear optimisation routine.

The overarching motivation for developing a CCP-based method for the estimation of cardiac output and $S_{\bar{v}}O_2$ was that the techniques currently available in clinical practice are invasive, inaccurate, impractical, or a combination of these. It was therefore necessary to apply the experimental CCP methods to representative populations, where a comparison of accuracy and practicality could be made against the reference standards of measurement. This thesis presents the work from three cohort studies, including two, the pulmonary hypertension and cardiac surgery cohorts, where cardiac output and $S_{\bar{v}}O_2$ monitoring is indicated with relative frequency. The remaining study, using healthy volunteers, was conducted to compare exogenous and endogenous gas-based methods for the estimation of

cardiopulmonary parameters, as well as to examine the overall feasibility of using CO_2 for this purpose. The conclusions from the three cohort studies are discussed below.

6.1 Pulmonary Hypertension Cohort

In chapter 3, the pulmonary hypertension cohort study was designed with the goal of bringing a practical, non-invasive, and accurate technique for the estimation of cardiac output and $S_{\bar{v}}O_2$ in the non-ventilated patient population. The rebreathing method used to facilitate the wash-in of the tracer gases, CH_4 and C_2H_2, improved upon the practicality of open-circuit configurations used in previous studies. Here, the anaesthetic reservoir bag used for rebreathing could be pre-filled, negating the need for the MFS to be connected to gas supply lines. The protocol length, less than five minutes, also reduces the barrier to uptake of this method in clinical and research settings.

Due to the multiple points of novelty with this experimental configuration, a new modelling approach was developed. The effects of different termination sensitivities within the nonlinear optimisation algorithm were examined. It was determined that the granularity offered by progressively more sensitive tolerances was beyond the level of physiological significance required. As part of this wider analysis, each participant's dataset was run 36 times (12 times for each of the three termination sensitivity sets) to obtain a coefficient of variation for the sum of the squared residual and cardiac output ($\dot{Q}$ CV). A cutoff value of 5% was implemented for the $\dot{Q}$ CV, where datasets above this value flagged as being unreliable. As a quality control indicator, this process has now been taken forward to other CCP studies, including the ones presented in this thesis.

The CCP estimates of cardiac output for participants where the $\dot{Q}$ CV was less than 5%, i.e. non-flagged participants, were comparable, and potentially slightly superior, to the corresponding thermodilution measurements when compared with the reference direct Fick measurements. While the caveat of this statement referring to non-flagged participants should not be ignored, the promise of this rebreathing technique using exogenous tracer

gases is clear. The $S_{\bar{v}}O_2$ estimates compared less well with the direct Fick measurements and highlighted a limitation of the study, which was that pulse oximetry was used to estimate the arterial content of O_2.

The presence of a percentage of alveolar dead space in healthy individuals was discussed as a possibility, based on findings from Sandhu et al.(94) The effect of adding this dead space to the model lung was examined, with the overall result showing an increase in CCP-estimated cardiac output, and therefore comparing more favourably to the direct Fick measurements than the fits without dead space added.

The results of the pulmonary hypertension study represent a significant advancement in the application of CCP to estimate cardiac output and $S_{\bar{v}}O_2$. As stated above, the number of flagged participants cannot be ignored, and work is required from a protocol setup and modelling standpoint to reduce and eliminate datasets with high $\dot{Q}$ CVs. Despite this, the fact that unreliable datasets are identified early through this mechanism allows for results with a low $\dot{Q}$ CV to be used with greater confidence.

6.2 Healthy Volunteer Cohort

In chapter 4, the healthy volunteer study was conceived in equal parts to test the rebreathing circuit configuration (subsequently carried forward to the pulmonary hypertension study) and to compare cardiac output and $S_{\bar{v}}O_2$ estimates from exogenous and endogenous (CO_2) tracer gas-based methods. The motivation for using CO_2 as a tracer gas was to increase the potential uptake of the method in settings where it would be difficult or impossible to use exogenous tracer gases, such as in mechanically ventilated patients.

This study was limited by the lack of a reference measurement for both cardiac output and $S_{\bar{v}}O_2$. As a result, comparisons between the four different protocols, the exogenous rebreathing and open-circuit and two CO_2 rebreathing protocols, were required. This included the use of correlations and Bland-Altman plots to examine the relative bias of

each protocol. An adapted estimation of the intraclass correlation coefficient (ICC) was then used to examine the relative precision between the protocols. While the relatively small sample size of the cohort made definitive conclusions difficult to make, the differences in parameter estimates between the two CO_2 protocols as well as high $\dot{Q}$ CV values only appearing for CO_2 and not exogenous tracer gas datasets, suggest that there are inherent difficulties with using CO_2 as a tracer gas. Another finding of note was that the rebreathing exogenous tracer gas protocol yielded the highest cardiac output estimates. Given the findings of the pulmonary hypertension cohort, where this nearly identical protocol underestimated the direct Fick measurements, it is likely that the CO_2 protocols (and open-circuit exogenous protocol) in the healthy volunteer study were underestimating the true cardiac output to a greater degree.

6.3 Cardiac Surgery Cohort

Chapter 5 presented the results from the cardiac surgery cohort. In contrast to patients in the pulmonary hypertension cohort—where pulmonary artery catheterisation is required not only for mixed venous O_2 sampling and cardiac output monitoring but also for measuring pulmonary artery pressures (and therefore cannot be replaced)—a larger proportion of cardiac surgery patients could benefit from a non-invasive alternative to the pulmonary artery catheter (PAC)-based approach. Currently, cardiac output monitoring is routinely avoided, or minimally invasive options, such as pulse contour analysis, which lack accuracy, are used due to the risks associated with PAC insertion. The utility of a non-invasive and mass-balanced approach, as CCP is, is therefore clear.

This study was limited by two major factors. Firstly, the reluctance to insert PACs due to safety concerns meant that the sample size was much smaller than anticipated. Secondly, the technical issues with the MFS when connected to mechanically ventilated participants affected the measured data and subsequent modelling, even with a post-hoc correction to flow during the data processing stage. Due to the latter factor, the CCP estimates of cardiac output and $S_{\bar{v}}O_2$ compared poorly with the invasive reference measure-

ments. Despite this, when considering only the small number of non-flagged participants, where the uncorrected N_2 balance was good, the comparisons were far more favourable. This indicates a certain degree of promise that the technique developed in this study is viable, once the technical issues are rectified (or improved upon significantly).

Since all participants in this study had arterial blood gas samples taken during MFS data collection, it was possible to directly estimate the alveolar dead space fraction, rather than relying on the literature value used in the pulmonary hypertension and healthy volunteer cohorts. In the healthy volunteer cohort study, cardiac output was found to be significantly higher following the addition of alveolar dead space to the model lung for the CO_2 datasets compared with the exogenous tracer gas datasets. Therefore, for the cardiac surgery participants, it was anticipated that the modelled cardiac outputs, calculated with the additional dead space included, would also be higher than those obtained without incorporating dead space, as a CO_2-based method was also used here to estimate cardiac output. This was not entirely the case, however, with some cardiac output values being lower following the addition of dead space. It is currently unclear whether this finding is confounded by the technical issues with the data collection or whether the expectation that the addition of alveolar dead space to the model should increase the cardiac output is based on incorrect assumptions.

6.4 Future Work

The three studies discussed in this thesis provide several avenues for the improvement of CCP techniques and informing future studies. For all three studies, only single measurements of cardiac output and $S_{\bar{v}}O_2$ were taken (one per different protocol for the healthy volunteer study). It is entirely possible, however, to estimate these parameters on a more frequent basis to guide acute therapy. Postoperative cardiac surgery patients would be an example of this, where the CCP technique used in chapter 5 of hyper-/hypoventilating the patient to effect a CO_2 change could be conducted as often as every 30 minutes (based on the model run time), with steady states in between.

While in certain clinical situations, cardiac output and $S_{\bar{v}}O_2$ measures more frequent than what CCP can offer may be required, the true value of these CCP estimates may lie in longer-term clinical and research applications. The current invasive nature of accurate measurements of cardiac output and $S_{\bar{v}}O_2$ limits the use of these parameters in population-based studies. However, certain published studies indicate the benefit of exploring this area. Bown et al. demonstrated that a reduction in cardiac output, measured at baseline, 18 months, 3 and 5 years, may be associated with cognitive decline in multiple domains.(123) Additionally, single measurements of cardiac output and $S_{\bar{v}}O_2$ in patients admitted to hospital may be useful in predicting long-term morbidity and mortality. Hamdan et al. and Hsieh et al. showed higher rates of mortality and morbidity associated with a lower cardiac output-dependent measure (cardiac index and cardiac power output, respectively) in patients with heart failure.(124; 125) Similarly, for $S_{\bar{v}}O_2$, with measurements taken upon admission to the intensive care unit (ICU), Holm et al. and Kaakinen et al. both showed worse short- and long-term outcomes for patients with $S_{\bar{v}}O_2$ values less than 60%.(126; 127)

As discussed earlier in this chapter, certain weaknesses of the pulmonary hypertension cohort study must be addressed for the protocol to be taken forward for further clinical and research applications. Namely, these weaknesses were the number of participants for which the $\dot{Q}$ CV was greater than the cutoff value of 5% and the bias towards the CCP values of cardiac output underestimating the direct Fick values. For the former, the work should be focused around trialling new protocols with an input stimulus with more power than from the current method. This may include measures such as extending the period of rebreathing, or including an O_2 washout period, to more accurately estimate the lung inhomogeneity and volume parameters. For the latter, the work in this thesis explored increasing the modelled dead space to address the underestimation of cardiac output. This did not entirely correct the phenomenon, however. As CCP is rooted in mass balance, the presence of residual bias suggests that there are flaws in the modelling. Two future pieces of work to address this should be considered. Firstly, the exchange of C_2H_2

with the airways during tidal breathing should be explored. Specifically, the question to be answered is whether a fraction of C_2H_2 is absorbed by the airways during inspiration and released back during expiration, and is therefore not available for uptake into the systemic circulation, as currently modelled. Secondly, further validatory work concerning the recirculation within the circulatory and body gas stores (CBGS) sub-model should be conducted. In particular, the blood volumes for the central compartments and the recirculation times for C_2H_2 should be reevaluated.

For the healthy volunteer cohort, multiple participants were flagged for having a high $\dot{Q}$ CV when undertaking the CO_2 rebreathing protocol. No participants were flagged for this reason in either of the exogenous tracer gas protocols. As such, the future work, similar to the pulmonary hypertension cohort protocol, should centre around finding a protocol which provides more power in the input signal. This would then help inform further protocol designs for ventilated subjects, where CO_2 is used as a tracer gas.

With reference to future studies involving mechanically ventilated participants, the two factors which severely limited the cardiac surgery cohort study must be addressed. The issues surrounding N_2 balance may be addressed in the first instance by installing a newly acquired third version of differential pressure sensors, which address the stability issues encountered with the first set and the slow response time with the second set. Another factor to address, which is more complex to address, relates to altering the geometry of the flow path within the MFS head. Here, the challenge is to develop a method for sampling pressure radially as well as circumferentially across the measurement mesh. A potential issue with circumferential sampling in mechanically ventilated subjects is that the rapid transience between inspiration and expiration may create patterns of flow which differ between the centre and peripheries of the flow path, thereby causing inaccuracies in data measurement. Once the flow sensing has been fixed so that low values for N_2 exchange are consistently obtained in mechanically ventilated subjects, a preliminary study in participants without PACs should be conducted to examine whether $\dot{Q}$ CVs below the

5% cutoff can reliably be achieved.

The second factor which affected the cardiac surgery cohort study was the small sample size, due to the difficulty in recruiting participants with PACs. For future research studies where the aim is to validate the presented CCP technique, a centre (potentially overseas) where PAC use is more frequent should be used. However, this should only be attempted once the aforementioned technical issues are rectified.

Conclusion

The results of three studies, examining the use of computed cardiopulmonography for the non-invasive estimation of cardiac output and $S_{\bar{v}}O_2$ have been discussed. While each study presented challenges and limitations to overcome, these results represent meaningful advances in our understanding of CCP. This includes definitive points of improvement, which can clearly and tangibly be addressed in future studies.

7 Appendix: Contributions

The studies presented in this thesis included healthy volunteers and patients, where contributions from multiple individuals were required for the design and safe execution of the experimental protocols conducted. Listed below are the acknowledgements of the contributions made by these individuals for each study. In addition to this list, the design of the studies and analysis and interpretation of the data reported within this thesis was undertaken entirely by the author under the supervision of Professor Peter Robbins.

Pulmonary hypertension cohort study

Dr Nick Talbot: Chief investigator; assistance in securing ethical approval.

Dr Dominic Sandhu: Development and improvement to computational model; assistance in securing institutional ethical approval.

Dr Graham Richmond: Technical assistance with molecular flow sensor.

Dr Francesco Lo Giudice: Assistance recruiting participants; clinical proceduralist during experimental protocols.

Professor Luke Howard: Assistance recruiting participants; clinical proceduralist during experimental protocols; assistance in securing institutional ethical approval.

Healthy volunteer cohort study

Dr Nick Talbot: Chief investigator; assistance in securing ethical approval; conception and design of study.

Dr Dominic Sandhu: Development and improvement to computational model.

Ms Hazel Bott: Assistance in recruiting participants, assistance with dataset processing.

Dr Graham Richmond: Technical assistance with experimental protocol and molecular flow sensor.

Dr Nicholas Smith: Technical assistance with experimental protocol and molecular flow sensor; conception and design of open-circuit exogenous gas protocol.

Cardiac surgery cohort study

Dr Andrew Johnson: Trust-based chief investigator; assistance in securing ethical approval; assistance recruiting participants; support during experiments.

Dr Dominic Sandhu: Development and improvement to computational model.

Dr Graham Richmond: Assistance in N_2 balance issue investigation; design and development of flow correction program, assistance with experimental protocol.

Dr Nicholas Smith: assistance with experimental protocol.

Dr John Couper: Design and development of physical support structures for molecular flow sensor.

References

[1] Michael A Gropper, Lars I Eriksson, Lee A Fleisher, Jeanine P Wiener-Kronish, Neal H Cohen, and Kate Leslie. *Miller's anesthesia, 2-volume set E-book*. Elsevier Health Sciences, 2019. ISBN 0323612644.

[2] Peter Kam and Ian Power. *Principles of Physiology for the Anaesthetist*. CRC Press, 2020. ISBN 0429288212.

[3] H. Thomas Robertson. Dead space: the physiology of wasted ventilation. *European Respiratory Journal*, 45(6):1704–1716, 2015. ISSN 0903-1936. doi: 10.1183/09031936.00137614.

[4] Marc Humbert, Gabor Kovacs, Marius M. Hoeper, Roberto Badagliacca, Rolf M. F. Berger, Margarita Brida, Jørn Carlsen, Andrew J. S. Coats, Pilar Escribano-Subias, Pisana Ferrari, Diogenes S. Ferreira, Hossein Ardeschir Ghofrani, George Giannakoulas, David G. Kiely, Eckhard Mayer, Gergely Meszaros, Blin Nagavci, Karen M. Olsson, Joanna Pepke-Zaba, Jennifer K. Quint, Göran Rådegran, Gerald Simonneau, Olivier Sitbon, Thomy Tonia, Mark Toshner, Jean Luc Vachiery, Anton Vonk Noordegraaf, Marion Delcroix, Stephan Rosenkranz, Markus Schwerzmann, Anh Tuan Dinh-Xuan, Andy Bush, Magdy Abdelhamid, Victor Aboyans, Eloisa Arbustini, Riccardo Asteggiano, Joan Albert Barberà, Maurice Beghetti, Jelena Čelutkienė, Maja Cikes, Robin Condliffe, Frances De Man, Volkmar Falk, Laurent Fauchier, Sean Gaine, Nazzareno Galié, Wendy Gin-Sing, John Granton, Ekkehard Grünig, Paul M. Hassoun, Merel Hellemons, Tiny Jaarsma, Barbro Kjellström, Frederikus A. Klok, Aleksandra Konradi, Konstantinos C. Koskinas, Dipak Kotecha, Irene Lang, Basil S. Lewis, Ales Linhart, Gregory Y. H. Lip, Maja Lisa Løchen, Alexander G. Mathioudakis, Richard Mindham, Shahin Moledina, Robert Naeije, Jens Cosedis Nielsen, Horst Olschewski, Isabelle Opitz, Steffen E. Petersen, Eva Prescott, Amina Rakisheva, Abilio Reis, Arsen D. Ristić, Nicolas Roche, Rita Rodrigues, Christine Selton-Suty, Rogerio Souza, Andrew J. Swift, Rhian M. Touyz, Silvia Ulrich, Martin R. Wilkins, and Stephen John Wort. 2022 esc/ers guidelines

for the diagnosis and treatment of pulmonary hypertension. *European Heart Journal*, 43(38):3618–3731, 2022. ISSN 0195-668X. doi: 10.1093/eurheartj/ehac237.

[5] Marius M. Hoeper, Marc Humbert, Rogerio Souza, Majdy Idrees, Steven M. Kawut, Karen Sliwa-Hahnle, Zhi-Cheng Jing, and J. Simon R. Gibbs. A global view of pulmonary hypertension. *The Lancet Respiratory Medicine*, 4(4):306–322, 2016. ISSN 2213-2600. doi: 10.1016/s2213-2600(15)00543-3.

[6] Bradley A. Maron. Revised definition of pulmonary hypertension and approach to management: A clinical primer. *Journal of the American Heart Association*, 12(8), 2023. ISSN 2047-9980. doi: 10.1161/jaha.122.029024.

[7] Yen-Chun Lai, Karin C. Potoka, Hunter C. Champion, Ana L. Mora, and Mark T. Gladwin. Pulmonary arterial hypertension. *Circulation Research*, 115(1):115–130, 2014. ISSN 0009-7330. doi: 10.1161/circresaha.115.301146.

[8] Parul Pahal and Sandeep Sharma. *Secondary Pulmonary Hypertension*. StatPearls Publishing, Treasure Island (FL), 2025.

[9] Adaani Frost, David Badesch, J. Simon R. Gibbs, Deepa Gopalan, Dinesh Khanna, Alessandra Manes, Ronald Oudiz, Toru Satoh, Fernando Torres, and Adam Torbicki. Diagnosis of pulmonary hypertension. *European Respiratory Journal*, 53(1):1801904, 2019. ISSN 0903-1936. doi: 10.1183/13993003.01904-2018.

[10] National Institute for Cardiovascular Outcomes Research (NICOR). National adult cardiac surgery audit 2024 summary report. Report, National Institute for Cardiovascular Outcomes Research, 2024.

[11] Abdelhadi Ismail, George Semien, Sanjeev Sharma, Sara A Collier, and Szabolcs Y Miskolczi. *Cardiopulmonary bypass*. StatPearls Publishing, 2024.

[12] John H. Alexander and Peter K. Smith. Coronary-artery bypass grafting. *New England Journal of Medicine*, 374(20):1954–1964, 2016. ISSN 0028-4793. doi: 10.1056/nejmra1406944.

[13] Furqan A Rajput and Roman Zeltser. Aortic valve replacement. In *StatPearls [Internet]*. StatPearls Publishing, 2023.

[14] Gregory A. Fishbein and Michael C. Fishbein. Mitral valve pathology. *Current Cardiology Reports*, 21(7), 2019. ISSN 1523-3782. doi: 10.1007/s11886-019-1145-5.

[15] Arthur C. St. André and Anthony Delrossi. Hemodynamic management of patients in the first 24 hours after cardiac surgery. *Critical Care Medicine*, 33(9):2082–2093, 2005. ISSN 0090-3493. doi: 10.1097/01.ccm.0000178355.96817.81.

[16] J. M. Ferrao De Oliveira. Mitral valve repair: better than replacement. *Heart*, 92 (2):275–281, 2006. ISSN 1355-6037. doi: 10.1136/hrt.2005.076208.

[17] Christian Besler, Joerg Seeburger, Holger Thiele, and Philipp Lurz. Treatment options for severe functional tricuspid regurgitation: indications, techniques and current challenges. *ESC European J Cardiol Practice*, 16, 2018.

[18] Adolf Fick. Ueber die messung des blutquantum in den herzventrikeln. *Sb Phys Med Ges Worzburg*, pages 16–17, 1870.

[19] Leroy D Vandam and John A Fox. Adolf fick (1829–1901), physiologist: a heritage for anesthesiology and critical care medicine. *The Journal of the American Society of Anesthesiologists*, 88(2):514–518, 1998. ISSN 0003-3022.

[20] Gary J Gazibarich, John Edward Boland, and Louis W Wang. *Analysis and interpretation of Fick and thermodilution cardiac output determinations*, pages 221–232. CRC Press, 2019.

[21] O Klein. Zur bestimmung des zirkulatorischen minutenvolumens beim menschen nach dem fickschen prinzip. *Munchen Med Wochenschr*, 77:1311–2, 1930.

[22] Jiří Widimský. Otto klein—the forgotten founder of diagnostic cardiac catheterization. *European Heart Journal*, 29(3):422–423, 2007. ISSN 0195-668X. doi: 10.1093/eurheartj/ehm549.

[23] Andre Cournand and Hilmert A Ranges. Catheterization of the right auricle in man. *Proceedings of the Society for Experimental Biology and Medicine*, 46(3):462–466, 1941. ISSN 0037-9727.

[24] A Cournand, HD Lauson, RA Bloomfield, ES Breed, and E de F Baldwin. Recording of right heart pressures in man. *Proceedings of the Society for Experimental Biology and Medicine*, 55(1):34–36, 1944. ISSN 0037-9727.

[25] AR Cournand, RL Riley, ES Breed, E deF Baldwin, DW Richards, MS Lester, and M Jones. Measurement of cardiac output in man using the technique of catheterization of the right auricle or ventricle. *The Journal of Clinical Investigation*, 24(1):106–116, 1945. ISSN 0021-9738.

[26] Renate Forssmann-Falck. Werner forssmann: A pioneer of cardiology. *The American Journal of Cardiology*, 79(5):651–660, 1997. ISSN 0002-9149. doi: 10.1016/S0002-9149(96)00833-8.

[27] Arthur Grollman. The determination of the cardiac output of man by the use of acetylene. *American Journal of Physiology-Legacy Content*, 88(3):432–445, 1929. ISSN 0002-9513.

[28] August Krogh and J Lindhard. Measurements of the blood flow through the lungs of man 1. *Skandinavisches Archiv Für Physiologie*, 27(2):100–125, 1912. ISSN 0370-839X.

[29] A. Bornstein. Eine methode zur vergleichenden messung des herzschlagvolumens beim menschen. *Pflüger's Archiv für die Gesammte Physiologie des Menschen und der Tiere*, 132(5-7):307–318, 1910. ISSN 0031-6768. doi: 10.1007/bf01680346.

[30] EK Marshall Jr and Arthur Grollman. A method for the determination of the circulatory minute volume in man. *American Journal of Physiology-Legacy Content*, 86(1):117–137, 1928. ISSN 0002-9513.

[31] Carleton B Chapman, Henry Longstreet Taylor, Craig Borden, Richard V Ebert, Ancel Keys, and Walter S Carlson. Simultaneous determinations of the resting

arteriovenous oxygen difference by the acetylene and direct fick methods. *The Journal of Clinical Investigation*, 29(6):651–659, 1950. ISSN 0021-9738.

[32] Leon Cander and Robert E Forster. Determination of pulmonary parenchymal tissue volume and pulmonary capillary blood flow in man. *Journal of Applied Physiology*, 14(4):541–551, 1959. ISSN 8750-7587.

[33] Marvin A Sackner, Delmas Greeneltch, Martin S Heiman, Sanford Epstein, and Neal Atkins. Diffusing capacity, membrane diffusing capacity, capillary blood volume, pulmonary tissue volume, and cardiac output measured by a rebreathing technique. *American Review of Respiratory Disease*, 111(2):157–165, 1975. ISSN 0003-0805.

[34] Gabriel Laszlo. Respiratory measurements of cardiac output: from elegant idea to useful test. *Journal of Applied Physiology*, 96(2):428–437, 2004. ISSN 8750-7587.

[35] Dinesh G Haryadi, Joseph A Orr, Kai Kuck, Scott McJames, and Dwayne R Westenskow. Partial co2 rebreathing indirect fick technique for non-invasive measurement of cardiac output. *Journal of Clinical Monitoring and Computing*, 16:361–374, 2000. ISSN 1387-1307.

[36] Nikhil Narang, Jennifer T Thibodeau, William F Parker, Justin L Grodin, Sonia Garg, Ryan J Tedford, Benjamin D Levine, Darren K McGuire, and Mark H Drazner. Comparison of accuracy of estimation of cardiac output by thermodilution versus the fick method using measured oxygen uptake. *The American Journal of Cardiology*, 176:58–65, 2022.

[37] Alessandro Candreva, Emanuele Gallinoro, Marcel van't Veer, Jeroen Sonck, Carlos Collet, Giuseppe Di Gioia, Monika Kodeboina, Takuya Mizukami, Sakura Nagumo, and Danielle Keulards. Basics of coronary thermodilution. *Cardiovascular Interventions*, 14(6):595–605, 2021. ISSN 1876-7605.

[38] Bart F Geerts, Leon P Aarts, and Jos R Jansen. Methods in pharmacology: measurement of cardiac output. *British Journal of Clinical Pharmacology*, 71(3): 316–330, 2011.

[39] Sheila Harvey, David A. Harrison, Mervyn Singer, Joanne Ashcroft, Carys M. Jones, Diana Elbourne, William Brampton, Dewi Williams, Duncan Young, and Kathryn Rowan. Assessment of the clinical effectiveness of pulmonary artery catheters in management of patients in intensive care (pac-man): a randomised controlled trial. *The Lancet*, 366(9484):472–477, 2005. ISSN 0140-6736. doi: 10.1016/s0140-6736(05)67061-4.

[40] Giles Coverdale and Mathew Patteril. Do pulmonary artery catheters have a role in the 21st century intensive care unit? *British Journal of Anaesthesia*, 129(1):3–7, 2022.

[41] James A Brown, Edgar Aranda-Michel, Arman Kilic, Derek Serna-Gallegos, Valentino Bianco, Floyd W Thoma, and Ibrahim Sultan. The impact of pulmonary artery catheter use in cardiac surgery. *The Journal of Thoracic and Cardiovascular Surgery*, 164(6):1965–1973.e6, 2022. ISSN 0022-5223.

[42] Jörn Grensemann. Cardiac output monitoring by pulse contour analysis, the technical basics of less-invasive techniques. *Frontiers in Medicine*, 5, 2018. ISSN 2296-858X. doi: 10.3389/fmed.2018.00064.

[43] Mary Rodriguez Ziccardi and Nauman Khalid. Pulmonary artery catheterization. In *StatPearls Internet*. StatPearls Publishing, 2023.

[44] Sheila E. Harvey, Catherine A. Welch, David A. Harrison, Kathryn M. Rowan, and Mervyn Singer. Post hoc insights from pac-man—the u.k. pulmonary artery catheter trial*. *Critical Care Medicine*, 36(6):1714–1721, 2008. ISSN 0090-3493. doi: 10.1097/ccm.0b013e318174315d.

[45] Ramon P. Clement, Jaap J. Vos, and Thomas W.L. Scheeren. Minimally invasive cardiac output technologies in the icu: putting it all together. *Current Opinion in Critical Care*, 23(4):302–309, 2017. ISSN 1070-5295. doi: 10.1097/mcc.0000000000000417.

[46] Onkar Judge, Fuhai Ji, Neal Fleming, and Hong Liu. Current use of the pulmonary

artery catheter in cardiac surgery: a survey study. *Journal of Cardiothoracic and Vascular Anesthesia*, 29(1):69–75, 2015. ISSN 1053-0770.

[47] Takuma Maeda, Kohshi Hattori, Miho Sumiyoshi, Hiroko Kanazawa, and Yoshihiko Ohnishi. Accuracy and trending ability of the fourth-generation flotrac/vigileo system™ in patients undergoing abdominal aortic aneurysm surgery. *Journal of Anesthesia*, 32:387–393, 2018. ISSN 0913-8668.

[48] Koichi Suehiro, Katsuaki Tanaka, Mika Mikawa, Yuriko Uchihara, Taiki Matsuyama, Tadashi Matsuura, Tomoharu Funao, Tokuhiro Yamada, Takashi Mori, and Kiyonobu Nishikawa. Improved performance of the fourth-generation flotrac/vigileo system for tracking cardiac output changes. *Journal of Cardiothoracic and Vascular Anesthesia*, 29(3):656–662, 2015. ISSN 1053-0770.

[49] Kohshi Hattori, Takuma Maeda, Tetsuhito Masubuchi, Atsushi Yoshikawa, Keigo Ebuchi, Kuniko Morishima, Masataka Kamei, Kenji Yoshitani, and Yoshihiko Ohnishi. Accuracy and trending ability of the fourth-generation flotrac/vigileo system in patients with low cardiac index. *Journal of Cardiothoracic and Vascular Anesthesia*, 31(1):99–104, 2017. ISSN 1053-0770.

[50] Marcus Carlsson, Ruslana Andersson, Karin Markenroth Bloch, Katarina Steding-Ehrenborg, Henrik Mosén, Freddy Stahlberg, Bjorn Ekmehag, and Hakan Arheden. Cardiac output and cardiac index measured with cardiovascular magnetic resonance in healthy subjects, elite athletes and patients with congestive heart failure. *Journal of Cardiovascular Magnetic Resonance*, 14(1):50, 2012. ISSN 1097-6647. doi: 10.1186/1532-429x-14-51.

[51] L. E. R. McLure and A. J. Peacock. Cardiac magnetic resonance imaging for the assessment of the heart and pulmonary circulation in pulmonary hypertension. *European Respiratory Journal*, 33(6):1454–1466, 2009. ISSN 0903-1936. doi: 10.1183/09031936.00139907.

[52] Patrickh Knight, Stanislawp Stawicki, Neelabh Maheshwari, Jafar Hussain, Michael

Scholl, Michael Hughes, Thomasj Papadimos, Weidunalan Guo, James Cipolla, and Nicholas Latchana. Complications during intrahospital transport of critically ill patients: Focus on risk identification and prevention. *International Journal of Critical Illness and Injury Science*, 5(4):256, 2015. ISSN 2229-5151. doi: 10.4103/2229-5151.170840.

[53] Xavier Monnet and Jean-Louis Teboul. Transpulmonary thermodilution: advantages and limits. *Critical Care*, 21:1–12, 2017.

[54] Neil Herring and David J Paterson. *Levick's introduction to cardiovascular physiology*. CRC Press, 2018.

[55] Hanan Keren, Daniel Burkhoff, and Pierre Squara. Evaluation of a noninvasive continuous cardiac output monitoring system based on thoracic bioreactance. *American Journal of Physiology-Heart and Circulatory Physiology*, 293(1):H583–H589, 2007. ISSN 0363-6135.

[56] Jan Penaz. Photoelectric measurement of blood pressure, volume and flow in the finger. In *Digest of the 10th International Conference on Medical and Biological Engineering-Dresden, 1973*, volume 104, 1973.

[57] Jasper Truijen, Johannes J van Lieshout, Wilbert A Wesselink, and Berend E Westerhof. Noninvasive continuous hemodynamic monitoring. *Journal of Clinical Monitoring and Computing*, 26:267–278, 2012. doi: 10.1007/s10877-012-9375-8.

[58] Torsten Bossert, Jan F. Gummert, Hartmuth B. Bittner, Markus Barten, Thomas Walther, Volkmar Falk, and Friedrich W. Mohr. Swan-ganz catheter-induced severe complications in cardiac surgery: Right ventricular perforation, knotting, and rupture of a pulmonary artery. *Journal of Cardiac Surgery*, 21(3):292–295, 2006. doi: 10.1111/j.1540-8191.2006.00235.x.

[59] Kate E. Drummond and Edward Murphy. Minimally invasive cardiac output monitors. *Continuing Education in Anaesthesia Critical Care Pain*, 12(1):5–10, 2012. ISSN 1743-1816. doi: 10.1093/bjaceaccp/mkr044.

[60] Peter Baylor. Lack of agreement between thermodilution and fick methods in the measurement of cardiac output. *Journal of Intensive Care Medicine*, 21(2):93–98, 2006. doi: 10.1177/0885066605285234.

[61] Albertus van Grondelle, R. V. Ditchey, Bertron M. Groves, Wiltz W. Jr Wagner, and John T. Reeves. Thermodilution method overestimates low cardiac output in humans. *American Journal of Physiology-Heart and Circulatory Physiology*, 245(4): H690–H692, 1983.

[62] L Jacquet, G Hanique, D Glorieux, P Matte, and Martin Goenen. Analysis of the accuracy of continuous thermodilution cardiac output measurement: Comparison with intermittent thermodilution and fick cardiac output measurement. *Intensive Care Medicine*, 22:1125–1129, 1996. ISSN 0342-4642.

[63] Uri Elkayam, Robert Berkley, Stanley Azen, Laura Weber, Boaz Geva, and Walter L. Henry. Cardiac output by thermodilution technique. *Chest*, 84(4):418–422, 1983. ISSN 0012-3692. doi: 10.1378/chest.84.4.418.

[64] John H. Stevens. Thermodilution cardiac output measurement. *JAMA*, 253(15): 2240, 1985. ISSN 0098-7484. doi: 10.1001/jama.1985.03350390082030.

[65] Karim Kouz, Frederic Michard, Alina Bergholz, Christina Vokuhl, Luisa Briesenick, Phillip Hoppe, Moritz Flick, Gerhard Schön, and Bernd Saugel. Agreement between continuous and intermittent pulmonary artery thermodilution for cardiac output measurement in perioperative and intensive care medicine: a systematic review and meta-analysis. *Critical Care*, 25(1), 2021. ISSN 1364-8535. doi: 10.1186/s13054-021-03523-7.

[66] M Cecconi, D Dawson, R Casaretti, RM Grounds, and A Rhodes. A prospective study of the accuracy and precision of continuous cardiac output monitoring devices as compared to intermittent thermodilution. *Minerva Anestesiologica*, 76(12):1010, 2010. ISSN 0375-9393.

[67] CG LaFarge and OS Miettinen. The estimation of oxygen consumption. *Cardiovascular Research*, 4(1):23–30, 1970. ISSN 1755-3245.

[68] A Bergstra, RB Van Dijk, HL Hillege, KI Lie, and GA Mook. Assumed oxygen consumption based on calculation from dye dilution cardiac output: an improved formula. *European Heart Journal*, 16(5):698–703, 1995. ISSN 1522-9645.

[69] Nikhil Narang, M. Odette Gore, Peter G. Snell, Colby R. Ayers, Santiago Lorenzo, Graeme Carrick-Ranson, Tony G. Babb, Benjamin D. Levine, Amit Khera, James A. De Lemos, and Darren K. McGuire. Accuracy of estimating resting oxygen uptake and implications for hemodynamic assessment. *The American Journal of Cardiology*, 109(4):594–598, 2012. ISSN 0002-9149. doi: 10.1016/j.amjcard.2011.10.010.

[70] Susanna Desole, Anne Obst, Dirk Habedank, Christian F Opitz, Christine Knaack, Franziska Hortien, Alexander Heine, Beate Stubbe, and Ralf Ewert. Comparison between thermodilution and fick methods for resting and exercise-induced cardiac output measurement in patients with chronic dyspnea. *Pulmonary Circulation*, 12 (3):e12128, 2022.

[71] Beth Cummings, Michelle L. Hamilton, Luca Ciaffoni, Timothy R. Pragnell, Rob Peverall, Grant A. D. Ritchie, Gus Hancock, and Peter A. Robbins. Laser-based absorption spectroscopy as a technique for rapid in-line analysis of respired gas concentrations of o2 and co2. *Journal of Applied Physiology*, 111(1):303–307, 2011. ISSN 8750-7587. doi: 10.1152/japplphysiol.00119.2011.

[72] Mikhail Mazurenka, Andrew J. Orr-Ewing, Robert Peverall, and Grant A. D. Ritchie. Cavity ring-down and cavity enhanced spectroscopy using diode lasers. *Annual Reports Section "C" (Physical Chemistry)*, 101:100, 2005. ISSN 0260-1826. doi: 10.1039/b408909j.

[73] Theresa Julia Zielinski, Erica Harvey, Robert Sweeney, and David M. Hanson. *Quantum States of Atoms and Molecules*. ACS Publications, 2005.

[74] Jinyi Li, Ziwei Yu, Zhenhui Du, Yue Ji, and Chang Liu. Standoff chemical detection using laser absorption spectroscopy: A review. *Remote Sensing*, 12(17):2771, 2020. ISSN 2072-4292. doi: 10.3390/rs12172771.

[75] Ronald K Hanson, R Mitchell Spearrin, and Christopher S Goldenstein. *Spectroscopy and Optical Diagnostics for Gases*, volume 1. Springer, 2016.

[76] C. D. Rodgers and A. P. Williams. Integrated absorption of a spectral line with the voigt profile. *Journal of Quantitative Spectroscopy and Radiative Transfer*, 14(4): 319–323, 1974. ISSN 0022-4073. doi: 10.1016/0022-4073(74)90113-7.

[77] Nicholas M. J. Smith, John Couper, Graham Richmond, Dominic Sandhu, Gus Hancock, Peter A. Robbins, and Grant A. D. Ritchie. Development of in-airway laser absorption spectroscopy for respiratory based measurements of cardiac output. *Scientific Reports*, 11(1):5252, 2021. ISSN 2045-2322. doi: 10.1038/s41598-021-84649-0.

[78] Luca Ciaffoni, David P O'Neill, John H Couper, Grant AD Ritchie, Gus Hancock, and Peter A Robbins. In-airway molecular flow sensing: A new technology for continuous, noninvasive monitoring of oxygen consumption in critical care. *Science Advances*, 2(8):e1600560, 2016. ISSN 2375-2548.

[79] Inc. The MathWorks. Optimization toolbox (r2024b), 2024.

[80] James E Mountain, Peter Santer, David P O'Neill, Nicholas M. J. Smith, Luca Ciaffoni, John H Couper, Grant A. D. Ritchie, Gus Hancock, Jonathan P Whiteley, and Peter A Robbins. Potential for noninvasive assessment of lung inhomogeneity using highly precise, highly time-resolved measurements of gas exchange. *Journal of Applied Physiology*, 124(3):615–631, 2018. ISSN 8750-7587.

[81] J. P. Whiteley, D. J. Gavaghan, and C. E. W. Hahn. A tidal breathing model of the inert gas sinewave technique for inhomogeneous lungs. *Respiration Physiology*, 124 (1):65–83, 2000. ISSN 0034-5687. doi: 10.1016/S0034-5687(00)00185-7.

[82] Snapper R. M. Magor-Elliott, Christopher J. Fullerton, Graham Richmond, Grant A. D. Ritchie, and Peter A. Robbins. A dynamic model of the body gas stores

for carbon dioxide, oxygen, and inert gases that incorporates circulatory transport delays to and from the lung. *Journal of Applied Physiology*, 130(5):1383–1397, 2021. ISSN 8750-7587. doi: 10.1152/japplphysiol.00764.2020.

[83] R. L. Riley and A. Cournand. 'ideal' alveolar air and the analysis of ventilation-perfusion relationships in the lungs. *Journal of Applied Physiology*, 1(12):825–847, 1949.

[84] Walter S Snyder, M. J. Cook, E. S. Nasset, L. R. Karhausen, G. Parry Howells, and I. H. Tipton. *Report of the Task Group on Reference Man*, volume 23. Pergamon Oxford, 1975.

[85] J. Valentin. Basic anatomical and physiological data for use in radiological protection: reference values. *Annals of the ICRP*, 32(3-4):1–277, 2002. ISSN 0146-6453. doi: 10.1016/S0146-6453(03)00002-2.

[86] David P O'Neill and Peter A Robbins. A mechanistic physicochemical model of carbon dioxide transport in blood. *Journal of Applied Physiology*, 122(2):283–295, 2017. doi: 10.1152/japplphysiol.00318.2016.

[87] Nicholas M. J. Smith, John Couper, Christopher J. Fullerton, Graham Richmond, Nick P. Talbot, Gus Hancock, Ian Pavord, Grant A. D. Ritchie, Peter A. Robbins, and Nayia Petousi. Novel measure of lung function for assessing disease activity in asthma. *BMJ Open Respiratory Research*, 7(1), 2020. doi: 10.1136/bmjresp-2019-000531.

[88] Asma Alamoudi, Lorenzo Petralia, Nicholas M. J. Smith, Haopeng Xu, Dominic Sandhu, Graham Richmond, Nick P. Talbot, Grant Ad Ritchie, Ian Pavord, Peter A. Robbins, and Nayia Petousi. Effects of biologic therapy on novel indices of lung inhomogeneity in patients with severe type-2 high asthma. *BMJ Open Respiratory Research*, 12(1):e002721, 2025. ISSN 2052-4439. doi: 10.1136/bmjresp-2024-002721.

[89] Snapper RM Magor-Elliott, Asma Alamoudi, Rebecca R Chamley, Haopeng Xu, Tishan Wellalagodage, Rory P McDonald, David O'Brien, Jonathan Collins, Ben

Coombs, and James Winchester. Altered lung physiology in two cohorts after covid-19 infection as assessed by computed cardiopulmonography. *Journal of Applied Physiology*, 133(5):1175–1191, 2022. doi: 10.1152/japplphysiol.00436.2022.

[90] Josep Roca and Peter D. Wagner. Contribution of multiple inert gas elimination technique to pulmonary medicine. 1. principles and information content of the multiple inert gas elimination technique. *Thorax*, 49(8):815–824, 1994.

[91] Brian J Whipp and Karlman Wasserman. Alveolar-arterial gas tension differences during graded exercise. *Journal of Applied Physiology*, 27(3):361–365, 1969.

[92] AB Dubois, AG Britt, and WO Fenn. Alveolar co2 during the respiratory cycle. *Journal of Applied Physiology*, 4(7):535–548, 1952.

[93] Zachary Messina and Herbert Patrick. Partial pressure of carbon dioxide. In *StatPearls [Internet]*. StatPearls Publishing, 2022.

[94] Dominic Sandhu, Snapper RM Magor-Elliott, Nayia Petousi, Nick P Talbot, Alexander N Bennett, David A Holdsworth, Grant AD Ritchie, and Peter A Robbins. Alveolar deadspace and intrapulmonary shunt in healthy individuals and in individuals who have recovered from covid-19 infection. *Experimental Physiology*, 2025.

[95] Catherine E Farrow, Robert A Robles, G Kim Prisk, Piotr Harbut, Atul Malhotra, Terence C Amis, Peter D Wagner, and Kristina Kairaitis. Increased intrapulmonary shunt and alveolar dead space post-covid-19. *Journal of Applied Physiology*, 135(5): 1012–1022, 2023.

[96] Graham L Hall, Nicole Filipow, Gregg Ruppel, Tolu Okitika, Bruce Thompson, Jane Kirkby, Irene Steenbruggen, Brendan G Cooper, Sanja Stanojevic, and Bert Arets. Official ers technical standard: Global lung function initiative reference values for static lung volumes in individuals of european ancestry. *European Respiratory Journal*, 57(3), 2021. ISSN 0903-1936.

[97] J. Ibañez and J. M. Raurich. Normal values of functional residual capacity in the sitting and supine positions. *Intensive Care Medicine*, 8(4):173–177, 1982. ISSN 0342-4642. doi: 10.1007/bf01725734.

[98] A. Garland and P. Hopton. Airway closure in anaesthesia and intensive care. *BJA Education*, 22(4):126–130, 2022. ISSN 2058-5349. doi: 10.1016/j.bjae.2021.12.001.

[99] Joshua E. Brinkman, Fadi Toro, and Sandeep Sharma. *Physiology, Respiratory Drive*. StatPearls Publishing, Treasure Island (FL), 2025.

[100] P. K. Weathersby and L. D. Homer. Solubility of inert gases in biological fluids and tissues: a review. *Undersea Biomedical Research*, 7(4):277–296, 1980.

[101] GOMIDAS Jibelian, RICHARD R Mitchell, and ERIC S Overland. Influence of hematocrit and temperature on solubility of acetylene and dimethyl ether. *Journal of Applied Physiology*, 51(5):1357–1361, 1981. ISSN 8750-7587.

[102] Inc The MathWorks. Optimization toolbox™ user's guide. 2024.

[103] Caroline Thomas and Andrew B Lumb. Physiology of haemoglobin. *Continuing Education in Anaesthesia, Critical Care & Pain*, 12(5):251–256, 2012. ISSN 1743-1824.

[104] James H Nichols, Tony Cambridge, Neldis Sanchez, and Debra Marshall. Clinical validation of a novel quality management system for blood gas, electrolytes, metabolites, and co-oximetry. *The Journal of Applied Laboratory Medicine*, 6(6):1396–1408, 2021.

[105] R. K. Webb, A. C. Ralston, and W. B. Runciman. Potential errors in pulse oximetry: Ii. effects of changes in saturation and signal quality. *Anaesthesia*, 46(3):207–212, 1991. ISSN 0003-2409.

[106] MD Hammond, GE Gale, KS Kapitan, A Ries, and PD Wagner. Pulmonary gas exchange in humans during normobaric hypoxic exercise. *Journal of Applied Physiology*, 61(5):1749–1757, 1986. ISSN 8750-7587.

[107] H. Kobayashi, B. Pelster, J. Piiper, and P. Scheid. Diffusion and perfusion limitation in alveolar o2 exchange: shape of the blood o2 equilibrium curve. *Respiration Physiology*, 83(1):23–34, 1991. ISSN 0034-5687. doi: 10.1016/0034-5687(91)90090-6.

[108] A. C. Ralston, R. K. Webb, and W. B. Runciman. Potential errors in pulse oximetry: I. pulse oximeter evaluation. *Anaesthesia*, 46(3):202–206, 1991. ISSN 0003-2409.

[109] Scott A Sasse, Priscilla A Chen, Richard B Berry, Catherine S. H. Sassoon, and C. Kees Mahutte. Variability of cardiac output over time in medical intensive care unit patients. *Critical Care Medicine*, 22(2):225–232, 1994.

[110] Chung-Chi Huang, Ying-Huang Tsai, Ning-Hung Chen, Meng-Chih Lin, Thomas CY Tsao, Cheng-Huei Lee, and Kuang-Hung Hsu. Spontaneous variability of cardiac output in ventilated critically ill patients. *Critical Care Medicine*, 28(4):941–946, 2000.

[111] Sarah L Richardson, Alzbeta Hulikova, Melanie Proven, Ria Hipkiss, Magbor Akanni, Noémi B. A. Roy, and Pawel Swietach. Single-cell o2 exchange imaging shows that cytoplasmic diffusion is a dominant barrier to efficient gas transport in red blood cells. *Proceedings of the National Academy of Sciences*, 117(18):10067–10078, 2020.

[112] Erwin E. Argueta and David Paniagua. Thermodilution cardiac output. *Cardiology in Review*, 27(3):138–144, 2019. ISSN 1061-5377. doi: 10.1097/crd.0000000000000223.

[113] David Liljequist, Britt Elfving, and Kirsti Skavberg Roaldsen. Intraclass correlation–a discussion and demonstration of basic features. *PloS One*, 14(7):e0219854, 2019.

[114] Terry K Koo and Mae Y Li. A guideline of selecting and reporting intraclass correlation coefficients for reliability research. *Journal of Chiropractic Medicine*, 15 (2):155–163, 2016.

[115] Abhilasha J Patel, Robert Wesley, Susan F Leitman, and Barbara J Bryant. Capillary versus venous haemoglobin determination in the assessment of healthy blood donors. *Vox Sanguinis*, 104(4):317–323, 2013.

[116] Göran Hedenstierna and Lennart Edmark. Mechanisms of atelectasis in the perioperative period. *Best Practice & Research Clinical Anaesthesiology*, 24(2):157–169, 2010.

[117] W Habre, T Asztalos, PD Sly, and F Petak. Viscosity and density of common anaesthetic gases: implications for flow measurements. *British Journal of Anaesthesia*, 87(4):602–607, 2001. ISSN 1471-6771.

[118] Wallace O Fenn, Hermann Rahn, and Arthur B Otis. A theoretical study of the composition of the alveolar air at altitude. *American Journal of Physiology-Legacy Content*, 146(5):637–653, 1946.

[119] Radiometer Medical ApS. *ABL700 Series Reference Manual*. Radiometer Medical ApS, Bronshoj, Denmark, 2004.

[120] Radiometer Medical ApS. *ABL800 FLEX User Manual*. Radiometer Medical ApS, Bronshoj, Denmark, 2015.

[121] Charlotte Urell, Elisabeth Westerdahl, Hans Hedenström, Christer Janson, and Margareta Emtner. Lung function before and two days after open-heart surgery. *Critical Care Research and Practice*, 2012(1):291628, 2012. doi: 10.1155/2012/291628.

[122] Barry Dixon, Duncan J Campbell, and John D Santamaria. Elevated pulmonary dead space and coagulation abnormalities suggest lung microvascular thrombosis in patients undergoing cardiac surgery. *Intensive Care Medicine*, 34(7):1216–1223, 2008. doi: 10.1007/s00134-008-1042-7.

[123] Corey W Bown, Rachel Do, Omair A Khan, Dandan Liu, Francis E Cambronero, Elizabeth E Moore, Katie E Osborn, Deepak K Gupta, Kimberly R Pechman, Lisa A Mendes, et al. Lower cardiac output relates to longitudinal cognitive decline in aging adults. *Frontiers in Psychology*, 11:569355, 2020. doi: 10.3389/fpsyg.2020.569355.

[124] Righab Hamdan, Fida Charif, Ali Zein, Mohamad Issa, Claudette Najjar, Hadi Abdallah, Saleh Fakih, and Mohamad Saab. Noninvasive monitoring of cardiac

output: a useful tool yet? *Journal of Cardiovascular Echography*, 29(4):165–168, 2019. doi: 10.4103/jcecho.jcecho_38_19.

[125] Ming-Jer Hsieh, Jih-Kai Yeh, Yu-Chang Huang, Ming-Yun Ho, Dong-Yi Chen, Cheng-Hung Lee, Chao-Yung Wang, Shang-Hung Chang, Chun-Chi Chen, and I-Chang Hsieh. Cardiac power output associated with hospitalization and mortality in coronary artery disease patients at stage b heart failure. *IJC Heart & Vasculature*, 55:101521, 2024. doi: 10.1016/j.ijcha.2024.101521.

[126] Jonas Holm, Erik Håkanson, Farkas Vánky, and Rolf Svedjeholm. Mixed venous oxygen saturation predicts short-and long-term outcome after coronary artery bypass grafting surgery: a retrospective cohort analysis. *British journal of anaesthesia*, 107 (3):344–350, 2011. doi: 10.1093/bja/aer166.

[127] Timo I Kaakinen, Tomi Ikäläinen, Tiina M Erkinaro, Jaana M Karhu, Janne H Liisanantti, Pasi P Ohtonen, and Tero I Ala-Kokko. Association of low mixed venous oxygen saturations during early icu stay with increased 30-day and 1-year mortality after cardiac surgery: a single-center retrospective study. *BMC anesthesiology*, 22 (1):322, 2022. doi: 10.1186/s12871-022-01862-8.